STRASBOURG

OCTOBER 26-27 2021

JEMP 2021

Biennial French InterPore Conference

Book of abstracts

Institut Terre & Environnement de Strasbourg | ITES | UMR 7063 de l'Université de Strasbourg & CNRS & ENGEES

France InterPore Chapter

TESCAN PERFORMANCE IN NANOSPACE

SYNERGIE 4

General overview

Every two years, the JEMP (Journées d'Etudes des Milieux Poreux), which were initiated in 1993 at Toulouse - France, are the ideal meeting place for scientific and industrial communities whose common purpose is the understanding of the complex behavior of porous media. The fifteenth edition of JEMP took place at Le Palais Universitaire at Strasbourg (France) from 26th to 27th October 2021.

STEERING COMMITTEE

Laboratory: ITES UMR7063
Research group: TrHyCo

Yves ARMANDO (IE, CNRS)
Benjamin BELORT (MCF, Strasbourg University)
Marwan FAHS (MCF, ENGEES)
François LEHMANN (PR, Strasbourg University)
Gerhard SCHAFER (PR, Strasbourg University)

LOCAL SCIENTIFIC COMMITTEE

Ackerer Philippe (ITES, Strasbourg)
Belfort Benjamin (ITES, Strasbourg)
Brendle Jocelyne (IS2M, Mulhouse)
Bueno Marie-Ange (LPMT, Mulhouse)
Chaplais Gérald (IS2M, Mulhouse)
Daou Jean (IS2M, Mulhouse)
Delay Frédéric (ITES, Strasbourg)
Di Chiara Raphaël (ITES, Strasbourg)
Lehmann François (ITES, Strasbourg)
Mose Robert (Icube, Strasbourg)
Pac Marie-José (LPMT, Mulhouse)
Ryzhikov Andrey (IS2M, Mulhouse)
Toussaint Renaud (ITES, Strasbourg)
Weill Sylvain (ITES, Strasbourg)
Younes Anis (ITES, Strasbourg)

NATIONAL SCIENTIFIC COMMITTEE (FIC)

Amaziane Brahim (LMA, Pau)
Coussot Philippe (IFSTTAR, Champs-sur-Marne)
De Dreuzy Jean-Raynald (Geosciences Rennes, Rennes)
Delmas Agnès (CETHIL, Lyon)
Descamps Cedric (SAFRAN CERAMICS, Le Haillan)
Erhel Jocelyne (INRIA, Rennes)
Fahs Marwan (LHYGES, Strasbourg)
Geindreau Christian (3SR, Grenoble)
Golfier Fabrice (GeoRessources, Nancy)
Goyeau Benoit (EM2C, Chatenay-Malabry))
Granet Sylvie (EdF, Palaiseau)
Grégoire David (IPRA/LFCR, Pau)
Lasseux Didier (I2M, Bordeaux)
Martins Jean (LTHE, Grenoble)
Masson Roland (Dieudonné, Nice)
Mercury Lionel (ISTO, Orléans)
Mghazli Zoubida (U. Ibn Tofail, Maroc)
Moyne Christian (LEMTA, Nancy)
Noetinger Benoit (Ifpen, Reuil-Malmaison)
Quintard Michel (IMFT, Toulouse)
Rochais Denis (CEA, Tours)
Rousseau Benoit (LteN, Nantes)
Saad Mazen (U. Nantes, Nantes)
Schäfer Gerhard (ITES, Strasbourg)
Talon Laurent (FAST, Orsay)
Topin Frédéric (IUSTI, Marseille)
Thovert Jean-François (Pprime, Poitiers)
Vignoles Gérard (LCTS, Bordeaux)

List of chairpersons:
Philippe Ackerer, Gérald Chaplais, Jean Daou, Hannelore Derluyn, Christian Geindreau, Fabrice Golfier, Alberto Guadagnini, Didier Lasseux, Benoit Noetinger, Laurent Orgogozo, Michel Quintard, Denis Rochais, Didier Stemmelen, Renaud Toussaint, Mghazli Zoubida

List of sponsors

TESCAN world-class technology delivers complete solutions for researchers in all branches of science. No matter what is the type and size of the sample, and what questions are being asked, there is always a dedicated solution available to solve all required tasks. Due to the high versatility and customisable design of all TESCAN systems, it is very easy to design and manufacture dedicated instruments suited exactly to the customer's needs.

Tescan is a "SILVER PARTNER" of JEMP2021.

SYNERGIE4 est depuis 1994, l'interlocuteur privilégié pour ce qui concerne la microanalyse, la micro tomographie par rayons X, le dépôt de couches minces et la microscopie électronique. Nous proposons des solutions complètes pour : * des microscopes électroniques de table (MEB), * des systèmes EDS, WDS, µXRF et EBSD, * des appareils de micro tomographie, * des Pico et Nano-Indenteurs pour MEB et MET, * des appareils de découpe et de polissage par faisceau d'ions, * des appareils de dépôts de couches minces. Toujours à la recherche de la satisfaction de nos clients, nous assurons : l'installation, la formation sur site, le suivi technique ainsi que la fourniture de consommables pour tous les produits que nous distribuons.

Synergie4 is a "BRONZE PARTNER" of JEMP2021.

List of partners

Other supports

Plenary lectures

Numerical models for evaluating the competitive use of the subsurface: the influence of energy storage and production in groundwater

Rainer HELMIG, Institute for Modelling Hydraulic and Environmental Systems, Stuttgart University, Germany.

Abstract

The subsurface is being increasingly utilised both as a resource and as an energy and waste repository. Historically, there have been few issues of concern related to competition between resources, with groundwater contamination being a notable exception. However, with increasing exploitation, resource conflicts are becoming increasingly common and complex. Current issues in this regard include, for example, the long-range impact of mechanical, chemical and thermal energy storage on groundwater resources, and the complex effects surrounding hydraulic fracturing in both geothermal and shale gas production. To analyse and predict the mutual influence of subsurface projects and their impact on groundwater reservoirs, advanced numerical models are necessary. In general, these subsurface systems include processes of varying complexity occurring in different parts of the domain of interest. These processes mostly take place on different spatial and temporal scales. It is extremely challenging to model such systems in an adequate way, accounting for the spatially varying and scale-dependent character of these processes. We will describe the fundamental properties and functions of a compositional multi-phase system in a porous medium. The basic multi-scale and multi-physics concepts are introduced and conservation laws formulated and explain the numerical solution procedures for both decoupled and coupled model formulations. Two applications of multi-physics and multi-scale algorithms will be presented and discussed.

Short biography

Rainer H. Helmig is head of the Department of Hydromechanics and Modelling of Hydrosystems in the Faculty of Civil and Environmental Engineering at the University of Stuttgart, Germany. He gained his doctoral degree from the University of Hannover in 1993 and an advanced research degree (Habilitation) from the University of Stuttgart in 1997. In 1995, he was awarded the renowned "Dresdner Grundwasserforschungspreis" for his doctoral thesis on "Theory and numerics of multiphase flow through fractured porous media". His habilitation thesis was published by Springer in the much-cited textbook "Multiphase flow and transport processes in the subsurface: A contribution to the modeling of hydrosystems". From 1997 to 2000, Rainer Helmig held a professorship in "Computer Applications in Civil Engineering" at the Technical University of Braunschweig. Rainer Helmig's research covers fundamental research and applied science in the field of porous-media flow. A major focus is on developing methods for coupling hydrosystem compartments and complex flow and transport processes.

Design of silica and zeolites monoliths for process intensification in heterogeneous (bio)catalysis and in wastewater treatment

Anne GALARNEAU, Institut Charles Gerhardt Montpellier (ICGM) UMR 5253 CNRS-UM-ENSCM, University of Montpellier, France

Abstract

Silica monoliths with hierarchical porosity (macro-/mesoporous), prepared by combining phase separation (spinodal decomposition) and sol-gel process, have demonstrated remarkable potential as supports for catalysts and adsorbents with improved efficiency and productivity of a number of applications in heterogeneous (bio)catalysis, adsorption, separation, water treatments. Monoliths productivities reach 2-4 times the one of packed-bed and 3-10 times the one in batch. This is due to their perfect homogeneous interconnected macroporous network enabling an exceptional mass transfer and a fine control of contact time. In their thin skeleton, their large mesopore volume combined with large mesopore diameters and high surface area allow high diffusion of reactants and products and high reactivity. Silica monoliths have been functionalized by an important variety of moities and techniques, such as grafting with versatile species (acidic, basic), by alumina coating, immobilization of ionic liquids, of enzymes, in-situ synthesis of nanoparticles of Pd and MOF. Their skeleton has been transformed into MCM-41 and zeolites (SOD, LTA, FAU-X) by pseudomorphic transformation. Carbon monoliths have been obtained by replica of silica monoliths. These functional materials reveal great opportunities for process intensification. For examples, LTA and FAU-X monoliths have removed selectively Sr^{2+} and Cs^{+}, respectively, in simulated radioactive water with perfect breakthrough curves.

Short biography

Dr Anne Galarneau obtained a PhD in Materials Sciences in the Institute of Materials in Nantes, France, in 1993 on the study of lamellar phosphatoantimonic acids for heterogeneous catalysis under the supervision of Y. Piffard and M. Tournoux in collaboration with Rhône-Poulenc. She carried out a post-doc at Michigan State University, USA, in 1993-1995, where she discovered the synthesis of Porous Clay Heterostructures using surfactant-templated mechanism in the group of T. Pinnavaia. She became a CNRS researcher in France in 1995 and joined the Institute Charles Gerhardt in Montpellier, where she developed new synthesis of mesoporous silica prepared by surfactants templating (MCM-41, MCM-48, HMS, SBA-15, KIT-6) with the use of natural surfactants (lecithin) highly suitable for enzymes encapsulation. In particular she discovered the concept of pseudomorphic transformation – inspired by the mineral world – to independently control the textural properties and the morphology (particles, monoliths) of mesoporous silica and zeolites (SOD, LTA, FAU-X). Another key achievement was the characterization of materials porosity to elucidate the complex texture of SBA-15 and mesoporous FAU-Y. Her most recent works concern the elaboration of monoliths with hierarchical porosity, directly usable as reactors, which reveal remarkable performance in (bio)(photo)catalysis and wastewater treatments. She authored 157 publications and 6 patents (h-index 44).

Unravelling pore-scale processes in geomaterial

Veerle CNUDDE, *Dept. of Geology, Ghent University, Belgium. Holder of the chair "Porous media imaging techniques", Utrecht University, The Netherlands.*

Abstract:

Physical, chemical and biological weathering has a constant effect on the earth's landscape. This also impacts our building infrastructure, as stone and masonry are damaged by a combination of different processes, such as chemical attack, biological colonization, water infiltration and changes in temperature. Fluid flow, reactive transport, nucleation, dissolution, precipitation and mass transport are crucial processes occurring inside the pore system of geomaterials. To fully understand the macroscopical behavior of geomaterials in this context, their pore scale properties and processes have to be understood. The stone's mineralogy and pore structure strongly affect key internal pore scale processes. These processes have been studied indirectly by micro- and macroscopic observations and laboratory experiments. Although this provides valuable information, the key drivers of these processes are to be studied at the pore scale. To explore these dynamic pore-scale processes, several non-destructive 3D and 4D methods are currently available. These tools provide additional important insights. Unravelling pore-scale processes in combination with pore scale modelling is an essential step towards understanding and predicting a geomaterial's macroscopic behavior correctly.

The presentation discusses the current possibilities and challenges in non-destructive pore-scale imaging of geomaterials and how this data can be used as input for fluid flow models and their validation. Additional new developments at the synchrotron and on lab-based X-ray systems related to material characterization as well as to the understanding of pore-scale processes are discussed. Examples will be given of different experiments related to the characterization and the imaging of dynamic pore scale processes in (geo)materials.

Short biography

Prof. Veerle Cnudde received a PhD in Geology in 2005 from Ghent University (Belgium) where she has been a research professor since 2010. She is team leader of PProGRess (www.pprogress.ugent.be), the Pore-scale Processes in Geomaterials Research group (Dept. of Geology, UGent) and is one of the coordinators of the Ghent University Expertise Centre for X-Ray Tomography (UGCT). She was one of the co-founders of the UGCT spin-off company Inside Matters, which later merged with the spin-off company XRE, now part of TESCAN.

She specializes in non-destructive imaging of geomaterials and has a strong expertise in real-time imaging of processes in the pore space. Research projects which she has initiated are strongly linked to weathering and fluid flow processes of porous sedimentary rocks, as well as conservation of building stones.

Prof. Veerle Cnudde has published more than 100 peer-reviewed journal articles. She is currently the Chair of the Proposal Review Committee (PRC) of the TOMCAT beamline at Swiss Light Source (SLS). She is one of the co-founders of InterPore BENELUX and an elected Council Member of InterPore. In 2019, she became a part-time Full Professor at the Environmental Hydrogeology group at Utrecht University in the field of "Porous media imaging techniques". Prof. Veerle Cnudde has been selected by the InterPore award commitee Kimberly-Clark lecturer 2020.

Wetting mechanisms of fibrous materials: from yarn to textile scales

Jan CARMELIET[1], Robert Fischer[1,2,3], Jianlin Zhao[1], Christian M. Schlepütz[4], René M. Rossi[2], Dominique Derome[5]

[1]*Chair of Building Physics, ETHZ, Switzerland*
[2]*Laboratory for Biomimetic Membranes and Textiles, Empa, Switzerland*
[3]*Laboratory of Multiscale Studies in Building Physics, Empa, Switzerland*
[4]*Swiss Light Source, PSI, Switzerland*
[5]*Department of Civil and Building Engineering, Université de Sherbrooke, Canada*

Abstract

Textiles are ubiquitous as clothing, in medical, sport or hygienic care, but also in engineering or architecture. The control of liquid spreading in these materials is often crucial or desirable, such as e.g. moisture management in functional clothing or durability of fiber reinforced materials.

Fast X-ray tomographic microscopy and neutron radiography are used to monitor the imbibition process in yarns at micrometer and centimeter scale, respectively. Observed is a step-wise water uptake process characterized by fast pore filling events of long and narrow pores in the order of seconds and long waiting times between filling events up to several minutes. This step-wise dynamics results in an uptake behavior not following a square root behavior as described by Washburn's law. The step-wise dynamics are analyzed in terms of the balance between free energy and viscous dissipation, showing waiting times are corresponding to quasi-stable water configurations of almost vanishing free energy gradient.

A pore network model is developed based on the typical pore network topology of yarns and waiting time distributions as observed at micron scale. This network model is upscaled to millimeter scale and validated with the Neutron measurements. The network model allows to analyse in detail the interplay of pore scale processes and pore network topology at lower scales and their impact on experimentally observed processes at macroscale.

We finally study the imbibition process in two connected yarns, called interlaces. We observe that the imbibition process between two yarns may vary highly due to variations in pore connectivity in the contact area. The distribution of waiting times for the transport between two yarns is shifted to longer waiting periods as compared to the distribution of waiting times for the yarn pores.

Short biography

Since June 2008, Jan Carmeliet is full professor at the Chair of Building Physics at the department of Mechanical Engineering at ETH Zürich Switzerland.

Jan Carmeliet, graduated from the Katholieke Universiteit Leuven (K.U.Leuven) and has been Professor at K.U.Leuven since 1998 and part-time Professor at T.U.Eindhoven. He was in 2007 on sabbatical leave at the University of Illinois at Urbana Champaign and at Los Alamos Governmental Laboratories.

His research resulted in more than 330 scientific journal papers.

His research interests concern urban climate and urban heat island mitigation, multiscale behaviour of porous materials and their fluid interactions, and multi-energy decentralized systems at building and urban scale.

He was research councillor of the National Science Foundation Switzerland and expert of the Swiss Innovation Agency (InnoSuisse). He was director of the graduate program 'master integrated building systems' at ETHZ. He was member of the research commission of ETH Zürich, the scientific commission of the CCEM (Centre of Competence Energy and Mobility) and the Board of Energy Science Centre ETH Zürich. He plaid a very active role in acquiring and organizing the SCCER (Swiss competence centre energy research) FEEB&D (Future energy efficient buildings and districts).

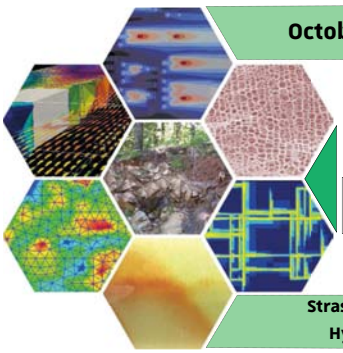

October 26–27 2021

France InterPore Chapter

JEMP 2021

Strasbourg (France)
Hybrid format

Institut Terre & Environnement de Strasbourg | ITES | UMR 7063 de l'Université de Strasbourg & CNRS & ENGEES

TESCAN PERFORMANCE IN NANOSPACE

SYNERGIE 4

Program – Tuesday, 26 October

Virtual talks in red

08:30 Welcome of in-presence participants – Palais Universitaire

09:00 Opening of JEMP2021 by scientific committee (room PASTEUR)

09:20 Keynote: **Rainer HELMIG** (room PASTEUR)

Numerical models for evaluating the competitive use of the subsurface: the influence of energy storage and production in groundwater

10:15 Coffee break (AULA)

10:40 Keynote: **Anne GALARNEAU** (room PASTEUR)

Design of silica and zeolites monoliths for process intensification in heterogeneous (bio)catalysis and in wastewater treatment

11:35 Short break

Room PASTEUR	Room 118	Room 119
11:45 **Djibo Soumana Aboubacar** *Modelling of heat conduction in granular porous media*	**Chaguer Mouna** *Development of the integrated hydrological model NIHM: Implementation of transport processes*	**Guo Juncheng** *Mechanisms of gas separation through 2D porous graphene membranes : theory and molecular simulations*
12:10 **Keita Seny** *Development of quantitative detection methods for mass spectrometry of non-interfering and interfering gases such as mixtures of H_2, He, Ne, O_2, Ar, N_2, CO_2, CH_4, C_2H_6, C_3H_8, i-C_4H_{10}, n-C_4H_{10} and C_5H_{12}*	**Mallya Nithin** *Topology Optimization of Encapsulated Macro-Porous Phase Change Materials for Thermal Energy Storage*	**Zhang Yijun** *Photopolymerization of zeolite/polymer based composite and corresponding application in the fields of 3D printing and gas adsorption*

12:30 LUNCH (« Restaurant universitaire GALLIA »)

Coffee Break (« Restaurant universitaire GALLIA »)

14:00 **Noetinger Benoit** *Equivalent hydraulic conductivity, connectivity and percolation in 2D and 3D random binary media*	**Ferhat Hamida Rabie** *Investigation of calcium sulfate carbonation processes using geological labs on a chip: experimental and thermo-kinetic modelling approaches*	**Blosse Sarah** *Enzymatic degradation of plant biomass : a porous media approach*
14:25 **Prieto Espinoza Maria** *Dichloromethane degradation in porous media under dynamic hydrogeological conditions*	**Mostafa Ahmad** *Pore-scale hydro-mechanical modeling of gas transport in coal matrix*	**Berjamin Harold** *Nonlinear acceleration waves in soft porous media*
14:50 **Ariskina Kristina** *Molecular dynamics study of methane diffusion in flexible microporosity of source rock's organic matter*	**Hajizadeh Javaran Mohammad Reza** *Application of deep neural networks in predicting natural convection on two dimensional porous media*	Assemat Pauline *How mechanical strain might modify transport properties of a biological tissue-mimicking porous media; an experimental approach*
15:15 **Bourel Christophe** *Modeling of shallow aquifers in interaction with overland water*	**Stemmelen Didier** *Swelling of polymeric hydrogels observed by MRI*	**Barthes Antoine** *Study of the nanoscopic fluid film involved in the crystallization of water in a porous material by a Non-Local Density Functional Theory framework*

15:35 Coffee Break (AULA)

16:00 FIC General Assembly (room PASTEUR)

17:00 Posters session & partners' exhibition (AULA)

18:40 Free time

20:00 Gala DINNER
(Restaurant L'Ancienne Douane – 6 rue de la douane – Strasbourg)

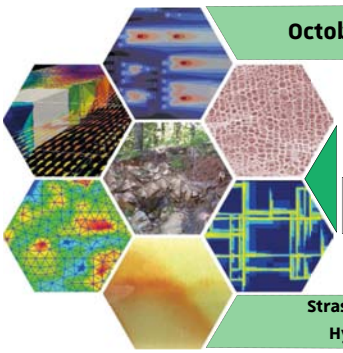

October 26–27 2021

France InterPore Chapter

JEMP 2021

Strasbourg (France)
Hybrid format

Institut Terre & Environnement de Strasbourg | ITES | UMR 7063 de l'Université de Strasbourg & CNRS & ENGEES

TESCAN PERFORMANCE IN NANOSPACE

SYNERGIE 4

Program – Wednesday, 27 October

Virtual talks in red

08:10 Welcome of in-presence participants – Palais Universitaire

08:30 Keynote: **Veerle CNUDDE (virtual talk - room PASTEUR)**
Unravelling pore-scale processes in geomaterial

09:25 Short break

	Room PASTEUR	Room 118	Room 119
09:30	**Bouvet Lisa** *Towards a pore scale model of snow cover metamorphism under isothermal conditions*	**Licsandru Glad-Calin** *Laboratory controlled NaCl salt crusts*	**Recalcati Chiara** *Statistical characterization of the micro-scale spatial distribution of calcite dissolution rates*
09:55	**Koohbor Behshad** *Modeling coupled DNAPL migration and complex resistivity evolution in saturated porous media*	**Mghazli Zoubida** *Mathematical modeling and numerical approximation of the compressible two-phase flow in a landfill*	**Stigliano Luca** *Geostatistical description of calcite surface roughness resulting from dissolution at close-to-equilibrium conditions*
10:20	**Mokhtari Omar** *How high-stress elastic filaments control flows of viscoelastic fluids through porous media?*	**Okumko Victor** *Investigating haloclasty as a potential cause of French Basque Country Coastline erosion*	**Noiriel Catherine** *Evaluation of mineral precipitation into single fractures*
10:40	Coffee break (AULA)		
10:55	**Koohbor Behshad** *On the use of ERT data for numerical modeling of seawater intrusion in fractured coastal aquifers*	**Maiza Safa** *Modeling of Evaporative Soil Salinization induced By Salt Recycling In Irrigated Arid Regions (Tunisia)*	**Lu Renchao** *Pore-scale modeling of acid etching in a carbonate fracture*
11:20	**Ahmed Maloum Mohamed El Moustafa** *Characterization of Transport Properties for the Microporous Layer of PEMFC from 3D Tomographic Images*	**Alamooti Amir** *Analysis of the displacement behavior of DNAPL in contaminated soils by injecting densified polymer suspension*	**Chekai Tinhinane** *Structural, chemical and hygric characterization of antique Dutch tiles and their susceptibility to salt damage*
11:45	**Fontaine Vincent** *Hybridizable interior penalty discontinuous Galerkin methods for degenerate advection-Diffusion-reaction problems*	**Mansouri-Boroujeni Mahdi** *The link between corner flows and Haines jumps dynamics during two phase flow in subsurface reservoirs using microfluidics*	**Ha Quoc Dat** *Study on the poromechanical behavior of coalbed methane affected by gas mixture adsorption in nanopores of complex geometry*
12:10	**Ahusborde Etienne** *Numerical simulation of coupled two-phase flows and geochemical reactions in porous media: contribution to a new CO 2 benchmark*	**Ghiringhelli Elisa** *Experimental study of drying in the presence of fluorescent colloidal particles in model system*	**Mannai Aroua** *Numerical Modeling of Evaporative Salinization and Crystallization-Induced Deformations in Building Stone*
12:30	LUNCH (« Restaurant universitaire GALLIA »)		
	Coffee Break (« Restaurant universitaire GALLIA »)		
14:00	**Perez Sarah** *On the estimation of permeability uncertainty due to unresolved pore-scale features*	**Etangsale Grégory** *Primal hybridizable discontinuous Galerkin methods for modeling flow in fractured porous media*	**Sarkis Marilyn** *Influence of the contact properties on the behavior of biocemented sand*
14:25	**Tinet Anne-Julie** *Comparison of morphological and effective properties of 3D reconstructed nanoporous medium from 2D FIB-SEM slices*	**Hoteit Hussein** *A pressure transient analysis approach to estimate CO_2 entrapment in fractured reactive formation*	**Fernandes Bruno** *Microstructure of concrete made with recycled concrete aggregates after exposure to elevated temperatures*
14:50	**Ryzhikov Andrey** *High Pressure Intrusion of Aqueous Salt Solutions in MFI-type Zeosil: Influence of Cation Nature*	**Mezquita Gonzalez Jesus Alberto** *Near surface geophysics to quantify groundwater storage heterogeneity in weathered/fractured hard rock aquifers*	Soumane Youness *Clogging of a 2D model porous media by a non brownian suspension*
15:10	Coffee Break (AULA)		
15:30	Keynote: **Jan CARMELIET (virtual talk - room PASTEUR)** *Wetting mechanisms of fibrous materials: from yarn to textile scales*		
16:30	FIC PhD Prize Awarding (Best PhD poster) Closure of the conference		
17:10			

Table of contents

Numerical modeling of flows in porous media

Characterization of Transport Properties for the Microporous Layer of PEMFC from 3D Tomographic Images

M. Maloum[a], M. Quintard[a], M. Prat[a], P. Duru[a], M. Marcoux[a], T. David[b], L. Guetaz[b], J. Pauchet[b]

[a] *Institut de Mécanique des Fluides de Toulouse (IMFT), Université de Toulouse, CNRS, 31400 Toulouse, France*
[b] *Atomic Energy and Alternative Energies Commission (CEA), Laboratory of Innovation on Technologies for new Energies and Nanomaterials (LITEN), University Grenoble Alpes, F-38054 Grenoble, France*

Keywords: Fuel cell, Porous medium, Upscaling, X-ray Tomography

1. Introduction

PEM fuel cells are well positioned in the current industrial market, notably in the automobile industry, as a clean solution for the supply of energy. Current research on fuel cells aims to increase their lifespan and lower their construction costs, in addition to increasing their power. As shown in fig.1-a, a fuel cell uses the chemical energy of hydrogen and oxygen to produce electricity. To ensure the performance of these electrochemical processes, several layers of different characteristics are present in the fuel cell:
GDL: Gas Diffusion Layer, designed to optimize gas diffusion (O_2 and H_2, water vapor)
CCL & ACL: Cathode and Anode Catalytic Layers are two layers of nanometer-scale porosity where electrochemical reactions take place.
MPL: Micro-Porous Layer is a thin layer between the GDL and the CCL, which helps to regularize the transition between these two layers.
The work presented here consists in characterizing the MPL layer by calculating its effective properties

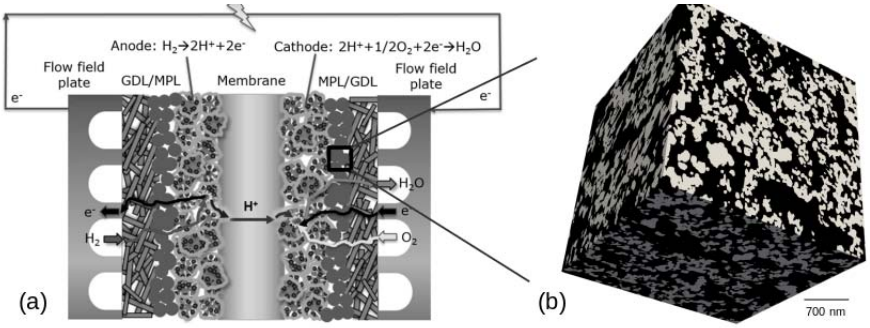

Figure 1: (a) Representation of the PEMFC [1], (b) 3D segmented tomographic image of the MPL (CEA-LITEN)

such as its thermal and electrical conductivity and effective diffusivity.

2. Effective Properties Numerical Computation

We proceed by direct numerical simulation based on the 3D image of the MPL in fig.1-b acquired by FIB/SEM (focus ion beam/scanning electron microscopy) and segmented by the project partner CEA-LITEN who used machine learning tools to perform the segmentation.
Given the size of the segmented 3D image (5.6 billion Voxels), we decided to use the sequential approach sketched in fig.2-a. We break down the image into several blocks of chosen size l. Then we calculate the effective properties of each block. This thus lead to a Darcy-scale map of anisotropic tensor. Medium is a heterogeneous medium made of two phases. We present below the case of thermal conduction. A pure diffusion problem would be treated by a penalization technique by imposing a sufficiently small diffusion coefficient in the non-condductive material.

2.1. Governing equations and boundary conditions

The steady-state conduction equation is written as:

$$\nabla.(\underline{\underline{\lambda}}(\underline{x}).\nabla T) = 0 \tag{1}$$

where $\underline{\underline{\lambda}}$ is the thermal conductivity tensor, isotropic at the local scale. The tool is generic but for the present application we take the values: $\lambda(air) = 0.024\ W.m^{-1}.K^{-1}$ and $\lambda(carbon) = 95\ W.m^{-1}.K^{-1}$ [2]. At the Darcy-scale the conductivity tensor will be an anisotropic tensor noted $\underline{\underline{\lambda}}^*$ (effective property per block). Because images are not periodic systems, we use the permeameter type of approach to estimate the effective properties at the various steps. Various types of permeameter boundary conditions may be used [3], in this work we use the classical inlet-outlet condition in one direction, and zero gradients on the sides. This makes it possible to calculate the effective properties in this direction by calculating the averages of the fluxes. Three simulations are necessary to find the effective property tensor, which can be obtained through:

$$\begin{pmatrix} \lambda^*_{xx} & \lambda^*_{xy} & \lambda^*_{xz} \\ \lambda^*_{yx} & \lambda^*_{yy} & \lambda^*_{yz} \\ \lambda^*_{zx} & \lambda^*_{zy} & \lambda^*_{zz} \end{pmatrix} . \begin{pmatrix} \overline{\nabla T_x}^1 & \overline{\nabla T_x}^2 & \overline{\nabla T_x}^3 \\ \overline{\nabla T_y}^1 & \overline{\nabla T_y}^2 & \overline{\nabla T_y}^3 \\ \overline{\nabla T_z}^1 & \overline{\nabla T_z}^2 & \overline{\nabla T_z}^3 \end{pmatrix} = \begin{pmatrix} \overline{Q_x}^1 & \overline{Q_x}^2 & \overline{Q_x}^3 \\ \overline{Q_y}^1 & \overline{Q_y}^2 & \overline{Q_y}^3 \\ \overline{Q_z}^1 & \overline{Q_z}^2 & \overline{Q_z}^3 \end{pmatrix} \tag{2}$$

where indices 1,2,3 indicate the number of the simulation associated with a direction.
We solve this system to find the conductivity tensor $\underline{\underline{\lambda}}^*$, which will be used in the Darcy-scale equation.

2.2. Preliminary results

Fig.2 illustrates the results from the image depicted in fig.1-b. On the right is represented the PDF of λ_{xx} for various block sizes, from which the sought effective property can be eventually determined.

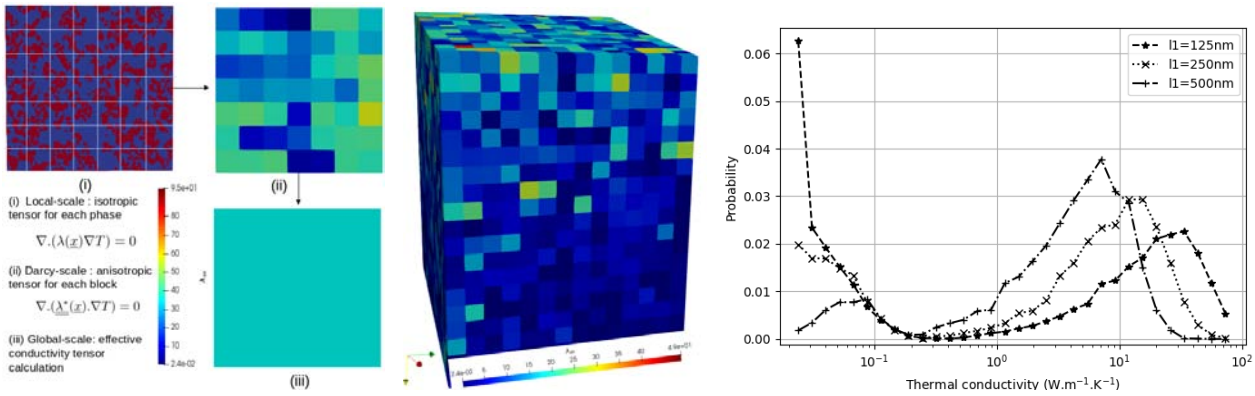

Figure 2: Left (a) Schematization of 2-step sequential approach, Middle (b) λ_{xx} map at a Dary-scale (l=500nm), Right (c) Probability density of λ_{xx} for different decomposition sizes (l_1)

3. Next Steps

The next step will be to characterize the impact of cracks (not visible in Fig.1b but visible at the scale of X-Ray tomographic images) on the MPL effective properties. Also, the presented numerical approach will be used for the characterization of the other porous layers, CCL, GDL, in the fuel cell.

Acknowledgments This project has received funding from the Fuel Cells and Hydrogen 2 Joint Undertaking under grant agreement No. 875025 (FURTHER-FC project). This Joint Undertaking receives support from the European Union's Horizon 2020 Research and Innovation program, Hydrogen Europe and Hydrogen Europe Research.

References

[1] J Jankovic et al. *Multi-scale imaging and transport modeling for fuel cell electrodes*, J. Mater. Res. 34, 579-591 (2019).
[2] F Barbir, *PEM Fuel Cells: Theory and Practice*, P 102. Elsevier Academic Press, USA (2005).
[3] R Guibert et al. *Comparison of Various Methods for the Numerical Evaluation of Porous Media Permeability Tensors from Pore-Scale Geometry.* Math Geosci 48, 329-347 (2016).

Molecular dynamics study of methane diffusion in flexible microporosity of source rock's organic matter

K. Ariskina, G. Galliero, A. Obliger

Lab. of Complex Fluids and their Reservoirs, UMR 5150,
E2S UPPA, University of Pau and the Pays de l'Adour/Total/CNRS - Pau, 64000

Keywords: methane diffusion, kerogen, molecular dynamics

1 Introduction

Over the last decades shale gas production from deep rock formations has become increasingly important in the gas industry. This has led to thorough examinations of fluid transport properties by molecular dynamics simulations in the organic part of the porous medium, such as those found in unconventional reservoirs, so called kerogen. Most of these studies have been done by considering the microporous structure of kerogen as a rigid solid [1-3]. However, a recent study [4] has revealed that accounting for the kerogen flexibility while investigating the hydrocarbon transport in an immature kerogen matrix could play a crucial role. Flexibility can lead to a significant increase in the free volume due to the adsorption-induced swelling that increases fluid transport when the fluid loading increases, as opposed to what found in the rigid case. This study has only been performed for a few set of thermodynamics conditions and collective diffusion has not been studied yet. All this calls for the need of in-depth studies of the flexibility effects on transport properties in immature kerogen.

2 Results and discussion

In this work methane diffusion in kerogen for a wide range of conditions (pressure, temperature) and fluid loading is investigated. It is proven that the collective effect on fluid transport through a deformable matrix of kerogen can be neglected. That means that the fluid-fluid interplay has no meaningful effect on the transport properties due to strong adsorption.

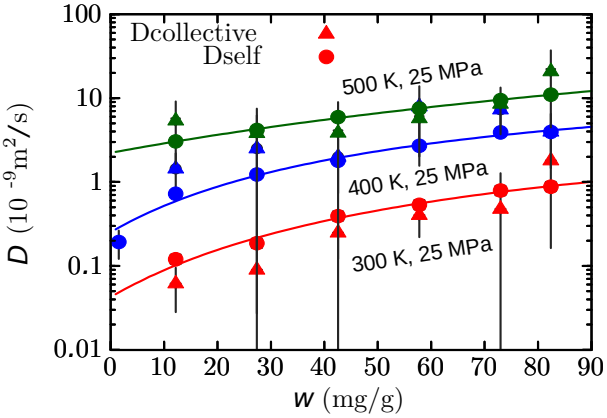

Figure 1: Methane diffusion coefficients versus the fluid loading per gram of kerogen.

It is also shown that the trend of diffusion coefficient increases via fluid loading can be well captured using free volume scaling.

Furthermore, we have started studying the carbon dioxide diffusion in the kerogen matrix. These results contribute to the investigation of fluid transport properties in such microporous medium and will be extended to study transport of carbon dioxide and methane mixtures in a near future.

References

[1] J. Collell *et al.*, Molecular Simulation of Bulk Organic Matter in Type II Shales in the Middle of the Oil Formation Window, *Energy & Fuels*, *28*(12), 7457–7466 (2014).
[2] K. Falk *et al.*, Subcontinuum mass transport of condensed hydrocarbons in nanoporous media, *Nature communications*, *6(1),* 6949 (2015).
[3] A. Obliger *et al.*, Poroelasticity of Methane-Loaded Mature and Immature Kerogen from Molecular Simulations, *Langmuir, 34(45), 13766–13780* (2018).
[4] A. Obliger *et al.*, Methane Diffusion in a Flexible Kerogen Matrix, *Journal of Physical Chemistry B*, 123(26), 5635–5640 (2019).

Towards a pore scale model of snow cover metamorphism under isothermal conditions

L. Bouvet[a,b], N. Calonne[b], F. Flin[b], C. Geindreau[a]

[a] *Univ. Grenoble Alpes, CNRS, Grenoble INP, Laboratoire 3SR, 1270 rue de la Piscine, 38400 Saint Martin d'Hères, France*

[b] *Univ. Grenoble Alpes, Université de Toulouse, Météo-France, CNRS, CNRM, Centre d'Études de la Neige, 38000 Grenoble, France*

Keywords: Snow microstructure, isothermal metamorphism, 3D model

1. Introduction

Snow on the ground evolves through processes of mass redistribution due to thermodynamic mechanisms called snow metamorphism. Different types of snow metamorphism take place depending on the temperature gradient intensity. Representing snow metamorphism for low temperature gradient (isothermal metamorphism) is key to model the evolution and properties of the snow cover. Recently, a new phase-field model allowing to describe 3D microstructure induced by curvature effects has been proposed [1]. In the present work, this model is used to simulate isothermal metamorphism of snow at the pore scale, considering the only process of moving interfaces by sublimation-deposition driven by curvatures. This model runs on real 3D microtomographic images and gives a temporal series of 3D images simulating isothermal metamorphism.

2. Calibration

The condensation coefficient involved in such modelling has been calibrated by reproducing the time evolution of the specific surface area (SSA) measured during isothermal experimental time-series at -2°C [2]. This parameter represents the efficiency of the integration of vapor molecules into the crystalline lattice of ice and is key to model metamorphism. However, it is still poorly understood and quantified, notably because of its complex dependencies to temperature, humidity and crystalline orientation [4]. This calibration has led to a value of the condensation coefficient $\alpha = (9.92 \pm 0.59)10^{-4}$. This value has been validated by simulating another experiment of isothermal metamorphism at -2°C [3].

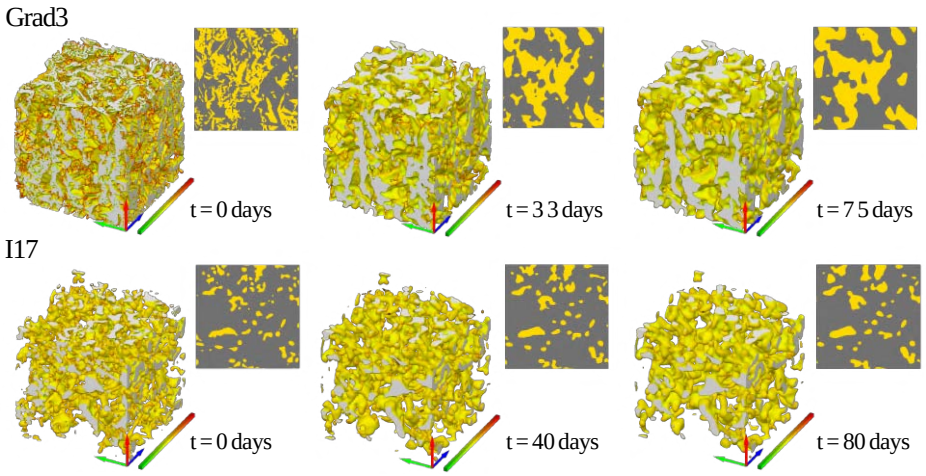

Figure 1: Simulated time series - 3D views and their vertical slices taken at the center of each cube.

3. Results

Finally, 4 images representing different types of snow microstructures have been chosen as input to simulate an isothermal metamorphism at -2°C during 75 days. 2 of the 4 simulated series are shown in Figure 1. Grad3 is an anisotropic faceted sample that underwent high temperature gradient and I17 is made of decomposing precipitation particles with rounded shapes. We see the effect of isothermal metamorphism: rounding, coarsening, and sintering of the ice grains. The obtained temporal series of 3D images were then used to calculate microstructural properties (porosity, SSA, covariance length, mean curvature distribution) and physical transport properties (thermal conductivity, effective diffusion, permeability) evolution during the metamorphism. Numerical estimations of physical properties are shown along with their current parameterizations to assess that the model conforms with current knowledge. An interesting new result arising from the simulations is the conservation or enhancement of the structural anisotropy for very anisotropic snow samples under isothermal conditions, which can be observed in Figure 2. This structural anisotropy can be linked to the vertical structure strengthening of Grad3 during the simulation in Figure 1, and questions the rather well established idea that isothermal conditions tend to decrease the anisotropy index.

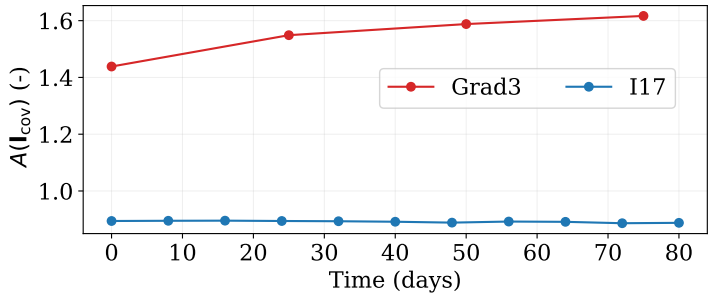

Figure 2: Anisotropy of covariance length evolution defined as $\mathcal{A}(\mathbf{l}_{\text{cov}}) = \mathbf{l}^z_{\text{cov}}/\mathbf{l}^{xy}_{\text{cov}}$.

4. Conclusion

We present a consistent model for isothermal metamorphism through the only process of condensation-sublimation. We calibrated the condensation coefficient using an experimental series, and evaluated it with a good agreement using another independent series. This model enables to study features of the isothermal metamorphism for different snow types leading to interesting results such as the conservation/enhancement of the anisotropy of initially anisotropic samples.

References

[1] Bretin, Elie ; Denis, Roland ; Lachaud, Jacques-Olivier ; Oudet, Edouard: Phase-field modelling and computing for a large number of phases. In: *ESAIM: Mathematical Modelling and Numerical Analysis* 53 (2019), Mai, Nr. 3, S. 805–832

[2] Flin, Frédéric ; Brzoska, Jean-Bruno ; Lesaffre, Bernard ; Coléou, Cécile ; Pieritz, Romeu A.: Three-dimensional geometric measurements of snow microstructural evolution under isothermal conditions. In: *Annals of Glaciology* 38 (2004), S. 39–44

[3] Hagenmuller, Pascal ; Flin, Frederic ; Dumont, Marie ; Tuzet, François ; Peinke, Isabel ; Lapalus, Philippe ; Dufour, Anne ; Roulle, Jacques ; Pézard, Laurent ; Voisin, Didier ; Ando, Edward ; Roscoat, Sabine Rolland du ; Charrier, Pascal: Motion of dust particles in dry snow under temperature gradient metamorphism. In: *The Cryosphere* 13 (2019), September, Nr. 9, S. 2345–2359

[4] Libbrecht, Kenneth G. ; Rickerby, Mark E.: Measurements of surface attachment kinetics for faceted ice crystal growth. In: *Journal of Crystal Growth* 377 (2013), August, S. 1–8

Modeling of shallow aquifers in interaction with overland water

C. Bourel[a], C. Choquet[b], C. Rosier[a], M. Tsegmid[a]

[a] *LMPA, Université du Littoral Côte d'Opale, France.*
[b] *MIA, Université de La Rochelle, France.*

Keywords: Fluid flow modeling, Saturated and unsaturated porous media, Numerical simulations, Asymptotic analysis, Vertical Richards equations, Dupuit Hypothesis

1. Presentation of the models

We present a new class of efficient models for water flow in shallow aquifers, providing an alternative to the classical but less tractable 3d-Richards model (see [2]). Those models are tuned to have exactly the same (dominant) behavior as the 3d-Richards model when when the ratio $\varepsilon =$*thickness over longitudinal length of the aquifer* is small. Thanks to a formal asymptotic analysis when $\varepsilon \to 0$, those dominant components of the flow have been obtained in several time-scale :

- **Fast component of the flow.** This component of the flow is dominant on a small time scale. It is described by a collection of vertical 1d-Richards problems parameterized by the horizontal position;
- **Slow component of the flow.**That component of the flow corresponds to a large time scale, when the vertical flow appears instantaneous. The corresponding evolution of the hydraulic head is independent of the vertical variable and become a 2d-horizontal problem.

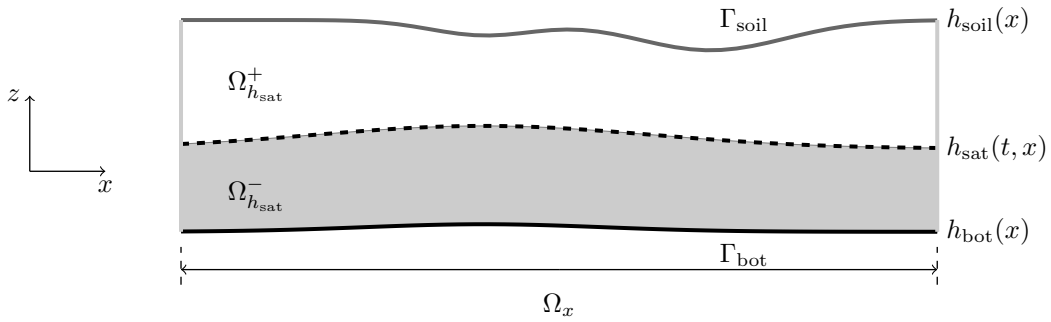

The new models are obtained by mimicking and coupling those two particular behaviours. The strategy is to introduce an artificial interface $h_{\text{sat}} = h_{\text{sat}}(t,x)$ between the two different types of flow. For each given h_{sat} (possibly depending on the other unknowns of the problem), we obtain one model of the class. Each of them consists in finding the fluid pressure $P = P(t,x,z)$ and an auxiliary hydraulic head $\tilde{H} = \tilde{H}(t,x)$ such that:

Flow in the upper part of the aquifer. In this part, only the fast component of the flow is described. We choose a collection of $1D$-Richards equations parameterized by $x \in \Omega_x$:

$$\begin{cases} \phi \dfrac{\partial s(P)}{\partial t} + \dfrac{\partial}{\partial z}\big(u \cdot e_3\big) = 0, \qquad u = -K\big(P\big)\left(\dfrac{1}{\rho\, g}\dfrac{\partial P}{\partial z} + 1\right) e_3 & \text{in }]0,T[\times\Omega^+_{h_{\text{sat}}} \\ \alpha(P, u\cdot n) = 0 & \text{in }]0,T[\times\Gamma_{\text{soil}} \\ P\big(t,x,h_a(t,x)\big) = \rho\, g(\tilde{H} - h_{\text{sat}}) & \text{in }]0,T[\times\Omega_x \end{cases} \tag{1}$$

where u is the flow velocity, $s(P)$ the soil saturation, $K(P)$ soil conductivity, ρ the fluid density, g the gravity constant, e_3 the unitary vector in direction 3 and α a given function describing the boundary condition on the top of the aquifer.

Flow in the lower part of the aquifer. In the lower part of the aquifer, bellow the level $z = h_a(t,x)$, the vertical flow is assumed to be instantaneous. The corresponding hydraulic head $\tilde{H}$ is constant with respect to z. We have, for $\tilde{K}(\tilde{H})$ an averaged conductivity tensor,

$$\begin{cases} P(t,x,z) = \rho\, g\big(\tilde{H}(t,x) - z\big) & \text{for } (t,x,z) \in]0,T[\times\Omega^-_{h_{\rm sat}} \\ -\operatorname{div}_x\big(\tilde{K}(\tilde{H})\,\nabla_x\tilde{H}\big) = -u\big|_{\Gamma_{h_{\rm sat}}} \cdot e_3 & \text{for } (t,x) \in]0,T[\times\Omega_x \end{cases} \tag{2}$$

2. Some remarks and results about the models

We obtain a new class of model, parameterized by the interface $h_{\rm sat}$ (under the constraint $h_{\rm bot} \leq h_{\rm sat} < h_{\rm bot}$). Roughly speaking, this kind of model can be seen as the coupling of 1d-vertical Richard models with a 2d-horizontal flow under the classical Dupuit hypothesis (first equation of (2)). The same kind of models can be find in [1] and [3] in a situation of a water table remaining far from the soil level (and treated from a numerical point of view). The main difference here is that the model (1)-(2) admit exactly the same dominant behavior as the 3d-Richards one, in a large range of time scale when $\varepsilon \to 0$. Moreover this convergence hold independently of the choice of $h_{\rm sat}$ so that every model of the class approximate the 3d-Richards model. This makes possible to tune $h_{\rm sat}$ a priori in view to improve the approximation when ε is not vanishing.

In the other hand, it should be noted that the main interest of this model is related to its good description of the vertical flow between the ground level and the water table. This is crucial when studying the transport of chemical components in the aquifer, in particular since many chemical reactions are expected in the first meters of the subsoil, where oxygen is still very present.

3. Numerical simulations

For the numerical approximation of coupled problem (1)-(2), we use a time implicit scheme. Each new time step is reached by using Picard fixed-point iterations in which we solve alternatively the collection of the one-dimensional Richards problems (1) and the 2D problem (2). We present in figure 1 an experiment of water infiltration and overflowing in the case where Ω_x is an interval of $\mathbb{R}$.

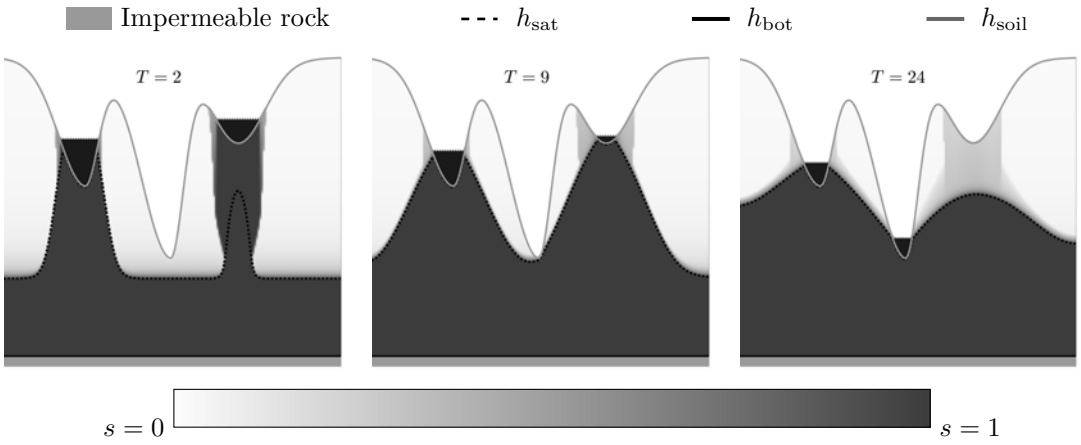

Figure 1: Evolution of saturation in a case of overland water which infiltrates the soil and reaches the water table.

References

[1] MB Abbott, JC Bathurst, JA Cunge, PE O'connell, and J Rasmussen. An introduction to the european hydrological system - systeme hydrologique europeen,"SHE", 2: Structure of a physically-based, distributed modelling system. *Journal of Hydrology*, 87(1):61–77, 1986.

[2] Christophe Bourel, Catherine Choquet, Carole Rosier, and Munkhgerel Tsegmid. Modeling of shallow aquifers in interaction with overland water. *Appl. Math. Model.*, 81:727–751, 2020.

[3] Mary F Pikul, Robert L Street, and Irwin Remson. A numerical model based on coupled one-dimensional Richards and Boussinesq equations. *Water Resources Research*, 10(2):295–302, 1974.

Modelling of heat conduction in granular porous media

A. Djibo Soumana[a], M. Poulleau[a], M.L. Zanota[b], B. Maschke[a], I. Pitault[a]

[a] *Univ. Lyon, UCBL Lyon1, CNRS, LAGEPP UMR 5007, 43 boulevard du 11 novembre 1918, F-69100 Villeurbanne, France*

[b] *Univ. Lyon, CNRS, CPE Lyon, UCBL, CP2M UMR 5128, 43 boulevard du 11 novembre 1918, F-69100 Villeurbanne, France*

Keywords: Packed-bed modelling, Port-Hamiltonian System, Graph, Image Processing

1. Introduction

This paper deals with the modelling of the heat transfer in packed bed reactors using their geometric and topological properties. The models used to simulate transport phenomena in granular fixed beds are generally of two types : the process engineering-type models that are either so-called pseudo-homogeneous or heterogeneous models and the Computational Fluid Dynamics (CFD) type which represent the porous medium as either homogeneous with uniform meshing or heterogeneous with complex meshing. Process engineering-type models give acceptable results if the reactor diameter (D) is about 15 times larger than the particle size (d) i.e. $D/d > 15$ [1] and if the chosen models and correlations are suited to the studied problem. But when the $D/d < 15$, like for instance fixed bed reactors used for methane steam reforming where very endothermic chemical reactions take place with high temperature conditions (approximately 800Â° C), these models cannot accurately simulate the heat transport. As for CFD-type models, they can be precise but require very significant computing resources and time [2].

In this paper, an alternative approach is considered, using graphs derived from tomography as an extension of [3]. Indeed, the packed bed two phases are represented by two dual graphs obtained using X-ray tomography or Discrete element method (DEM) combined with Image Processing using iMorph software. A third solid-fluid coupling graph is built representing the two-phase transfer. The balance equations are written and solved using a pseudo Port-Hamiltonian System (PHS) formulation. The work presented here is limited to the modelling of the heat diffusion in a bed of spherical particles containing stagnant fluid.

2. Methodology

Using iMorph software, the packed bed 3D image (see Figure 1(a)) is constructed and graphs of fluid and solid phases derived (see the solid graph in Figure 1(b) for instance). In the solid graph, nodes and edges are associated to respectively particles and contact surfaces at the interface of two neighboring particles, which can be either solid-solid contacts or solid-fluid-solid contacts as defined in [4]. For the fluid graph, constructed using the Plateau method, one associates nodes and edges to respectively fluid cells and interfaces of two neighboring fluid cells (see Figure 1(c) for illustration). Furthermore, some geometrical properties such as volumes and surfaces of solid and fluid phase elements, are extracted and associated with those of the graphs. The heat transfer in an α-phase (solid or fluid) is described using first order PDE system as :

$$\begin{pmatrix} \partial_t u^\alpha \\ F^\alpha \end{pmatrix} = \begin{pmatrix} 0 & -div \\ -grad & 0 \end{pmatrix} \begin{pmatrix} T^\alpha \\ \phi^\alpha \end{pmatrix} and \begin{pmatrix} e_\partial^\alpha \\ f_\partial^\alpha \end{pmatrix} = tr \begin{pmatrix} T^\alpha \\ \phi^\alpha \end{pmatrix} \tag{1}$$

Where u, T and ϕ are respectively the internal energy density, the temperature and the heat flux density. The differential operator in eq. 1 is skew-symmetric then can be considered as Hamiltonian. e_∂ and f_∂ are the port boundary variables and $tr()$ is the trace operator at the domain boundary. The state variables u and T are related through the equation $du = C_V dT$ with C_V the heat capacity in constant volume. The constitutive relations are defined as : $\phi = -\lambda F$ and $F = -gradT$, the thermodynamic

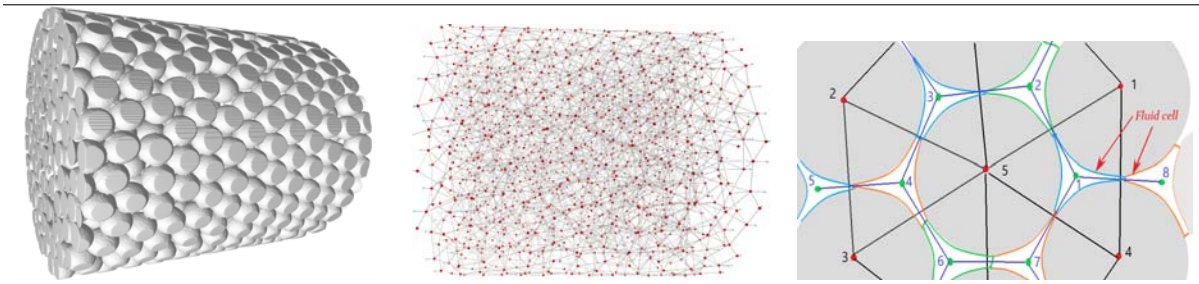

(a) (b) (c)

FIGURE 1 – (a)Packed bed X-ray CT image reconstruction (b)Solid graph (1777 solid nodes and 6208 fluid cells) (c) representation of 2D solid and fluid elements

driving force, with λ the actual heat conductivity of the phase.

After discretization of the eq. (1) for the two phases and their coupling via the discrete relationship $\phi_{ij}^{sf} = h_{ij} F_{ij}^{sf}$, representing the heat flux density between a solid element i and a fluid element j, one can derive a finite-dimensional pseudo-PHS for the packed bed filled with stagnant fluid as :

$$\begin{bmatrix} \partial_t \mathbf{U^s} \\ \partial_t \mathbf{U^f} \\ \mathbf{F^s} \\ \mathbf{F^f} \\ \mathbf{F^{sf}} \end{bmatrix} = \begin{bmatrix} 0 & 0 & -D_1^T & 0 & -M_s^T \\ 0 & 0 & 0 & -D_2^T & M_f^T \\ -D_1 & 0 & 0 & 0 & 0 \\ 0 & -D_2 & 0 & 0 & 0 \\ M_s & -M_f & 0 & 0 & 0 \end{bmatrix} \begin{bmatrix} \mathbf{T^s} \\ \mathbf{T^f} \\ \mathbf{\Phi^s} \\ \mathbf{\Phi^f} \\ \mathbf{\Phi^{sf}} \end{bmatrix} + \begin{bmatrix} 0 & 0 & -D_{1b}^T & 0 \\ 0 & 0 & 0 & -D_{2b}^T \\ -D_{1b} & 0 & 0 & 0 \\ 0 & -D_{2b} & 0 & 0 \end{bmatrix} \begin{bmatrix} \mathbf{T_b^s} \\ \mathbf{T_b^f} \\ \mathbf{\Phi_b^s} \\ \mathbf{\Phi_b^f} \end{bmatrix} \quad (2)$$

With subscripts s, f and b standing for solid , fluid and boundary respectively. $\mathbf{U^s}$, $\mathbf{U^f}$, $\mathbf{F^s}$, $\mathbf{F^f}$, $\mathbf{T^s}$, $\mathbf{T^f}$, $\mathbf{\Phi^s}$, $\mathbf{\Phi^f}$ and $\mathbf{\Phi^{sf}}$ are vectors collecting the discrete U_i^s, U_j^f, F_{ik}^s, F_{jl}^f, F_{ij}^{sf}, T_i^s, T_j^f, ϕ_{ik}^s, ϕ_{jl}^f and ϕ_{ij}^{sf}, determined by volume-averaging, respectively. D_1 and D_2, and their transposes D_1^T and D_2^T, represent solid and fluid incidence matrices obtained from dual graphs. The matrices M_s and M_f with their transposes M_s^T are M_f^T are two-phase interconnection matrices.

3. Conclusions & perspectives

We presented in this paper a new approach, for modelling heat diffusion in packed bed containing stagnant fluid, based on a pseudo Port Hamiltonian System formalism. The model was constructed taking into account the actual solid-fluid structure, i.e the topology and geometry. The future work will focus on thermal convection and particle type effect.

Références

[1] Schweich, Daniel, *Génie de la réaction chimique* Chap10, 610. Ed. Tec. & doc., place (2001).
[2] Dixon, Anthony G, Local transport and reaction rates in a fixed bed reactor tube : Endothermic steam methane reforming, *Chemical Engineering Science*, 168, 156–177 (2017).
[3] Louati H. et al., Network-Based Modeling of Transport Phenomena in Solid and Fluid Phases of Open-Cell Foams : Construction of Graphs, *Advanced Engineering Materials*, 22, 1901468 (2020).
[4] Fei W. et al.,Network analysis of heat transfer in sphere packings, *Powder Technology*, 362, 790–804s (2020).

Hybridizable interior penalty discontinuous Galerkin methods for degenerate advection-diffusion-reaction problems

G. Etangsale[a], M. Fahs[b], V. Fontaine[a], A.R. Isa-Abadi[c]

[a]*Department of Building and Environmental Sciences, University of La Réunion - South Campus, France.*
[b]*Université de Strasbourg, CNRS, ENGEES, LHYGES UMR 7517, F-67000 Strasbourg, France.*
[c]*Department of Water Engineering, Shahrekord University, Shahrekord, Iran.*

Keywords: Primal hybridizable discontinuous Galerkin, interior penalty methods, degenerate second-order elliptic problems, upwind and Scharfetter–Gummel schemes, numerical experiments

Abstract

Degenerate second-order elliptic equations are well-established models to describe a wide variety of phenomena in real-life applications, such as pure diffusion or advection problems and mixed problems combining the above mechanisms for a wide range of Péclet numbers [4]. A detrimental situation may arise in the context of locally evanescent diffusivity. Indeed, its mathematical nature is nonuniform over the entire domain, as it can be purely hyperbolic in a subregion and elliptic in the rest. Consequently, the state variable can be discontinuous at interfaces separating both subregions according to the wind flow sense. This critical situation is easily encountered in mass transport in fractured porous media and is thus quite delicate to solve numerically. During the past decades, different authors have analyzed this model problem, although mainly in the context of discontinuous Galerkin (DG) methods [3] (see e.g., [1] and the extensive references therein). However, DG methods are generally more expensive than most other numerical methods due to their high number of coupled degrees of freedom (DOFs) and large stencils. We here favored HDG formalisms considered as a new class of DG methods eligible for static condensation. An additional discrete variable is introduced corresponding to the trace approximation of the state variable on the mesh skeleton. Thus, the interior-based DOFs can be easily eliminated by solving a local problem at the element level so that only skeleton-based DOFs remain. In practice, HDG methods turn out to be more accurate than their DG counterparts in many situations, and they are thus more efficiently implementable and highly parallelizable. Despite all of these assets, the literature is relatively scarce concerning the resolution of degenerate elliptic equations by the class of HDG methods. Only Di Pietro et al. recently designed a primal discontinuous skeletal method based on the hybrid-high order (HHO) formalism for the diffusive part to address this kind of issue. Here, we focus instead on the class of interior penalty HDG methods denoted by H-IP and its three well-known variants, namely, the incomplete (H-IIP), symmetric (H-SIP), and nonsymmetric (H-NIP) schemes. Both diffusive and advective-reactive contributions are discretized separately. The stability is ensured by adding jump-penalty terms, which correspond to the discrepancy between interior- and interface-based DOFs, on the mesh skeleton. The stabilization penalty parameters are selected with respect to the nature of the local cellwise problem reducing to an upwinding-based scheme in the hyperbolic subregion and the Scharfetter–Gummel (SG) scheme elsewhere. Thus, the stated H-IP formalism can automatically treat the pure diffusion or advection-reaction processes or (mixed) advection-diffusion-reaction processes characterized by a diffusion- or advection-dominated regime, i.e., a wide range of Péclet numbers - including the delicate situation of local evanescent diffusion. A stability analysis is then investigated by checking favorable properties such as the consistency and discrete coercivity to ensure existence and uniqueness of the discrete solution. Numerical experiments are also presented to prove the following assertions, such as the high-order accuracy and robustness of the discretization method. *A complete description of the proposed H-IP method for solving degenerate elliptic problems is available at the* arXiv *repository [2] and downloaded at the following address*[1]

[1] `https://arxiv.org/pdf/2106.00226.pdf`

References

[1] Di Pietro D.A., Droniou J. and Ern A., A discontinuous-skeletal method for advection-diffusion-reaction on general meshes, *SIAM Journal on Numerical Analysis*, 53, 2135-2157 (2015).

[2] Etangsale G., Fahs M., Fontaine V. and Isa-Abadi A.R., Families of hybridizable interior penalty discontinuous Galerkin methods for degenerate advection-diffusion-reaction problems, *arXiv:2106.00226* [math.NA], June 2021.

[3] Houston P., Schwab C. and Süli E., Discontinuous hp-Finite Element Methods for Advection-Diffusion-Reaction Problems, *SIAM Journal on Numerical Analysis*, 39, 2133-2163 (2002).

[4] Oleĭnik, O. and Radkevič, E.V., *Second-Order Equations With Nonnegative Characteristic Form*, VII p. 259. Springer US, Boston (1973).

Development of quantitative detection methods for mass spectrometry of non-interfering and interfering gases such as mixtures of H_2, He, Ne, O_2, Ar, N_2, CO_2, CH_4, C_2H_6, C_3H_8, i-C_4H_{10}, n-C_4H_{10} and C_5H_{12}.

S. Keita[a,b,c], S. Noirez[b], G. Berthe[b], A. Vinsot[c], B. S. Kim[b], M. Mascle[b], M. Lundy[c], B. Garcia[b]

[a]*Sorbonne Université – ED n° 398 : Géosciences, Ressources Naturelles et Environnement (GRNE)*
[b]*IFP Energies nouvelles – 1 et 4 avenue de Bois-Préau, 92852 Rueil-Malmaison, France*
[c]*Andra, Centre de Meuse/Haute-Marne, F-55290 Bure, France*
[d]*IFP Energies nouvelles – Direction Scientifique, 1-4 Avenue de Bois-Préau 92852 Rueil-Malmaison, France*

Keywords: in situ gas monitoring, calibration method and tests, Underground Research Laboratory.

Introduction

Clay-rich rocks are under consideration in Europe to host long-lived radioactive waste geological repositories. Thus, the study of water-gas-rock interactions in clay underground has benefited in recent decades from the creation of underground research laboratories (URL) in this type of environment in Belgium and Switzerland as well as in France. These URL facilitate simultaneous access to two or even three phases (water, gas, rock) during in situ experiments. Andra's Meuse/Haute-Marne URL galleries (-490 meters depth) are ventilated with outdoor air from the surface. This air interacts with all the surfaces of the rock (Callovo-Oxfordian clay) it encounters and also with the laboratory building materials as concrete, steel…. It becomes enriched with water vapor coming from the rock and other gases present in a dissolved state in the rock pore water (like nitrogen, light alkanes and alkenes, carbon dioxide). On the other hand, oxygen from the air is consumed by reacting mainly with pyrites present in the rock [1].

In order to evaluate underground work chemical evolution over time, numerous gas composition analyses are performed in the URL. This presentation focuses on the analyzer's choices and the calibration methods to monitor the gases evolution in partly closed underground micro-tunnels.

Materials and methods

To track the composition of the gas contained in the underground works, IFPEN has developed a gas monitoring station called "Flair soil™" bringing together two analyzers: a mass spectrometer and an infrared laser spectroscope (Picarro®). Unlike infrared analyzer, mass spectrometer requires precise calibration. A quantitative method of online gas analysis has been developed using quadripolar mass spectrometry to measure the composition of a complex gas mixture. For a complex gas mixture, it is difficult to separate certain species due to spectral interference and fragmentation of the ions produced [2]. Alkanes, for example, have complex fragmentation models. This method belongs to the class of multivariate calibration [3]. In this work, the calibration is carried out using the individual gases of known concentrations in a nitrogen matrix and the ionic currents obtained from the measurement of each gas. To determine the interferences, we analyzed simple mixtures : 5000 ppm C_2H_6, 500 ppm C_3H_8, 500 ppm i-C_4H_{10}, 100% n-C_4H_{10}, 500 ppm C_5H_{12}, 1% Ar and 1% Ne, each gas is in a N_2 matrix except n-C_4H_{10} and complex mixtures : H_2, He, CO_2, CH_4, O_2, in N_2 matrix at different contents. In the simple mixture the nitrogen matrix represents more than 99% and in the complex mixture it (N_2) represents more than 79%.

Results

The calibration method we are developing is based on a mathematical approach. The matrix calculations link the Xi chemical species to the measured y_i ion currents. Thus, for every y_i ion current measured, we can write (Eq. 1):

$$y_i = \sum_j a_{ij} x_j \quad (1)$$

With a_{ij} the response coefficient of the chemical species j on the current yi, and Xj its concentration. This equation is written for each of the measured y_i currents, giving a system of linear equations of n*k dimensions (n measured ion currents and k chemical species considered). This system is described by the following matrix system (Eq. 2):

$$\begin{pmatrix} y_1 \\ \vdots \\ y_n \end{pmatrix} = \begin{pmatrix} a_{11} & \cdots & a_{ik} \\ \vdots & \ddots & \vdots \\ a_{nj} & \cdots & a_{nk} \end{pmatrix} \cdot \begin{pmatrix} X_1 \\ \vdots \\ X_k \end{pmatrix} \quad (2)$$

$$Y = A \cdot X \quad (3)$$

In this system (Eq. 3), Y represents the vector of measured y_i ion currents (size n), X represents the vector of relative concentration of chemical species considered x_i (size k), and A represents the matrix containing all the response coefficients (a_{ij}) of each chemical species j on each of the currents i (size n*k). The calibration is made using standard gases, for which the chemical composition is known. The measurement of the ion currents of an unknown gas mixture can then be used to calculate relative concentrations according to equation 4.

$$X = A^{-1} \cdot Y \quad (4)$$

The concentrations obtained (X_{cal}) by this method and the ones determined (X_{ac}) by the supplier (AirProducts) are represented in Table 1. Our results agree with those of the supplier for 6 out of 11 species; for the others tests are underway to improve them. The sum of the concentrations obtained is greater than 100%, this is due to the fact that nitrogen which constitutes the matrix, is overdetermined.

Table 1: Compositions of different gas mixtures used in the calibration and measurements results

Gaz	H_2 %mol	He %mol	CH_4 %mol	Ne %mol	N_2 %mol	C_2H_6 %mol	O_2 %mol	C_3H_8 %mol	Ar %mol	CO_2 %mol	C_5H_{12} %mol	iC_4H_{10} %mol	nC_4H_{10} %mol
X_{ac}	0.05	0.005	0.001	0.05	99.74	0.001	0	0.001	0.10	0.05	0.001	0.001	0
X_{cal}	0.07	0.005	0.001	0.07	101.59	0.001	0	0.003	0.12	0.05	0.001	0.001	0

Conclusion

A multivariate calibration method for the mass spectrometry of non-interfering and interfering gases, such as H_2, He, Ne, O_2, Ar, N_2, CO_2, CH_4, C_2H_6, C_3H_8, i-C_4H_{10}, n-C_4H_{10} and C_5H_{12}, was developed. This method allows a quantitative analysis of complex gas mixtures containing interference that contribute to the same mass-to-charge ratios (m/z).

References

[1] Vinsot, A., Lundy, M. and Linard, Y. (2017) O_2 Consumption and CO_2 Production at Callovian-oxfordian Rock Surfaces. Procedia Earth and Planetary Science 17, 562-565.

[2] Hoffmann ED, Stroobant V. Mass spectrometry principles and applications. 3rd ed. John Wiley & Sons Ltd.; 2007.

[3] Binninger, T., Pribyl, B., Pătru, A., Ruettimann, P., Bjelić, S. et Schmidt, T. J. (2018). Multivariate calibration method for mass spectrometry of interfering gases such as mixtures of CO, N_2 and CO_2. Journal of mass spectrometry : JMS, 53(12), 1214–1221. doi:10.1002/jms.4299.

On the use of ERT data for numerical modeling of seawater intrusion in fractured coastal aquifers

B. Koohbor[a], A. Gonzalez Quiros[b], M. Fahs[c], J. Deparis[a], J.-C. Comte[b]

[a] *Bureau de Recherches Géologiques et Minières (BRGM), France*
[b] *University of Aberdeen, School of Geosciences, UK*
[c] *CNRS, ENGEES, ITES UMR 7063, University of Strasbourg, Strasbourg, France*

Keywords: Electrical Resistivity Tomography (ERT); Fractured coastal aquifers; Seawater intrusion; Discrete fracture model; Uncertainty Analysis

Abstract

Coastal aquifers are the first source of freshwater for more than 40% of the world's population. These aquifers are currently in a critical situation in many parts of the world due to the contamination by seawater intrusion (SWI) which is exacerbated by aquifer over-pumping and climate changes. While the effect of aquifers heterogeneity on SWI has been widely discussed in the literature, SWI in fractured coastal aquifers (FCAs) has been less studied and related processes are still poorly understood. Yet, FCAs are found globally (e.g. France, USA, Greece, Italy, Ireland, UK and in the Mediterranean zone).

Variable density flow (VDF) models have become common tools that are widely used in SWI studies for multiple theoretical and practical purposes. In fractured aquifers, coupling the VDF and discrete fracture (DF) models appear as an appropriate way to consider the effect of fractures or faults on SWI. This coupling is more realistic than equivalent models that cannot reproduce preferential flow in fractures. However, DF models require detailed information about the fracture characteristics, which can be a challenging task in field applications.

Due to the resistivity contrast between salt and fresh water, Electrical resistivity tomography (ERT) is commonly used for characterizing SWI in coastal aquifers [1], and these geophysical data are widely used for aquifers characterization and modeling. However, the relevance of ERT data for modeling SWI in fractured coastal aquifers specifically is still not investigated. Recent works, in inland fractured aquifers, showed promising results on the use of ERT in identifying parameters of single continuum porous equivalent [2] or dual continuum models (e.g. see [3]). Few studies used ERT data for discrete fracture characterization [4]. The significance of ERT data in the parametrization of DF models is still poorly understood. This work aims at addressing these gaps by evaluating the efficacy of surface ERT data in the parameterization of a VDF-DF model for SWI in FCAs. Our goal is also to provide a methodology for reliable simulations of SWI in FCAs by integrating ERT profiles, a DF model and advanced uncertainty analysis.

Thus, we consider the case of Clashnessie Bay, NW Scotland. The study site is underlain by fractured Precambrian gneisses affected by a major regional fault zone. A cross- sectional ERT profile was carried orthogonal to the fault. ERT results revealed a ~100 m wide vertical zone of low resistivity coinciding with the fault zone, which indicates highly weathered/fractured rock. Either side of the fault zone was characterized by high resistivities, indicating poor bedrock weathering/fracturing. Resistivity data can be used to estimate the porosity within and outside the fault zone and associated uncertainties [5]. This will further help to build the DF model for SWI, but inherent uncertainties related to its hydrodynamic characteristics and topology of fractures can affect the model output. To handle these uncertainties, we perform a propagation uncertainty analysis that allows for identifying the most significant characteristics of fractures that can affect SWI predictions. The results of the uncertainty analysis can be used in performing new ERT surveys to accurately identify the most significant parameters.

References

[1] *De Franco, R., Biella, G., Tosi, L., Teatini, P., Lozej, A., Chiozzotto, B., ... & Gasparetto-Stori, G. (2009). Monitoring the saltwater intrusion by time lapse electrical resistivity tomography: The Chioggia test site (Venice Lagoon, Italy). Journal of Applied Geophysics, 69(3-4), 117-130.*

[2] *Comte, J.C. et al., , 2019, Catchment-scale heterogeneity of flow and storage properties in a weathered/fractured hard rock aquifer from resistivity and magnetic resonance surveys: implications for groundwater flow paths and the distribution of residence times. Geological Society, London, Special Publications, 479(1), pp.35-58.*

[3] *Sreeparvathy et al. 2019, Application of ERT, Saline Tracer and Numerical Studies to Delineate Preferential Paths in Fractured Granites, Groundwater. https://doi.org/10.1111/gwat.12663*

[4] *Robinson J. et aL. 2015, Challenges and opportunities for fractured rock imaging using 3D cross-borehole electrical resistivity, GEOPHYSICS, VOL. 80, NO. 2; 10.1190/GEO2014-0138.*

[5] *Mezquita G. et al. 2021, Quantification of groundwater storage heterogeneity in weathered/fractured basement rock aquifers using electrical resistivity tomography: Sensitivity and uncertainty associated with petrophysical modelling. Journal of Hydrology, 593, p.125637.*

Modeling coupled DNAPL migration and complex resistivity evolution in saturated porous media

Behshad Koohbor, Jacques Deparis, Hossein Davarzani, Philippe Leroy, Stéfan Colombano
Bureau de Recherches Géologiques et Minières (BRGM), Orléans, France

Keywords: Induced Polarization; Dense Non-Aqueous Phase Liquid (DNAPL); Two-Phase flow in porous media; COMSOL Multiphysics®; Complex resistivity

Abstract

Induced Polarization (IP) is the measurement of the response of electrical conductivity (or resistivity) to an applied range of frequency (usually between a few millihertz to a few tens of kilohertz). It can be applied as a non-intrusive method to investigate Dense Non-Aqueous Phase Liquid (DNAPL) contamination/remediation process. Multiphase flow in porous media can be coupled with the electrical current to simulate the process of DNAPL migration and deliver a broader view in space and time esp. when the results are supported by field measurements or laboratory experiments. In addition to previous works in the literature regarding the coupled simulations of two-phase flow and in-phase electrical resistivity, in this work, we aimed to perform coupled simulations of two-phase flow in porous media and sinusoidal electrical current (i.e. frequency ranging from 0.7Hz to 3000Hz) via the application of complex electrical resistivity.

The domain and the scenarios of the simulations (i.e. fill-up and pumping) are based on previously published laboratory experiments [1,2]. The simulations are developed in 3D and are performed in COMSOL Multiphysics®. The fluid flow equations are, first, discretized (i.e. by Finite Element Method) and solved using the pressure-saturation approach and by application of the Van Genuchten-Mualem constitutive relationships. Then, the saturation of water and the DNAPL is translated into in-phase and quadrature conductivities via the chosen petrophysical relationships [3,4] and then the system of partial differential equations governing the electrical current (i.e. Amper's law) is solved and the electrical potential is calculated in the domain for each time-step. The electrical potential, then, can be translated into complex resistance and then to complex resistivity. The results of the fluid flow and the phase transport are validated against the results of laboratory experiment measurement. Figure 1 shows selected results of the phase transport validation for the pumping scenario. The results of the complex resistivity measurements and simulations are validated and one of the electrical injection configurations for the fill-up scenario is selected and shown in Figure 2.

The used formulation and tool for simulation of the fluid flow (i.e. pressure-saturation in 3D) has been discussed briefly to give insights regarding the application of three-phase flow in future studies. The choice of petrophysical relationships for in-phase and quadrature conductivity are verified and are consistent with the experimental study, yet the exponents of the water in the petrophysical relationship were estimated to be lower than those reported previously by the experimental study [2]. The simulations and the experiments are in complete accordance with each other in the parts of the domain where the saturation of DNAPL is relatively low (esp. in the cone of depression in the pumping scenario). The simulations also predict the time of evolution of in-phase and quadrature resistivity (i.e. when DNAPL front passes the injection and potential electrodes) with satisfying accuracy. However, the points associated with high saturation of DNAPL (i.e. close to $S_n=1-S_{rw}$) show high errors between the results of in-phase resistivity calculated simulations and the previously reported experiments. Yet, this error is decreased when comparing the quadrature resistivities. The present study can be regarded as a preliminary study toward further applications of coupled IP-Multiphase flow for more accurate detection and monitoring of non-aqueous phase liquids. We suggest that our choice of tool/approach can be extended to larger-scale studies for further investigation.

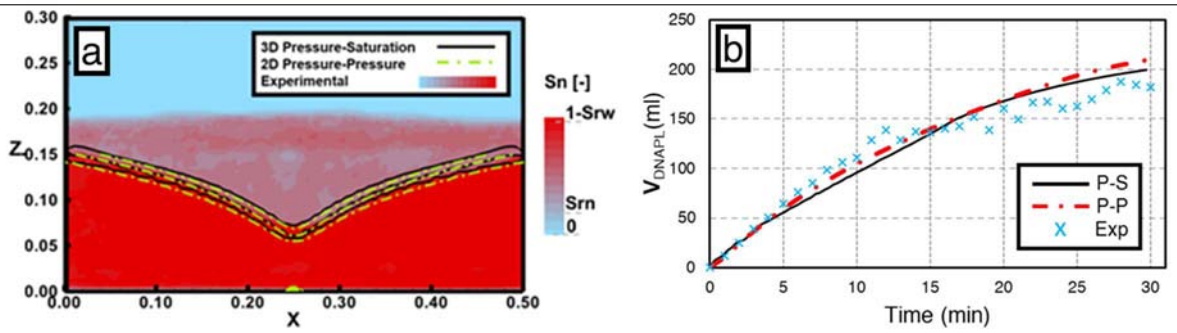

Figure 1. Simultaneous representation of experimental measurements and two simulation approaches for the 150 ml.min^{-1} flowrate for: (a) distribution of water and DNAPL at the end of pumping scenario and (b) temporal evolution of the retrieved DNAPL

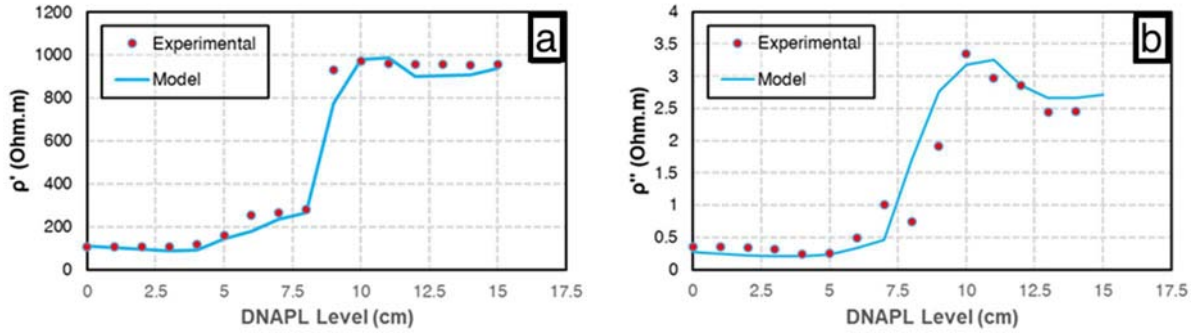

Figure 2. Simultaneous results of complex resistivity evolution through the fill-up scenario for an electrical injection/potential configuration at the bottom part of the domain: (a) in-phase resistivity and (b) quadrature resistivity

Reference

[1] *Colombano, S., Davarzani, H., van Hullebusch, E.D., Huguenot, D., Guyonnet, D., Deparis, J., Lion, F., Ignatiadis, I., 2021. Comparison of thermal and chemical enhanced recovery of DNAPL in saturated porous media: 2D tank pumping experiments and two-phase flow modelling. Science of The Total Environment 760, 143958.* https://doi.org/10.1016/j.scitotenv.2020.143958

[2] *Colombano, S., Davarzani, H., van Hullebusch, E.D., Huguenot, D., Guyonnet, D., Deparis, J., Lion, F., Ignatiadis, I., 2021a. Comparison of thermal and chemical enhanced recovery of DNAPL in saturated porous media: 2D tank pumping experiments and two-phase flow modelling. Science of The Total Environment 760, 143958.* https://doi.org/10.1016/j.scitotenv.2020.143958

[3] *Vinegar, H.J., Waxman, M.H., 1984. Induced polarization of shaly sands. GEOPHYSICS 49, 1267–1287.* https://doi.org/10.1190/1.1441755

[4] *Glover, P.W.J., 2010. A generalized Archie's law for n phases. GEOPHYSICS 75, E247–E265.* https://doi.org/10.1190/1.3509781

How high-stress elastic filaments control flows of viscoelastic fluids through porous media ?

O. Mokhtari[a,b], J.-C. Latché[c], R. de-Loubens[b], M. Quintard[b], Y. Davit[b]

[a] *Institut de Mécanique des Fluides de Toulouse (IMFT), France*
[b] *Total E&P, CSTJF de Pau, France*
[c] *Institut de Radioprotection et de Sûreté Nucléaire (IRSN), France*

Keywords: Viscoelastic fluid flows, Birefringent Strand, Flow channelisation

Abstract

The flow of dilute polymer solution in model porous media consisting of an array of cylinder is considered. Numerical [1] and experimental [2] studies show that such flows are subject to the intensification of preferential flow paths. These pathways tend to favour shear stress and thus increase viscous dissipation and decrease permeability.
We seek to study the mechanisms of reinforcement of these preferential flow paths which are crucial to the understanding of these flows. We consider here the Oldroyd-B model of dilute polymer solutions. The equations of the model are solved using a time prediction-correction scheme and MAC discretization in finite volume in space.
The flow around two cylinders in a channel is first studied. As experimentally observed in [3], preferential flows appear, depending on the gap between the cylinders. We show that the reinforcement mechanism of the preferential flow paths is linked to the appearance of elastic filaments which will interact with the flow. Like gates, they will guide the flow to areas where the velocity is initially high.
We then show how this mechanism works in the flow through an array of cylindres and study its impact on the flow and its macroscopic properties. This viewpoint allows us to better understand many interesting properties such as flow anisotropy or hysteresis. It also gives us clues to try to understand the origin of instabilities that lead to viscoelastic turbulence.

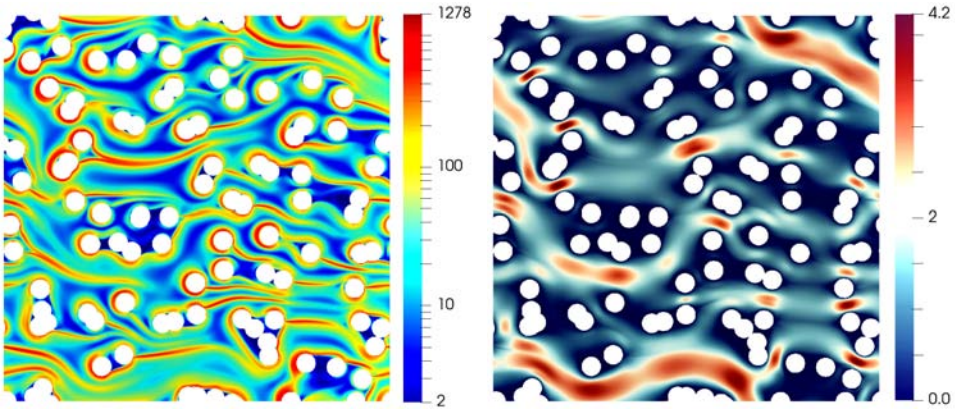

Viscoelastic fluid flow in a model porous media.
Elastic stress (left) and velocity magnitude (right).

References

[1] S. De, J.A.M. Kuipers, E.A.J.F. Peters, and J.T. Padding. Viscoelastic flow simulations in random porous media. *Journal of Non Newtonian Fluid Mechanics*, 248 :50-61, 2017.
[2] D.M. Walkama, N. Waisbord, and J.S. Guasto. Disorder suppresses chaos in viscoelastic flows. *Phys. Rev. Lett.*, 124 :164501, Apr 2020.
[3] C.C. Hopkins, S.J. Haward, and A.Q. Shen. Tristability in viscoelastic flow past side-by-side microcylinders. *Phys. Rev. Lett.*, 126 :054501, Feb 2021.

Dichloromethane degradation in porous media under dynamic hydrogeological conditions

Maria Prieto[a*], Raphaël Di Chiara[a], Benjamin Belfort[a], François Lehman[a], Jérémy Masbou[a], Carmen Lázaro-Sanchez[b], Emilie Muller[b], Stéphane Vuilleumier[b], Sylvain Weill[a], Gwenaël Imfeld[a]

[a] *University of Strasbourg, CNRS/EOST, ITES UMR 7063, Institut Terre et Environnement Strasbourg (ITES), France*
[b] *University of Strasbourg, CNRS, GMGM UMR 7156, Génétique Moléculaire, Génomique, Microbiologie, Strasbourg, France*

Keywords: Reactive transport model, dichloromethane, biodegradation, isotope fractionation, saturated zone

Reactive transport in porous media involves a complex interplay of multiple processes relative to flow of water and gases, transport of elements, chemical reactions and microbial activities. At surface-groundwater interfaces, the role of the capillary fringe is of particular interest as water table variations influence the transfer of gases (e.g., O_2), the evolution of redox conditions and the adaptation of bacterial populations and communities controlling biodegradation pathways of halogenated contaminants, such as dichloromethane (DCM). DCM is a toxic and volatile halogenated compound frequently detected in multi-contaminated aquifers. Mechanisms of bacterial degradation of DCM under both aerobic and anaerobic conditions have been described [1, 2, 3, 4, 5, 6]. However, little is known about the relationships between the hydrogeochemical variations caused by water table fluctuations, and their effects on the diversity and distribution of bacterial communities and degradation pathways in aquifers. Here, two laboratory aquifers fed with contaminated groundwater from the industrial site Thermeroil (France) were set up to collect groundwater samples at high-resolution across the flow path and to examine the reactive transport of DCM under steady and dynamic hydrogeological conditions. Hydrochemical, microbial and isotopic composition (i.e., $\delta^{13}C$ and $\delta^{37}Cl$) of DCM was examined to determine mass removal and degradation pathways. For the latter, dual-element isotope analysis allows the comparison of stable isotope ratios of two elements in a dual plot, and the slope (i.e., $\Lambda^{C/Cl} = \Delta\delta^{13}C/\Delta\delta^{37}Cl$) provides a quantitative parameter of contaminant transformation pathways [7, 8].

Under both conditions, O_2-depleted concentrations (<0.9 mg/L) in the saturated zone and increasing Fe^{2+} concentrations at lower depths of the laboratory aquifers suggested iron-reducing conditions. Although mass transfer of O_2 increased during water table fluctuations, rapid equilibrium was observed after each imbibition period. Pronounced carbon isotope fractionation of DCM was associated with larger mass removal of DCM under transient conditions (B>90%, $\Delta\delta^{13}C$ = 60‰) than under steady state (B = 42%, $\Delta\delta^{13}C$ = 12‰). $\Lambda^{C/Cl}$ values are independent of complicating masking effects, and thus reflect reaction mechanisms. Dual C-Cl isotope plots suggested distinct DCM degradation pathways under steady and transient conditions with $\Lambda^{C/Cl}$ values of 1.92 ± 0.30 and 3.58 ± 0.42, respectively. The RTM model CubicM was further developed to include dual-element CSIA (i.e., $\delta^{13}C$ and $\delta^{37}Cl$) and biological processes, such as growth, decay, attachment, detachment or dormancy, and relate changes in redox conditions with DCM degrading populations. The two-phase flow model (i.e., water and gas) accounts for volatilization and associated transport processes of DCM. Four distinct microbial populations potentially involved in distinct DCM degradation pathways are implemented following Michaelis-Menten kinetics. Each DCM degradation pathway is modelled according to pathway-specific reaction rates and isotope fractionation [9]. Furthermore, DOC is considered as a carbon source for non-DCM degraders and serves as supplier of CO_2, for DCM fermentative pathways. Simulations under steady-state conditions shows that (i) DCM volatilization is restricted across the capillary fringe, (ii) DCM can be degraded via four distinct competing pathways, and (iii) bacterial parameters such as the maintenance factor, defined as the energy consumed for functions other than the production of new cell material [10], may play an important role during early stages of bacterial adaptations. Transient conditions are currently simulated to improve our understanding of DCM natural attenuation at contaminated sites under dynamic conditions.

[*] Corresponding author: prietoespinoza@unistra.fr

References

[1] Kleindienst S, Chourey K, Chen G, Murdoch RW, Higgins SA, Iyer R, Campagna SR, Mack EE, Seger ES, Hettich RL, Löffler FE. (2019). Proteogenomics reveals novel reductive dehalogenases and methyltransferases expressed during anaerobic dichloromethane metabolism. Applied Environmental Microbiology, 85:e02768-18.

[2] Mägli, A., Messmer, M., & Leisinger, T. (1998). Metabolism of dichloromethane by the strict anaerobe *Dehalobacterium formicoaceticum*. Applied and Environmental Microbiology, 646-650.

[3] Nikolausz, M., Nijenhuls, I., Ziller, K., Richnow, H.-H., & Kästner, M. (2006). Stable carbon isotope fractionation during degradation of dichloromethane by methylotrophic bacteria. Environmental Microbiology, 8, 156-164

[4] Torgonskaya, M., Zyakun, A., Trotsenko, Y., Laurinavichius, K., Kümmel, S., Vuilleumier, S., & Richnow, H. (2019). Individual stages of bacterial dichloromethane degradation mapped by carbon and chlorine stable isotope analysis. Environmental Sciences, 147-160

[5] Trueba-Santiso, A., Parladé, E., Rosell, M., Lliros, M., Hatijah Mortan, S., Martinez-Alonso, M., Gaju, N, Martín-González, L., Vicent, T., Marco-Urrea, E. (2017). Molecular and carbon isotopic characterization of an anaerobic stable enrichment culture containing *Dehalobacterium* sp. during dichloromethane fermentation. Science of the Total Environment, Volumes 581-582, 640-648

[6] Vuilleumier, S., & Leisinger, T. (1996). Protein engineering studies of dichloromethane dehalogenase/glutathione S-transferase from *Methylophilus* sp. strain DMll Serl2 but not Tyr6 is required for enzyme activity. Eur. J. Biochem., 410-417

[7] Elsner, M. (2010). Stable isotope fractionation to investigate natural transformation mechanisms of organic contaminants: Principles, prospects and limitations. Journal of Environmental Monitoring, 12(11), 2005–2031.

[8] Ojeda, A. S., Phillips, E., & Sherwood Lollar, B. (2020). Multi-element (C, H, Cl, Br) stable isotope fractionation as a tool to investigate transformation processes for halogenated hydrocarbons. Environmental Science: Processes & Impacts, 22,567-582.

[9] Jin, B., Nijenhuis, I. & Rolle, M. (2018) Simulation of dual carbon–bromine stable isotope fractionation during 1,2-dibromoethane degradation, Isotopes in Environmental and Health Studies, 54, 418-434

[10] van Bodegom P. (2007). Microbial maintenance: a critical review on its quantification. Microbial ecology, 53, 513–523.

Numerical simulation of coupled two-phase flows and geochemical reactions in porous media: contribution to a new CO_2 benchmark

E. Ahusborde[a], B. Amaziane[a], M. Kern[b]

[a] *Universite de Pau et des Pays de l'Adour, E2S UPPA, CNRS, LMAP, Pau, France.*
[b] *INRIA Paris, France*

Keywords: Multiphase flow, Reactive transport, Porous media, Fully implicit scheme, Finite volume, DuMu^X, HPC, DSA

1. Introduction

Reactive multiphase flows in porous media play a significant role in many applications related to subsurface environmental and energy issues. For instance, we can mention non exhaustively long-term safety assessment for CO_2 storage and nuclear waste repositories, petroleum engineering, hydrogeology or geothermal energy production [1]. Such flows are governed by a set of highly nonlinear system of degenerate partial differential equations (PDEs) that describes a multiphase compositional flow, coupled with algebraic and/or ordinary differential equations (related to geochemistry), requiring special numerical treatment. Numerical simulation of large-scale reactive multiphase flows in complex porous media remains one of the outstanding challenges in the field of reservoir engineering. One of the reasons for this complexity is the highly nonlinear nature of the coupled equations that govern the system. For decades, many researchers have explored alternative forms of the governing equations, and have sought specialized numerical algorithms so as to improve the computational performance of a simulator. Here, we consider a Direct Substitution Approach (DSA) that incorporates the mass action laws directly in the mass conservation laws [2]. In this talk, we present a parallel, fully coupled, fully implicit, finite volume scheme for modeling isothermal reactive multiphase flow based on the DSA formulation mentioned above. The method has been implemented in the DuMu^X platform [3], using High Performance Computing, and has been validated by numerous 1D, 2D and 3D test cases including a recent benchmark. Several numerical tests will be presented.

2. Mathematical model and numerical scheme

We consider a two–phase reactive flow process in a porous medium. Chemical reactions can involve solutes, sorbed species and mineral precipitation or dissolution. The problem is modeled by a mass conservation law for each component in each phase, Darcy's law, a capillary pressure law, equations of state and solubility laws. Geochemical reactions are modeled through their reaction rates. These reaction rates depend on the reaction type, they are given as nonlinear functions of concentrations in the case of kinetic reactions and are unknowns for the equilibrium reactions. Equilibrium rates are usually eliminated through relevant transformations and the system is then closed by mass action laws, which are algebraic equations relating species activities.

A fully coupled, fully implicit, approach using a DSA formulation as mentioned in the introduction will be examined here to tackle this strongly nonlinear system. An implicit Euler scheme is used for time discretization. The spatial discretization is performed by a cell-centered finite volume method combining an upwind scheme for the convective terms and a two-point flux approximation for the diffusive terms. Our strategy has been implemented in DuMu^X [3]. The nonlinear system are solved using an appropriate Newton's method with variable time stepping. The control of the time-step is based on the number of iterations required by Newton's method to achieve convergence for the previous time step. The linear systems at each Newton iteration are solved by solvers provided by DUNE [4](Bi-conjugate Gradient Stabilized (BiCG-STAB) with AMG preconditioner).

3. Numerical results

Our numerical strategy has been validated on numerous 1D, 2D and 3D test cases. Here we show an example proposed in [5] that models mineral trapping by considering a chemical system with three equilibrium precipitation-dissolution reactions. The given configuration generates a precipitation/dissolution front. Figure 1 displays the profiles for gas saturation and concentrations after 20 days, using the DSA strategy [2]. They present a very good match with those obtained in [5].

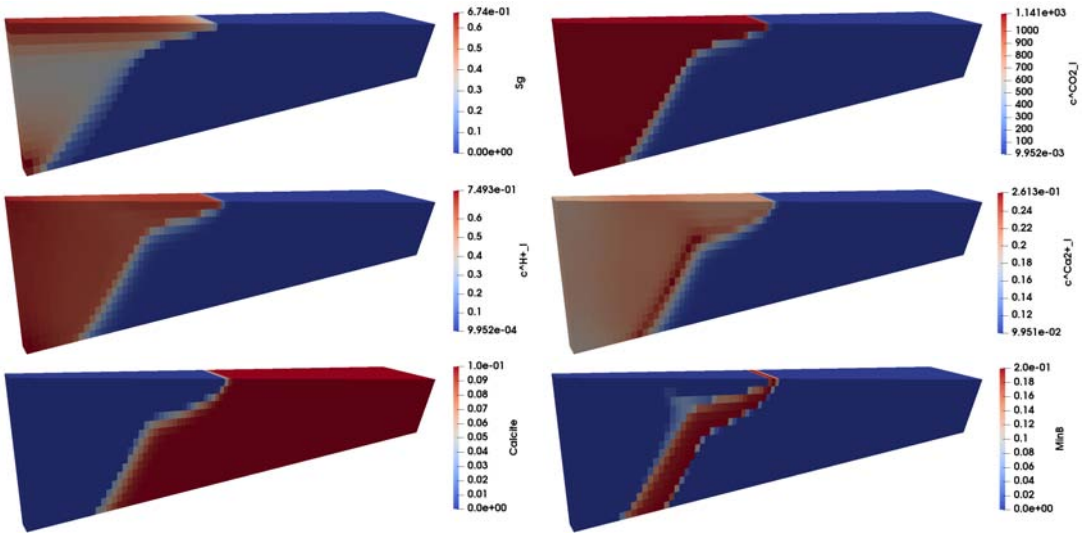

Figure 1: Profiles for gas saturation and concentrations after 20 days for test case presented in [5].

We will also present results from a recently proposed benchmark that models scenarios of CO_2 geological storage into a deep saline aquifer. Our results will be compared with those obtained by other participants.

4. Acknowledgements

This research has been partly supported by the Carnot Institute ISIFoR project (Institute for the sustainable engineering of fossil resources) and New Aquitaine Region. This project has received funding from the European Union's Horizon 2020 research and innovation programme under grant agreement n^o 847593. Their support is gratefully acknowledged. We also thank the CINES (National Computing Center for Higher Education) to give us access to their computing resources facility. This work was granted access to the HPC resources of CINES under the allocation A0080610019 made by GENCI. Computer time for a part of this study was also provided by the computing facilities MCIA (Mésocentre de Calcul Intensif Aquitain) of the Université de Bordeaux and of the Université de Pau et des Pays de l'Adour.

References

[1] Y. Xiao (Editor), F. Whitaker (Editor), T. Xu (Editor) and C. Steefel (Consulting Editor), *Reactive Transport Modeling: Applications in Subsurface Energy and Environmental Problems*. John Wiley & Sons Ltd, (2018).

[2] E. Ahusborde, B. Amaziane, M. Id Moulay, High Performance Computing of 3D reactive multiphase flow in porous media: application to geological storage of CO_2, *Submitted to Computational Geosciences*, (2020).

[3] T. Koch *et al*, DuMu^X 3 - an open-source simulator for solving flow and transport problems in porous media with a focus on model coupling, *Computers & Mathematics with Applications*, 81, 423-443 (2021).

[4] P. Bastian, M. Blatt, A. Dedner, N.A. Dreier, C. Engwer, R. Fritze, C. Gräser, D. Kempf, R. Klöfkorn, M. Ohlberger, O. Sander, The DUNE framework: Basic concepts and recent developments, *Computers & Mathematics with Applications*, 81, 75-12 (2021).

[5] F. Brunner, P. Knabner, A global implicit solver for miscible reactive multiphase multicomponent flow in porous media, *Computational Geosciences*, 23, 127-148 (2019).

Equivalent hydraulic conductivity, connectivity and percolation in 2D and 3D random binary media.

Iván Colecchio[a,c], Alejandro D. Otero[b,d], Benoît Noetinger[e,], Alejandro Boschan[a,c]

[a] *Grupo de Medios Porosos, Facultad de Ingeniería, Universidad de Buenos Aires, Paseo Colón 850, Buenos Aires, Argentina*
[b] *Departamento de Energía, Facultad de Ingeniería, Universidad de Buenos Aires, Paseo Colón 850, Buenos Aires*
[c] *CONICET, Buenos Aires, Argentina*
[d] *Centro de Simulación Computacional, CSC - CONICET, Godoy Cruz 2390, Buenos Aires, Argentina*
[e] *IFP Energies Nouvelles 1 & 4, avenue de Bois-Préau, 92852 Rueil-Malmaison Cedex - France*

Keywords: percolation, up-scaling, binary media, stochastic

1. Introduction

Achieving a precise description of a representative equivalent hydraulic conductivity (K_{eq}) of heterogeneous media is of great interest in several subsurface related disciplines [1, 2, 3]. The equivalent hydraulic conductivity (K_{eq}) relates the spatial averages of flux and head gradient in a block of heterogeneous media. In this article, we study the influence of connectivity on K_{eq} of media samples composed of a high conductivity (k^+) and a low conductivity (k^-) facies. A stochastic approach is applied to study how connectivity affects the probability distribution of K_{eq} in binary media. Binary media have a proportion p of a high conductivity facies (k^+) and a proportion (1-p) of a low conductivity facies (k^-). Multi-gaussian samples of spatially uncorrelated and correlated media are generated, using an exponential covariance function, with different integral scales (I_c). The binary media samples are obtained by truncation of the multi-gaussian ones. The k^+ facies of the correlated samples are given high, intermediate or low connectivity structures by operating on the truncation scheme. Figure 1 illustrates various 2D and 3D binary media. Using several realizations, setting $k^+ = 100$ and $k^- = 0.01$ and using the so-called permeameter method [2, 3], sets of K_{eq} were computed that depend on input parameters.

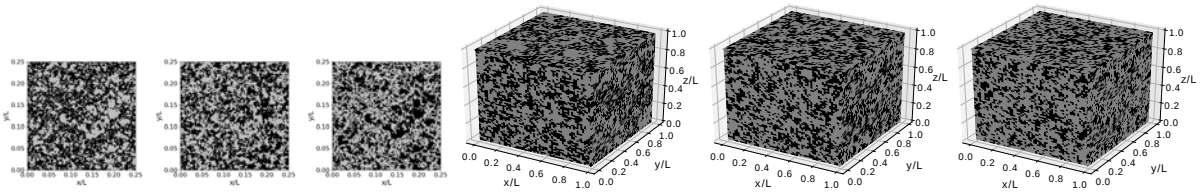

Figure 1: Maps of $k(\mathbf{r})$ for the binary samples used in the present study. (Black): k^+, (gray): k^-. (left): 2D binary samples (only a part of them is shown for clarity), with $p = 0.5$ and $l_c = 3\Delta$. (Right): 3D binary samples, with $p = 0.4$ and $l_c = 2\Delta$. (Left): high; (center): intermediate; and (right): low connectivity structure types.

2. Results of a Monte Carlo study for K_{eq} distributions

A cluster identification function is applied to compute the critical value of p for which percolation of the k^+ facies occurs (p_{av}), for each connectivity structure type and I_c. The relationship between p_{av} and I_c follows a linear trend for both 2D and 3D. The results show that the mean of K_{eq} of correlated media is always greater than that of the uncorrelated media in 3D, but not in 2D. The distribution of K_{eq} values approaches a lognormal distribution in all cases, as illustrated in figure 2. The corresponding mean ($\langle K_{eq} \rangle$) and variance ($\sigma^2_{\log(K_{eq})}$) were studied too.

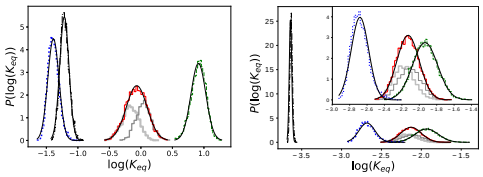

Figure 2: Distributions $P(\log(K_{eq}))$. (Left): 2D at $p = 0.566$ and $l_c = 2\Delta$. (Right): 3D at $p = 0.247$ and $l_c = 1.5\Delta$. For both: (): $l_c = 0.001\Delta$ (no structure). (): Low connectivity structure type. (): High connectivity structure type. The values of p are chosen so that, for the case of the intermediate connectivity structure type (), half of the realizations percolate ($\langle N_p \rangle = 0.5$) while the other half do notdon't. Their distributions corresponding to each half are depicted in dark and light gray lines respectively. (): Fits by a gaussian function. Inset: DetailZoom of the distributions for 2D media with low, high and intermediate connectivity structure types. As a reference, when $p = 0$ or $p = 1$, the media are homogeneous and $k(\mathbf{r}) = k^-$ or $k(\mathbf{r}) = k^+$ respectively. [inline]This caption was modified but not highlighted

The probability distribution of K_{eq} values, and the critical value of p for which percolation occurs (p_{av}), are studied as a function of these connectivity parameters. In 3D, when there is a connectivity structure, K_{eq} is always greater (and p_{av} smaller) than when there is not ($l_c \to 0$). The same behavior is observed in 2D, except that, for media samples with a low connectivity structure (i.e. when the k^+ facies is disconnected), K_{eq} is smaller (and p_{av} greater) than when there is no structure. The existence of a connectivity structure always leads to a greater K_{eq} in 3D, but not in 2D. The mean $\langle K_{eq} \rangle$ and the variance $\sigma^2_{\log(K_{eq})}$ show a collapse if expressed in terms of $p - p_{av}$ (for $\sigma^2_{\log(K_{eq})}$, notably, even if 2D and 3D data are plotted together). This indicates that any influence of the connectivity parameters on K_{eq} is well accounted for by a shift in the percolation threshold p_{av}.

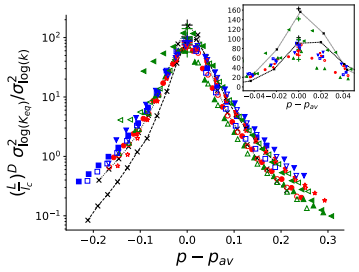

Figure 3: Normalized variance of $\log(K_{eq})$ (scaled by $(L/l_c)^D$) as a function of $(p - p_{av})$. (Empty markers): $l_c = 2\Delta$ in 2D and $l_c = 1.5\Delta$ in 3D. (Solid markers): $l_c = 3\Delta$ in 2D and $l_c = 2\Delta$ in 3D. ($\triangle$: 2D / $\triangleleft$: 3D): High; connectivity structure type. (: 2D / : 3D): Intermediate connectivity structure type. (: 2D / $\triangledown$: 3D): Low connectivity structure type. (: 2D /: 3D): $l_c = 0.001\Delta$ (no structure). (): Results for $p = p_{av}$. (Inset): DetailZoom of the percolation region in linear scale.

3. Conclusions

The main outcome of the present study is that the percolation threshold p_{av} contains the essential information over the connectivity of the k+ facies for a wide range of connectivity scenarios both in 2D and 3D. This is, the mean and variance curves of K_{eq})q collapse if expressed in terms of p-p_{av}, as illustrated in figure 3. For the variance, notably, this is so even if 2D and 3D results are plotted together.

References

[1] Hunt, A.G., Sahimi, M., Flow, transport, and reaction in porous media:Percolation scaling, critical-path analysis, and effective medium approximation. *Reviews of Geophysics* 55, 993â1078. doi:10.1002/2017RG000558 (2017).

[2] Boschan, A., Noetinger, B., Scale dependence of effective hydraulic con-ductivity distributions in 3D heterogeneous media: A numerical study, *Transport in Porous Media*, 94, 101â121. doi:10.1007/s11242-012-9991 (2012).

[3] Colecchio, I., Boschan, A., Otero, A.D., Noetinger, B., On the multiscale characterization of effective hydraulic conductivity in random heterogeneous media: A historical survey and some new perspectives, *Advances in Water Resources*, 140, 103594. doi:10.1016/j.advwatres.(2020).

Parameters identification in porous media

Application of deep neural networks in predicting natural convection on two-dimensional porous media

Mohammad Reza Hajizadeh Javaran[1], Amadou-oury Bah[2], Mohammad Mahdi Rajabi[1], Gabriel Frey[3], Florence Le Ber[3], Marwan Fahs[2,*]

[1]*Civil and Environmental Engineering Faculty, Tarbiat Modares University, PO Box 14115-397, Tehran, Iran.*

[2]*Université de Strasbourg, CNRS, ENGEES, ITES UMR 7063, 67000 Strasbourg, France.*

[3]*Université de Strasbourg, CNRS, ENGEES, ICube UMR 7357, 67000, Strasbourg, France*

E-mail: fahs@unistra.fr

Keywords: deep neural network, natural convection, convolutional neural network

1 Introduction

Natural convection is an important concept in porous media problems [4]. It is encountered in several applications such as in heat storage in aquifers, CO_2 sequestration in geological formations, geothermal energy extraction and geological deposition of nuclear waste. Physics-based numerical models are commonly used for simulating natural convection in porous media. Despite the effectiveness of these models in most cases, they encounter some important challenges. One key challenge is the computational time cost, which is more noticeable at large time and space scales, especially in repetitive runs. In recent years, several meta-models, such as polynomial chaos expansions and feed-forward neural networks, have been proposed in order to reduce the simulation time of natural convection models. These meta-models have demonstrated acceptable performance in low-dimensional domains, but they do not scale well to high-dimensional problems [1]. To overcome this challenge, we propose the use of a convolutional neural network (CNN) architecture [2]. We apply the proposed CNN in the context of '*image-to-image'* regression to: (a) estimate the entire heat distribution resulting from a specified permeability, and (b) estimate the permeability from a heat map.

2 Methodology

We apply the proposed CNN to model the hypothetical problem of a porous square enclosure filled with a saturated porous medium. Using a numerical modeling tool, the heat maps resulting from a number of constant, randomly selected Rayleigh numbers are generated for steady-state conditions. Rayleigh number is a parameter controlling the heat transfer processes, which is proportional to the permeability. The generated dataset of Rayleigh-temperature distribution images is employed to train a CNN architecture developed after a series of trials and errors. All images are in square shape of 32 × 32, and pixel values of images are normalized between 0 and 1 in the preprocessing step of neural network training. After data preparation, we trained the model with a maximum number of 2,000 samples, where 50% are used for training, 30% for validation and 20% for testing. A similar methodology has also been employed to develop a model that acts as an *optimizer* to estimate the Rayleigh number from the heat distribution. The CNNs models have been developed using Keras and Tensorflow python machine learning libraries

3 Results and discussion

We trained two CNNs, one as a meta-model and the other as an optimizer. Different numbers of training input-output images (including 100, 500, 1000, and 2000) generated from the numerical model are employed to evaluate the performance of proposed networks. Two evaluation criteria are used to assess the performance of the developed CNN modes: (1) the root mean squared error (RMSE), which shows the error between predicted and actual samples [3] and (2) the coefficient of determination (R^2-score), a number that shows a good prediction as it gets closer to 1 [5]. As an example of the results, the performance of CNN used as the meta-model is visualized for a specific value of the Rayleigh number in Figure 1. In this figure, we compare the CNN's predicted heat map with numerical modeling result, which shows a prediction with a very low error. The spatial distribution of the error, that is, the absolute value of the difference between CNN and numerical model predictions of temperature, are calculated pixel by pixel. In the meta-model case, we can see that in the middle of the domain, errors are more prominent. The total RMSE and R^2-score for all predicted cases is 0.0102 and 0.999, respectively.

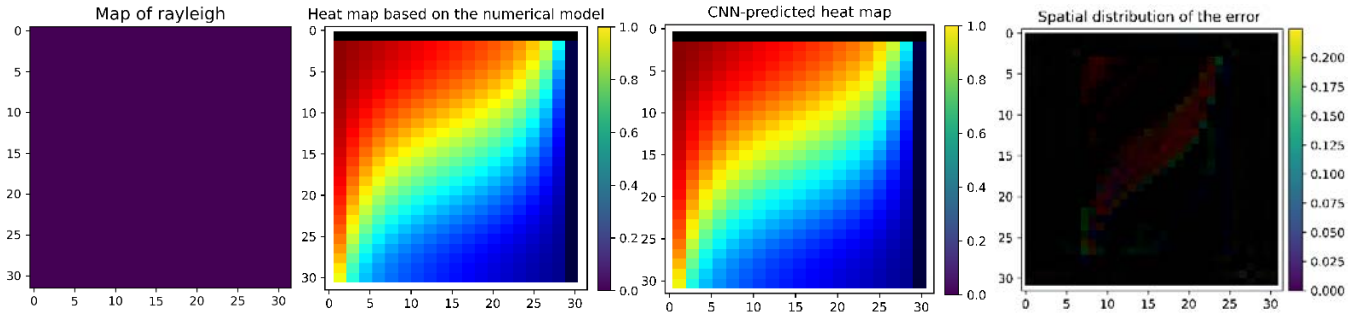

Figure 1. Comparison of the numerical model and CNN prediction for a meta-model.

4 References

[1] Fajraoui, N., Fahs, M., Younes, A., & Sudret, B. (2017). Analyzing natural convection in porous enclosure with polynomial chaos expansions: Effect of thermal dispersion, anisotropic permeability and heterogeneity. *International Journal of Heat and Mass Transfer*, *115*, 205-224.

[2] Ji, X., Yan, Q., Huang, D., Wu, B., Xu, X., Zhang, A., ... & Wu, M. (2021). Filtered selective search and evenly distributed convolutional neural networks for casting defects recognition. Journal of Materials Processing Technology, 292, 117064.

[3] Kumar, D., Roshni, T., Singh, A., Jha, M. K., & Samui, P. (2020). Predicting groundwater depth fluctuations using deep learning, extreme learning machine and Gaussian process: a comparative study. *Earth Science Informatics*, *13*(4), 1237-1250.

[4] Nield, D. A., & Bejan, A. (2017). Convection in Porous Media. Cham: *Springer International Publishing*. https://doi.org/10.1007/978-3-319-49562-0

[5] Zhu, Y., Zabaras, N., Koutsourelakis, P. S., & Perdikaris, P. (2019). Physics-constrained deep learning for high-dimensional surrogate modeling and uncertainty quantification without labeled data. *Journal of Computational Physics*, *394*, 56-81.

Coupled processes in porous media

Development of the integrated hydrological model NIHM: Implementation of transport processes

M. Chaguer[a], S. Weill[a], ¨P. Ackerer[a], ¨F. Delay[a]

[a]*Université de Strasbourg, CNRS, ENGEES, ITES UMR 7063, F-67000 Strasbourg, France*

Keywords: subsurface solute transport, model reduction, low-dimensional model, advection-dispersion equation, transport scheme

Abstract

Solute transport models based on the resolution of the 3-D Advection-Dispersion-Reaction (ADR) are frequently burdened with several numerical problems, in addition to the high computational cost. A model reduction approach that couples surface and subsurface flow in watersheds was newly established in the form of the hydrological model NIHM (Normally Integrated Hydrological Model). In this paper, we introduce a numerical technique to implement a non-intrusive subsurface transport scheme into the low-dimensional model NIHM and reduce the dimensionality of the subsurface solute transport problem. The model NIHM was previously evaluated and applied to actual hydrosystems, without addressing mass transfers. The low-dimensionality in the subsurface compartment results from an integration along the local direction normal to the bedrock of the aquifer. That being said, the model reduction could reduce the precision of velocity fields estimations required for mass transfer problems. The accuracy and computational efficiency of the proposed model have been thoroughly examined through applications to various synthetic test cases, under different hydrodynamic conditions to assess the influence of the reduction of dimensionality on solute transport simulations. The findings of this study prove that the established reduction method could be suitable for predicting subsurface solute transport behaviors in porous domains, while providing an important gain in computation time, which might be appealing for actual groundwater quality management plans.

Laboratory controlled NaCl salt crusts

G. Licsandru[a,b], C.Noiriel[b], S. Geoffroy[c], A. Abou Chakra[c], P.Duru[a], M. Prat[a]
[a]*IMFT (Institut de Mécanique des Fluides de Toulouse), Université de Toulouse, CNRS – Toulouse, France*
[b]*GET (Géosciences environnement Toulouse) Observatoire Midi Pyrénées, Université de Toulouse, CNRS, IRD, France*
[c]*LMDC (Laboratoire Matériaux et Durabilité des Constructions), Université de Toulouse, INSAT, UPS, France*

Keywords: Evaporation; saline solution; crystallization; salt crust

Abstract

Drying of saline solutions in porous media leads to several phenomena that are still largely open problems. To name only a few, one can mention the detrimental impact of salt crust on evaporation, the crust blistering and doming phenomena [1], and the formation of regular patterns. In order to provide a better understanding of these phenomena, we have developed a series of laboratory experiments both in 2D and 3D where such phenomena are reproduced and analyzed by a combination of optical visualization and X-Ray Micro-Tomography techniques. Modelling and numerical simulations are also developed in conjunction with the experiments as an additional tool to support the analysis and interpretation.

As an illustration, Fig.1 shows the crust obtained in a 3D setup and observed by X-Ray Micro-Tomography. As shown, the crust, is actually a multilayer layer crust with well-defined air gaps. This is also a clear illustration of crust blistering. As proposed in [2] the formation of the air gap and the associated upper crust detachment process can be attributed to a dissolution-precipitation phenomenon. In the presentation, we will discuss such a dissolution-precipitation process and also an overview of the insights gained on the afore-mentioned phenomena with the aid of controlled crust experiments.

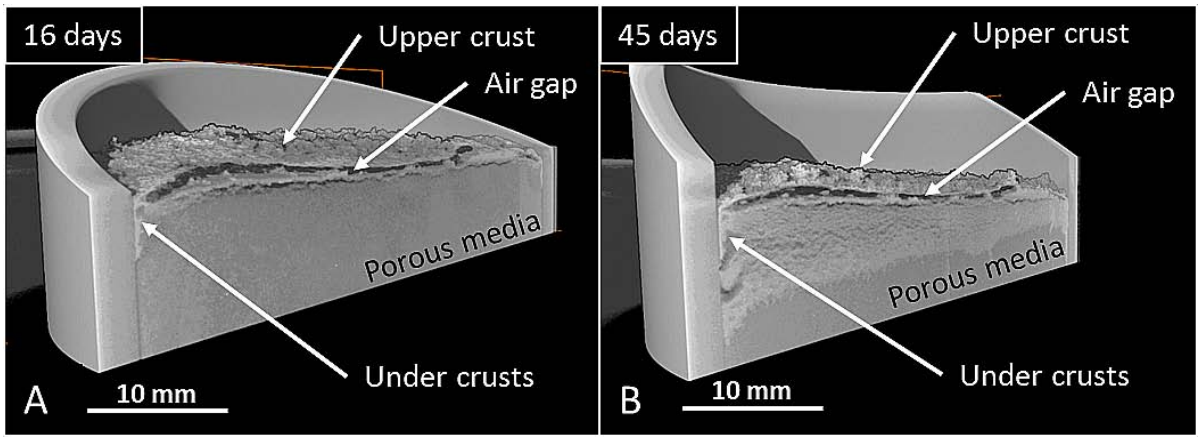

Figure 1: (A, B) Illustration of crust development in time by X-Ray Micro-Tomography. Note the air gap between the upper and under crusts.

References

[1] U. Nachshon, N. Weisbrod, R. Katzir et A. Nasser, «NaCl Crust Architecture and Its Impact on Evaporation: Three-Dimensional Insights,» *Geophysical Research Letters,* vol. 45, pp. 6100-6108, 2018.

[2] G. Licsandru, C. Noiriel, P. Duru, S. Geoffroy, A. Abou Chakra et M. Prat, «Dissolution-precipitation-driven upward migration of a salt crust,» *Physical Review E,* vol. 100, p. 032802, 9 2019.

Mathematical modeling and numerical appproximation of the compressible two-phase flow in a landfill

Z. Mghazli[a], Z. Belhachmi[b], S. Ouchtout[a,b]

[a] *Equipe d'Ingénierie Mathématique (EIMA), Laboratoire EDP, Algèbre et Géométrie Spectrale, Ibn Tofaïl University, Kénitra, Morocco.*
[b] *University of Haute-Alsace, IRIMAS UR 7499, F-68100 Mulhouse, University of Strasbourg, France.*

Keywords: Anaerobic biodegradation, Compressible two-phase flow, Biogas production

1. Introduction

Waste management and renewable energy generation are two key issues in nowadays society. A major research field arising in recent years focuses on combining the two aforementioned topics by developing new techniques to handle waste and to use it in the energy production. The anaerobic digestion process is a natural biological process of decomposition of organic matter by microorganisms (bacteria) activated in the absence of oxygen. It consists of complex chemical reactions. In the long term, the organic matter is transformed into "biogas" which is a mixture of methane and carbon dioxide.

The reactions of the degradation of organic mater for biogas production are classically described with a system of ordinary differential equations (ODEs) based on the principle of mass conservation and specific growth rates associated with each step of the mater decomposition (e.g. see [2]).

A bacterial dynamics model proposed by Bernard et al. [4], introduces a mere two step process that single out the dominant part in the bio-chemical transformations, namely, the acidogenesis using Monod's kinetics, and the methanogenesis using Haldane's kinetics. This approach, become now very popular in the field and constitutes our starting point in this work (e.g. see [5]).

Besides, the household waste landfill is a multi-phases medium consisting of solid, liquid and gas and considered as a reactive porous medium governed a coupled PDE-ODEs system describing the biological activity and the fluid flow, in which the biodegradation process produces a biogas (see [6], [1]). This approach is largely used in the field, particularly in the control and the optimization of the biogas production. However, it has some limitations, mainly due to the omission of the non-homogeneous character of the porous medium and the spatial distribution of the biological activity.

2. Aim

In this work, we present a new coupled model combining the biological and the mechanical aspects describing respectively the process of the biogas production and the compressible two-phase leachate-biogas flow during the anaerobic biodegradation of the organic mater in a landfill considered as a reactive porous medium.

The anaerobic digestion is a biological process that mineralizes organic substrates in the absence of oxygen. The organic material is then transformed by microorganisms to a mixture (biogas) of methane (CH_4) and carbon dioxide (CO_2) through a complex reactions in parallel and/or in series. The methane production process considered in this work is described as follows: a first step of hydrolysis / acidogenesis of the organic mater, represented by its concentration that we denote X, leads to the formation of carbon dioxide (CO_2) and simple soluble organic mater S. The latter is used as a substrate by methanogenic bacteria B which in turn produce carbon dioxide (CO_2) as well as methane (CH_4). At their death, the methanogenic bacteria in turn constitute a complex substrate to hydrolysis step (see FIGURE 1). The model given in [3] describes both the biological activity and the leachate single phase flow, represented by a system of reaction-diffusion coupled with Darcy flow equations, during the anaerobic digestion process in two-step for biogas production onsidering a landfill as a reactive porous medium. In this

work, we extend this approach to a two phases flow where the gaseous phase "biogas" is included in the model.

We carry out the full-discretization of the PDEs problem by using the second order BDF2 scheme in time and the P1-conforming finite ele-ment approximation in a variational framework. The numerical simulations in 2D and 3D will be given.

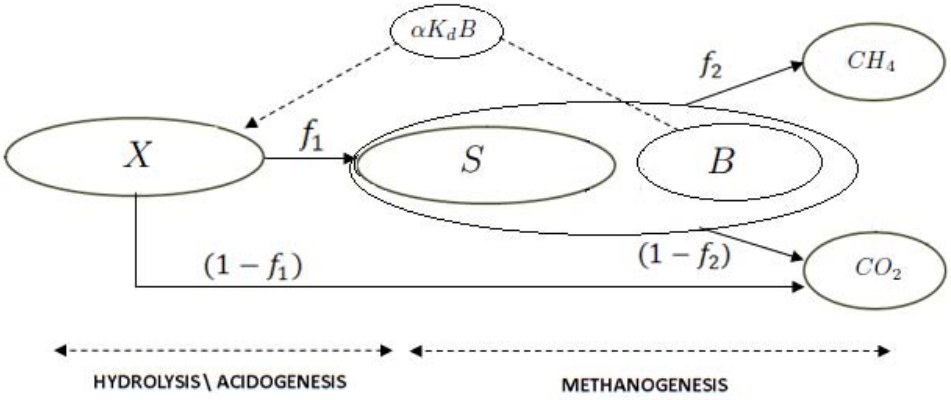

Figure 1: PScheme used for modeling anaerobic degradation of organic mater

References

[1] Agostini, F., Sundberg, C., Navia, R. (2012) , Is biodegradable waste a porous environment? A review. Waste Management, Research, 30(10), 1001-1015.

[2] Bastin, G. and Dochain, D. (1991), On-line estimation and adaptive control of bioreactors. Elsevier, Amsterdam, 1990 (ISBN 0-444-88430-0). xiv+ 379 pp. Price US 146.25/Dfl. 285.00.

[3] Belhachmi, Z., Mghazli, Z., Ouchtout, S. (2021), Mathematical modelling and numerical approximation of a leachate flow in the anaerobic biodegradation of waste in a landfill. Journal of Mathematics and Computers in Simulation, 2021, vol. 185, p. 174-193.

[4] Bernard, O., Hadj-Sadok, Z., Dochain, D., Genovesi, A., Steyer, J. P. (2001), Dynamical model development and parameter identification for an anaerobic wastewater treatment process. Biotechnology and bioengineering, 75(4), 424-438.

[5] Ouchtout, S., Mghazli, Z., Harmand, J., Rapaport, A., Belhachmi, Z. (2020), Analysis of an anaerobic digestion model in landfill with mortality term. Communications on Pure and Applied Analysis, 19(4), 2333.

[6] Pinder, G. F., Gray, W. G. (2008), Essentials of multiphase flow and transport in porous media. John Wiley and Sons.

Pore-scale hydro-mechanical modeling of gas transport in coal matrix

Ahmad Mostafa[1], Luc Scholtès[2], Fabrice Golfier[1]

[1]Université de Lorraine, Laboratoire GeoRessources, Nancy, France
[2]Université Clermont-Auvergne, Laboratoire Magmas et Volcans, Clermont-Ferrand, France

Keywords: DEM, PFVM, coal matrix, solvation pressure, hydro-mechanical coupling, nanoporous material.

Coal beds are dual permeability systems characterized by a porous matrix enclosed within sets of orthogonal fractures known as cleats. Production of coalbed methane (CBM) consists in desorbing methane from the low permeable coal matrix to the high permeable cleat system. Unlike in conventional reservoirs exploitation, sorption mechanisms cause shrinkage and swelling of the matrix which increase the complexity of the phenomena at stake, leading to complex reservoir behaviors in terms of production.

A 3D discrete element method (DEM) coupled to a pore scale finite volume method (PFVM) is used here to better understand the different mechanisms at stake. The model, implemented in the open source software Yade Open DEM (Smilauer et al., 2015), based on the hydro-mechanical model proposed by Catalano et al. (2014). The coal matrix is treated as an assembly of bonded particles interacting one with another through elastic-brittle contact laws. The pore space is discretized into tetrahedra, generated from a regular triangulation of the particle assembly. Both Knudsen and surface diffusion as well as sorption processes are modeled considering the coal matrix as a microporous material. The method is hydro-mechanically coupled in the sense that changes in pore pressure produce hydrostatic forces that deform the solid skeleton, while deformation of the pore space induces pore pressure changes that promote interporal flow. In addition, sorption induced deformations are taken into account by considering an additional pressure term related to the concentration of gas within the medium (the so-called solvation pressure).

In this work, we first present the model and its constitutive equations. We assess its capabilities by comparing its predictions to well established solutions describing diffusive flow in porous media as well as to classic poroelasticity concepts. In particular, we focus on the influence of sorption induced deformations on the Biot coefficient estimation taking into consideration different adsorption isotherm types (Linear and Langmuir adsorption). Finally, we compare the model predictions to swelling test data from the literature to illustrate its consistency.

REFERENCES

- V. Smilauer et al. (2015), Reference manual. In Yade Documentation 2nd ed. The Yade Project, http://yade-dem.org/doc/
- E. Catalano, B. Chareyre, E. Barthélemy. Pore-scale modeling of fluid-particles interaction and emerging poromechanical effects, International Journal for Numerical and Analytical Methods in Geomechanics,2014, 38(1),pp.51-71.
- L. Brochard, M. Vandamme, R. Pellenq. Poromechanics of microporous media. Journal of the Mechanics and Physics of Solids, 2012, 60 (4), pp.606-622.

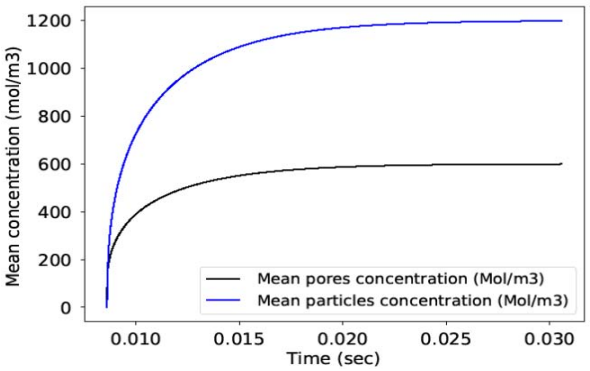

Figure 1. Evolution of mean pore concentration and mean particle concentration with time.

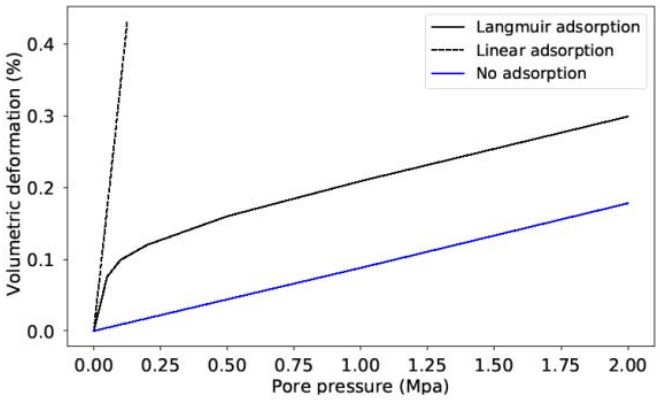

Figure 2. Evolution of volumetric deformation with respect to fluid pore pressure considering different adsorption isotherms.

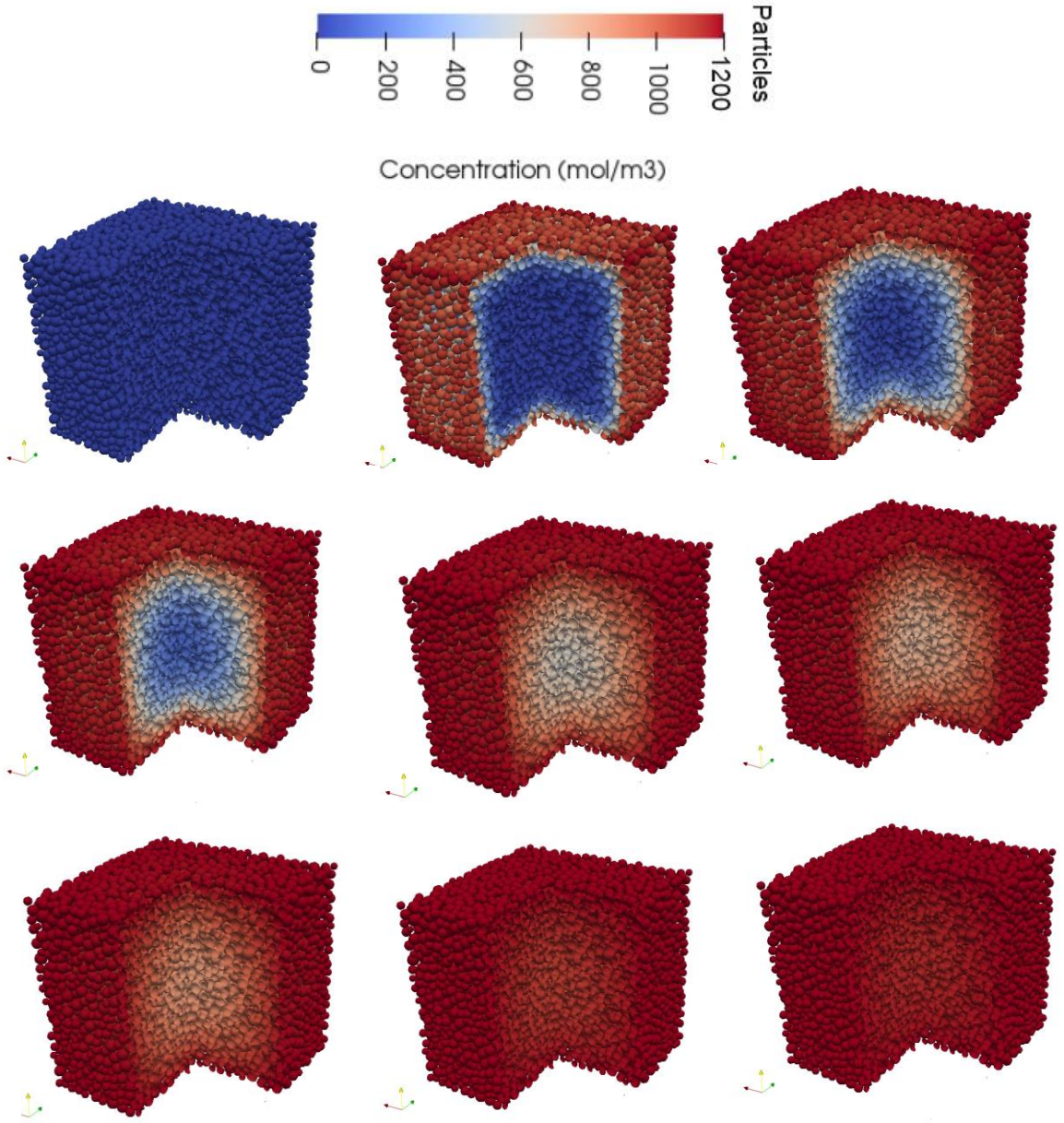

Figure 3. Evolution for particles concentration at different times

Topology Optimization of Encapsulated Macro-Porous Phase Change Materials for Thermal Energy Storage

N. Mallya [a], S. Haussener [a]

[a] *Laboratory of Renewable Energy Science and Engineering, EPFL, 1015 Lausanne, Switzerland*

Keywords: digital 3D porous structures, neural network, phase change, topology optimization

Thermal energy storage using latent heat provides a competitive edge to the existing storage technologies for large-scale integration of renewable sources with a suitably selected phase change material (PCM) with large latent heat, high melting point and optimized design. Metal alloys [1] can be used in place of commonly used low conductivity PCMs (organic acids, salts) for high-energy and high-power density applications [2]. Due to the two orders of magnitudes higher thermal conductivity of the metal alloys, the convective heat transfer rate from the heat transfer fluid (HTF) to the PCM becomes limiting making encapsulated macro-porous structures with larger surface areas promising. Structural optimization is required to tailor the specific storage capacity, charging-discharging rates, and storage unit design to the final application. Computational analyses of porous structures often involve approximated or volume averaged models. We provide a computational methodology to generate, mesh and simulate with ordered and random structures that resemble their realistic counterparts and investigate and optimize the effect of the structure on the phase change characteristics.

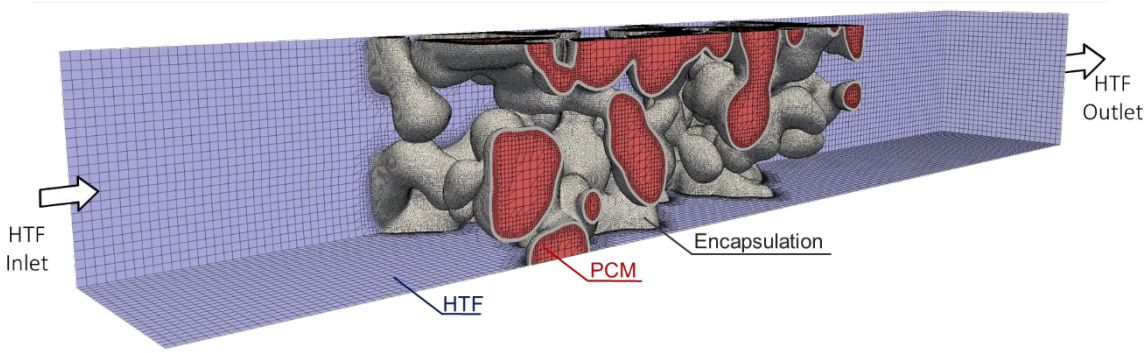

Figure 1: Unit cell of a randomly generated 3D monolithic encapsulated macro-porous heat storage structure.

We report a machine learning approach to optimize the topology of a macro-porous structure for a specific energy and power density by training it to predict the heat transfer and temperature distribution during phase change. Unit cells of random and ordered 3D percolating encapsulated macro-porous structures were artificially generated and disconnected pores and solid structures were removed to obtain a monolithic structure that can be used as a periodic unit cell. Hexahedral meshing of the structures was performed using snappyHexMesh and mesh convergence was verified. Transient fluid-solid conjugate heat transfer and the effective heat capacity method [3] in ANSYS Fluent to predict the phase change inside the encapsulated PCM. In this method, we implement an increased specific heat capacity of the PCM during phase change to account for the latent heat. Air was used as the HTF with constant properties, and the PCM was assumed to be homogeneous, isotropic and with temperature dependent thermal heat capacity and conductivity. Due to the low Stefan numbers, the natural convection inside the PCM encapsulations was neglected [2]. Porosity, average pore-size, and especially the surface area between the HTF and the PCM had a significant effect on the distribution of the HTF-PCM heat flux and thus the phase change time during dis/charging of the heat storage.

The entire set of generated and ordered encapsulated macro-porous structures and their simulated heat and mass transfer performance was used as training data for a mesh-based convolution neural network that predicts the results of the phase change simulations [4]. Gradient descent optimization was used to generate optimized, application specific macro-porous encapsulations. While training of the neural network required tens of hours, optimization could be performed in the matter of a few minutes.

The approach presented allows to generate macro-porous encapsulations with designs tailored to specific applications with requirements on storage capacity, dis/charging rates, and storage unit design, and represents an important design tool for transferable solutions.

References

[1] Binder, S.; Haussener, S. *Applied Surface Science*, 505 (2019).
[2] Mallya, N.; Haussener, S. *International Journal of Heat and Mass Transfer*, 164 (2021).
[3] Poirier, D.; Salcudean, M. *Journal of Heat Transfer*, 110, 562–570 (1988).
[4] Baqué, P.; Remelli, E.; Fleuret, F.; Pascal, F. *International Conference on Machine Learning* (2018).

Investigating haloclasty as a potential cause of French Basque Country Coastline erosion

V. Okumko[a], D. Herluyn[a,b], G. Pijaudier-Cabot[a,c] , D. Grégoire[a,c]

[a]*Universite de Pau et des Pays de l'Adour, E2S UPPA, CNRS, Total, LFCR, Anglet & Pau, France*
[b]*Universite de Pau et des Pays de l'Adour, E2S UPPA, CNRS, DMEX, Pau, France*
[c]*Institut Universitaire de France (IUF)*

Keywords: haloclasty, mirabilite, quasi-simultaneous Neutron and X-ray tomographic (NeXT)

Forecasting the evolution and momentum of coastal erosion under current climate changes and forthcoming sea level rise remains a scientific challenge. The Ezponda project aims at studying and hierarchizing the different key parameters (haloclasty, rain, storms), which drives coastal erosion and coastal protection building damage.

Haloclasty is a natural rock failure process driven by salt crystallization and salt weathering. When saline fluids are present in the pore space of a material, salt crystal might precipitate upon changes in temperature or humidity conditions, leading to salt precipitation in the pores. The confined crystal growth within the pores might lead to a build-up of crystallization-induced stresses, which can eventually cause fractures in the porous medium [1-2].

In this context, this work aims to build an experimentally reliable database that allows for the comparison and validation of further numerical models developed in parallel within the Ezponda project.

A simple lab-designed protocol is proposed with well-defined boundary conditions allowing for an easy reproduction with numerical tools. The protocol consists of keeping the base of a cylindrical sample in a 3 molal concentration of sodium sulfate solution at an approximate temperature of 34 ˚C with room temperature controlled at 20 ˚C. Upon capillary uptake and natural evaporation, mirabilite may form within the rock porous network and produce damage as already observed in various civil engineering contexts [3]. Digital Image Correlation (DIC) is applied to characterize the rock deformation and cracking on the sample surface. To localize the damage appearing inside the sample upon crystallization, acoustic sensors were attached to the sample under the same experimental protocol to monitor acoustic emissions within the sample. Finally, the experimental protocol is reproduced at the D50 beam line [4] of the Institut Laue-Langevin for a better insight of the multi-physics couplings between salt crystallization and damage in a porous medium. The acquisition of quasi-simultaneous Neutron and X-ray tomographic (NeXT) scans of the sample under the experimental protocol helps elucidate on the interplay of salt crystallization and damage in porous rock material [5-7].

The study focuses on the erosion of the French Basque Country coastline between Hendaye and Saint-Jean-de-Luz, which is mainly composed of Santonian flysch rock formation - a very low porosity and tight material with few diffused heterogeneities. In addition, different rock materials: Vosges sandstone, Lavoux limestone and a pre-cracked concrete are also studied in order to test the robustness of the on-going numerical model.

References

[1] Scherer, G. (2004). *Cement and Concrete Research*, 34(9), 1613-1624.
[2] Steiger, M. (2005). *Journal of Crystal Growth*, 282(3), 455-469.
[3] Lubelli et al., (2018). *Materials and Structures*, 51(2), 55.
[4] Tengattini et al. (2020). *Nucl. Instrum. Methods. Phys. Res. A*, 968, 163939.
[5] Grégoire et al. (2019). *Institut Laue-Langevin (ILL)*, UGA-61.
[6] Grégoire et al. (2020). *Institut Laue-Langevin (ILL)*, UGA-90.
[7] Grégoire et al. (2020). *Institut Laue-Langevin (ILL)*, UGA-115.

Acknowledgements: This work is partially financed by FEDER funds through the EZPONDA project and by the E2S UPPA hub Newpores. H. Derluyn gratefully acknowledges the financial support from the European Research Council (ERC) under the European Union's Horizon 2020 research and innovation programme (grant agreement No 850853). The authors gratefully acknowledge Alessandro Tengattini and Lukas Helfen for their help and support during the experimental tests carried out at the D50 beamline of the Institut Laue-Langevin (Grenoble, France).

Swelling of polymeric hydrogels observed by MRI

D. Stemmelen[a], S. Leclerc[a], F. Xu[a], J. Peixinho[b]

[a]*LEMTA, UMR 7563 CNRS – Université de Lorraine, 54505 Vandoeuvre-les-Nancy*
[b]*Laboratoire PIMM, UMR 8006, CNRS, Arts et Métiers Institute of Technology, CNAM, HESAM Université, 75013 Paris*

Keywords: ionic hydrogels; superabsorbent polymer; swelling; MRI; surface instabilities; diffusiophoresis

1 Introduction

Super-absorbent polymeric hydrogels are a variety of porous media that can swell up to more than 100 times their original volume when immersed in water. They are composed of polymer chains linked together in a lightly crosslinked network and exhibiting an affinity for water due to the existence of hydrophilic groups [1]. In fact, during the swelling process, water molecules come to occupy the hydrophilic sites, which leads to an expansion of the polymer network and a macroscopic swelling of the hydrogel. The crosslinking of the polymer chains, even if it is weak, makes it possible to avoid the breakdown of the hydrogel at high water contents and gives it some rigidity. Due to the ionic nature of hydrogels, their swelling is generally accompanied by complex mechanisms involving electro-hydro-chemo-mechanical couplings. MRI technique is an attractive way to observe the swelling of hydrogels and the associated coupling phenomena.

2 Method

When a spherical bead of dry hydrogel is immersed in water, a transient phenomenon of gel formation on the surface of the polymer bead is observed, but also of the appearance of lobes, then their coalescence, to result in again to a spherical geometry of the full of water hydrogel bead [1, 2].

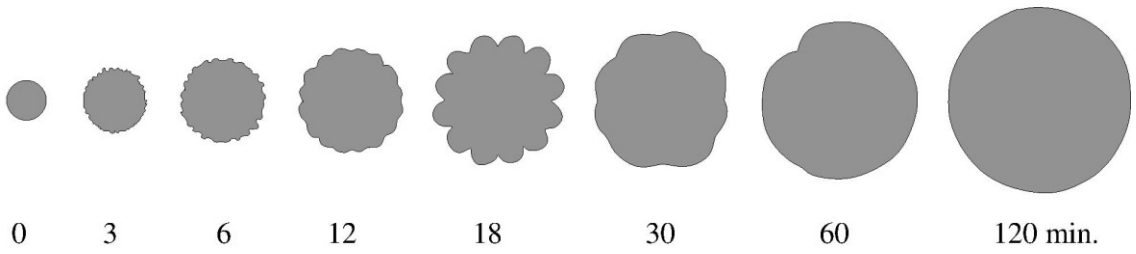

Figure 1: Sketch of the transient swelling process of a hydrogel bead.

Observing by MRI the swelling of a hydrogel bead immersed in a volume of water is not an easy task because once expanded, the hydrogel contains more than 99% water. It is therefore difficult to distinguish its interface from the water in which it bathes. Hence, it is necessary to add a contrast agent (paramagnetic Cu^{2+} ions, for example) to differentiate the NMR relaxation parameters of the solution and of the hydrogel [3]. However, the presence of ions in solution can also significantly affect the hydrogel swelling process.

3 Results

A preliminary study was carried out to get an insight into the maximum swelling of hydrogel (sodium polyacrylate) beads immersed in copper sulphate solutions at different concentrations. This kind of hydrogel has a strong tendency to bind Cu^{2+} cations. This consequently leads to additional crosslinks within polymer chains which decrease the swelling of the hydrogel.

We then performed MRI images according to the swelling kinetics of these hydrogel beads in different concentrations of copper sulphate varying between 0.1 mM to 5 mM. The images were acquired using an NMR spectrometer (Bruker 600 MHz Wide Bore) equipped with a micro-imaging device. As expected, these experiments allow us to follow the swelling of the hydrogel beads over time: the formation of the gel on the surface of the polymer bead, the appearance of lobes, then their coalescence, and also the gradual disappearance of the solid polymer seed within the sphere (Figure 2).

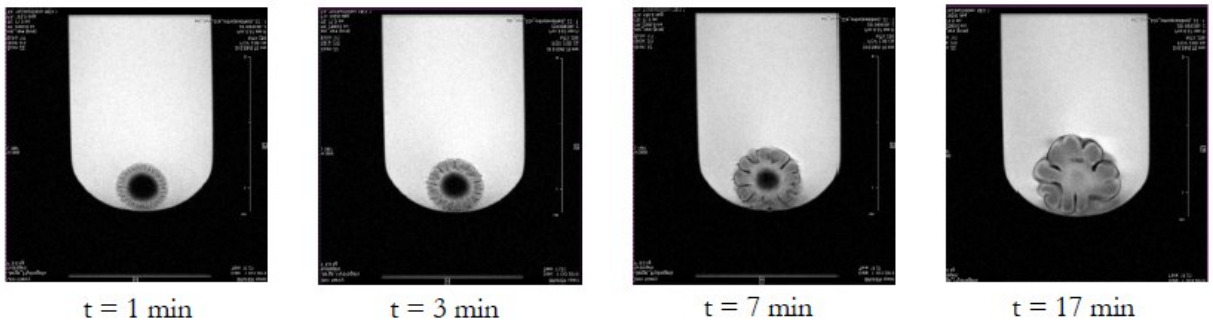

Figure 2: Observation over time, by MRI, of a hydrogel bead immersed in a 5 mM $CuSO_4$ solution. The diameter of the dry polymer bead and the test tube are 3.2 mm and 20 mm respectively.

For the tests carried out at high concentrations, $[CuSO_4] > 1$ mM, we observe complex mechanisms coupling the diffusion and adsorption of Cu^{2+} ions in the hydrogel. The adsorption of cations leads to a crosslinking of the polymer chains which decreases the swelling of the hydrogel. It is even possible to observe in this case, after a first phase of swelling, a second phase of shrinkage associated with osmotic drying of the hydrogel. It seems to us that this second phase is not reported in literature and we have tried to understand this phenomenon. In parallel to these complex phenomena, we have also visualized by MRI the mechanisms of diffusiophoresis [4] in the solution in which the hydrogel is immersed (Fig. 3). The method was also carried out with a gadolinium chelate (Gd^{3+} DTPA) as a contrast agent for MRI and results are in all respects similar.

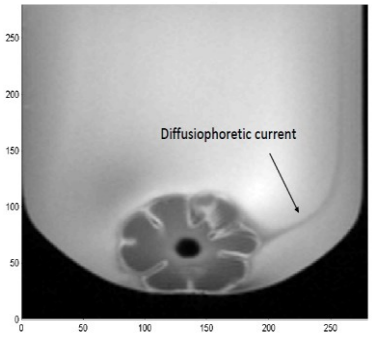

Figure 3: Observation of diffusiophoretic convection currents.

4 Conclusion

This study shows the possibility of using MRI techniques to analyze water and ions transport as well as mechanical deformations during the swelling of polymeric hydrogels. It allows to collect morphological quantities (core diameter, number and dimensions of folds), which will be beneficial for the validation of swelling models.

References

[1] T. Bertrand, J. Peixinho, S. Mukhopadhyay and C.W. MacMinn, *Phys. Rev. Appl.*, 6, 064010 (2016).
[2] M. Curatolo, P. Nardinocchi, E. Puntel and L. Teresi, *J. Appl. Phys.*, 122, 145109 (2017).
[3] W. Barros Jr., E.N. de Azevedo and M. Engelsberg, *Soft Matter,* 8, 8511-8516 (2012).
[4] D. Florea, S. Musa, J.M. Huyghe and H.M. Wyss, *Proc. Natl. Acad. Sci. USA*, 111, 6554-6559 (2014).

Investigation of calcium sulfate carbonation processes using geological labs on a chip: experimental and thermo-kinetic modelling approaches

Rabie Ferhat Hamida[1], Olivier Nguyen[1], Mohamed Azaroual[2] and Samuel Marre[1]

[1]CNRS, Univ. Bordeaux INP. ICMCB, UMR 5026 F-33600, Pessac, France

[2]BRGM, 3 Avenue Claude-Guillemin BP 36009, 45060 Orléans cedex 02 France

Key Word: reactive transport, CO_2 geological storage, Lab-On-Chip, kinetics, thermodynamic equilibrium, gypsum carbonation.

The geological subsoil has been used for a long time, to extract natural resources (water, heat, gas, useful mineral substances, etc.) or to inject or store undesirable compounds (industrial water and desalination brines, petroleum brines, radioactive wastes, acid gases, CO_2, etc.). This requires the mastering of reactive transport processes in porous and fractured geological environments at different time and space scales.

The objective of this work is to study, at the pore scale, the precipitation and the dissolution processes of carbonate and sulfates minerals, in order to understand the physical and chemical mechanisms at the interface of different phases (mineral/water/gas). For this purpose, we control the parameters that are likely to affect the reaction rates, like pH (from 5 to 10), temperature (from 25 to 100 °C) and the concentration of alkaline earth minerals (Ca, Mg). The recent development of the geological Lab-On-Chip (GLoCs) [1] for the study of reactive transport mechanisms at the conditions of geological reservoirs (25 <T <100° C and 1 <P <200 bar) have demonstrated the applicability of these devices and their adaptability to study geochemical processes.

We used the GLoCs devices coupled with different *in-situ* characterization techniques (*i.e.*, high speed optical imaging, Raman spectroscopy, etc.) to study the calcium sulfate carbonation mechanisms and the kinetics of the following reaction at 25°C and 1 bar:

$$CaSO_4 + CO_3^{2-} \rightarrow CaCO_3 + SO_4^{2-} \qquad (1)$$

The gypsum crystals ($\mathrm{CaSO_4.2H_2O}$) were first precipitated on chip in small pools (diameter = 2 mm and depth = 45 µm) by mixing of 0.08 M $\mathrm{CaCl_2}$ and 0.08 M $\mathrm{Na_2SO_4}$ aqueous solutions under ambient conditions [2]. The saturation state of reactive fluid with respect to calcium sulfate phases was calculated using PHREEQC V3: $S_{Gypsum} = 0.83$, $S_{Anhydrite} = 0.65$ (S = log Q/K) [4]. The function Q is the Ionic Activity Product of a mineral and the K, is its thermodynamic equilibrium constant. Gypsum precipitation reaction approaches equilibrium within 2-4 hours. The carbonation of gypsum began after the injection of Na_2CO_3 into the pools that contain equilibrated gypsum crystals in saturated fluid. Diffusion of carbonate ion into pools changes the reactive fluid leading to the starting dissolution of gypsum crystals monitored using real-time observation by *in-situ* confocal microscopy. This highlights the precipitation of calcite and vaterite 1 hour after the gypsum dissolution started. It was observed thanks to image treatment that the gypsum dissolution kinetic is accelerated by calcite and vaterite formation [3]. The sequence in which calcite and vaterite form is interpreted taking into consideration diffusion mechanism and the qualitative evolution of several chemical parameters in the reactive fluid: SO_4^{2-}/CO_3^{2-} activity ratio, pH and aqueous species distribution.

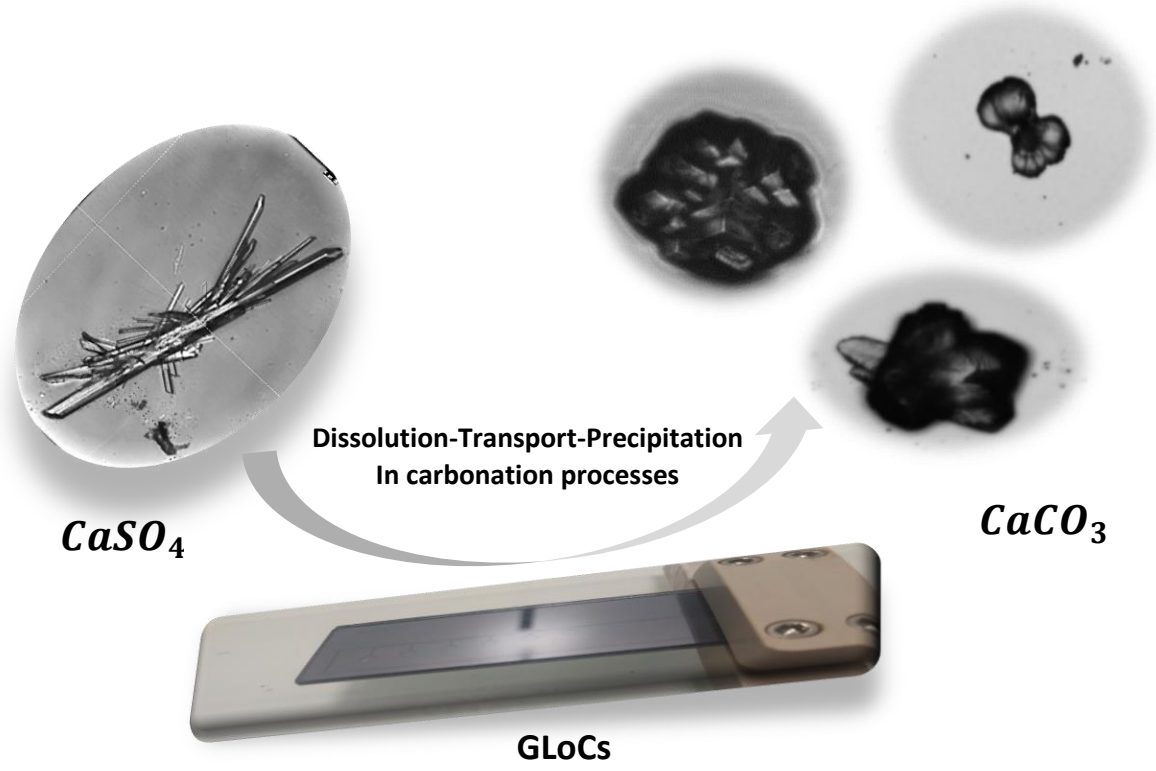

Figure 1: Using Lab-On-Chip to study gypsum carbonation at 25°C and 1 bar

The reactive transport coupling dissolution-diffusion-precipitation mechanisms will improve our knowledge of the carbonation kinetics for CO_2 storage applications by understanding its interaction with gypsum in saturated fluid (Ca^{2+}, Mg^{2+} and SO_4^{2-}). Then, the impacts of these reactions on the porosity and the permeability evolutions of the geological porous media can be quantified. Experimental results will be used for thermo-kinetic modelling using PHREEQC V3 (Parkhurst et Appelo, 2013). In our results, the gypsum was completely dissolved (disappeared) within 5 hours. The image treatment allowed to estimate the mean surface evolution of the gypsum dissolution reaction, 2.79×10^{-2} µm^2/s. In the literature, the dissolution rate constant of gypsum during its carbonation is $1.1 \pm 0.1 \times 10^{-7}$ mol/m^2/s [2]. On the other hand, vaterite crystals were precipitated within 3 to 5 hours with a parabolic form for the crystal area evolution. Polynomial equations were fitted to integrate the surface evolutions in the kinetic equation (according to the Transition State Theory, TST approach) of gypsum dissolution and carbonate precipitation rate laws.

References

[1] S. Morais, A. Cario, N. Liu, D. Bernard, C. Lecoutre, Y. Garrabos, A. Ranchou-Peyruse, S. Dupraz, M. Azaroual, R.L. Hartman, S. Marre, studying key processes related to CO2 underground storage at the pore scale using high pressure micromodels, Reaction Chemistry and Engineering, 2020, 5, 1156-1185.

[2] Lei Yu, Leyla M. Daniels, Josephina J.P.A. Mulders, Giuseppe D. Saldi, Anna L. Harrison, Li Liu, Eric H. Oelkers, an experimental study of gypsum dissolution coupled to CaCO3, Chemical Geology, 2019, 525, 447–461.

[3] L. Fernandez-diaz, C.M. Oina, J. Manuel Astilleros, N. Sanchez-Pastor, the carbonatation of gypsum: Pathways and pseudomorph formation, American Mineralogist, Volume 94, pages 1223–1234, 2009.

[4] Parkhurst, D.L., Appelo, C.A.J., 2013. Description of input and examples for PHREEQC version 3—a computer program for speciation, batch-reaction, one-dimensional transport, and inverse geochemical calculations. In: Techniques and Methods 6–A43. U.S. Geological Survey, Denver, Colorado URL. https://pubs.usgs.gov/tm/06/a43/.

Multiphase - multi-components systems

Analysis of the displacement behavior of DNAPL in contaminated soils by injecting densified polymer suspension

Amir Alamooti [a,b,c] Stéfan Colombano [a], Sagyn Omirbekov [a,b], Azita Ahmadi-Sénichault [b], Hossein Davarzani [a]

[a] *BRGM (French Geological Survey)*
[b] *Institut de Mécanique et Ingénierie de Bordeaux (I2M), Arts et Métiers Institute of Technology, CNRS, Talence, 33405, France*
[c] *Agence de la transition écologique (ADEME), Angers, France*

Keywords: densification, DNAPL, non-Newtonian fluid, clogging

1 Introduction

The process of contaminant removal from the zones near groundwater resources has drawn great attention due to the high importance of these vital resources [1]. In the case of Dense Non-Aqueous Phase Liquids (DNAPL) owing to their high density, they form discontinuous insoluble lenses below the groundwater level. In addition, due to their high interfacial tension and high viscosity an efficient way beyond the common approaches like pump-and-treat method is required to remediate them from the contaminated zones. Furthermore, due to their presence near the groundwater zones using methods such as surfactant injection might be inappropriate as the surface tension decreases, and in the case of the foam injection the stability would be critical [2, 3]. In high permeable soils in the absence of capillary forces, using polymer solutions without any additives can increase the viscose forces but in the case of very dense DNAPL it might be not efficient enough as the buoyancy forces are working against the lateral displacement of the DNAPL [4]. In addition, due to high permeability of the soils the redistribution or more precisely backward movement of the remaining DNAPL to the displacement zone after remediation is challenging.

2 Material and Methods

Here, we are going to present our results on using densified polymer solutions to displace the chlorinated DNAPL from the contaminated soil below the groundwater level. Barite particles were selected to be added to the polymer solution for not only densification but also their strong clogging behavior inside the high permeable displaced zone that can properly prohibit the redistribution of remaining DNAPL. In order to have a stable suspension, the addition of several polymers including guar gum, xanthan gum, and carboxymethyl cellulose (CMC) was examined and it was found that CMC polymer can provide the most stable polymer solution. Then several barite-polymer solutions with densities more, equal, and less than that of DNAPL were prepared and the rheological behavior of these solutions was analysed. To evaluate the efficiency of the barite-polymer solution on the displacement of DNAPL below the groundwater level in real site, a decimetric-scale 2D-sandbox was used. Then the solutions with different densities were injected to the zone containing DNAPL at the bottom of the 2D-sandbox. The injection of each solution was continued to reach to the maximum recovery. The displacement procedure was monitored using an advanced imaging technique and the production and injection process were analyzed using mass balance interpretation. In addition to assess the clogging behavior of barite-polymer solution, the densities of produced fluids after post barite-polymer injection through a fully water saturated 1D- columns of sand were measured.

3 Results and conclusion

The results showed that using a polymer solution to displace the DNAPL cannot lead to appropriate displacement when the gravity forces are dominant. We found that adding the barite particles increases the lateral displacement of DNAPL. The displacement efficiencies were increased up to 213%, 345%, and 367% for the solutions with densities of 0.78, 1, and 1.14 times the density of DNAPL respectively in comparison to the case where only a polymer was individually used (Figure 1). Also, it was shown that the barite-

polymer solution can cause a permeability reduction in the sands up to 55%, 70%, and 72% for different solutions with increasing trend of densities mentioned above. The experimental process was numerically simulated using generalized Darcy's law and the continuity equation. To assign the non-Newtonian behavior of the barite-polymer solution the power-law relationship obtained from the rheological investigation of the polymer was introduced into the model. Also to consider the clogging behavior of the suspension solution, the transport equation of diluted species was imported into the model and then the relationship between the permeability and porosity reduction was described by Carman-Kozney equation. The displacement behavior of the phases inside the porous media obtained by simulation was validated by images analysis and data obtained from mass balance.

We showed that the densification of a polymer solution by overcoming to the gravity forces can result in more lateral displacement of DNAPL and consequently can improve the displacement efficiency. It is shown that barite particles by decreasing the permeability of the displaced zone can block the redistribution of the remaining DNAPL. We anticipate the results of this work can be effectively used in the case of contaminated fields with DNAPL near the groundwater, as this method not only can astonishingly remediate the polluted soil but also can prevent the further groundwater contamination with remaining DNAPL.

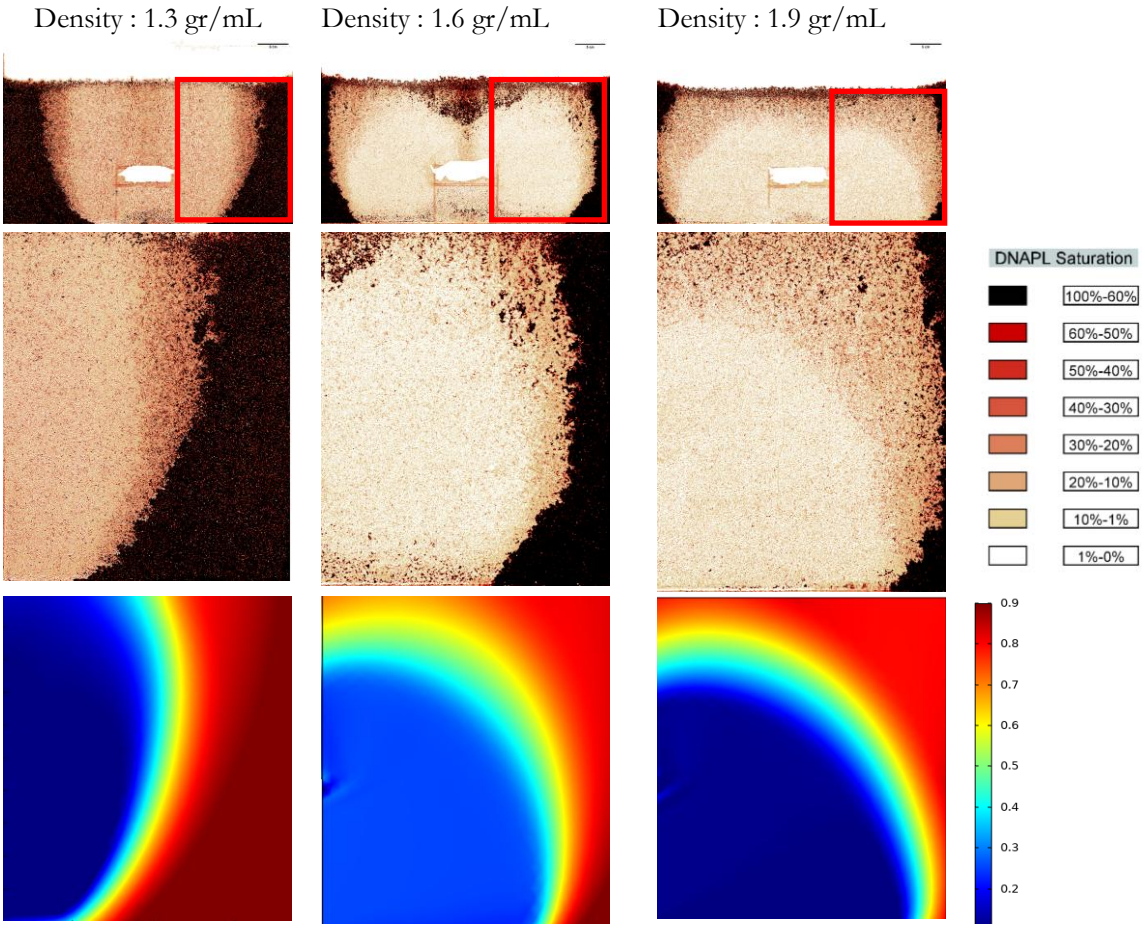

Figure 1: Displacement patterns and comparison between the modelling and experimental results

References

[1] Colombano, S., Davarzani, H., Hullebusch, E. D. van, Huguenot, D., Guyonnet, D., Deparis, J., Lion, F. and Ignatiadis, I., Comparison of Thermal and Chemical Enhanced Recovery of DNAPL in Saturated Porous Media: 2D Tank Pumping Experiments and Two-Phase Flow Modelling, Science of The Total Environment, vol. 760, p. 143958, 2021.

[2] Maire, J., Joubert, A., Kaifas, D., Invernizzi, T., Marduel, J., Colombano, S., Cazaux, D., Marion, C., Klein, P.-Y. and Dumestre, A., Assessment of Flushing Methods for the Removal of Heavy Chlorinated Compounds DNAPL in an Alluvial Aquifer, Science of The Total Environment, vol. 612, pp. 1149–58, 2018.

[3] Omirbekov, S., Davarzani, H., Colombano, S. and Ahmadi-Senichault, A., Experimental and Numerical Upscaling of Foam Flow in Highly Permeable Porous Media, Advances in Water Resources, vol. 146, p. 103761, 2020.

[4] Miller, C. T., Hill, E. H. and Moutier, M., Remediation of DNAPL-Contaminated Subsurface Systems Using Density-Motivated Mobilization, Environmental Science & Technology, vol. 34, no. 4, pp. 719–24, 2000.

Experimental study of drying in the presence of fluorescent colloidal particles in model system

E. Ghiringhelli, M. Prat, M. Marcoux

Institut de Mécanique des Fluides de Toulouse, U.M.R. C.N.R.S., INP/UPS No 5502, Avenue du professeur Camille Soula, 31400 Toulouse, France

Keywords: Evaporation, Porous media, Particles tracking, Particles deposit

1 Motivation

The motivation for the present study stems from visualizations of the PTFE distribution in the gas diffusion layer (GDL) of Proton Exchange Membrane Fuel Cell (PEMFC). The GDL is a fibrous carbon layer treated with polytetrafluoroethylene (PTFE), by drying a layer saturated with a solution of PTFE particles, to improve hydrophobicity [1, 2, 3]. During the fabrication, internal surfaces appears to be hardly covered homogenously causing a mixed wettability in the medium, indeed it is showed in [4] that PTFE distribution strongly depends on evaporation conditions, such as the surrounding pressure.

2 Study on a model system

The objective of the work is to study the pattern formed by fluorescent particles (1 μm) in the porous media after the evaporation of the water, in different geometries, starting from a single pore before moving to a pore network on micro-models and/or with different initial conditions. The first step was to use a transparent material to make the porous medium (polymer), filling it with a solution of fluorescent red colloids and let it dry at constant temperature and humidity. Using fluorescent colloids will allow us to follow their position during evaporation, therefore compute the velocity field and connect it to the final deposit. The flow of water during evaporation and the pattern of deposited particles were observed at a microscope using a confocal green source, in the pictures below the particles are bright.

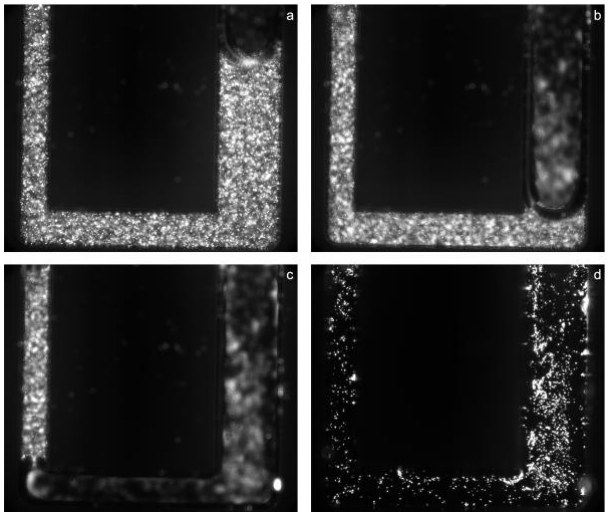

Figure 1: (a), (b) and (c) are different stages of evaporation in a plexiglass pore 3mm x 3mm of a solution with concentration 2×10^{-5} % (timesteps: 20 minutes, 1 hour and 40 minutes and 3 hours), while (d) is the deposit of the bright particles after drying.

We notice that the largest channel is the first one to dry out, similarly to the invasion pattern of pure water, on the other hand the deposit of particles can result in two different configurations: the particles are forced to move on the other side or they deposit from the moving meniscus. This last phenomenon can be observed in Figure 1 (d) in an overall heterogeneous pattern of deposited particles, with higher concentration in the bigger channel.

The final aim is to be able to analyse and predict the materials properties such as wettability, contact angle, hydrophobicity of particles, etc…on polymer micromodels. These procedures would allow us to explain how the fluid moves while drying, thanks to the tracking of particles, how it influences the colloids' deposition and finally, find procedures to improve GDL's properties for better fuel cells operation.

References

[[1] Tatsumi Kitahara, Toshiaki Konomi, and Hironori Nakajima. Microporous layer coated gas diffusion layers for enhanced performance of polymer electrolyte fuel cells. Journal of Power Sources, 195(8):2202–2211, April 2010.
[2] Hasan K. Atiyeh, Kunal Karan, Brant Peppley, Aaron Phoenix, Ela Halliop, and Jon Pharoah. Experimental investigation of the role of a microporous layer on the water transport and performance of a PEM fuel cell. Journal of Power Sources, 170(1):111–121, June 2007.
[3] Chung-Jen Tseng and Shih-Kun Lo. Effects of microstructure characteristics of gas diffusion layer and microporous layer on the performance of PEMFC. Energy Conversion and Management, 51(4):677–684, April 2010.
[4] Hiroshi Ito, Katsuya Abe, Masayoshi Ishida, Akihiro Nakano, Tetsuhiko Maeda, Tetsuo Munakata, Hironori Nakajima, and Tatsumi Kitahara. Effect of through plane distribution of polytetrafluoroethylene in carbon paper on in-plane gas permeability. Journal of Power Sources, 248:822–830, February 2014.

The link between corner flows and Haines jumps dynamics during two phase flow in subsurface reservoirs using microfluidics

Mahdi Mansouri-Boroujeni[a], Mohamed Azaroual[a,b], Sophie Roman[b]

[a] *Univ. Orléans, CNRS, BRGM, ISTO, UMR 7327, F-45071, Orléans, France.*
[b] *BRGM, 3 Avenue Claude Guillemin, 45100 Orléans, France.*

Keywords: Corner flow, Capillary dominated flow regime, Haines jumps

1. Introduction

Multiphase flow in porous media is an inherent process in many environmental and industrial systems. Variations in fluid and porous media properties, and flow condition leads into different front behaviors, forming various displacement patterns, which are classically categorized into capillary, viscous and stable flow regimes. These flow regimes are represented based on two dimensionless numbers, describing active forces (viscosity ratio, $M = \frac{\mu_{displacing}}{\mu_{displaced}}$, and capillary number, $Ca = \frac{\mu_{displaced} v}{\sigma \cos\theta}$, where μ, v, σ and θ represent viscosity, velocity, interfacial tension and contact angle) [1]. Distinct interface displacement mechanisms are triggered during pore invasions in each flow regime. Haines jumps mechanism are the dominant pore invasion mechanisms when capillary forces are dominant in porous media, capillary flow regime. Abrupt displacement of interface preceded by pinning intervals at constrictions are of characteristics of this mechanism [2]. Although, many studies have targeted displacement under this mechanism, still the dynamics of Haines jumps and the nature of this pinning-jumping behavior is not clear. In this research we aim to cast light on the dynamics of Haines jumps as a pore invasion mechanism at capillary flow regime.

2. Materials and methods

Microfluidics devices are well-known for their ability to provide a well controlled pore and throat structure along with the transparency and enabling the visualization of the displacement process and the interface dynamics. A high-resolution camera coupled with a microscope enabled us to capture image sequences of different drainage process stages. We benefit from micro-PIV (Particle Image Velocimetry at microscopic scale) technique to measure the velocity field in the body of the wetting fluid [3]. In order to have representation of successions of pores and throats in subsurface formations and avoid complex interactions of interconnected porous systems, a modified pore doublet geometry, composed of two undulated capillaries, was considered as porous media pattern. DI water and air/silicone oil are the wetting and the non-wetting phases, respectively, in our PDMS (a type of elastomer) micromodels. This consideration of materials is analogous to displacement condition of CO_2 sequestration in the phase diagram ($-2 < M < -1$ and $Ca < -3$). A model based on volume averaging for Navier-Stokes equation is developed and is applied on presented pore doublet model,

$$-\rho^{(2)}\frac{d}{dt}\left(\left(A(h_i)\dot{h_i}\right)\Theta(h_i)\right) - \mu^{(2)}A(h_i)\dot{h_i}\Phi(h_i) - \sigma\kappa(h_i)\cos(\theta) = -\rho^{(2)}\frac{d}{dt}\left(\left(A(h_{ii})\dot{h_{ii}}\right)\Theta(h_{ii})\right) - \mu^{(2)}A(h_{ii})\dot{h_{ii}}\Phi(h_{ii}) - \sigma\kappa(h_{ii})\cos(\theta), \quad (1)$$

where $A, h, \theta, \mu, \sigma, \kappa$ and ρ represent cross-section surface area of the capillary, distance of interface from the inlet, contact angle, viscosity, interfacial tension, curvature of the interface and density and subscriptions i and ii and superscripts (1) and (2) are related to first and second capillary and displacing

and displaced phase respectively and Φ and Θ are defined as following, knowing Γ and M are density and viscosity ratios,

$$\Theta(h) = \Gamma \int_0^h \frac{1}{A(x)}\, dx + \int_h^L \frac{1}{A(x)}\, dx,$$

and

$$\Phi(h) = M \int_0^h \frac{1}{A(x)K(x)}\, dx + \int_h^L \frac{1}{A(x)K(x)}\, dx.$$

It is able to predict the interface position during the displacement process at different viscosity ratios and capillary numbers.

3. Main results and new highlights

Experimental data on interface dynamics at low flow rates will be presented and compared to the developed model. Additionally, micro-PIV is applied to monitor residual wetting fluids at corners of porous media during pore invasion process. In agreement with previous studies, Haines jumps are found to be the main pore invasion mechanism at low capillary numbers. As a part of pore invasion process with this mechanism, the interface pins at a constriction followed by drastic interface velocity increase. Model is able to predict the sudden interface velocity change. However, it can not explain the pinning period when the interface and fluids seem to be static. During the pinning interval, we observe a continuous flow of the wetting phase toward the interface front through the corners of drained pores, see Fig. 1. Dynamics of Haines jumps and the waiting time at the pore throat (i.e. the time that interface waits at a constriction before a jump) are associated to dynamics of corner flow and the existing pressure gradient between interface and corners. A range of viscosity ratios are explored to compare time scale of events at different displacement conditions. This work highlights the effect of front instabilities and interfacial forces at immiscible capillary-dominated flow regimes and brings new data on dynamics of pore invasion at this flow condition. Further investigations regarding the effect of wettability, pore shape will be performed and the role of corner flow dynamics on CO_2 storage capacity and storage mechanisms will be considered as future steps.

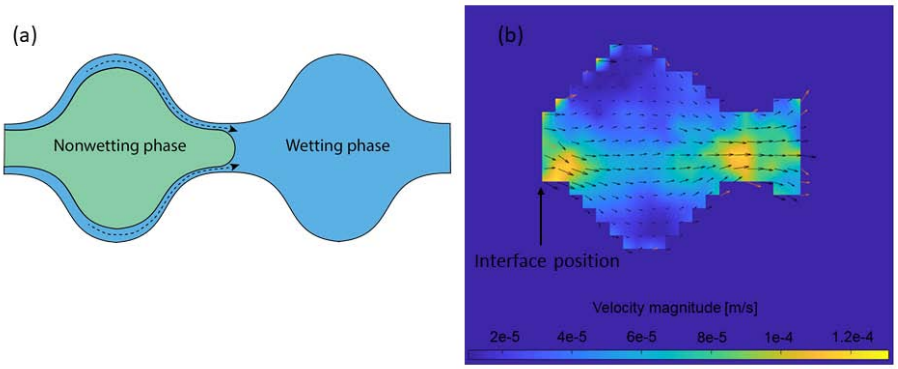

Figure 1: (a) The front is pinned at a constriction before an invasion by Haines jumps mechanism. The pressure gradient from corner wetting fluid to the front is specified schematically by the direction of corner flows. (b) Micro-PIV results in the wetting fluid in porous media during the pinning behavior of the interface. Velocity vectors are average of the velocity over the time-span of the pinning behavior.

References

[1] Lenormand. R, Numerical models and experiments on immiscible displacements in porous media, *Journal of fluid mechanics*, 189, 165–187 (1988).

[2] Moebius. F, Interfacial jumps and pressure bursts during fluid displacement in interacting irregular capillaries, *Journal of colloid and interface science*, 377, 406–415 (2012).

[3] Roman. S, Particle velocimetry analysis of immiscible two-phase flow in micromodels, *Advances in Water Resources*, 95, 199–211, (2012).

Modeling of Evaporative Soil Salinization induced By Salt Recycling in Irrigated Arid Regions (Tunisia)

S. Maiza[a], E.Mejri[a], N.Zemni[a], I.Askri[c], J.Hommel[b], R. Helmig[b], and R. Bouhlila [a]

[a]Department of Modeling in Hydraulics and Environment, National Engineering School of Tunis, University Tunis El Manar, Tunisia.
[b]Department of Hydromechanics and Modeling of Hydrosystems, University of Stuttgart, Stuttgart, Germany.
[c] Department of Civil Engineering, National Engineering School of Gabes, Tunisia

Keywords: Coupled Free Flow- Porous Media system, Evaporative salinization, Irrigation Return flow, Salt precipitation, Numerical Modeling.

1 Introduction

Evaporative soil salinization is a predominant problem worldwide, especially in the long-term irrigated lands with brackish shallow groundwater in arid regions. This white hazard represents a real threat to the environment and sustainable agriculture [4]. The process of soil salinization is well investigated in the literature by focusing on saline water evaporation from porous medium and land-atmosphere interaction processes [6]. However, most of these studies are conducted without consideration of the complete soil salinization cycle.

The objective of the present work is the modeling of evaporation-soil salinization processes induced by salt recycling through irrigation return flow, with a particular focus on the evaporation front [2].

The numerical model accounts for a single-phase compositional gas flow for the free-flow region coupled with a non-isothermal multi-phase compositional porous medium flow [2][3]. The constructed model is implemented in the numerical modeling framework and open-source simulator DuMux [1].

The newly developed model will be calibrated and validated through laboratory experimental data and applied for simulating sequences of evaporation and salt precipitation under real climatic conditions related to a Southern Tunisian oasis.

References

[1] Flemisch, B., Darcis, M., Erbertseder, K., Faigle, B., Lauser, A., Mosthaf, K., Mthing, S., Nuske, P., Tatomir, A., Wolff, M. and R. Helmig, DuMux: DUNE for Multi-Phase, Component, Scale, Physics, ...Flow and Transport in Porous Media. Advances in Water Resources 34(9): 1102-1112 (2011).

[2] Jambhekar, V. A., Helmig, R., Schröder, N., & Shokri, N, Free–Flow–Porous–Media Coupling for Evaporation-Driven Transport and Precipitation of Salt in Soil. Transport in Porous Media, 110(2), 251–280. doi:10.1007/s11242-015-0516-7(2015).

[3] Mejri, E, Modelling and analyses of salt precipitation on evaporation processes in the unsaturated zone, Ph.D. thesis in Hydraulic Engineering, National Engineering School of Tunis.133p (2018).

[4] Askri, B., Bouhlila, R., & Job, J. O, A conceptual hydrologic model for studies of salinization in Tunisian Oases. International Journal of Water Ressources and Arid Environments 1(6): 428-439 (2011).

[5] Milnes, E., & Perrochet, P., Direct simulation of solute recycling in irrigated areas. Advances in Water Resources, 29(8), 1140–1154. doi: 10.1016/j.advwatres.2005.09.004 (2006)

[6] Slama, F., Zemni, N., Bouksila, F., De Mascellis, R., & Bouhlila, R., Modeling the Impact on Root Water Uptake and Solute Return Flow of Different Drip Irrigation Regimes with Brackish Water. Water, 11(3), 425. doi:10.3390/w11030425 (2019).

Mechanics of porous media: deformation, failure, damage

Structural, chemical and hygric characterization of antique Dutch tiles and their susceptibility to salt damage

T. Chekai[a,b], R. Wijnhorst[c], P. Senechal[b], M.P. Isaure[d], S. de Miranda[e], L. Pel[f], N. Shahidzadeh[c], H. Derluyn[a,b]

[a]*Universite de Pau et des Pays de l'Adour, E2S UPPA, CNRS, TOTAL, LFCR UMR 5150, Pau, France*
[b]*Universite de Pau et des Pays de l'Adour, E2S UPPA, CNRS, DMEX UMS 3360, Pau, France*
[c]*Van der Waals-Zeeman Institute, Institute of Physics, University of Amsterdam, Science Park 904, 1098 XH Amsterdam, The Netherlands*
[d]*Universite de Pau et des Pays de l'Adour, E2S UPPA, CNRS, IPREM UMR 5254, Pau, France*
[e]*Department of Civil, Chemical, Environmental, and Materials Engineering (DICAM), University of Bologna, Viale del Risorgimento 2, Bologna 40136, Italy*
[f]*Eindhoven University of Technology, Department of Applied Physics, Transport in Permeable Media, P.O. Box 513, 5600 MB Eindhoven, The Netherlands*

Keywords: Crystallization damage, layered porous materials, tiles, x-ray tomography

1 Introduction

Cultural heritage is exposed to many deteriorating processes around the world. Degradation induced by salt crystallization is one of the main mechanisms that threaten artefacts such as sculptures, ceramics, or frescoes. These artworks are typically made of an assembly of layered materials with different physicochemical properties. Although much progress has been made in recent years to understand the impact of salt crystallization on single porous media, many questions remain unanswered when salt damage occurs in layered materials and on the role of the interfaces between the material layers. This gave the motivation for the JPI-CH project CRYSTINART that aims to develop an integrated approach for modelling and analysis of the decay of artworks due to salt crystallization in layered materials.

In that context, the purpose of this study is to characterize the structural, chemical and hygric properties of antique Dutch tin-glazed tiles from the 19th century, and the effect of these properties on the susceptibility to salt damage. These tiles are ceramics that are mainly made of a mixture of calcium-rich clays coated with glaze. This material is prone to different types of glaze defects induced by salt weathering, they are manifesting by (1) glaze peeling, (2) crazing which is glaze cracking due to high surface tension and (3) shivering which is a process that occurs when the separation between the glaze and the body induces the removal of a portion from the body [1].

2 Experimental study

2.1 Structural, chemical and hygric characterization

The tiles' structure was studied by scanning electron microscopy and X-ray micro-tomography, as depicted in Figure a-b. The tiles consist of a glaze layer of about 380µm thickness and a clay body of about 8mm in height. The glaze itself is in principle non-porous, but air and gas bubbles can be formed during the firing of the tile in the manufacturing process (black square in Figure a-b) [6]. The open porosity of the bi-layered material was determined from a vacuum saturation test (standard NF EN 1936) and also using the X-ray images of the material and amounts to 29%. The full porosity of the clay as well as for the glaze was estimated using CT images of samples of the material, and it was estimated to 26% for the clay part, and 14% for the glaze layer. The tile clay body was analyzed by X-ray diffraction and X-ray fluorescence to characterize its crystallized mineral phases and chemical composition, respectively. The main crystal phases are quartz, calcite, albite and muscovite, and calcium, iron, and lead are abundant. No salts were detected, implying that the source for salt damage must be external.

A common external source of salts is capillary rise [2], [3], [4]. By varying environmental conditions (relative humidity, temperature), the material is then exposed to cycles of drying and rewetting, inducing salt weathering. To characterize the hygric behavior of the tiles, a drying test, as well as a hygroscopic test, was performed with pure water on two types of tiles: (1) with intact glaze, (2) with craquelure (red square in Figure a-b), i.e. with fractured glaze. For the drying test, saturated cylindrical samples of 5mm in diameter and 8mm

in height were sealed circumferentially and at the bottom, and subsequently exposed to an environment of 57% RH and 21 °C. As such, drying could only occur via the glaze layer. The samples with craquelure showed a faster drying, which is logical since the vapor permeability is increased in the presence of the fractures. Surprisingly, also the samples with intact glaze dried, indicating that the glaze layer is not fully impermeable. For the hygroscopic test, samples of 2x2x0.8cm were exposed to steps in relative humidity at 23°C, without sealing the surfaces. The hygroscopic moisture content was determined once the samples were in equilibrium with the surrounding environment. The hygroscopic sorption curves are presented in Figure c, showing a change in the hygroscopic behavior of the tile when the glaze is fractured. The higher moisture uptake for samples with craquelure suggests that the fracture network increases the hygroscopic sorption capacity of the tile. Further tests are ongoing in order to elucidate on the moisture transport through the glaze layer.

2.2 Salt weathering

Cylindrical samples (5mm in diameter and 8mm in height) with and without craquelure are being weathered through wetting-drying cycles, using a 5.5 molal NaCl solution and a 1.26 molal Na_2SO_4 solution. The tiles are exposed to the solutions for 10 minutes, then let to dry at 25% RH and 21°C with sealing of all the sides except the one of the glaze. X-ray scans are performed on the tiles before, during and after the salt weathering test to monitor structural changes and crystallization damage.

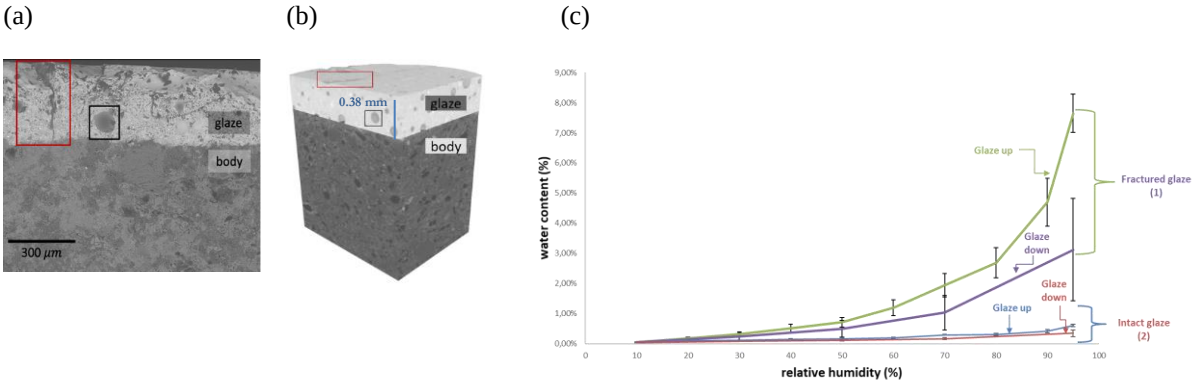

Figure 1: (a)-(b): SEM image and 3D X-ray CT reconstruction of the glaze-body interface. An example of craquelure is marked in the red square and an example of an air bubble within the glaze in the black square. (c) Hygroscopic sorption curve of the Dutch tile: fractured glaze (1), intact glaze (2).

Acknowledgement

The authors acknowledge the support from the European project CRYSTINART through the joint Programming initiative on cultural Heritage (JPI-CH).

References

[1] B. H. Wilson, Monograph and Bibliography on Terra Cotta, *J. Am. Ceram. Soc.*, vol. 9, no. 2, pp. 94–136 (1926).
[2] E. Sebastián, G. Cultrone, D. Benavente, L. Linares Fernandez, K. Elert, and C. Rodriguez-Navarro, Swelling damage in clay rich sandstones used in the church of San Mateo in Tarifa (Spain), *J. Cult. Herit.*, vol. 9, no. 1, pp. 66–76 (2008).
[3] H. Derluyn, H. Janssen, and J. Carmeliet, Influence of the nature of interfaces on the capillary transport in layered materials, *Constr. Build. Mater.*, vol. 25, no. 9, pp. 3685–3693 (2011).
[4] R. M. Espinosa-Marzal and G. W. Scherer, Impact of in-pore salt crystallization on transport properties, *Environ. Earth Sci.*, vol. 69, no. 8, pp. 2657–2669 (2013).
[5] L. Dei, M. Mauro, P. Baglioni, C. Manganelli Del Fà, and F. Fratini, Growth of crystal phases in porous media, *Langmuir*, vol. 15, no. 26, pp. 8915–8922 (1999).
[6] K, van Lookeren Campagne et al., "Understanding 17th-18th century Dutch Tin-glaze Through the Interpretation and Reconstruction of Historical Recipes." GlazeArt2018, pp 150-164.

Microstructure of concrete made with recycled concrete aggregates after exposure to elevated temperatures

B. Fernandes[a], C. Gaborieau[b], H. Carré[a], J.-C. Mindeguia[b], C. Perlot[a], Y. Anguy[b], C. La Borderie[a], L. Pigot[c]

[a] *Université de Pau et des Pays de l'Adour, E2S UPPA, SIAME, Anglet, France*
[b] *I2M, UMR CNRS 5295, 33405 Talence, France*
[c] *G&E / Carnot Isifor – Ensegid, 33607 Pessac, France*

Keywords: concrete, temperature, microstructure

1 Introduction

Standard concrete is usually composed of cement paste (binders and water), fine aggregates (such as sand) and coarse natural aggregates (NA). In the last years, recycled concrete aggregates (RCA) have gained popularity as a partial or total substitute to NA, as RCA have the potential to produce sustainable concrete with a relative good mechanical performance [1], [2]. Although much work has been done over the past years, some issues need to be further addressed to promote the usage of RCA in concrete. One of these issues is the high temperature behaviour (e.g. during a fire) of concrete made with RCA.

When exposed to high temperature, concrete suffers physicochemical changes, resulting in modified mechanical properties, cracking and spalling [3]. These changes are directly related to changes in the underlying microstructure. This is even more important in the case of RCA, due to its nested microstructure. The RCA itself is indeed composed of two different materials: natural aggregates and attached (or adhered) old cement paste. Therefore, concrete with RCA presents a larger variety of interfaces than standard concrete i.e. interfacial transition zone (ITZ) between (old) aggregates and old cement paste, between new cement paste and (old and new) aggregates, and interfaces between old and new cement pastes [4]. The latter may be regarded as one of the most significant features of RCA-based concrete.

The aim of this study is to evaluate the microstructural behavior of concrete made with RCA after exposure to high temperatures. Scanning electron microscopy (SEM) and energy dispersive X-ray spectrometry (EDS) were used to evaluate the microstructure and the interfaces after exposure to elevated temperatures.

2 Methodology

Concrete cubes of 15 x 15 x 15 cm were produced. The concrete mix was done with Cement CEM II/A-L 42.5 R (420 kg/m^3), limestone filler Betocarb (60 kg/m^3), Alluvial Sand (799.8 kg/m^3), RCA 4/10 (291.5 kg/m^3) and RCA 10/20 (630.3 kg/m^3). Concrete presented a water/cement ratio of 0.4 and to improve workability, superplasticizer SIKA ViscoCrete Tempo-483 was used (0.9 %). Concrete presented a slump of 180 mm and a 28-days compressive strength of 45.5 MPa.

From these cubes, small prisms of 4.5 x 3 x 2 cm were cut using a diamond saw. These samples were dried in an oven at 80 °C for 24 hours. Then, the samples were heated in an electric furnace to different target temperatures: 200 °C, 400 °C and 600 °C. After each one of these thermal cycles, ex-situ analyses were carried. The microstructural analysis was done using an environmental SEM (FEI Quanta FEG 250) and the chemical mapping was done with an EDAX energy dispersive X-ray spectrometer (EDS). The same regions were analyzed for each temperature.

3 Results

A sample of concrete made with RCA dried at 80 °C was used to illustrate the microstructural analysis. By combining SEM images (Fig. 1A) and X-ray EDS elemental chemical maps (Figs. 1B-C), it is possible to delineate accurately the abovementioned interfaces, and in particular the transition between the new and the old cement paste. In the elemental maps of magnesium (Mg) (Fig. 1B) and potassium (K) (Fig. 1C), there is a clear distinction between the old cement paste of the RCA (on top of the image) less concentrated in Mg and more concentrated in K compared to the new paste used to make this RCA-based concrete. In these images, fine aggregates, mostly sand grains, appears in black in Figs. 1B-C and in mid-grey in Fig. 1A.

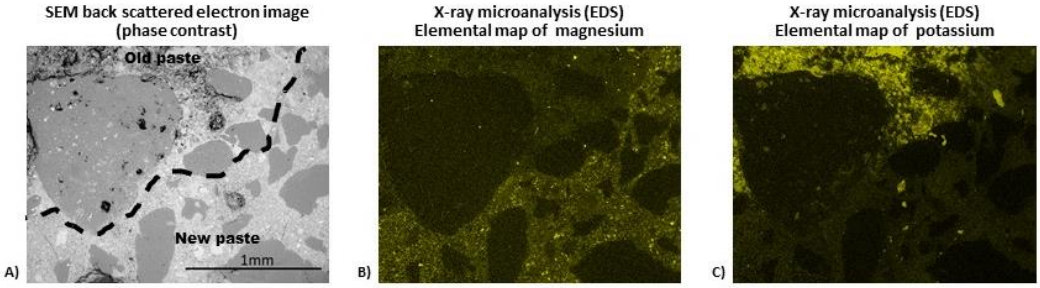

Figure 1: SEM image (back scattered electrons) (A) and X-ray EDS elemental chemical maps (B and C)

Fig. 2 illustrates another zone of the same sample. In Fig. 2B, the collection of X-ray spectra acquired at each pixel in Fig. 2A is synthetized through a statistical approach which allows to exhibit N phases (N = 4), each phase being characterized by its average phase X-ray spectrum. The chemical quantification (ZAF method) of the average phase X-ray spectra reveals the presence of two different cement pastes i.e. phase 1 in blue (new paste) and phase 3 in green (old paste) whose interface is again clearly delineated.

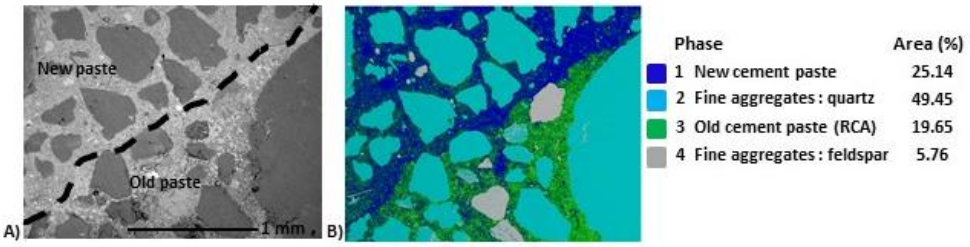

Figure 2: A) SEM image (back scattered electrons (80°). B) Statistical phase reconstruction based on the X-ray chemical spectra acquired at each pixel in Fig. 2A.

Regarding the high temperature behavior, the question becomes whether the highlighted paste–paste interfaces, which characterize RCA-based concrete, promote crack development. Fig. 3 shows SEM micrographs of the area shown in Fig. 2 at different temperatures. At 200 °C, cracks initiate around sand grains, both in the new and in the old cement paste. These cracks are essentially perpendicular to the new paste/old paste interface. In this respect, the paste-paste interface would not promote extra fractures. Further increase of the temperature leads to a higher connection between cracks. At 600 °C, crack opening significantly increases.

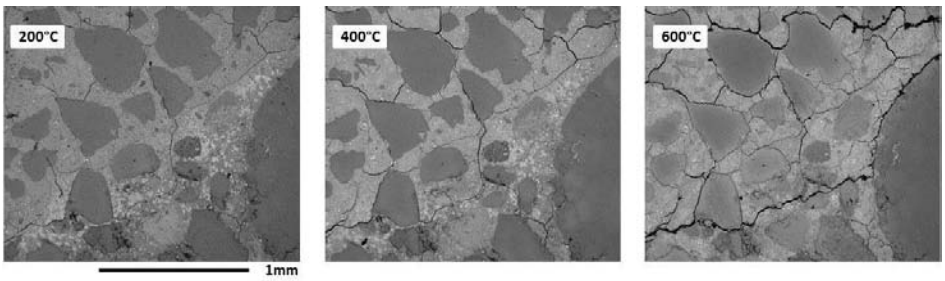

Figure 3: SEM micrographs of the are displayed in Fig. 2 (80°C) after heating the sample up to 600°C.

These structural and chemical exploratory analyses at the microscopic scale support that paste-paste interfaces do not promote extra fracture development. Hence, the different interfaces did not represent a major drawback in terms of concrete post-heating behaviour. Further analysis, comparing these results with concrete with NA, may validate the spreading use of RCA to make sustainable concrete.

References

[1] C. Shi, Y. Li, J. Zhang, W. Li, L. Chong, and Z. Xie, Performance enhancement of recycled concrete aggregate - A review, *Journal of Cleaner Production*, vol. 112, pp. 466–472 (2016).
[2] F. de Larrad and H. Colina, Concrete Recycling: Research and Practice. CRC Press (2019).
[3] B. Georgali and P. E. Tsakiridis, Microstructure of fire-damaged concrete. A case study; *Cement and Concrete Composite,* vol. 27, pp. 255-259 (2005).
[4] M. Pepe, R. D. Toledo Filho, E. A. B. Koenders, and E. Martinelli, Alternative processing procedures for recycled aggregates in structural concrete, *Construction and Building Materials,* vol. 69, pp. 124-132 (2014).

Study on the poromechanical behavior of coalbed methane affected by gas mixture adsorption in nanopores of complex geometry

Quoc Dat Ha[a], Tien Dung Le[a], Irina Panfilov[a], Christian Moyne[a]

[a]*University of Lorraine, CNRS, LEMTA, F-54000 Nancy, France*

Keywords: Poromechanics, Adsorption isotherm, Solvation force, Fundamental Measure Theory

1 Introduction

Gas adsorption phenomena play an important role in coalbed methane recovery as the main gas quantity is stored within the nanopore network in the coal matrix in adsorbed state. Moreover, the adsorbed gas pressure in the nanopore has a magnitude much larger than the bulk pressure in large pores which changes dramatically the mechanical behavior of the medium [1, 2, 3]. To enhance the methane recovery, CO_2 can be injected into the reservoir in order to replace the adsorbed CH_4 at the adsorption sites and increase the CH_4 production. However, due to the higher adsorption potential of CO_2, it may induce the matrix swelling and consequently close the natural fractures (cleats) and reduce the permeability [2, 3]. Understanding these phenomena allow us to predict the deformation of coal seam and the change of the permeability during the CH_4 production and CO_2 injection periods.

The present work aims at building a two-scale poromechanical model for the coalbed methane reservoir considering the adsorption effects of a fluid mixture in nanopores. The confined fluid mixture density profiles are computed by using the Density Functional Theory (DFT). The gas molecules are considered as hard-sphere fluids which interact between them by a Lennard-Jones potential. The hard sphere/hard sphere short range interaction is treated by the Fundamental Measure Theory (FMT). In addition, the fluid molecules/solid wall interaction is also considered as Lennard-Jones type interaction. The novelty of this work is the development of a new numerical method to compute the confined fluid mixture densities in any three-dimensional pore geometry. The nanopore is discretized in voxels and Fast Fourier Transform (FFT) is used to solve the convolution terms having tremendous advantage in terms of execution time, computer resources and calculation accuracy. Regardless of molecule diameters disparity, this approach is not limited to some ideal geometries reported in the literature as slit, cylindrical or spherical pores where analytical solutions exist. This provides a powerful tool to compute the fluid mixture adsorption in complex pore geometries. Given the fluid densities, the solvation force, which is the adsorption-induced-force exerted on the solid wall by the fluid, can be computed in arbitrary geometries for a Lennard-Jones fluid using a new formula developed within this work. It is shown that the solvation force is negative with a magnitude much larger than the bulk pressure. In this context, this force is taken into account in the two-scale poromechanical model giving an additional term in the macroscopic law due to the adsorption effect.

2 Gas adsorption isotherm and solvation force

The proposed method is applied to study the adsorption competition between CH_4 and CO_2 in an ellipsoidal nanopore. The dimensionless gas density distributions are presented in the Fig. 1 in two perpendicular planes Oxz and Oyz (where Ox and Oy refer to two semi-major axes, Oz the semi-minor one). The adsorption peaks for the both gases obtain the maximum values in the vicinity of pore surface (red color) as a consequence of hard-sphere/hard wall effect and solid/fluid Lennard-Jones type interaction. We can observe that with the same bulk density values, the adsorbed quantity of CO_2 is much larger than the CH_4 one due to the higher attractive potential of CO_2 with the solid wall. That explains why the CO2 injection can enhance the CBM recovery.

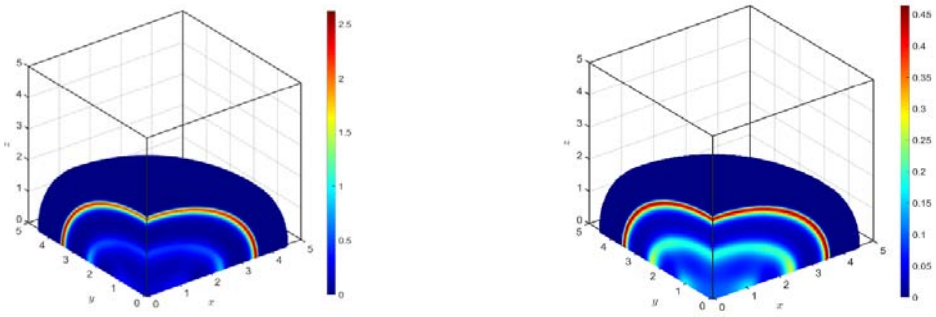

(CO_2) (CH_4)

Figure 1. Dimensionless gas densities in an ellipsoidal pore with $a = b = 4.5d_{\mathrm{CH_4}}, c = 3.5d_{\mathrm{CH_4}}$ and bulk densities $\rho^b_{\mathrm{CH_4}} d^3{}_{\mathrm{CH_4}} = \rho^b_{\mathrm{CO_2}} d^3{}_{\mathrm{CH_4}} = 0.05$ (a, b, c refer to two semi-major and semi-minor axes, $d_{\mathrm{CH_4}}$ the CH_4 molecule diameter)

Given the gas densities, the solvation force can be calculated at the surface of the ellipsoidal pore. We can observe in Fig. 2 that in complex geometries such as ellipsoidal cavities, the solvation force does not reduce to a uniform pressure but includes both normal and tangential components which are not uniform at the pore surface. The tangential part is considerably smaller than the normal part. This force, depending on the bulk densities, is generally negative with an absolute value much higher than the bulk pressure.

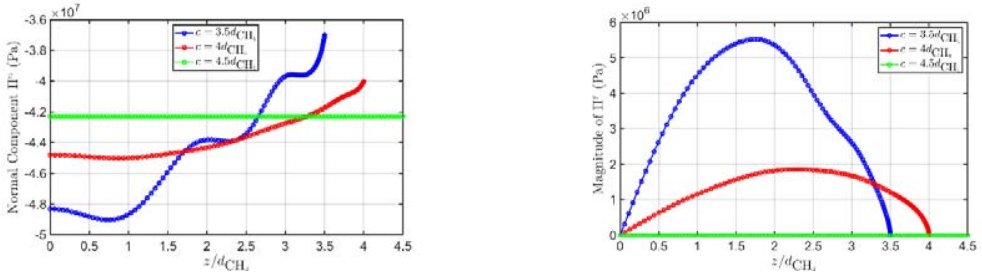

Normal component *Magnitude of tangential component*

Figure 2. Solvation force components

3 Two-scale poromechanical model

The mechanical problem at the pore-scale is developed considering the solvation force exerted on the solid surface by the fluid phase. Homogenization method is used to upscale the pore-scale model to derive the macroscopic law at the continuous scale of the coal matrix. The macroscopic total stress is composed of a classical elastic term characterized by an effective stiffness tensor and a second term related to the solvation force obtained by the resolution of a closure problem. In the case of spherical nanopore, this result reduces to a modified poroelastic Biot model where the fluid pressure in the classical model is replaced by the sum of the bulk pressure and the solvation force. Such macroscopic response provides a deep understanding of how the solvation force affects the volumetric deformation of the medium. Our simulation is applied to enhanced coalbed methane recovery for investigating the matrix swelling in increasing CO_2 pressure.

References

[1] Q. D. Ha, T. D. Le, I. Panfilov, and C. Moyne. *Solvation force and adsorption isotherm of a fluid mixture in nanopores of complex geometry based on fundamental measure theory*, Journal of Physics : Condensed Matter, 33(33) :335002 (2021).

[2] T. D. Le, C. Moyne, M. A. Murad, I. Panfilov, *A three-scale poromechanical model for swelling porous media incorporating solvation forces: Application to enhanced coalbed methane recovery*, Mechanics of Materials, 131, 47-60 (2019).

[3] T. D. Le, H. Q. Dat, I. Panfilov, C. Moyne, *Multiscale model for flow and transport in CO_2 -enhanced coalbed methane recovery incorporating gas mixture adsorption effects,* Advances in Water Resources, 144, 103706 (2020).

Numerical Modeling of Evaporative Salinization and Crystallization-Induced Deformations in Building Stone

A. Mannai[1], E. Mejri[1], L. Guellouz[1], J. Hommel[2], R. Helmig[2], and R. Bouhlila[1]

1 Department of Modeling in Hydraulics and Environment, National Engineering School of Tunis, University Tunis El Manar, Tunisia.
2 Department of Hydromechanics and Modeling of Hydrosystems, University of Stuttgart, Stuttgart, Germany.

Keywords: *Salt weathering, numerical modelling, drying evaporation, coupling, effective stress.*

Abstract

Crystallization of evaporites within and on rock surfaces often damage the host rock, this phenomenon is called salt weathering. The latter is commonly noticed as one of the major factors in deterioration of building materials and historical architecture. The environmental changes (especially relative humidity and fluctuations in temperature) can promote changes in the location and/or in the way salt crystallization and growth take place, either promoting the formation of efflorescence or generating sub-florescence which causes stone degradation resulting from high crystallization pressures [4].
The main objective of this work is modelling the process of salt crystallization in building materials under drying conditions, taking into account the interactions between the porous media mainly stone and the atmosphere and the mechanical effect of salt crystallization within the porous media.

Thanks to the developed Free Flow-Porous Medium model, we capture the complex interactions between varying environmental conditions and the processes inside the pore space during saline-water evaporation [3]. The model performance is illustrated by simulating sequences of evaporation and salt crystallization inducing rock damage under the influence of climatic conditions. Therefore, the fundamental laws of the mass, momentum and energy exchange between the FF and the PM region coupled with the theory of poro-mechanics [2] and crystallization kinetics, are used to construct the model which is implemented in the numerical modeling framework and open-source simulator DuMux [1].

A further experimental set up illustrating the impact of evaporation-driven salinization on the damage of monuments in an archeological site in Tunisia will be proposed in order to calibrate and validate the proposed framework.

References

[1] Flemisch, B., Darcis, M., Erbertseder, K., Faigle, B., Lauser, A., Mosthaf, K., Mthing, S., Nuske, P., Tatomir, A.,Wolff, M. and R. Helmig): DuMux: DUNE for Multi-Phase, Component, Scale, Physics, ...Flow and Transport in Porous Media. *Advances in Water Resources* 34(9): 1102-1112 (2011).

[2] Guellouz,L: Modélisation du couplage hydraulique mécanique dans les sols non saturés : Application aux barrages en terre, *Ph.D Dissertation of University AIX-MARSEILLE II.*150p (1995).

[3] Mejri, E.: Modelling and analyses of salt precipitation on evaporation processes in the unsaturated zone, *PhD thesis in Hydraulic Engineering, National Engineering School of Tunis.*133p (2018).

[4] Rodriguez-Navarro, C. Doehne, E: Salt weathering: influence of evaporation rate, supersaturation and crystallization pattern. *Earth Surface Processes and Landforms*, 24: 191-209 (1999).

Influence of the contact properties on the behavior of biocemented sand

M. Sarkis, A. Naillon, F. Emeriault, C. Geindreau

Univ. Grenoble Alpes, CNRS, Grenoble INP, Laboratoire 3SR
1270 rue de la Piscine, 38400 Saint Martin d'Hères, France
e-mail: marilyn.sarkis@univ-grenoble-alpes.fr

Keywords: Bio-cementation, D.E.M., Micro-mechanics

1 Introduction

In the early 21st century, it has been proven that bacterial activity in the soil matrix accelerates the calcite crystals ($CaCO_3$) deposit at the grain contacts [1]. This process, known as bio-calcification, soon became a novel way to reinforce sand [2], [3], by transforming the latter into sandstone by means of calcite bridges between the sand particles. Many mechanical tests on bio-cemented sand have been conducted the macroscopic behaviour of this material, and it has been shown that the mechanical properties are highly improved without affecting the permeability. Indeed, only a small volume fraction of calcite, is needed to dramatically increase the macroscopic properties However, what remains missing are the mechanics at the contact scale. For instance, the tensile and shear strengths of the bonds are unknown, and represent important input parameters for a numerical model that aims to predict the response of bio-cemented sand under different types of loadings. The final goal of this work is to develop a numerical model, using the discrete element method (D.E.M.), that is capable of reproducing the increase of the mechanical properties of bio-cemented sand under a triaxial loading observed experimentally, with the increase of the amount of precipitated calcite. Contacts properties of bio-cemented sand (contact surface area, percentage of cohesive contacts, tensile and shear strengths of the bonds…) represent important input parameters for a numerical model that aims to predict the response of bio-cemented sand under different types of loadings. In the present work, a first D.E.M. model is presented taking account the cohesive contact surface areas distribution and the percentage of cohesive contacts measured from X-ray tomography.

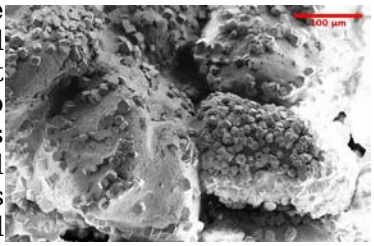

Figure 1: S.E.M. image of bio-cemented fontainebleau sand

2 D.E.M. model based on X-ray tomography measurements

The proposed model has been made with the discrete element method (D.E.M.) using the software Yade [4]. The contact law used is a cohesive law that uses Cundall's linear elastic plastic law with adhesion at the contacts [5]. This model takes as input some geometrical parameters, which are the contact surface area distribution that were measured from X-Ray tomography images in [6], as well as the different types of contacts : purely cohesive (new contact created by cementation), frictional (former frictionnal contact wich has not been cemented), or mixed (former frictional contact wich has been cemented). The adhesion forces, that represent in our case the calcite bonding, are calculated at each contact starting from the cohesive contact surface areas.

The fixed parameters are:

- The inter-particle friction angle: Φ=20°,
- The diameter of the sand particles: D=210 µm

- The tensile strength of the calcite: σ_{tens}=2.75 MPa, previously calibrated by [7],
- The density and poisson ratio of the sand and the calcite: ρ=2640 kg/m3 and ν=0.25.

As for the variable parameters, we have:

- The Young's modulus E_m of the grains that control the stiffness of the sample, that is changed depending on the degree of cementation,
- The mean cohesive contact surface area S_c and its standard deviation $\bar{\sigma}$, computed from X-ray tomography,
- The percentage of cohesive contacts.

Our model is capable of reproducing well the mechanical behaviour of bio-cemented sand under triaxial loading for a low degree of cementation (Figure 2(a)). However, in the case of a high degree of cementation, the model underestimates the stress peaks (Figure 2(b)). The numerically calculated friction angle does not exhibit a sharp increase with the increase of the degree of cementation compared to the experimental values (Figure 2(c)). However, the values of the cohesion are similar in both cases (Figure 2(d)).

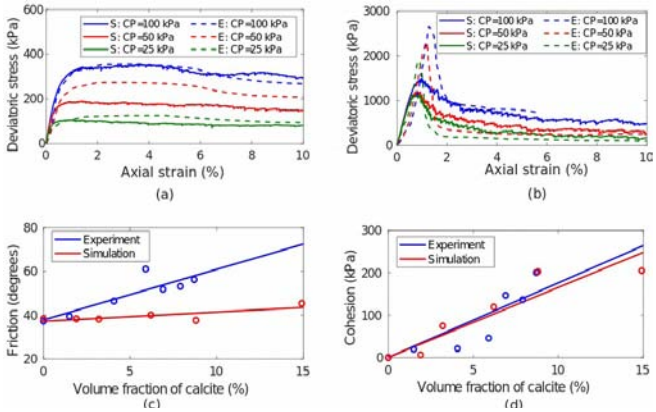

Figure 2: (a) Numerical and experimental response for low-cemented sand, (b) Numerical and experimental response for highly-cemented sand, (c) Evolution of the friction angle with the volume fraction of calcite, (d) Evolution of the cohesion with the volume fraction of calcite

Conclusion

As previously mentioned, the shear and tensile strengths of the cemented contacts were numerically calibrated, however there is no experimental data regarding the micro-mechanics of the material in question. Since these two parameters are essential inputs to our numerical model, and since the macroscopic behavior of bio-cemented sand is highly governed by what is happening at the contact scale, micro-mechanical experiments are currently being conducted in order to measure the tensile and shear strengths of one cemented contact between two grains of sand, as well as some other parameters.

References

[1] S. Castanier, G. Le Métayer-Levrel, and J.-P. Perthuisot, "Bacterial Roles in the Precipitation of Carbonate Minerals," in *Microbial Sediments*, R. E. Riding and S. M. Awramik, Eds. Berlin, Heidelberg: Springer Berlin Heidelberg, 2000, pp. 32–39.

[2] V. S. Whiffin, L. A. Van Paassen, and M. P. Harkes, "Microbial carbonate precipitation as a soil improvement technique," *Geomicrobiol. J.*, vol. 24, no. 5, pp. 417–423, 2007.

[3] J.-S. Lee and J. C. Santamarina, "Bender elements: performance and signal interpretation," *J. Geotech. geoenvironmental Eng.*, vol. 131, no. 9, pp. 1063–1070, 2005.

[4] V. Šmilauer *et al.*, "Yade Documentation," 2015, doi: 10.5281/zenodo.32409.

[5] F. Bourrier, F. Kneib, B. Chareyre, and T. Fourcaud, "Discrete modeling of granular soils reinforcement by plant roots," *Ecol. Eng.*, vol. 61, no. 1 PARTC, pp. 646–657, 2013, doi: 10.1016/j.ecoleng.2013.05.002.

[6] A. Dadda, C. Geindreau, F. Emeriault, S. Rolland du Roscoat, A. Esnault Filet, and A. Garandet, "Characterization of contact properties in biocemented sand using 3D X-ray micro-tomography," *Acta Geotech.*, vol. 14, no. 3, pp. 597–613, 2019, doi: 10.1007/s11440-018-0744-4.

[7] A. Dadda, "Étude Mécanique Et Microstructurale Des Sols Bio-Cimentés : Application Aux Ouvrages Hydrauliques En Terre," 2017.

Behavior of complex fluids in porous media

Study of the nanoscopic fluid film involved in the crystallization of water in a porous material by a Non-Local Density Functional Theory framework

A. Barthes[a*], M. Pérez[a], T. Bernet[b], M. Piñeiro[c], M. Conde[d], D. Grégoire[a,e], C. Miqueu[a]

[a]*Universite de Pau et de Pays de l'Adour, E2S UPPA, CNRS, LFCR, Anglet, France*
[b]*Department of Chemical Engineering, Imperial College London, UK*
[c]*Universidad de Vigo, Spain*
[d]*Universidad Politécnica de Madrid, Spain*
[e]*Institut Universitaire de France, Paris, France*
**corresponding author: abarthes@univ-pau.fr*

Keywords: nanopore, crystallization, Density Functional Theory, water

Abstract:

Water confined in porous materials has attracted great attention due to its large number of application (e.g. geosciences, biology, nanotribology). Crystallization of water in porous media involves extremely high pressures able to produce the deformation of the porous matrix. When crystallization occurs in a pore, the interactions between the crystal and the skeleton have led to the concept of "crystallization pressure" [1]. It has been supposed that the interaction should be mediated by the presence of a thin water fluid film (a few nanometer thick) located in between them. This study aims to describe the thin water film occurring between the ice crystal and the solid surface of a porous material during crystallization and to compute the pressure of this inhomogeneous film. A molecular non-local Density Functional Theory (NLDFT) [2] coupled with the Statistical Associative Fluid Theory for potential of variable range (SAFT-VR) [2] has been developed and employed to obtain the equilibrium distribution of water molecules confined into this slit-like nanopore consisting of the wall of ice on one side and a graphitic surface on the other side. Several configurations are explored by changing both the thermodynamic conditions and the water film width.

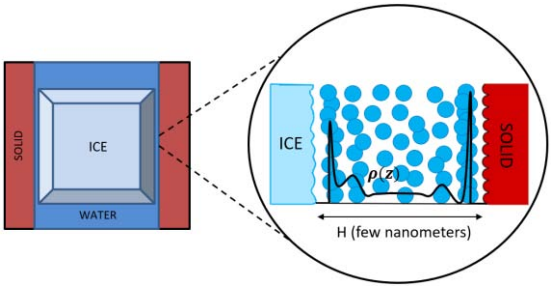

Figure 1: Ice crystal confined between two solid surfaces of a slit pore. Thin water film between a wall of ice and a graphitic surface with a schematic representation of the asymmetric water density profile ρ(z) obtained at equilibrium with NLDFT-SAFT-VR coupling.

Acknowledgements: This work is financed by the Investissement d'Avenir French programme (ANR-16-IDEX-0002) under the framework of the E2S UPPA hub Newpores.

References

[3] Steiger, M. Crystal growth in porous materials—I: The crystallization pressure of large crystals, *Journal of Crystal Growth*, 282, 455-469 (2005).
[4] Evans, R. The Nature of Liquid-Vapor Interface and Other Topics in the Statistical Mechanics of Non-Uniform Classical Fluids, *Advances in Physics*, 28, 143-200 (1979).
[5] Chapman, W.G, Gubbins, K.E., Jackson, G., Radosz, M. SAFT: Equation-of-state solution model for associating fluids *Fluid Phase Equilibria*, 52, 31-38 (1989).

Fractured porous media (prospecting, production, storage)

Primal hybridizable discontinuous Galerkin methods for modeling flow in fractured porous media

G. Etangsale[a], M. Fahs[b], V. Fontaine[a], H. Hoteit[c]

[a] *Department of Building and Environmental Sciences, University of La Réunion - South Campus, France.*
[b] *Université de Strasbourg, CNRS, ENGEES, LHYGES UMR 7517, F-67000 Strasbourg, France.*
[c] *Physical Science and Engineering Division, King Abdullah University of Science and Technology (KAUST), Thuwal, Saudi Arabia.*

Keywords: Hybridizable discontinuous Galerkin, high-order finite element, fractured porous media, Discrete Fracture-Matrix, numerical experiments, comparisons with COMSOL

Abstract

Modeling fluid flow in fractured porous media has received tremendous attention from engineering, geophysical, and other research fields over the past decades. We focus here on large fractures described individually in the porous medium, which act as preferential paths or barriers to the flow. Two different approaches are available from a computational aspect:

- The first one, and definitively the oldest, consists of meshing inside the fracture. In this case, the flow is governed by a single Darcy equation characterized by a large scale of variation of the permeability coefficient within the matrix region and the fracture, respectively. However, this description becomes quite challenging since it requires a considerable amount of memory storage, severely increasing the CPU time.
- A more recent approach differs by considering the fracture as an encapsulated object of lower dimension, i.e., $(d-1)$-dimension. As a result, the flow process is now governed by distinctive equations in the matrix region and fractures, respectively. Thus, coupling conditions are added to close the problem. This mathematical description of the fractured porous media has been initially introduced by Martin et al. in [4] and is referred to as the Discrete Fracture-Matrix (DFM) model.

The DFM description is particularly attractive since it significantly simplifies the meshing of fractures and allows the coupling of distinctive discretizations such as Discontinuous and Continuous Galerkin methods inside the bulk region and the fracture network, respectively. For instance, we refer the reader to the recent works of Antonietti et al. [1] (and references therein), where the authors coupled the Interior Penalty DG method with the (standard) H_1-Conforming finite element method to solve the DFM problem (see e.g., [3]). However, it is well-known that DG methods are generally more expensive than most other numerical methods due to their high number of coupled degrees of freedom (DOFs) and their large stencils. Therefore, in the present work, we favor families of Hybridizable Discontinuous Galerkin (HDG) methods which are more performant and competitive (thanks to the static condensation) than standard DG counterparts. Furthermore, HDG methods are particularly relevant in the DFM model due to the localization of their DOFs on the mesh skeleton. To our knowledge, only Chave et al. [2] recently designed a discontinuous skeletal approach based on the Hybrid High-Order (HHO) method to address this issue. Numerical experiments are then presented to corroborate our assertions. First, we measure the estimated convergence rates in simple situations characterized by a single fracture proving that the proposed discretization method converges optimally. We therefore investigate the ability of the HDG scheme to handle more complex geometries characterized by intersecting and immersed fractures by comparing our discrete solutions to those of commercial software such as COMSOL.

References

[1] Antonietti P. F., Facciolà C. and Verani M., Unified analysis of discontinuous Galerkin approximations of flows in fractured porous media on polygonal and polyhedral grids, *Mathematics in Engineering*, 2, 340–385 (2020)

[2] Chave F., Di Pietro D. A. and Formaggia L., A Hybrid High-Order method for Darcy flows in fractured porous media, *SIAM Journal on Scientific Computing*, 40, A1063–A1094 (2018)
[3] Kadeethum T., Nick H. M., Lee S. and Ballarin F., Flow in porous media with low dimensional fractures by employing enriched Galerkin method, *Advances in Water Resources*, 142, 103620 (2020)
[4] Martin V., Jaffré J. and Roberts J. E., Modeling fractures and barriers as interfaces for flow in porous media, *SIAM Journal on Scientific Computing*, 26, 1667–1691 (2005)

A pressure transient analysis approach to estimate CO_2 entrapment in fractured reactive formation

Ruben Figueroa-Hernandez, Abdirizak Omar, Hussein Hoteit

Physical Science and Engineering Division, King Abdullah University of Science and Technology, Thuwal, Saudi Arabia

Keywords: CO_2 sequestration, fractured media, fracture clogging, pressure transient analysis, analytical solutions

1 Introduction

The global increase in CO_2 emissions over the last few is of major concern. Long-term CO_2 storage by mineralization into fractured basalts is a promising method. This technology has been demonstrated in Iceland and has potential in Saudi Arabia and other places. Carbonated water injection into fractured basalt could lead to a reduction or increase in fracture conductivity caused by mineral precipitation and dissolution. In this work, we develop a novel method to quantify fracture conductivity alteration due to mineralization.

2 Approach

Using pressure-transient-analysis (PTA), we develop a novel semi-analytical model to identify and quantify the increase or reduction in fracture conductivity due to fracture closing or skin formation from CO_2 mineralization in fractured reactive formation. The fractures are assumed to be planar as shown if Figure 1.

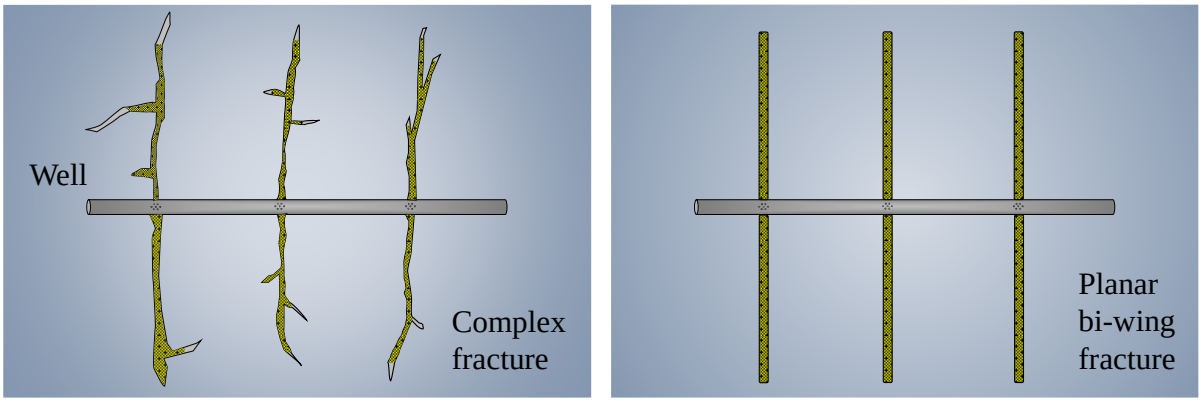

Figure 1: Complex hydraulic fractures (left) with their simplified configuration (right).

By coupling the fractured and matrix regions, we derive the diffusivity equations used to reproduce the pressure behavior during carbonated water injection. The coupled system of diffusivity equation is given by :

$$\frac{\partial^2 p_D}{\partial x_D^2} + \frac{\partial^2 p_D}{\partial y_D^2} = \frac{\partial p_D}{\partial t_D} \text{ in the matrix}$$

$$\frac{\partial^2 p_{f_D}}{\partial x_D^2} + \frac{2}{F_{CD}^*}\frac{\partial p_D}{\partial y_D} = \frac{1}{\eta_D}\frac{\partial p_{f_D}}{\partial t_D} \text{ in the fracture}$$

Where p_D is the dimensionless pressure and the other parameters reflects the fracture conductivity and compressibility. Using a numerical reservoir simulator, we validate our model by analyzing the pressure response for a fractured well. The semi-analytical model is solved in Laplace space to avoid time-dependency of the governing equations and then inverted to time-space. The derived model is capable of accurately capturing the pressure response due to fracture clogging or fracture opening. Comparison with a full-physics simulator showed a good match for the pressure response and its derivative. We also develop a diagnostic approach based on type-curves to quickly identify the current fracture conductivity and its rate of change (see Figure 2). We introduce an indicator parameter to capture the rate of fracture closure as a function of time. This approach provides an important indicator as it could be directly related to the degree and rate of mineralization in the fractures.

This work presents a novel method to identify and quantify fracture mineralization in fractured basalts during CO_2 storage. Complementary to lab studies and reactive transport simulation, type-curves can be used as a quick diagnostic tool to estimate the rate of fracture mineralization. This model can overcome the complexity of simulations and provides a robust approach to assess the success of CO_2 mineralization in fractured basalt and reactive formation.

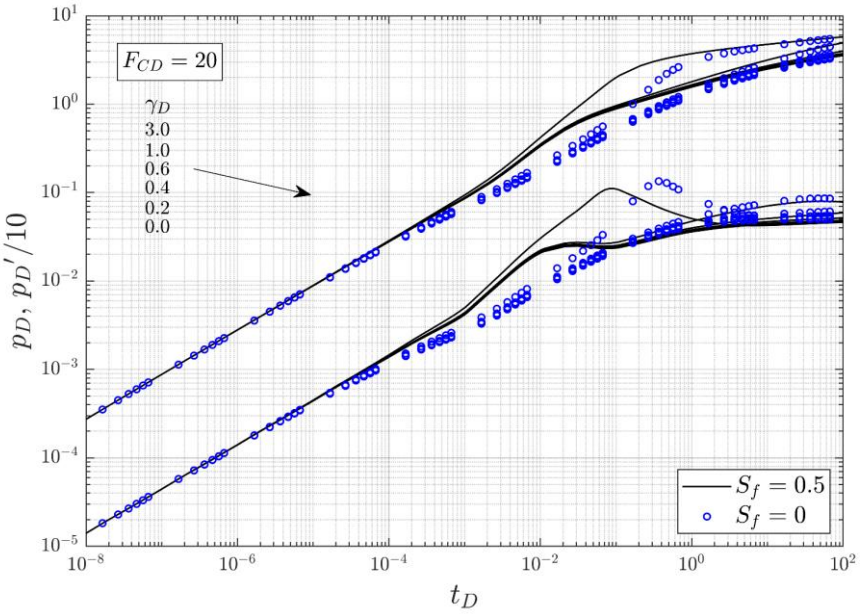

Figure 2: Type curves showing the dimensionless pressure and its derivative which include the effect of fracture clogging ($S_f = 0.5$) compared to original unclogged fracture ($S_f = 0$), where fracture clogging is a result of formation damage (skin) at the fracture inner walls.

References

[1] Lee, T., Park, D., Shin, C., Jeong, D., & Choe, J. Efficient production estimation for a hydraulic fractured well considering fracture closure and proppant placement effects. Energy Exploration & Exploitation, 34(4), 643-658 (2016).
[2] H. Cinco-Ley et al., "Transient pressure analysis for fractured wells," Journal of petroleum technology, vol. 33, no. 09, pp. 1–749, (1981).
[3]K. Liao, S. Zhang, X. Ma, and Y. Zou, "Numerical investigation of fracture compressibility and uncertainty on water-loss and production performance in tight oil reservoirs," Energies, vol. 12, no. 7, p. 1189 (2019).

Near surface geophysics to quantify groundwater storage heterogeneity in weathered/fractured hard rock aquifers

J. A. Mézquita González[a], J-C Comte[a]

[a]*University of Aberdeen, School of Geosciences, UK*

Keywords: Hydrogeophysics, hard rock aquifer, petrophysics, clay

1 Introduction

The problems of supplying fresh water to people around the world are opening new areas of investigation to satisfy the current demand. One of these areas is hydrogeophysics focusing on exploring and monitoring exploiting alternative sources of groundwater. Weathered/fractured basement rock aquifers (also called hard rock aquifers) have long overlooked for large scale water supply due to their relatively low storage capacity, but, since recently are being increasingly studied for their local hydrogeological and geothermal potential and resilience to climate change and pollutions. The actual hydrodynamic properties and behavior of these aquifers are not completely understood and often subject to assumptions, especially with respect to heterogeneity and storage capacity. In this study, near-surface geophysics was used to estimate basement aquifer storage heterogeneity in a non-invasive and cost-effective manner. We performed and analyzed 2D electrical resistivity tomography (ERT), induced polarization (IP), 1D magnetic resonance sounding (MRS) measurements, and borehole geophysical logging acquired in a micaschist catchment in Gortinlieve, Ireland. The dataset includes a variety of resolution scales allowing the development of new approaches to characterize hard rock aquifers in situ from borehole to catchment scales.

The results of this study showed that ERT derived porosities from Archie´s petrophysical model overestimates the values in comparison to Waxman & Smits (WS), a method that considers the influence of the cation exchange capacity (CEC) of clay minerals on the ERT measurements. WS porosities are closer to the specific yield estimated from pumping test in boreholes, MRS water content, and the typical ranges of hard rock aquifers demonstrating WS superiority to Archie and affirming that clay content cannot be neglected when characterizing storage properties in weathered/fractured hard rock aquifers. An important analysis using water content profiles from MRS corroborated the results with a particularly good match at three locations across the study area characterized by deep

weathering/fracturing associated with regional fracture zones. To further verify the ERT porosity models, we tested an alternative approach based on the differential effective medium (DEM) theory applied to time-domain IP data to recover CEC and porosity tomograms. Results of IP data analysis showed that chargeability measurements can be used to provide preliminary porosity estimates and cation exchange capacity (CEC) values when used under certain limits due to the parameters required. Importantly, this approach provides a methodology to estimate porosity without having direct clay minerals measurements. The findings confirmed that near-surface geophysical techniques are key instruments to assess groundwater conditions in hard rock aquifers and quantify spatial heterogeneity of storage properties at large field scales relevant to groundwater exploration and management.

Imaging, digital porous generation

On the estimation of permeability uncertainty due to unresolved pore-scale features

S. Perez[a], P. Poncet[a]

[a] *Universite de Pau et des Pays de l'Adour, E2S UPPA, CNRS, LMAP, Pau, France.*

Keywords: Pore scale modeling, DRP, Slip flows, Absolute permeability, Uncertainty management

In this presentation, we focus on two kinds of morphological uncertainties at the pore scale of porous rocks: on the one hand on uncertainty on the roughness of the pore surface, and on the other hand on the uncertainty of the surface location due to the blur of micro-tomography image processing.

Indeed, both can be translated into a slip boundary condition associated to a slip length denoted β. A surface roughness of the poral space typically scales in nanometers but may lead to slip lengths close to the micrometer: [4] reports a range $500 - 860nm$ for a mica/water interface with a roughness of $15nm$. Moreover, the case of blur can be translated to a slip length equal to a portion of the voxel width [1], that is to say also the micrometer scale. These two slip phenomena may also be in competition. However, we aim at quantifying the impact of the slip length β on the computed permeability

$$K_\beta = \phi\mu < u_\beta >_{\Omega_F} / < f >_{\Omega_F}, \tag{1}$$

in a rock sample whose fluid domain is denoted Ω_F, complementing the rock matrix domain Ω_S. In this expression (1), $< . >_{\Omega_F}$ represents the average in the fluid domain, f the driving force, μ the dynamic viscosity of the fluid, ϕ the sample porosity and $< u >_{\Omega_F}$ the averaged velocity on the fluid region ($\phi <u>$ is then the superficial velocity introduced in [7] for upscaling to the Darcy scale, see also [3]). The velocity u_β is carried out from the Stokes equation $-\Delta u + \nabla p = f$ and $\operatorname{div} u = 0$ in Ω_F (p is the pressure).

It satisfies a no-slip-through condition $u_\beta \cdot n = 0$ at the fluid/solid interface $\partial\Omega_F$ for its normal component (n is the unit inward normal field at the boundary), and a slip condition on its tangential components, that is to say

$$Tu - \beta T D(u) n = 0 \text{ with } T = I - n \otimes n \tag{2}$$

where T is the projector on the tangential field and $D(u) = (\nabla u + \nabla u^T)/2$ is the shear-rate tensor.

By computation, is it then possible to get a range of possible values $[K_\beta, K_0]$, where K_0 is the absolute permeability obtain for the full no-slip flow, instead of a single value K_0 subject to large uncertainty.

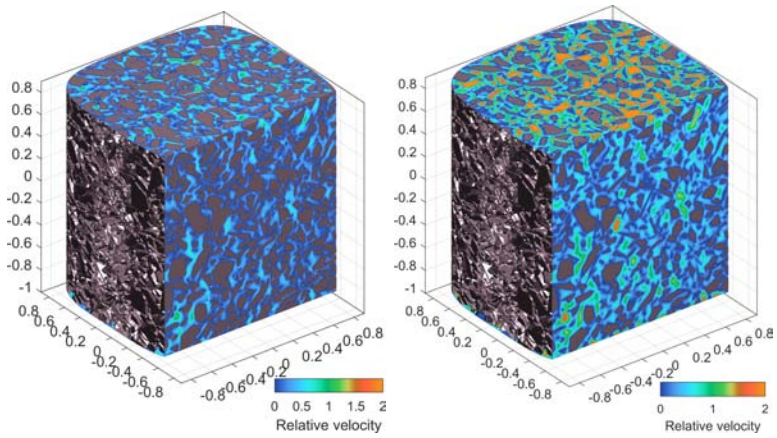

Figure 1: Flow in a compact sand pack sample at a resolution 512^3. To the left: using adherent boundary condition; To the right: using slip length $\beta/h = 0.76$.

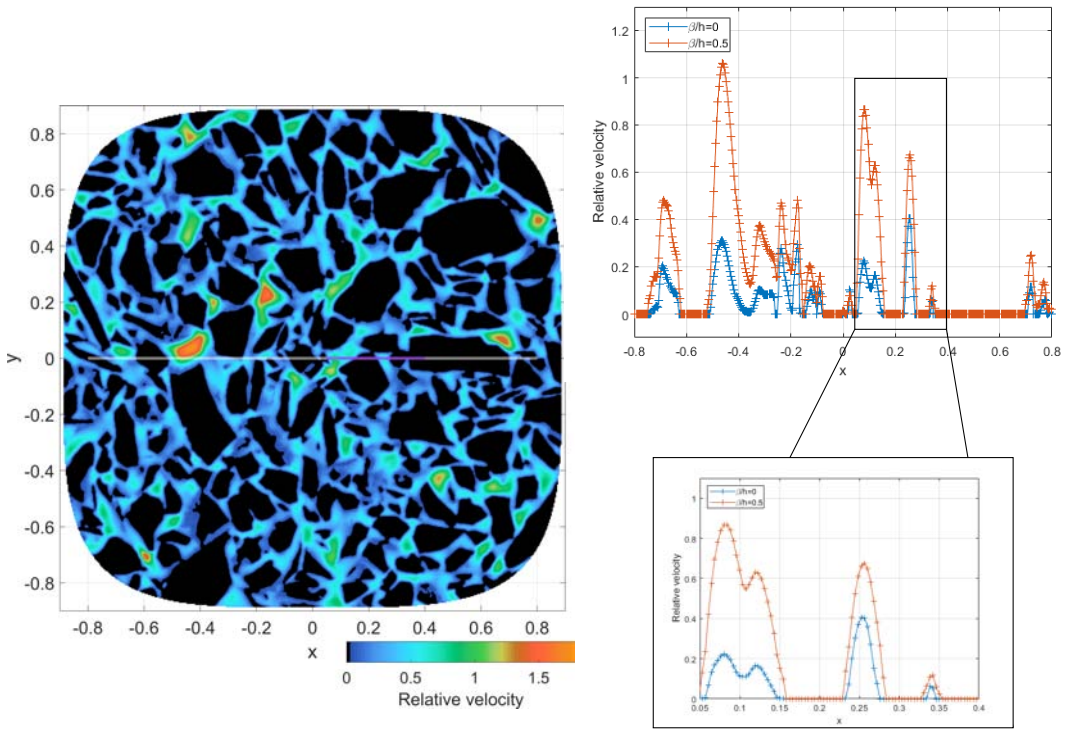

Figure 2: Velocities in the driving force direction, through a sectional profile at $z = -0.75$ and $y = 0$ in relative coordinates, for the sandpack sample: comparison between the adherent and slip boundary conditions for $\beta/h = 0.5$. A slice at $z = -0.75$ for a slip length $\beta/h = 0.5$ is displayed on the left-hand image. The white and magenta lines show the location, respectively, of the cuts of the unzoomed and zoomed curves to the right.

By means of asymptotic analysis, it is possible to provide an expansion of the permeability:

$$K_\beta = K_0 + \beta L_0 + \mathcal{O}(\beta^2) \tag{3}$$

We show that the linear deviation is given $L_0 = \phi\mu < U^1 >_{\Omega_F} / < f >_{\Omega_F}$ where U^1 is obtained by asymptotic analysis as the solution of a Stokes equation with prescribed velocity $T\,U^1 = T\,D(u_0)n$ at the boundary $\partial\Omega_F$, where u_0 is the no-slip solution giving K_0 (see [6] for details).

Several study cases will be described. To conclude, this technique is especially useful at an experimental level for microCT imaging with blur or difficult to threshold, and at numerical level for simulation of dissolution or crystallization whose reactive flow generates interfaces with intermediate values of porosity [5, 2].

References

[1] M. Bonnivard, A.-L. Dalibard, and D. Gérard-Varet. Computation of the effective slip of rough hydrophobic surfaces via homogenization. *Mathematical Models and Methods in Applied Sciences*, 24:2259–2285, 2014.

[2] J-M. Etancelin, P. Moonen, and P. Poncet. Improvement of remeshed lagrangian methods for the simulation of dissolution processes at pore-scale. *Advances in Water Resources*, 146:103780, 2020.

[3] L. Hume and P. Poncet. A velocity-vorticity method for highly viscous 3d flows with application to digital rock physics. *Journal of Computational Physics*, 425:109910, 2021.

[4] Eric Lauga and Michael P. Brenner. Dynamic mechanisms for apparent slip on hydrophobic surfaces. *Physical Review E*, 70(2):026311, 2004.

[5] S. Molins, C. Soulaine, N. I. Prasianakis, A. Abbasi, P. Poncet, A. J. C. Ladd, V. Starchenko, S. Roman, D. Trebotich, H. A. Tchelepi, and C. I. Steefel. Simulation of mineral dissolution at the pore scale with evolving fluid-solid interfaces: Review of approaches and benchmark problem set. *Computational Geosciences*, 2020.

[6] S. Perez, P. Moonen, and P. Poncet. On the deviation of computed permeability induced by unresolved morphological features of the pore space. *Under revision*, 2021.

[7] M. Quintard and S. Whitaker. Two phase flow in heterogeneous porous media: the method of large-scale averaging. *Transport in Porous Media*, 3:357–413, 1987.

Comparison of morphological and effective properties of 3D reconstructed nanoporous medium from 2D FIB-SEM slices

A-J. Tinet[a], F. Golfier[a], P. Collon[a], Q. Corlay[a]

[a]*Université de Lorraine, CNRS, GeoRessources, F -54000 Nancy, France*

Keywords: Nanoporous medium, Reconstruction, Effective properties, LBM

1 Introduction

The study of fluid transport within these porous media is essential for issues of storage barriers for gas (CO2, H2) or deep radioactive wastes [1]. These low permeability materials may have a high overall porosity (for instance around 20% for argillite) but more than 90% of this porosity is constituted by pores smaller than 100 nm. The connectivity and the topology of these pores influence the transfer mechanisms of such nanoporous media [2]. A better understanding of their pore structure is thus necessary to characterize their flow and transport behaviour. This can be done using a DRP (Digital Rock Physics) approach, consisting in the creation/acquisition of a 3D pore-scale model of the porous medium and numerical simulation of flow and transport equations on such a model.

Acquiring direct data on the porous structure (micropore, nanopore) is often a challenging task. The SEM (Scanning Electron Microscope) methods remain the most appropriate approaches to obtain nanoporosity information from thin sections (nanometric). FIB (Focused-Ion Beam) makes it possible to obtain nanometer-thick slices. Coupled with the SEM, it allows a 3D reconstruction of the pore space at high resolution [3, 4]. This technique is, however, very expensive and limited by the size of the sample to be analysed (usually of the order of a few μm^3). As a consequence, the imaged sample is generally smaller than the representative elementary volume (REV) especially for more complex processes, or more complex pore structure such as multimodal materials.

In this work, we evaluate the capacity of spacing the imaged SEM slices and numerically reconstructing the 3D volume at a larger scale using geostatistical methods [5] to accurately recover the desired properties of the material. To this end, we will test four different reconstruction methods on a fully-known set of FIB-SEM images of synthetic clay (from [6]). In order to assess the performance of the approaches, the reconstructed results will be compared through a variety of morphological and effective properties.

2 Materials and methods

For this comparative analysis, we use a stack of a segmented FIB-SEM serial-section images of a synthetic clay made from compacted illite powder, which has an overall porosity of 32% [6]. The original sample measures was acquired at 5 nm resolution. For computational efficiency, the reconstruction methods were developed and tested on against the reference grid of 180x180x180 voxels. 2D regularly-sampled parallel slices are then extracted and used as conditioning data for the 3D reconstruction.

The reconstruction methods used were a SIS (Sequential Indicator Simulation) and three derived versions of the MPS (Multi-Point Statistics) approach (a three directional aggregation MPS (3DA-MPS) [7], a slice sequential MPS [8] and a weighted three directional aggregation MPS) [9]. Reconstructed samples were generated for each method and for 3 three different amount of conditioning data. Five repetitions for each set of conditions was performed.

In order to assess the performance of the reconstructions, a set of morphological and effective properties were used. The morphological parameters (porosity, specific surface, Euler characteristic, tortuosity and pore size distribution) were computed using the image analysis software ImageJ and plug-ins (XLib and MorpholibJ). Effective properties (permeability, effective diffusion and longitudinal dispersion) were obtained using numerical upscaling with a Lattice Boltzmann Method for flow and transport equations [9, 10] (e.g. Figure 1, left).

3 Results and discussion

The SIS approach reveals a good agreement of averaged properties but also a lack of description of preferential patterns as indicated by the observed discrepancy for the Euler characteristic and hence for the predicted dispersion coefficient. In addition to exhibiting artefacts, the relevance of sequential approach is highly dependent on the amount of conditioning data. The image reconstruction is satisfying with high conditioning but quickly degrades. On the contrary, the 3DA-MPS approach exhibits very good results for all the transport properties when the density of conditioning data is large but with no post-processing required (Figure 1, right). When the distance between conditioning data is close to the characteristic, the reconstruction remains acceptable, but degrades strongly afterwards (Figure 1, right). Finally, the weighted-3DA-MPS approach shows better consistency with decreasing conditioning data (Figure 1, right), but leads to noise in the reconstructed images and is not as accurate at high conditioning as 3DA-MPS. It calls for more advanced weighting and post-processing steps.

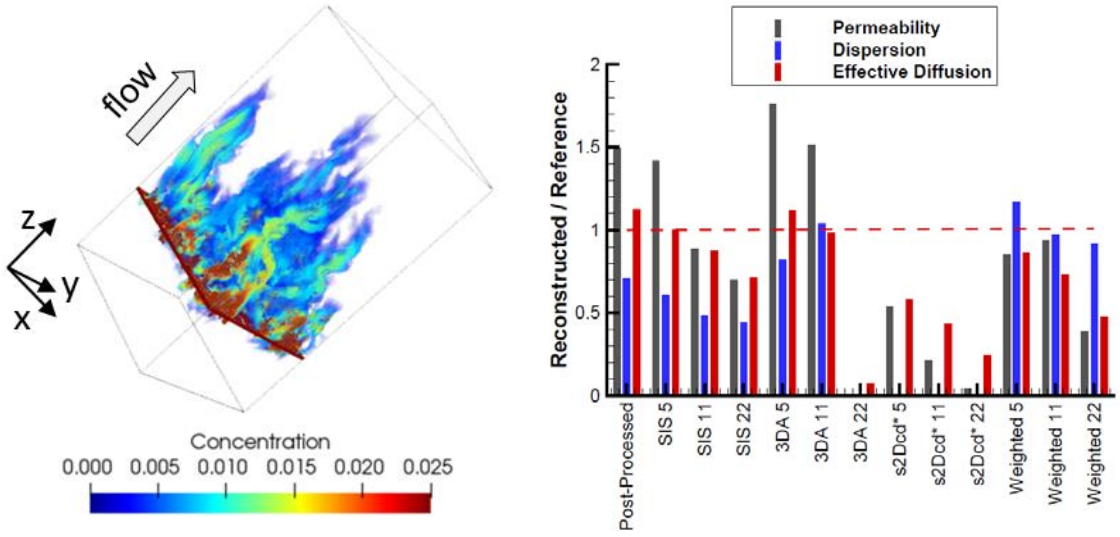

Figure 1: Left side: Concentration distribution for the reference case obtained by LBM transport simulation. Right side: Ratio of effective properties for one realisation of the reconstructed images to the reference.

References

[1] Marschall P. et al., Characterisation of Gas Transport Properties of the Opalinus Clay, a Potential Host Rock Formation for Radioactive Waste Disposal, *Oil & Gas Science and Technology*, 60(1), 121-139 (2005)

[2] Hu Q. el al., Low pore connectivity in natural rock, *Journal of Contaminant Hydrology*, 133, 76-83 (2012)

[3] Song Y. et al., Multi-scale pore structure of COx claystone: Towards the prediction of fluid transport, *Mar. Pet. Geol.*, 65, 63–82 (2015)

[4] Hemes S. et al., Multi-scale characterization of pore microstructures in Boom Clay (HADES, Mol, Belgium) using a combination of μ-CT, BIB-SEM and serial FIB-SEM techniques, *Microporous Mesoporous Mater.*, 208, 1–20 (2014)

[5] Tahmasebi P., Multiple Point Statistics: A review, *Springer International Publishing, Cham*, 613-643 (2018)

[6] Gaboreau S. et al., Optimization of pore-network characterization of a compacted clay material by TEM and FIB/SEM imaging, *Microporous Mesoporous Mater.*, 224, 116–128 (2016)

[7] Okabe H. and Blunt M.J., Pore space reconstruction of vuggy carbonates using microtomography and multiple-point statistics, *Water Resources Research*, 43(12) (2007)

[8] Comunian A. et al., 3D multiple-point statistics simulation using 2D training images, *Computers & Geosciences*, 40, 49-65 (2012)

[9] Tinet et al., Comparison of various 3D pore space reconstruction methods and implications on transport properties of nanoporous rocks, *Advances in Water Resources*, 103615 (2020)

[10] Pazdniakou et al., Numerical effciency assessment of the lattice Boltzmann model for digital nano-porous rock applications, *Advances in Water Resources*, 121, 44-56 (2018)

Organic porous media

Nonlinear acceleration waves in soft porous media

H. Berjamin[a]

[a]*School of Mathematics, Statistics and Applied Mathematics, NUI Galway, University Road, Galway, Republic of Ireland*

Keywords: Biological tissues, nonlinear waves, finite strain

1. Introduction

Poroelasticity theories have been employed in various biomechanical applications involving the deformation of hydrated porous biological tissues. Recently, biphasic mixture theory has received increasing attention in brain mechanics, where it is considered relevant for the modelling of time-dependent effects [1]. As such, head trauma involves highly time-dependent mechanical processes. Thus, it seems reasonable to include poroelastic behaviour in the constitutive modelling of brain tissue for wave propagation applications.

In the present study [2], we consider the propagation of nonlinear acceleration fronts in saturated porous media within the framework of the Biot–Coussy biphasic mixture theory [3], where both constituents are assumed incompressible (neo-Hookean elastic skeleton, and saturating fluid). In general, the amplitude of acceleration waves is governed by a Bernoulli equation. With the present constitutive assumptions, we find that the amplitude of 'slow' Biot compression waves follows a nonlinear evolution, while shear wave amplitudes evolve in a quasi linearly-degenerate fashion.

2. Equations of motion

Consider an unbounded incompressible poroelastic solid saturated by an incompressible fluid. The motion is described by the laws of mass balance and momentum balance where external body forces are neglected. The first governs the evolution of the volume fractions n^α for $\alpha \in \{\mathrm{s}, \mathrm{f}\}$ corresponding to the solid and fluid phases (second line of Eq. (1) below), while the second governs the evolution of the particle velocities $\boldsymbol{v}^\alpha$ (fourth and fifth lines of Eq. (1)). These equations of motion are constrained by the saturation condition $n^\mathrm{s} + n^\mathrm{f} = 1$, and the system is closed by suitable constitutive assumptions. In the Biot–Coussy mixture theory [3], the latter consist of a constitutive law for the dry solid combined with a poroelastic filtration law. Here, we consider a neo-Hookean porous solid where the fluid follows Darcy's law. The filtration law includes Biot's tortuosity effect, where the tortuosity coefficient $a = \frac{1}{2}(1 + 1/n^\mathrm{f})$ is derived from Berryman's formula.

In summary, using the Eulerian specification of motion, we may write the following first-order system of partial differential equations [2]

$$\begin{cases} \partial_t \boldsymbol{A} + \operatorname{grad}(\boldsymbol{A}\boldsymbol{v}^\mathrm{s}) = \boldsymbol{0}, \\ \partial_t n^\mathrm{f} + \operatorname{div}\big(n^\mathrm{f}(\boldsymbol{w} + \boldsymbol{v}^\mathrm{s})\big) = 0, \\ \operatorname{div}\big(n^\mathrm{f}\boldsymbol{w} + \boldsymbol{v}^\mathrm{s}\big) = 0, \\ \rho^\mathrm{f}\left[\partial_t \boldsymbol{v}^\mathrm{s} + (\operatorname{grad}\boldsymbol{v}^\mathrm{s})(\boldsymbol{w} + \boldsymbol{v}^\mathrm{s})\right] + a\rho^\mathrm{f}\left[\partial_t \boldsymbol{w} + (\operatorname{grad}\boldsymbol{w})(\boldsymbol{w} + \boldsymbol{v}^\mathrm{s})\right] = -n^\mathrm{f}\operatorname{grad} p - \frac{(n^\mathrm{f})^2}{k^\mathrm{f}}\boldsymbol{w}, \\ \rho^\mathrm{s}\left[\partial_t \boldsymbol{v}^\mathrm{s} + (\operatorname{grad}\boldsymbol{v}^\mathrm{s})\boldsymbol{v}^\mathrm{s}\right] + \rho^\mathrm{f}\left[\partial_t(\boldsymbol{w} + \boldsymbol{v}^\mathrm{s}) + \operatorname{grad}(\boldsymbol{w} + \boldsymbol{v}^\mathrm{s})(\boldsymbol{w} + \boldsymbol{v}^\mathrm{s})\right] = \operatorname{div}\boldsymbol{\sigma}^\mathrm{i}, \end{cases} \tag{1}$$

where the first line accounts for the evolution of the skeleton's deformation, and the third line is the saturation constraint. Here, we have introduced the seepage velocity $\boldsymbol{w} = \boldsymbol{v}^\mathrm{f} - \boldsymbol{v}^\mathrm{s}$, the permeability of the fluid k^f, the Lagrange multiplier p for the saturation constraint and the mixture's inner stress $\boldsymbol{\sigma}^\mathrm{i} = \boldsymbol{\sigma}^\mathrm{e} - p\boldsymbol{I}$, where $\boldsymbol{\sigma}^\mathrm{e}$ is Terzaghi's stress. Its dependence on the finite skeleton deformation follows from the neo-Hookean assumption, expressed in terms of the inverse $\boldsymbol{A} = \boldsymbol{F}^{-1}$ of the deformation gradient tensor $\boldsymbol{F}$.

3. Plane acceleration waves

To study plane wave solutions, we restrict the analysis to a one-dimensional configuration, assuming invariance along the y and z directions. Since both constituents are incompressible, linear plane waves are either longitudinal compression waves resulting from the interaction of both phases, or transverse shear waves mostly supported by the solid skeleton. Given the orders of magnitude of the poroelastic parameters for brain matter estimated in quasi-static tests [1], the present model is valid up to ultrasonic frequencies [2]. Thus, up to marginal adjustments, it might still be used in trauma-related configurations.

To gain insight into the physics of nonlinear waves, we derive the speed of a jump in the gradients of the primary variables (1), i.e. so-called *acceleration waves*. Using a symbolic calculus software, a closed-form expression of the characteristic wave velocities is obtained. Requiring real sound speeds then leads to the condition of hyperbolicity [2].

As shown by Ciarletta et al. [4], acceleration jump amplitudes are governed by a Bernoulli differential equation, in general. In the case of shear waves, we find that the amplitudes decay exponentially, in a similar fashion to what is known for linearly-elastic solids. For the compression waves, computations show that a nonlinear evolution is obtained, leading to blow-up in finite time. As stated in Müller and Ruggeri [5] p. 183, "if the initial discontinuity in the derivatives is too strong, it cannot be damped; instead it grows to infinity and thus the acceleration wave develops into a shock wave". Beyond a given critical amplitude, nonlinearity overpowers attenuation, leading to the formation of shock waves [2].

4. Conclusion

By analysing the speed and decay of nonlinear acceleration waves in soft Biot–Coussy porous materials, we have extended several works of the literature. Results show that poroelastic compression waves and shear waves propagate in a very different manner.

Acknowledgment

This work was supported by the Irish Research Council [project ID GOIPD/2019/328].

References

[1] E. Comellas, S. Budday, J.-P. Pelteret, G. A. Holzapfel, P. Steinmann, Modeling the porous and viscous responses of human brain tissue behavior, *Comput. Methods Appl. Mech. Engrg.* 369, 113128 (2020).

[2] H. Berjamin, Nonlinear plane waves in saturated porous media with incompressible constituents, arXiv:2101.09507 (2021).

[3] O. Coussy, *Poromechanics*. John Wiley & Sons Ltd, 2004.

[4] M. Ciarletta, B. Straughan, V. Tibullo, Acceleration waves in a nonlinear Biot theory of porous media, *Int. J. Non-Linear Mech.* 103 (2018)

[5] I. Müller, T. Ruggeri, *Rational Extended Thermodynamics*, Springer, 1998.

Enzymatic degradation of plant biomass: a porous media approach

S. Blosse[a,b], A. Bouchoux[b], P. Duru[a], C. Montanier[b]

[a] *Institut de Mécanique des Fluides de Toulouse (IMFT), Université de Toulouse, CNRS - Toulouse, France.*
[b] *Toulouse Biotechnology Institute, Université de Toulouse, CNRS, INRAE, INSA - Toulouse, France.*

Keywords: Plant Biomass, X-Ray Tomography, Enzymatic Degradation, Breakthrough Curves

1. Introduction

In the present era marked by the desire to build a bio-economy, plant biomass has a vast potential as a source of renewable and environmentally friendly molecules of interest. Deconstruction of plant biomass by a cocktail of enzymes is relevant at an industrial scale. Dry plant biomass such as wheat straw can be seen as a porous media where pores are dead cells separated by cell walls. At a smaller scale, the cell walls are composed of interpenetrating polymer networks, which are permeable and porous with pore sizes in the nanometer range. Achieving a better understanding of the intimate relationship between enzymatic activity and the exact course of deconstruction of such a complex, multiscale porous material is still needed. In this work -and we believe for the first time- we follow a porous media approach to contribute to this question. For that, we present results regarding enzymatic degradation of a model biomass, raw wheat straw, obtained with experimental approaches such as X-Ray tomography or breakthrough curve analysis, which are usually dedicated to more "conventional" porous media.

2. X-Ray Tomography: Study at the micron scale

First, we will present some results obtained using a laboratory-scale X-ray tomograph. Fully hydrated wheat straw samples, placed in a home-made 3D-printed thermostatically controlled bioreactor, are subjected to the action of a commercial enzymatic cocktail. In parallel, enzymatic activity is monitored using state of the art techniques in enzymology. In spite of a rather limited spatial resolution (voxel size is 1.25 μm), 3D X-ray tomography allows to highlight the selective effects of the enzymatic degradation. Notably, the disappearance of cellulose-rich cell walls (parenchyma) as a function of the duration of the enzymatic attack, can be quantified over the full scale of the wheat straw sample (i.e. a few mm in length) offering 3D pieces of information on the degradation process, which contrasts with the 2D picture classically obtained from 2D imaging, see Figures 1 and 2.

3. Elution Experiment: Study at the submicron scale

Second, in order to probe the effects of the enzymatic degradation at a sub-micron scale, we analyse breakthrough curves obtained by 2D X-ray radiography. This technique consist in flushing with pure water a wheat straw initially saturated with a radio-opaque molecular tracer. Experiments are conducted with untreated and degraded wheat straws. Breakthrough curve analysis is used to highlight the differences between these two kinds of samples, which traduce an alteration of the transport properties of the tracer within the wheat straw. Modelling the transport properties (e.g. through an effective diffusion coefficient) in relation with the enzymatic degradation mechanism (e.g. progressive disentangling of the polymer networks constitutive of the plan cell walls, prior to its disappearance as imaged on 3D images) is a key point and results of this on-going work will be presented.

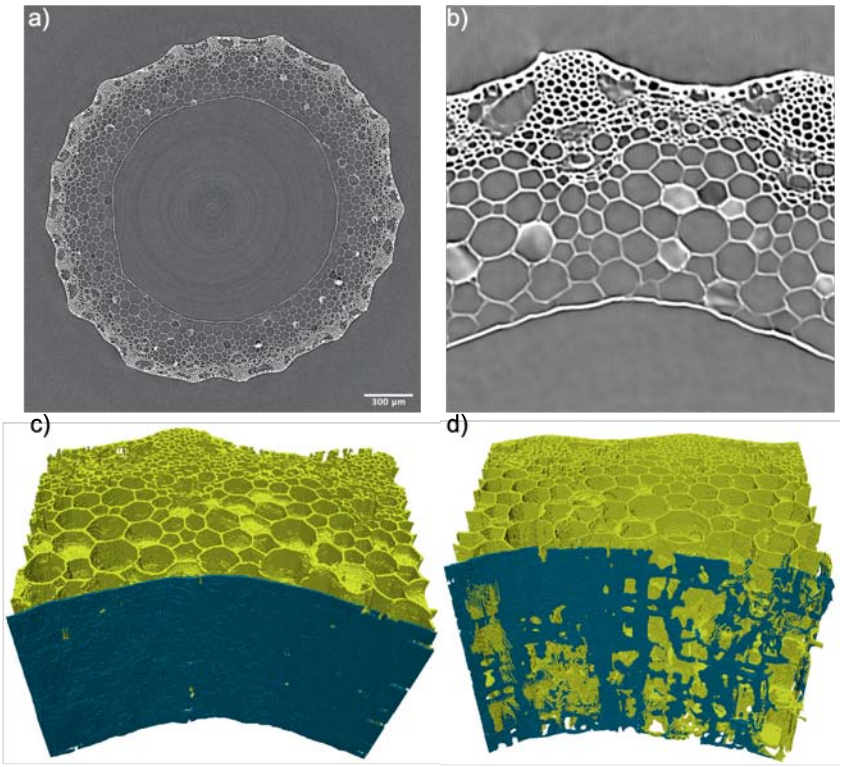

Figure 1: a) Transversal slice of a raw wheat straw from X-ray computed microtomography. b) Zoom on the transversal slice for detail. c) 3D rendering detail of a raw wheat straw. d) 3D rendering detail of a wheat straw after enzymatic degradation.

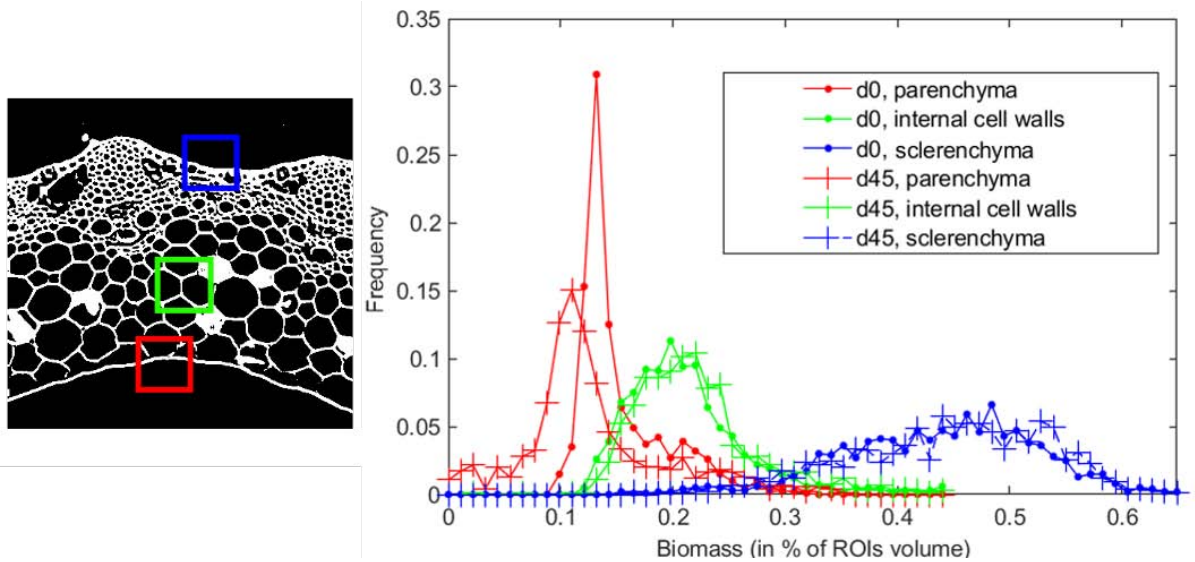

Figure 2: Binarized image of tomographic slice detail of wheat straw with three regions of interest (right). Amount of biomass in 1000 randomly located 3D ROIs for native (d0) and digested (d45) wheat straw (left) : the selective action of the cocktail on the parenchyma is highlighted.

How mechanical strain might modify transport properties of a biological tissue-mimicking porous media; an experimental approach

P. Lefebvre[a], V. Mansard[b], L. Malaquin[b], P. Assemat[a], P. Swider[a]
[a] *IMFT UMR 5502, Toulouse, France*
[b] *LAAS UPR 8001, Toulouse, France*

Keywords: poromechanics, biomaterials, transport properties, X-ray tomography, digital volume correlation

1 Introduction

Biofilms, cells, and tissues are evolving depending on mechanical strain, interstitial fluid flow and presence of bioactive materials and species [1, 2]. The interstitial flow is considered as a stimulus in cellular mechanotransduction and tissue mechanobiology. Therefore, knowledge of biophysical, structural and transport properties can improve diagnosis, therapeutic strategies and patient follow-up. Applications include pediatric and aging pathologies, cancer, infections.

Mesoscopic mechanical properties of porous media such as elasticity and transport properties such as permeability might be strongly dependent upon microarchitecture (porosity, tortuosity). Those equivalent properties can be complex and even scalable [1-6]. Whilst mixed multiscale approaches showed relevant results with generic materials [7,8], the identification of governing laws between microarchitecture, transport and strain remain an open question with biological tissue [9].

The poromechanical approach is useful for the in-situ study of a large variety of porous media [10], and can be relevant to explore multiscale couplings in biological media. With low Reynolds number, the filtration rate and pressure gradient can be linked by the effective permeability through Darcy's empirical law [5]. However limitations in the results interpretation arise for heterogeneous media such as biological tissues [10].

This study presents the implementation of a device that simultaneously characterize the evolving microarchitecture under loading in an X-ray microtomograph, and the effective permeability. Results were obtained on a sample of macro-porous PDMS, a material widely used in cell culture due to its biocompatibility and non-toxicity. Correlations could be extracted from these results between transport properties, deformation and flow.

2 Methods and results

The constitutive stress-strain equation of the porous media is expressed by equation (1a) which involves Lamé coefficients λ^e, μ^e, and Biot coefficient b. The Darcy law involving the intrinsic permeability κ^e, fluid pressure p^f and fluid flux $q^{f/s}$ is expressed by equation (1b). Under the hypotheses of quasi-static responses, small strains and incompressible phases, the evolving porosity ϕ^f, or structural fraction $\phi^s = 1 - \phi^f$, is associated with the mechanical transform $J = 1 + \text{trace}\,\boldsymbol{\varepsilon}$.

$$\boldsymbol{\sigma} = \lambda^e \cdot \text{trace}\,\boldsymbol{\varepsilon} \cdot \mathbf{I} + 2\mu^e \boldsymbol{\varepsilon} - b \cdot p^f \cdot \mathbf{I} \quad \text{(a)} \qquad \mathbf{q}^{f/s} = -\frac{\kappa^e}{\mu} \cdot \mathbf{grad}\, p^f \quad \text{(b)} \qquad (1)$$

The experimental device shown in Figure 1a is located into the chamber of an X-ray tomograph (RX Solution®) figure 1b, and volume strain is explored using the displacement field obtained by digital volume correlation (LaVision®). The PDMS specimen is sealed into a silicon tube with characteristic dimensions of 7 mm in length and 4 mm in diameter. This tube allows loadings to be monitored using the controlled axial displacement w_0.

The loaded configuration of the sample microarchitecture and the associated averaged volume strain are shown in Figure 1c and Figure 1 d, respectively. The correlation between the effective permeability and the

averaged volume strain is shown in Figure 1e. The fitting procedure, successively using a linear function, a power function, an exponential function, and a quadratic function, gives determination coefficients R^2 equal to 0.973, 0.988, 0.989, and 0.9897, respectively.

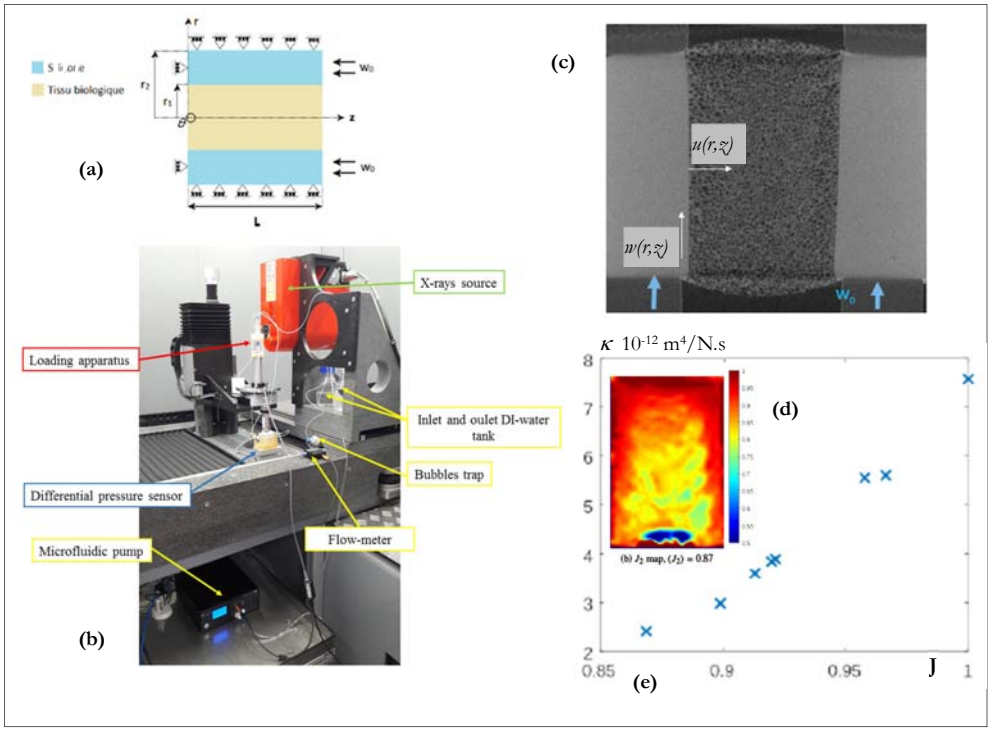

Figure 1: Experimental methodology. (a) Reference model, (b) Experimental device, (c) X-ray imaging of loaded sample, (d) Volume strain and (e) Correlation between the effective permeability and the averaged volume strain.

3 Conclusion

Preliminary results showed a robust and reproducible relationship, between permeability and volume strain variation induced by mechanical loadings. Thanks to the accurate exploration of the microarchitecture, the strain dependent porosity, the pore shape evolution and their incidence on transport properties have been accessible but were not commented here. Further studies will concern the proposition of governing laws associating transport properties, material elastic properties and evolving strain.

References

[1] Fung YC. 1993. Biomechanics, mechanical properties of living tissue, Springer.
[2] Cowin, S.C. (2001) Bone Mechanics Handbook. 2nd Edition, CRC Press, Boca Raton.
[3] *Biot MA, Willis DG. 1957. The elastic coefficients of the theory of consolidation" J. Ap Mech. 24: 594–601.*
[4] Dullien, F., *Porous media, fluid transport and pore structure.* 1992, USA: Academic Press.
[5] Coussy, O., *Poromechanics.*2004: J. Wiley & Sons.
[6] Ingrahama M.D., Bauera S.J., Kathleen A. Issenb, Thomas A. Dewersa. *Int. J. Rock Mech. Min. Sci.* 96 (2017), 1 - 10. Evol. of permeability and Biot coefficient at high mean stresses in high porosity sandstone.
[7] Misra A., Parthasarathy R., Singh V., Spencer P. Micro-poromechanics model of fluid-saturated chemically active fibrous media. *Z Angew Math Mech.* 2015. 95(2): 215–234.
[8] Moreno A, Quintard M, Mancini A, Gomez-Brouchet A, Swider P, Assemat P. *Upscaling of fluid flow in spatially heterogeneous bone tumors.* (2020). VPH 2020 Conference.
[9] Cheng AHD, poroelasticity, Springer, 2016.
[10] Arramon YP, Nauman EA.,. "The intrinsec permeability of cancellous bone." In *Bone mechanics*, 980. Cowin SE, 2001.

Multiscale fibrous media, nano and micro porous media

Clogging of a 2D model porous media by a non brownian suspension

Y. Soumane[a], A. Naillon[b], H. Bodiguel[a]

[a] *Univ. Grenoble Alpes, CNRS, Grenoble INP, LRP, Grenoble, France*
[b] *Univ. Grenoble Alpes, CNRS, Grenoble INP, 3SR, Grenoble, France*

Keywords: porous media, clogging, particle suspension, microfluidics

1. Introduction

Transport of particles in porous media is of great importance for many applications such as flows in biological systems [1], filtration [2], soil mechanics, petroleum engineering... During the flow of a dense suspension, particles can accumulate in certain regions, form plugs, reduce the permeability, and eventually clog the whole medium. In order to better understand the underlying mechanisms of this clogging, a direct observation seems interesting. Recently, plug formation at pore-scale has been studied using elementary structures such as simple constrictions [3], and clogging at the scale of the entire medium, but for uniform porous media [4]. In this work, we seek to extend these results in disordered micromodels. First, our goal is to analyze the effect of flow conditions and suspension properties on the clogging dynamics. In a second step, we propose a method to avoid or delay the clogging, by varying the injection conditions.

2. Experimental procedure

In order to study the clogging dynamics, we have designed a 2D model of disordered porous media in PDMS (figure 1). It is casted in a mold fabricated by photolithography, and covered by a glass slide. The micromodel is 8 mm long, 7.3 mm wide and 46 μm deep. Its porosity is 0.76 and the mean pore throat is around 55 μm.

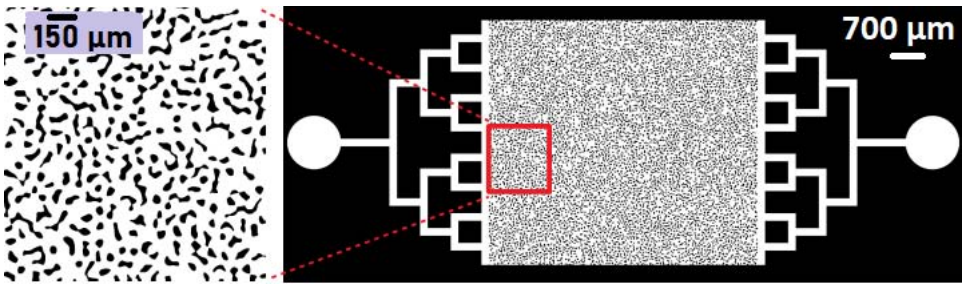

FIGURE 1: Image of the model porous medium. White represents the void space, black the walls.

Poly(methyl methacrylate) (PMMA) particles have been used to prepare the suspensions. The diameter of the particles has been varied between 6 μm and 20 μm, but remained highly monodisperse. The suspending fluid was a mixture of sodium iodide, demineralized water and 2-pyridinemethanol which allowed to match both density and refractive index of the particles. Its viscosity was about 12 $mPa.s$ (25^oC).

3. Results

3.1. Clogging

In this part, the experiment was flow-rate controlled. We have studied the effect of flow rate, suspension concentration and particle size on clogging. This last parameter had the most important consequences. Indeed, for 6 μm and 10 μm particles, no clogging was observed whatever the injection conditions. For 20 μm particles, the medium was always clogged. In contrast, for 15 μm particles, which corresponds to about 3 times the pore throat aperture, the medium was clogged or not, depending on

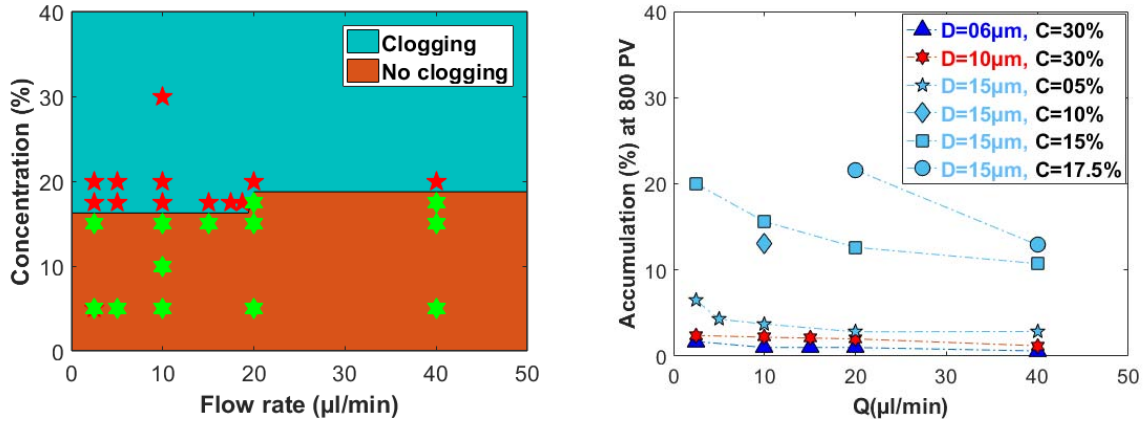

(a) (b)

FIGURE 2: **(a)** : Clogging phase diagramm for a suspension of 15 μm diameter particles. **(b)** : Accumulation as fonction of the flow rate at 800 PV for different concentrations and particle sizes.

the flow rate and on the suspension concentration. For this particle size, the concentration threshold for clogging was between 17.5% and 20% (figure 2a). Then, a quantitative analysis was performed to characterize the clogs. We determined the percentage of clogged space in the medium, called accumulation, the mean cluster size, and the mobility of the clusters, which quantifies the dynamics of growth and erosion of these. For example, in figure 2b, it is shown that the accumulation in non clogged medium decreased when increasing the flow rate, and increased when the suspension was more concentrated.

3.2. Preventing clogging

Here, the experiments were pressure controlled. We studied the effect of a non constant pressure drop on the clogging dynamics. A square signal has been used. The frequency of this signal varied from 0.4 Hz to 0 Hz, and its amplitude was varied from 0 to 25 mbar around 100 mbar. Surprisingly, these pressure oscillations have a strong influence on clogging. Indeed, the accumulation reached a steady state, which was lower than in the case of a constant pressure. Moreover, the higher the frequency, the lower the accumulation (figure 3a). For a given frequency, the more the amplitude, the less the accumulation (figure 3b). Interstingly, these oscillations also prevented the clogging, even in experimental conditions for which clogging occured at constant pressure drop.

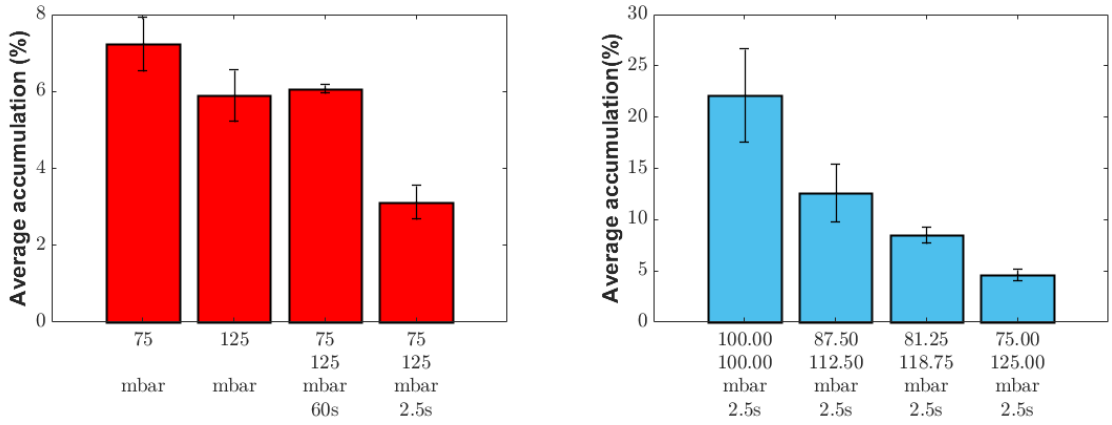

(a) (b)

FIGURE 3: Histogram of average accumulation. **(a)** at 300 PV as a function of pressure frequency (C=10%). **(b)** at 400 PV as a function of pressure amplitude (C=15%).

Références

[1] Sanderson, S Laurie and Cheer, Angela Y and Goodrich, Jennifer S and Graziano, Jenny D and Callan, W Todd, Crossflow filtration in suspension-feeding fishes, *Nature*, 412, 439–441 (2001).

[2] Datta, Somalee and Redner, S, Gradient clogging in depth filtration, *Journal*, 58, R1203 (1998).

[3] Marin, Alvaro and Lhuissier, Henri and Rossi, Massimiliano and Kähler, Christian J, Clogging in constricted suspension flows, *Physical Review E*, 97, 021102 (2018).

[4] Jung, Jongwon and Cao, Shuang Cindy and Shin, Young-Ho and Al-Raoush, Riyadh I and Alshibli, Khalid and Choi, Jin-Woo, A microfluidic pore model to study the migration of fine particles in single-phase and multi-phase flows in porous media, *Microsystem Technologies*, 24, 1071–1080 (2018).

Storage and absorption of mechanical energy in nanoporous materials

High Pressure Intrusion of Aqueous Salt Solutions in MFI-type Zeosil: Influence of Cation Nature

A. Astafan[a,b], T. J. Daou[a,b], H. Nouali[a,b], G. Chaplais[a,b], C. Marichal[a,b], A. Ryzhikov[a,b]

[a] *Université de Haute-Alsace, CNRS, IS2M UMR 7361, F-68100 Mulhouse, France.*
[b] *Université de Strasbourg, France.*

Keywords: high pressure intrusion-extrusion, aqueous salt solution, energy storage, influence of cations, zeosil, silicalite-1.

1 Introduction

Heterogeneous lyophobic systems, which consist of a porous matrix and a non-wetting liquid, are one of the most promising technologies for absorption and storage of mechanical energy. Their principle is based on the intrusion of liquid into the pores under high pressure, where the supplied mechanical energy is transformed into solid-liquid interfacial energy through the breaking of liquid intermolecular bonds. Since 2001, hydrophobic pure silica zeolites (zeosils) have been studied as porous matrix for high pressure water intrusion [1]. Depending on the zeolite structure, framework stability and the presence of defects, the "zeosil − water" system, when the pressure is released (extrusion), is able to restore, dissipate or absorb the mechanical energy supplied during the compression step (intrusion) and therefore to display a spring, shock absorber or bumper behavior [2]. Recently, it has been found that the intrusion-extrusion of saline aqueous solutions as non-wetting liquid presents a great advantage in this field. Indeed, the use of concentrated saline solutions increases the energy performance of zeosil-based systems [3], and the nature of the anion in these solutions provides a drastic influence on the behaviour of system and the value of the intrusion pressure [4]. A complementary study has been also conducted in order to investigate the influence of cation nature of different chloride salt solutions on intrusion-extrusion characteristics in MFI-type zeosil (silicalite-1). These results are reported here.

2 Experimental

Silicalite-1 was prepared in fluoride medium according to a procedure described previously [1]. The intrusion−extrusion experiments of chlorides aqueous solutions of alkali, alkaline earth and transition metals were performed at room temperature using a modified mercury porosimeter. The following salts MCl_n (with M stands for metal and n = 1, 2 or 3) were chosen: LiCl, NaCl, KCl, RbCl, CsCl, $MgCl_2$, $CaCl_2$, $ZnCl_2$, $MnCl_2$, $NiCl_2$, $CuCl_2$, $CdCl_2$... The aqueous solutions have been prepared at saturation concentrations and also by setting the molar H_2O/cation ratio at 12 and 18 in order to better compare cations impact. The latter ratios have been used to compare the performance of all the systems depending on cation nature.

3 Results and discussion

The examples of intrusion-extrusion curves are depicted in Figure 1. It has been observed that the cation nature has no significant influence on the behaviour of silicalite-1-based systems when saturated MCl_n solutions are used. All systems demonstrate a fully reversible spring behaviour except those with concentrated $ZnCl_2$ (H_2O/Zn^{2+} = 3.5, 6.0) and saturated CsCl (H_2O/Cs^+ = 5.0) solutions. With these solutions, a minor irreversibility of intrusion is present in the first intrusion-extrusion cycle (Figure 1) and corresponds to a combination of bumper and spring behaviors. This irreversibility phenomenon disappears for the next cycles or for lower salt concentrations.

Compared to "silicalite-1 − water", the intrusion of all saline solutions leads to a significant increase of intrusion pressure (97 MPa in the case of water) [1, 3]. It has been observed that LiCl and $ZnCl_2$ solutions with the lowest H_2O/M^{n+} ratios (2.8 and 3.5, respectively) provide the highest values of intrusion pressure close to 300 MPa. For the saturated $ZnCl_2$ solution (H_2O/Zn^{2+} = 1.75), the pressure is even supposed to exceed 400 MPa (measurement limit). In the same way, the dilution (increasing of H_2O/cation ratio) leads to a decrease of intrusion pressure.

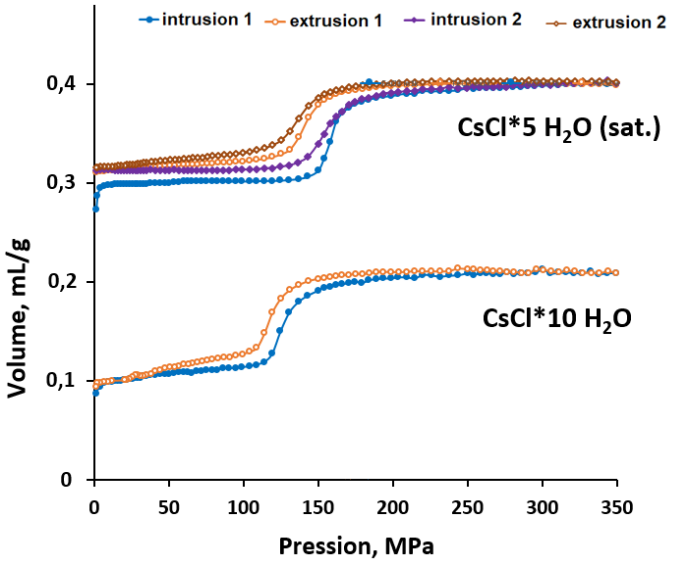

Figure 1: Intrusion-extrusion curves of "silicalite-1 – CsCl aqueous solution" systems.

4 Conclusions

The study of "silicalite-1 – chloride salt aqueous solution" systems shows that the cation nature influences considerably the intrusion pressure, whereas the spring behaviour remains essentially unchanged. It should be noticed that, in contrast to the cations, the anion nature impacts drastically intrusion-extrusion behaviour in "silicalite-1 – aqueous salt solution" systems [4]. For solutions with alkali and alkali earth metal cations and the same H_2O/M^{n+} ratio, the intrusion pressure increases with the ion diameter decrease. In the same way, the increase of cation charge leads to the pressure rise. The highest intrusion pressure values have been obtained for the solutions with lowest H_2O/M^{n+} ratio (LiCl and $ZnCl_2$ ones). Thus, these solutions are expected to be the most promising liquids for energy storage applications.

References

[1] V. Eroshenko, R. C. Regis, M. Soulard, J. Patarin, Energetics: A new field of applications for hydrophobic zeolites, *J. Am. Chem. Soc.*, 123, 8129-8130 (2001).

[2] L. Tzanis, M. Trzpit, M. Soulard, J. Patarin, Energetic performances of channel and cage-type zeosils, *J. Phys. Chem. C*, 116, 20389-20395 (2012).

[3] L. Tzanis, H. Nouali, T. J. Daou, M. Soulard, J. Patarin, Influence of the aqueous medium on the energetic performances of silicalite-1, *Mater. Lett.*, 115, 229-232 (2014).

[4] A. Ryzhikov, H. Nouali, T. J. Daou, J. Patarin, A drastic influence of the anion nature and concentration on high pressure intrusion–extrusion of electrolyte solutions in silicalite-1, *Phys. Chem. Chem. Phys.*, 20, 6462-6468 (2018).

Adsorption and separation by porous materials

Mechanisms of gas separation through 2D porous graphene membranes : theory and molecular simulations

J. Guo[a], R. Vermorel[a], G. Galliero[a]

[a]*Laboratory of Complex Fluids and their Reservoirs, University of Pau and Pays de l'Adour- Pau, France*

Keywords: gas separation, nanoporous graphene, molecular simulation

1 Introduction

In a context of energy transition, the growing share of gas (natural gas, hydrogen, bio-gas) in the energy mix, as well as the need to store CO2 and reduce its emissions, calls for an improvement in gas separation techniques. In this sense, free standing nanoporous graphene is a promising material because it makes it possible to exceed the selectivity to permeance ratio of other membrane materials.

In this study, we use molecular simulations to document the physical mechanisms governing permeation and gas separation through 2D graphene membranes, for different pore sizes and a range of thermodynamic conditions. Our objective is to identify, understand and quantitatively predict the transport properties of gases through these materials.

For pure species, we show that the permeation of a gas molecule consists of two successive steps: the permeation of the membrane plane through the pore and the desorption from the graphene sheet to the bulk. The first step is driven by steric effects in the pore plane. The second stage is the result of a competition between desorption kinetics and surface diffusion along the graphene sheet since an adsorbed molecule can recross the pore or diffuse towards another as long as it does not desorb. On the basis of these observations, we propose a theoretical model that allows us to reproduce the results of the simulations. This model shows that the potential of mean force between a permeating gas molecule and the graphene atoms in the pore region plays a central role.

In addition, we have simulated the separation of gas mixtures (CH4 / CO2, O2 / N2) through various nanoporous graphenes to investigate the selectivity of this type of membrane. Our data show the limits within which the results obtained for pure gases can be used to predict the separation of mixtures.

We believe that these recent results are of interest to help optimise the design of 2D graphene-based membranes, both from the point of view of the geometry or spatial distribution of the pores and their chemical functionalization.

References

[1] R. Vermorel; F. Oulebsir; G. Galliero, Communication: A method to compute the transport coefficient of pure fluids diffusing through planar interfaces from equilibrium molecular dynamics simulations, *The Journal of Chemical Physics*, 147, 101-102 (2017).
[2] F. Oulebsir; R. Vermorel; G. Galliero, Diffusion of Supercritical Fluids through Single- Layer Nanoporous Solids: Theory and Molecular Simulations, *Langmuir,* 34, 561-571 (2018).

Photopolymerization of zeolite/polymer based composite and corresponding application in the fields of 3D printing and gas adsorption

Yijun Zhang[a,b], Ludovic Josien[a,b], Angélique Simon-Masseron[a,b], Jacques Lalevée[a,b]

[a] *Institut de Science des Matériaux de Mulhouse (IS2M-CNRS), Université de Haute-Alsace - Mulhouse, 68100*
[b] *Université de Strasbourg - Strasbourg, 67081*

Keywords: Zeolite; 3D Printing; Composite; Photopolymerization; Gas Adsorption

1 Introduction

Zeolites are a set of crystalline aluminosilicates with a large amount of microporous structures, the large specific surface area and good adsorption. [1] Therefore, zeolites have been widely used in different applications, such as petrochemical industry, environmental protection and biological engineering. However, the direct utilization of powdery zeolites in chemical operation leads to a massive loss of raw materials and equipment contamination, which increases the cost in industrial applications. Therefore, zeolites are normally manufactured into various shapes to meet different industrial demands, such as pellets, beads, etc. Additive manufacturing (AM), as known as 3D printing, brings convenient, cheap, and promising opportunities to fabricate zeolite monoliths with adapted shape and size. [2] 3D printing via photopolymerization is developing rapidly and has been a turning point of additive manufacturing (AM), due to its mid reaction conditions, nearly no release of volatile organic compounds (VOCs), etc. In addition, zeolite also can be used as filler to improve or enhance the mechanical properties and functions of polymers. However, works have been rarely reported about the 3D printing via photopolymerization of zeolite/polymer, which can be applied to fabricate zeolite monoliths with bespoke shapes and manufacture functional composites. [3]

Here, we report the fabrication of LTA-5A zeolite/polymer based composite via photopolymerization (Figure 1). The results show that the zeolite filler content of this composite can reach at least 70 wt%, with good depth of cure and improved mechanical properties. Through SEM analysis, zeolites have a homogenous distribution in the composites, which provides a guarantee for the future 3D printing and fabrication of zeolite with bespoke structures. Although the issue of light penetration in filled samples is unavoidable, the production of 3D patterns can be performed through direct laser writing (DLW) as a lithography technique. Remarkably, a high zeolite porosity can be obtained with the 3D-printed structure, after debinding of the 3D-printed composite by thermal treatment. Compared with the corresponding pure zeolite powder, the porosity is only slightly reduced, which means these materials can be applied in field of adsorption and separation.

In conclusion, this work is expected to promote the valuable development of highly filled zeolite/polymer composites, and expand their potential application for 3D printing via photopolymerization in the field of high-performance lightweight materials, such as the fabrication of zeolitic objects with bespoke shapes for adsorption and separation.

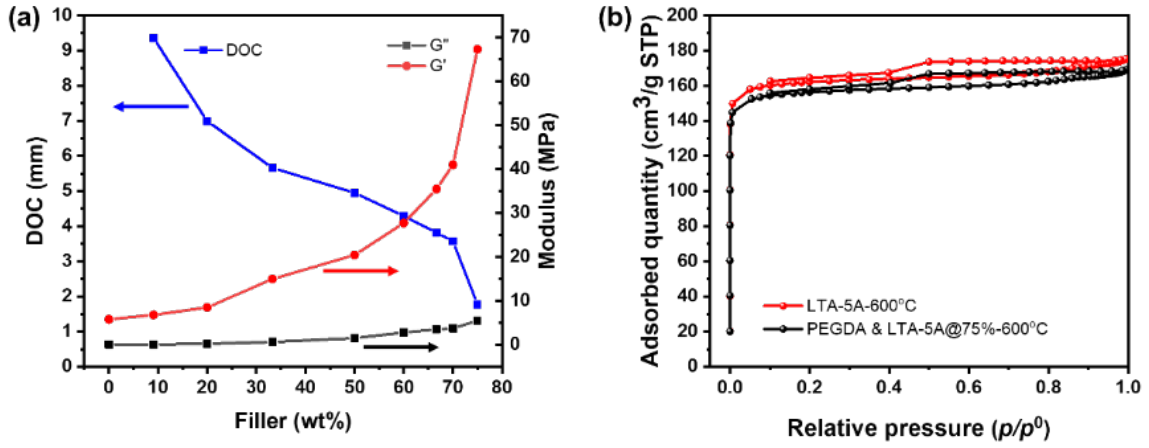

Figure 1: (a) The depth of cure (DOC) and the dynamic thermomechanical analysis (DMA) of PEGDA/LTA-5A based composite with different filler contents; (b) N_2 adsorption-desorption of LTA-5A powder (after 600 °C treatment) and PEGDA/LTA-5A based composite (75 wt%) after sintering at 600 °C.

References

[1] Simon V., Thuret A., Candy L., Bassil S., Duthen S., Raynaud C., Simon-Masseron A., Recovery of hydroxycinnamic acids from renewable resources by adsorption on zeolites, *Chem. Eng. J.* 280, 748-754 (2015).
[2] Zhang Y., Xu Y., Simon-Masseron A., Lalevée J., Radical photoinitiation with LEDs and applications in the 3D printing of composites, *Chem. Soc. Rev.* 50, 3824-3841 (2021).
[3] Zhang Y., Josien L., Salomon J.-P., Simon-Masseron A., Lalevée J., Photopolymerization of Zeolite/Polymer-Based Composites: toward 3D and 4D Printing Applications, *ACS Appl. Polym. Mater.* 3(1), 400-409 (2020).

Mechanical, chemical and thermal coupling between fluids and matrix in porous media

Pore-scale modeling of acid etching in a carbonate fracture

Renchao Lu[a], Xing-Yuan Miao[b], Olaf Kolditz[a,c,d], Haibing Shao[a]

[a] *Helmholtz Centre for Environmental Research - UFZ, Leipzig, Germany.*
[b] *Department of Energy Conversion and Storage, Technical University of Denmark, RisÃ¸ Campus, Frederiksborgvej 399, 4000 Roskilde, Denmark.*
[c] *Technische Universität Dresden, Dresden, Germany.*
[d] *TUBAF-UFZ Centre for Environmental Geosciences, Germany.*

Keywords: Pore-scale reactive transport modeling, Phase-field approach, Fracture acidizing, Evolution of fracture surface geometry

1. Introduction

Acid fracturing technique has been widely used in the oil and gas industry for improving the carbonate reservoir permeability. In recent years this chemical stimulation technique is borrowed from the oil and gas industry, tentatively employed in the enhanced geothermal system of Soultz-sous-Forêts [1]. In order to determine optimum operating conditions (e.g., acid type and acid injection rate), pore-scale acid-fracturing model is needed. The pore-scale model provides insight into the role of fracture surface geometry in acid etching of the fracture walls. Its core components consist in tracking the motion of the solid-liquid interface induced by acid etching. To date, a number of front tracking approaches (e.g., local remeshing technique, embedded boundary method, immersed boundary method, and level-set method) have been proposed by many researchers. In this work, we propose employing the phase-field approach to implicitly track the physically sharp concentration discontinuities across the solid-liquid interface.

2. Mathemetical description

The acid-fracturing process involves channeling flow, acid etching on the fracture wall, and solute transport process in the fracture. The fluid motion in the free-flow region and the low-porosity region is described by the Stokes-Brinkmann equations including the momentum balance equation and mass continuity equation. The acid etching formed by dissolution of carbonate is described by the phase-field equation. The dissolution of carbonate follows the classical transition-state-theory based reaction rate law. The solute transport in the vertically propagating fracture is described by the advection-dispersion-reaction equation.

3. Results

The 2-D acid-fracturing model involves a parallel-plate fracture of 100 μm in length and width and the bilateral low-permeability carbonate rock of 10 μm in thickness. A pad fluid of pH = 5.96 is continuously injected through the fracture at a constant injection velocity of 1 mm/s. The entire domain as shown in Fig. 1(a) is discretized into 58,286 Taylor-Hood elements. Fig. 1(a) and (b) show the evolution of the fracture surfaces during the time period between 10,000 s and 100,000 s. The acid etching causes a total surface recession of 6.2 μm. Fig. 1(c) and (d) show the contour plot of the fluid velocity. The maximum value of the transverse velocity component decreases from 1.4 mm/s to 1.35 mm/s as the flow channel gets wider. Fig. 1(e) and (f) show that the proposed pore-scale reactive transport model enables to capture the calcium concentration jump across the solid-liquid interface.

References

[1] Portier, S., Vuataz, F.-D., Nami, P., Sanjuan, B., Gérard, A., Chemical stimulation techniques for geothermal wells: experiments on the three-well EGS system at Soultz-sous-Forêts, France, Geothermics, 38(4), 349-359 (2009).

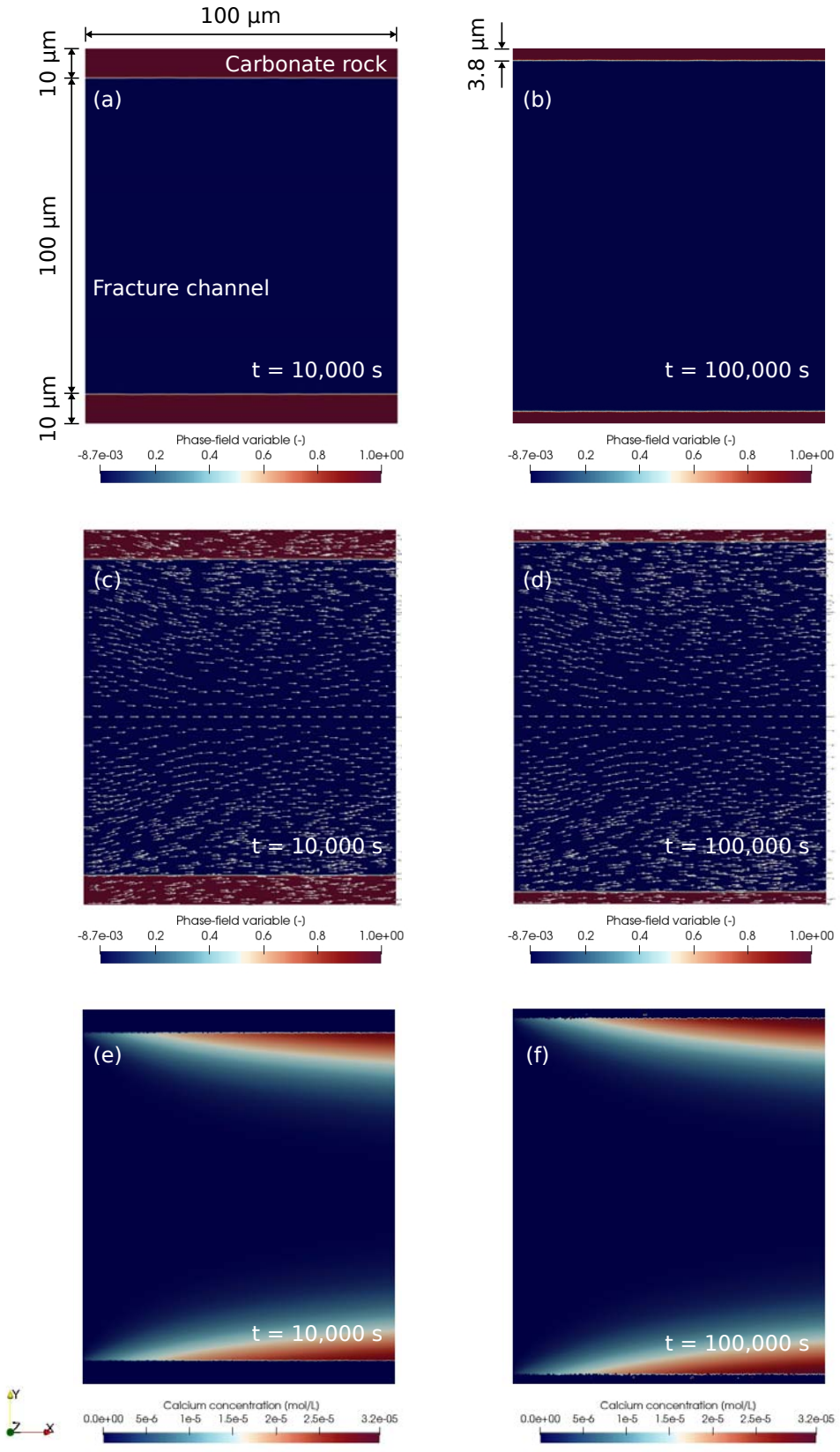

Figure 1: Contour plot of (a) and (b) phase-field variable, (c) and (d) fluid velocity, (e) and (f) calcium concentration in an acid-etched carbonate fracture for 100,000 s.

Evaluation of mineral precipitation into single fractures

Catherine Noiriel[a], Nicolas Seigneur[b], Pierre Le Guern[a], Vincent Lagneau[b]

[a]*Géosciences Environnement Toulouse, UMR 5533 Université Paul Sabatier, CNRS, IRD, CNES, 31400 Toulouse, France*
[b]*Mines Paris Tech, Centre de Géosciences, Université Paris Sciences Lettres, 77300 Fontainebleau, France*

Keywords: fracture, precipitation, reactive transport modelling

1 Introduction

Fractures are the principal path for fluid flow in low permeability rocks. Modification of their topology and transmissivity by reactive fluids is an important and complex geological process. In particular, the processes that affect reorganisation of flow and transport in fractures during precipitation are of prime interest for several geo-engineering applications (e.g. CO_2 geological sequestration, geothermal industry) to sustain injectivity and/or recovery of fluids. Given the complexity and heterogeneity of the pore structure, the wide range of chemical perturbations and the coupling between these different processes, obtaining a representative evolution of the effective properties of the porous medium in a continuum approach can be challenging [1]. However, although many advances have been made in pore scale modeling in recent year, it is necessary to continue relying on continuum approaches. In particular, continuum approaches can account for the feedback between flow and geochemistry and between volume of precipitate, evolving fracture aperture field and permeability, thus permitting a capture of the processes that are important to the understanding of fracture geometry alteration. Here, we present results of experimental and numerical investigation of precipitation of calcite into single fractures of artificial geometry in order to highlight the interplays between mineral precipitation, fracture geometry, flow field and growth substrate.

Experimental approach.

Calcite was precipitated from a supersaturated solution at two different flow rates into artificial fractures made in a dolomitic limestone. X-ray micro-tomography imaging was used to retrieve the precipitation rate in the fractures based on image difference (e.g., [2]). Results show that precipitation is highly dependent to the fracture geometry, local saturation index with respect to calcite in relationship with the flow field and the growth substrate. All the observations serve to constrain numerical modeling of the experiments.

Numerial reactive transport modeling in evolving fracture geometries.

The 2D multi-component reactive transport model HYTEC [3] was used to simulate fracture geometry evolution as a result of calcite precipitation. HYTEC solves numerically advection-dispersion-reaction equations. In particular, the model accounts for the feedback between calcite precipitation and the resulting changes of fracture porosity, permeability and flow. In the model, the fractures are discretized in 2D grid cells that approximate the geometry of the fracture planes. Different simulation configurations were tested to evaluate the impacts of three factors: (i) fracture geometry and (ii) Péclet and Damköhler numbers (which are related to the characteristic time for advection and precipitation relatively to diffusion, respectively), and (iii) growth substrate heterogeneity distribution, on the negative feedback between chemistry, transport and permeability reduction in fractures [4] (Figure 1).

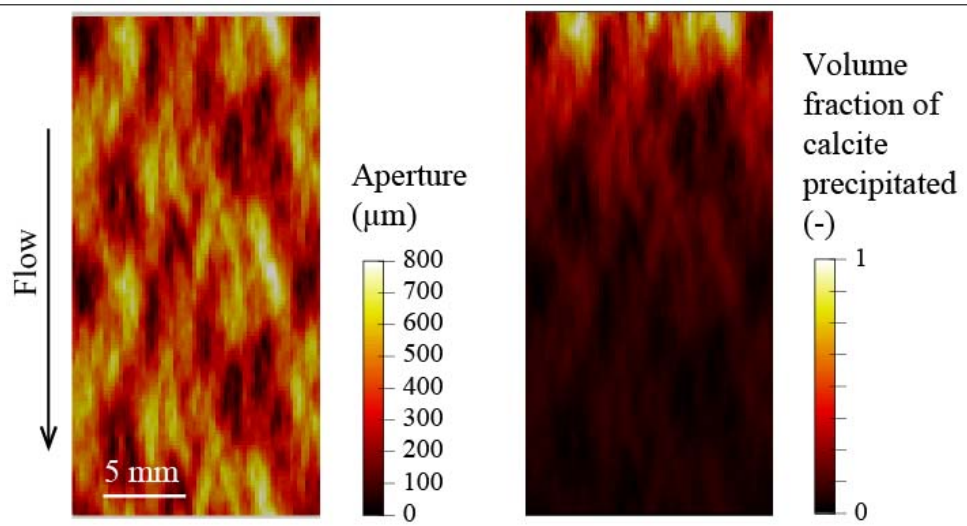

Figure 1: (left) Initial fracture geometry and (right) calcite volume fraction precipitated in a rough fracture, showing preferential precipitation in the areas (1) near the inlet, where the supersaturation is the highest, and (2) in the main flowpaths, where the supply of reactants is higher.

References

[1] Seigneur N., Mayer U. and Steefel C., Reactive Transport in Evolving Porous Media, Reviews in Mineralogy & Geochemistry 7 vol. 85, pp. 197-238 (2019).
[2] Noiriel C., Resolving time-dependent evolution of pore scale structure, permeability and reactivity using X-ray microtomography, Reviews in Mineralogy & Geochemistry, vol. 80., pp. 247-286, (2015).
[3] van der Lee J., De Windt L., Lagneau V. and Goblet P., Module-oriented modeling of reactive transport with HYTEC, Computers & Geosciences, 29, pp. 265-275, (2003).
[4] Noiriel C., Seigneur N., Le Guern P., and Lagneau V., Geometry and mineral heterogeneity controls on calcite precipitation in fractures: an X-ray micro-tomography and reactive transport modeling study. Advances in Water Resources (submitted).

Statistical characterization of the micro-scale spatial distribution of calcite dissolution rates

C. Recalcati[a], M. Siena[a], G. Bussetti[b], L. Duò[b], M. Riva[a], A. Guadagnini[a]

[a] *Department of Civil and Environmental Engineering, Politecnico di Milano, Italy*
[b] *Department of Physics, Politecnico di Milano, Italy*

Keywords: calcite, dissolution rate heterogeneity, stochastic modeling, Atomic Force Microscopy (AFM)

1 Introduction

A detailed knowledge of mineral dissolution/precipitation kinetics is of critical importance in several natural and industrial applications. Examples are processes such as aquifer contamination, geologic sequestration of carbon or hydraulic fracturing of reservoirs. Calcite has been widely studied due to its widespread presence in natural environments and to its propensity to react with pollutants, with potential impacts on groundwater quality [1], [2].

Estimates of dissolution/precipitation kinetics are traditionally assessed through bulk powder experiments. While this technique is simple and characterized by high reproducibility, large discrepancies in dissolution rate values are documented, even for experiments which are conducted under the same laboratory conditions [3]. High-resolution imaging techniques such as Atomic Force Microscopy (AFM) or Vertical Scanning Interferometry (VSI) allowing a direct observation of the processes taking place at the solid-fluid interface, have been intensively employed during the past years for the investigation of calcite dissolution and have dramatically contributed to enhance our understanding of reaction kinetics. Processes occurring on the surface at the microscopic level have been documented to be mainly related to local inhomogeneities and defects in the crystal lattice, which cause an uneven distribution of surface free energy and yield to marked spatial heterogeneities in the dissolution rate. Since the distribution of defects in the lattice may be regarded as random, several authors encourage a change of perspective towards a stochastic approach to capture spatial heterogeneities of dissolution rates [4], [5].

Here, we focus on reaction rate maps evaluated from topography images acquired via AFM imaging of a calcite sample subject to dissolution in deionized water. Our aims include (1) the characterization of the statistical behaviour of dissolution rate data and their spatial increments; (2) the identification of an appropriate interpretive model; (3) a quantitative evaluation of the temporal evolution of spatial heterogeneity of dissolution kinetics.

2 Materials and methods

Calcite samples (~5 × 3 × 1 mm^3) are prepared cleaving an Iceland Spar crystal pressing along the {104} plane with a razor blade immediately before the dissolution experiment. The sample is then placed in a fluid cell, magnetically attached to the measurement system, equipped with syringes allowing the replacement of the solution in the cell. Topography datasets, z, are acquired with an AFM in contact mode (see [6] for further details on the measurement apparatus), setting the scan frequency to 2.2Hz to cover an area of 6 × 6 μm^2 discretized in 512 × 512 pixel. Two diverse experimental conditions are considered: (1) static-solution experiment and (2) constant flow rate experiment. In the former case, the dissolving fluid is left as static in the cell for a temporal window of 30min, whereas in the latter one the entire volume of solution enclosed in the cell is renewed prior to each scan, assuring that the saturation of the fluid layer in direct contact with the sample is constant during the experiment.

Spatial distributions of dissolution rates, R, are evaluated as

$$R = \frac{z(t_1) - z(t_2)}{V_M(t_2 - t_1)} \tag{1}$$

where V_M is calcite molar volume. Characterization of the spatial heterogeneity of R rests on the assessment of the sample statistics of the zero mean fluctuations of dissolution rate, $R' = R(\boldsymbol{x}) - \langle R \rangle$, and of its

spatial increments, $\Delta R = R(\boldsymbol{x}+\boldsymbol{s}) - R(\boldsymbol{x})$ ($\boldsymbol{s}$ being a spatial distance, or lag, vector) from which we evaluate the spatial correlation, ρ, of the dissolution rate.

3 Results

We document the expected dissolution pattern of calcite at this saturation state according to [7], i.e., the nucleation of mono-layer and multi-layer etch pits. The two experiments considered exhibit diverse patterns of the temporal evolution of the surface, as depicted in Figure 1. Static solution experiments (Figure 1.a) show that the main mechanism driving the dissolution process changes over time, etch pits formation being followed by step retreat. Otherwise, surface features remain unchanged for the constant flow rate experiments (Figure 1.b).

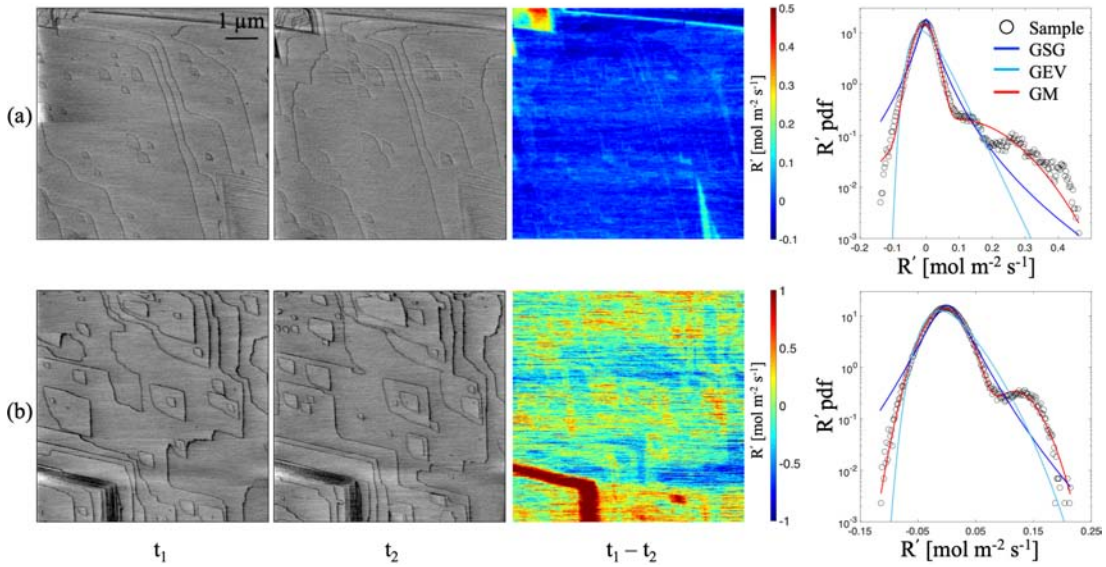

Figure 1: In situ AFM images (friction signal) showing surface pattern evolution in time for static solution (a) and constant flow rate (b) experiment together with the corresponding maps of dissolution rate fluctuation R'. The sample probability density (pdf) of R' and the interpretive models considered are also shown.

The sample statistics of dissolution rate are interpreted with various stochastic models, i.e., the Generalized Extreme Value (GEV) model, as suggested by [8], the Generalized Sub-Gaussian (GSG) model, as in [6], and the Gaussian Mixture (GM) model. The GM model emerges as most promising to capture the behavior of the sample probability densities of the rate in both experimental settings. Simple correlation models as well as nested models are employed to interpret spatial correlation of dissolution rates. The temporal trend of the model parameters is then investigated to provide quantitative insights on the temporal dynamics of the dissolution rate spatial organization.

References

[1] Heberling, F., Bosbach, D., Eckhardt, J.-D., Fischer, U., Glowacky, J., Haist, M., Kramar, U., Loos, S., Müller, H.S., Neumann, T., Pust, C., Schäfer, T., Stelling, J., Ukrainczyk, M., Vinograd, V., Vučak, M., Winkler, B.: Reactivity of the calcite–water-interface, from molecular scale processes to geochemical engineering. Appl. Geochem. 45, 158–190 (2014).

[2] Renard, F., Røyne, A., Putnis, C.V.: Timescales of interface-coupled dissolution-precipitation reactions on carbonates. Geosci. Front. 10, 17–27 (2019).

[3] Arvidson, R.S., Ertan, I.E., Amonette, J.E., Luttge, A.: Variation in calcite dissolution rates: geochim. Cosmochim. Acta. 67, 1623–1634 (2003).

[4] Luttge, A., Arvidson, R.S., Fischer, C.: A stochastic treatment of crystal dissolution kinetics. Elements 9, 183–188 (2013).

[5] Luttge, A., Arvidson, R.S., Fischer, C., Kurganskaya, I.: Kinetic concepts for quantitative prediction of fluid-solid interactions. Chem. Geol. 504, 216–235 (2019).

[6] Siena, M., Bussetti, G., Recalcati, C., Riva, M., Duò, L., Guadagnini, A.: Statistical characterization of heterogeneous dissolution rates of calcite from in-situ and real-time AFM imaging. Transp. Porous Media. Published online (2021).

[7] Teng, H.H.: Controls by saturation state on etch pit formation during calcite dissolution. Geochim. Cosmochim. Acta. 68, 253–262 (2004).

[8] Brand, A.S., Feng, P., Bullard, J.W.: Calcite dissolution rate spectra measured by in situ digital holographic microscopy. Geochim. Cosmochim. Acta. 213, 317–329 (2017).

Geostatistical description of calcite surface roughness resulting from dissolution at close-to-equilibrium conditions

Luca Stigliano[1,2], Martina Siena[2], Philippe Ackerer[1], Alberto Guadagnini[2], Damien Daval[1]

[1] Université de Strasbourg / CNRS / ENGEES, Institut Terre et Environnement de Strasbourg, UMR 7063. 1 Rue Blessig, 67084 Strasbourg, France.
[2] Dipartimento di Ingegneria Civile e Ambientale, Politecnico di Milano, Piazza L. Da Vinci 32, 20133 Milano, Italy.

Keywords: Calcite, Near equilibrium dissolution, Surface roughness, Geostatistics, Dissolution models

1 Introduction

Characterizing reactive processes at fluid-solid interfaces is key for the description of flow and transport phenomena in porous media, as they are known to affect several relevant properties, such as porosity and permeability [1-3]. Proper assessment of the dissolution kinetics is therefore critical for a number of applications including enhanced rock weathering for carbon dioxide removal from the atmosphere [4], radioactive waste storage [5], geothermal energy recovery [6] and geological storage of CO_2 [7], as well as for industrial sectors such as chemical engineering or medicine. As such, linking the evolution of the surface area (as quantified, e.g., through its spatial roughness) of grains to their dissolution rate is a key aspect of reactivity [8]. Unravelling the nature of its main features requires relying on approaches yielding a quantitative characterization of the temporal evolution of surface topography/roughness.

Here, a mechanically-polished {104} calcite surface was dissolved at room temperature and at close-to-equilibrium conditions (Ω=0.6) with an alkaline solution (pH = 8) across a temporal window of 8 days. Surface topography images were acquired daily using vertical scanning interferometry, the ensuing topography data being then embedded within a geostatistical analysis framework aimed at describing comprehensively the surface roughness evolution.

With the aim of obtaining insights on the underlying dissolution mechanism, three numerical models have been examined against the experimental observations. The model which was revealed as the most skillful to reproduce the observed statistical description of the system was then employed to assess the relative impact of initial surface roughness and fluid composition on the geostatistical evolution of the surface roughness.

2 Results

Time-resolved geostatistical analyses of a mechanically polished calcite surface reacting at close-to-equilibrium conditions were demonstrated to be a powerful tool to assess attainment of steady-state configuration for the reacting surface. This is reflected through the temporal dynamics of the key statistics and spatial semi-variograms of surface roughness which tend to stabilize after a given relaxation time

(approximately two days in our experiments). Our approach can be used as a quantitative reference to compare (i) differently polished (or unpolished, e.g., cleavage) calcite surfaces reacting at the same physico-chemical conditions, or (ii) mechanically polished calcite surfaces reacting at different physico-chemical conditions. In this context, additional investigations may contribute to possibly distinguish between the individual contribution given by the initial surface roughness and the reacting conditions to the plateau values of the statistical moments characterizing the dissolving surface area at steady-state.

The original numerical model developed in this work suggested that the influence of the initial surface roughness is limited, whereas potential empirical relations linking the surface roughness of reacted crystals to the saturation state at which they dissolved may be developed, which would allow to back-estimate the reacting conditions only based on topography data. The model also suggested that, under the investigated conditions, the dissolution of a calcite crystal is consistent with a mechanism based on the random generation of a number of areas dissolving preferentially, which tend to increase with time, and grow until they finally merge to attain a steady-state surface area.

Overall, our study suggests that potential empirical relations linking the surface roughness of reacted crystals to the saturation state at which they dissolved may be developed, which would make it possible to back-estimate the reacting conditions by simply measuring the topography of the reacted surface after attainment of steady-state.

References

1. Noiriel, C., P. Gouze, and D. Bernard, *Investigation of porosity and permeability effects from microstructure changes during limestone dissolution.* 2004. **31**(24).
2. Noiriel, C., et al., *Changes in reactive surface area during limestone dissolution: An experimental and modelling study.* Chemical Geology, 2009. **265**(1): p. 160-170.
3. Steefel, C.I. and K.T.B. MacQuarrie, *Approaches to modeling of reactive transport in porous media*, in *Reactive Transport in Porous Media*, P.C. Lichtner, C.I. Steefel, and E.H. Oelkers, Editors. 1996, Mineralogical Soc America: Washington. p. 83-129.
4. Beerling, D.J., et al., *Potential for large-scale CO2 removal via enhanced rock weathering with croplands.* Nature, 2020. **583**(7815): p. 242-248.
5. Frugier, P., et al., *SON68 nuclear glass dissolution kinetics: Current state of knowledge and basis of the new GRAAL model.* Journal of Nuclear Materials, 2008. **380**(1-3): p. 8-21.
6. Alt-Epping, P., et al., *Reactive transport modeling of the geothermal system at Bad Blumau, Austria: Implications of the combined extraction of heat and CO2.* Geothermics, 2013. **45**: p. 18–30.
7. Daval, D., *Carbon dioxide sequestration through silicate degradation and carbon mineralisation: promises and uncertainties.* npj Materials Degradation, 2018. **2**(1): p. 11.
8. Fischer, C., et al., *Variability of crystal surface reactivity: What do we know?* Applied Geochemistry, 2014. **43**(0): p. 132-157.

Poster

High pressure intrusion of non-wetting liquid in hydrophobic Zeolitic Imidazolate Frameworks for mechanical energy storage/absorption

A. Astafan[a,b], H. Nouali[a,b], A. Ryzhikov[a,b], T.J. Daou[a,b], C. Marichal[a,b], G. Chaplais[a,b]

[a] *Université de Haute-Alsace, CNRS, Institut de Science des Matériaux de Mulhouse (IS2M), UMR 7361, Axe Matériaux à Porosité Contrôlée (MPC), F-68100, Mulhouse, France*
[b] *Université de Strasbourg, F-67000 Strasbourg, France*

Keywords: mechanical energy storage, Zeolitic Imidazolate Frameworks, high pressure intrusion-extrusion, water, aqueous electrolyte solutions

Since 2001, our team has been studying the process of intrusion-extrusion of non-wetting liquids into a lyophobic porous material for absorption and storage of mechanical energy [1, 2]. Such systems, composed of a porous material (M) and a non-wetting liquid (L), are called also Heterogeneous Lyophobic Systems "HLS" and usually referred as "M–L".
From a conceptual point of view, the intrusion step, which is associated with the transformation of the liquid into a multitude of molecular clusters in the pores, occurs by applying an external pressure. During this compression step, the supplied mechanical energy is thus converted into interfacial energy. In the extrusion step, when the pressure is released, the system may induce an expulsion of the liquid out of the pores (extrusion). Depending on various physicochemical and structural parameters related to porous material combined with the nature of non-wetting liquid, HLS is able to restore, dissipate or absorb the mechanical energy supplied during the intrusion step and therefore to display a spring, shock-absorber or bumper behavior. Figure 1 presents the idealized Pressure-Volume diagrams of these three main energetic behaviors.

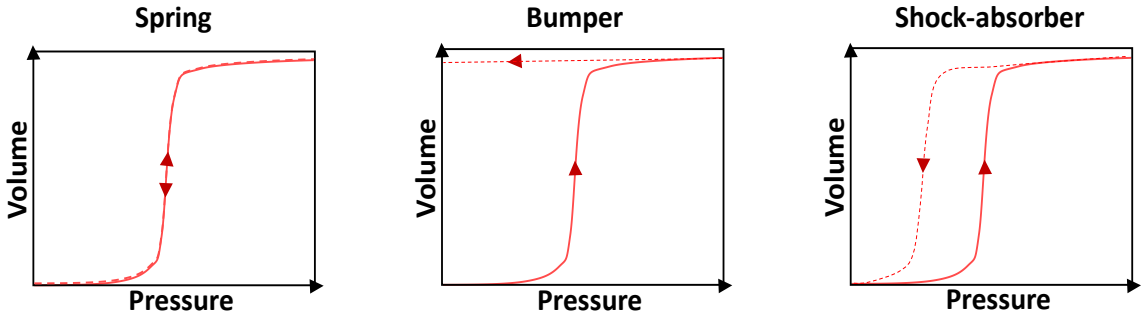

Figure 1: Idealized Pressure-Volume diagrams of the three main energetic behaviors. The intrusion curve is represented in continue line while the extrusion curve is depicted in dotted line.

Zeolitic Imidazolate Frameworks (ZIFs), a subclass of metal-organic frameworks, constructed from divalent metal ions (Zn^{2+}, Co^{2+}, Cd^{2+}, Fe^{2+} cations) and imidazolate-type linkers, may display both a hydrophobic and porous nature. Thus, such materials are of high interest in their use in HLS as a porous matrix, combined with water or electrolyte aqueous solutions as non-wetting liquids.
In 2013, our team paved the way for the study of energetic performances for ZIFs-based systems by using intrusion-extrusion experiments with the "ZIF-8−water" system. It has been shown that this system acts as a spring with a stored energy of 13 $J.g^{-1}$ [2]. Since then, the energetic performances of others ZIFs-based HLS have been studied. These studies have emphasized the various effects of the crystals size and shape, the nature of linker, the topology as well as the nature of non-wetting liquid on the energetic performances of the investigated systems [3-8].
In this work, we particularly highlight the influence of the anion nature on the energetic performances of "ZIFs–potassium salts aqueous solutions" systems.

References

[1] V. Eroshenko, R. Regis, M. Soulard, J. Patarin, Energetics: A new field of applications for hydrophobic zeolites, *J. Am. Chem. Soc.*, 123, 8129-8130 (2001).
[2] G. Ortiz, H. Nouali, C. Marichal, G. Chaplais, J. Patarin, Energetic performances of the metal-organic framework ZIF-8 obtained using high pressure water intrusion-extrusion experiments, *Phys. Chem. Chem. Phys.*, 15, 4888-4891 (2013).
[3] G. Ortiz, H. Nouali, C. Marichal, G. Chaplais, J. Patarin, Versatile Energetic Behavior of ZIF-8 upon High Pressure Intrusion-Extrusion of Aqueous Electrolyte Solutions, *J. Phys. Chem. C.*, 118, 7321-7328 (2014).
[4] G. Ortiz, H. Nouali, C. Marichal, G. Chaplais, J. Patarin, Energetic Performances of "ZIF-71-Aqueous Solution" Systems: a Perfect Shock-Absorber with Water, *J. Phys. Chem. C.*, 118, 21316-21322 (2014).
[5] I. Khay, G. Chaplais, H. Nouali, C. Marichal, J. Patarin, Water intrusion–extrusion experiments in ZIF-8: impacts of the shape and particle size on the energetic performances, *RSC. Adv.*, 5, 31514-31518 (2015).
[6] I. Khay, G. Chaplais, H. Nouali, G. Ortiz, C. Marichal, J. Patarin, Assessment of the energetic performances of various ZIFs with SOD or RHO topology using high pressure water intrusion–extrusion experiments, *Dalton. Trans.,* 45, 4392-4400 (2016).
[7] B. Mortada, G. Chaplais, V. Veremeienko, H. Nouali, C. Marichal, J. Patarin, Energetic Performances of ZIF-8 Derivatives: Impact of the Substitution (Me, Cl, or Br) on Imidazolate Linker, *J. Phys. Chem. C.*, 122, 3846-3855 (2018).
[8] B. Mortada, G. Chaplais, H. Nouali, C. Marichal, J. Patarin, Phase transformations of Metal-Organic Frameworks MAF-6 and ZIF-71 during intrusion-extrusion experiments, *J. Phys. Chem. C.*, 123, 4319-4328 (2019).

Hydrodynamic modelling of geothermal reservoir around Site U1517

G. Akhmetova[a], I. Panfilov[a], A. Pereira[a], S. Bourlange[b],

[a]*LEMTA, 2 Avenue de la Forêt de Haye, Université de Lorraine, Vandœuvre-lès-Nancy, 54500*
[b]*GeoRessources, 2 rue du Doyen Marcel Roubault, Université de Lorraine, Vandœuvre-lès-Nancy, 54500*

Keywords: gas hydrates, bottom simulating reflector, landslide, numerical modelling

1 Introduction

The Hikurangi Margin is an active subduction area located in the eastern side of New Zealand, where the Pacific oceanic plate and the Australian continental plate encounter and is the cause of a number of earthquakes each year bringing geological catastrophes and damage to the infrastructures.

The objective of the present study is to obtain an accurate picture of the fluid circulation and temperature distribution in the area so as to determine how the seafloor stability is affected by a submarine landslide located above the Hikurangi Margin, and by the presence of gas hydrates revealed in seismic images [1] by a bottom simulating reflector (BSR). BSRs are a physical boundary indicator between gas-hydrates bearing sediments and free-gas saturated sediments, and are usually located a few hundred meters below the seabed in the continental slope, especially in the accretion prisms of the subduction zone, parallel to the seafloor.

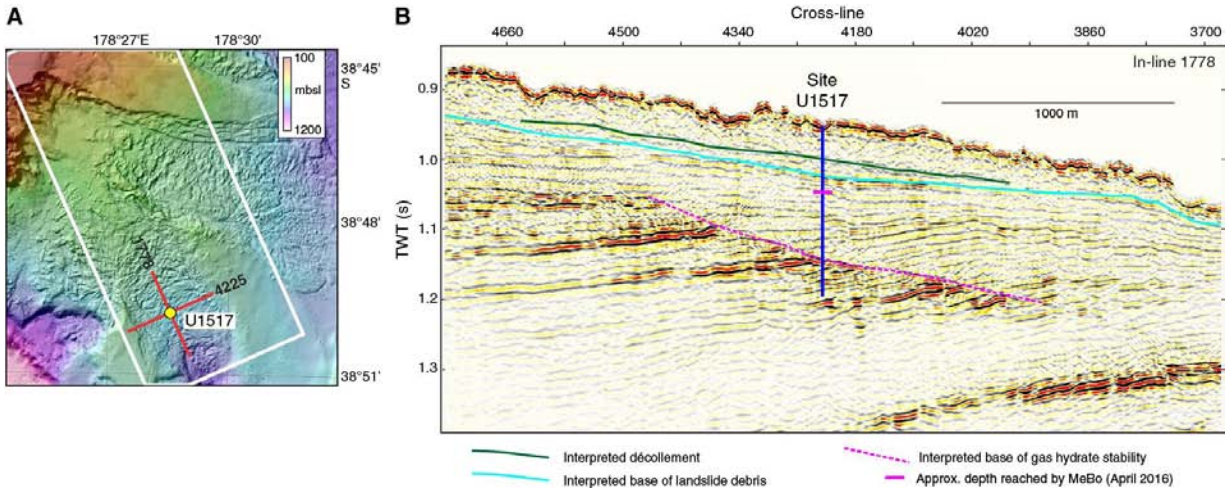

Figure 1: Bathymetry around Site U1517 with in-line and cross-line tracks from the 3-D seismic cube (A). Seismic section from the 3-D cube crossing Site U1517 with interpreted key horizons(B) [2].

2 Numerical modelling methods

A thermal and hydrodynamic model of the Hikurangi Margin area, taking into account gas hydrate transition phases, was constructed from data available around the U1517 site (see figure 1). The geometry

and physical parameters used are obtained from the structure defined in the seismic section and the physical properties of the U1517 cores [2]. The time evolution of heat and fluid fluxes, pressure and temperature distributions, as well as gas hydrate transition boundaries, are calculated using a finite element code. Different scenarios were tested considering a realistic range of background lateral fluid fluxes and dissolved methane concentrations.

3 Results

The several temperature and pressure distributions obtained from the present numerical study allowed us to determine the position of the BSR inside the geothermal reservoir matching the one appearing on seismic images. The dependence of the BSR position on the reservoir parameters such as water density, layers permeability and thermal properties of the sediments is examined as well as the methane distribution evolution. The crucial role played by the faults zones in the area is also emphasized.

References

[1] Barnes, Tectonic and geological framework for gas hydrates and cold seeps on the Hikurangi, *Marine Geology*, 272, 26-48 (2010).
[2] Barnes, Proceedings of the International Ocean Discovery Program, Volume 372A, *publications.iodp.org,* (2019).

Sink vs. tilt penetration into shaken dry granular matter: the role of foundation

L. Alonso-Llanes[a,b], G. Sánchez-Colina[a], A. J. Batista-Leyva[c,a], C. Clément[b], E. Altshuler[a], R. Toussaint[b,d]

[a] *Group of Complex Systems and Statistical Physics, Physics Faculty, University of Havana, 10400 Havana, Cuba.*
[b] *Université de Strasbourg, CNRS, Institut Terre et Environnement de Strasbourg, UMR7063, 67000 Strasbourg, France.*
[c] *Instituto Superior de Tecnologías y Ciencias Aplicadas (InSTEC), Universidad de la Habana, La Habana 10400, Cuba.*
[d] *PoreLab, The Njord Centre, Department of Physics, University of Oslo, P.O. Box 1074 Blindern, 0316 Oslo, Norway.*

Keywords: shaken granular matter, liquefaction, intruder penetration

1. Abstract

We study the behavior of cylindrical objects as they sink into a dry granular bed fluidized due to lateral oscillations (Fig. 1). Somewhat unexpectedly, we have found that, within a large range of lateral shaking powers, cylinders with flat bottoms sink vertically, while those with a "foundation"consisting in a shallow ring attached to their bottom, tilt besides sinking. The latter scenario seems to dominate independently from the nature of the foundation when strong enough lateral vibrations are applied. We are able to explain the observed behavior by quasi-2D numerical simulations, and the vertical sink dynamics with the help of a Newtonian equation of motion for the intruder. Our findings may shed light on the behavior of buildings and other man-made constructions during earthquakes.

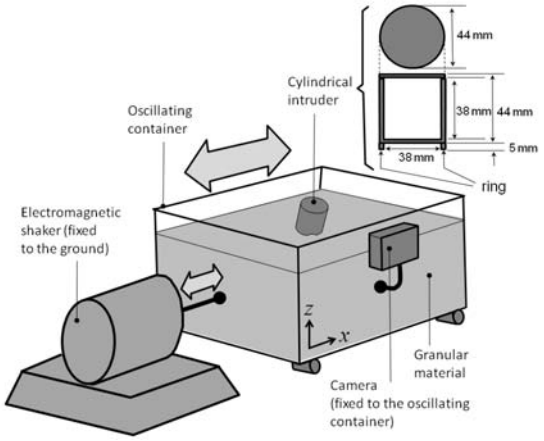

Figure 1: Experimental setup. At the upper right, we have illustrated the intruder consisting in a cylinder with ring.

Chemo-mechanical effects of salt crystallization in 3D porous media: dynamic studies by X-ray tomography

Syrine Ben Elhadj Hamida [a,b], Pascale Senechal [b], Peter Moonen [a,b], Hannelore Derluyn [a,b]
[a]Université de Pau et des Pays de l'Adour, E2S UPPA, CNRS, Total, LFCR, Pau, France
[b]Université de Pau et des Pays de l'Adour, E2S UPPA, CNRS, DMEX, Pau, France

Keywords: Porous media, salt crystallization, X-ray μCT

1 Introduction

Saline aquifers have a large capacity for gas storage, such as CO_2 or natural gas. This storage leads to perturbations of the underground environment, and might induce the precipitation of salts, natural constituents of brines present inside the host rock. When precipitation occurs inside the pores, the rock's permeability might decrease. Crystallization stresses might build up as well which can eventually fracture the rock [1]. As such, the injectivity can be highly impacted. Crystallization-induced fracturing is also a main cause of the weathering of building stones and construction materials, and as such can drastically reduce the lifetime of a building or structure.

It is therefore essential to understand the relationship between salinity, pore structure and the risk for pore clogging and fracture formation, to be able to control this risk in future geoengineering and civil engineering applications. In the framework of the ERC project PRD-Trigger (Precipitation triggered rock dynamics – the missing mesoscopic link), the purpose of this study is to identify the key correlations between morphological identifiers of the pore space (pore size, shape, connectivity), fluid and salt distributions and precipitation-induced damage based on quantitative image processing of 4D X-ray μCT experiments.

2 Experimental study

As a first step, artificial 3D porous media have been designed, allowing to precisely control the pore size distribution and porosity. The model porous media are composed of glass beads within a glass capillary tube (8 mm inner diameter) that are joined together by an epoxy-resin method [2], representative for an artificial rock core that is sealed circumferentially. By varying the mix of bead sizes, samples with unimodal or multimodal pore size distributions are created. The porosity, pore size distribution and connectivity are quantified from an X-ray tomographic scan of the artificial porous medium.

Two salts are used in this study, sodium chloride (NaCl) and sodium sulphate (Na_2SO_4). They are two of the most abundant salts found in building materials upon salt weathering damage. Sodium sulphate can be considered as a 'model' salt for hydration reactions, whereas sodium chloride can be regarded as a 'model' salt for coastal conditions, as well as for reservoir brines.

The thenardite (Na_2SO_4) → mirabilite ($Na_2SO_4 \cdot 10H_2O$) transition reaction of sodium sulphate at room temperature is known to induce cracking easily, due to the generation of high supersaturations and thus high crystallization pressures [3]. Thenardite crystallization is provoked in the samples by rapid drying-out in an oven. Thenardite crystals then serve as nucleation points for mirabilite precipitation, which is provoked by rewetting the sample at room temperature. Multiple drying-rewetting cycles at room temperature are subsequently imposed until the occurrence of damage.

NaCl is known to have the potential to create high crystallization pressures at high supersaturations (up to 200 MPa [4]), and its precipitation follows from the drying-out of a sample imbibed with sodium chloride solution. To that extent, dry gas is injected at a constant flow rate from the bottom of the sample, percolating upward due to buoyancy.

X-ray tomographic scans performed at regular time intervals and followed by image processing allow to determine different characteristics of crystals and their location in relation to the distribution of the brine

and the pore space characteristics (pore size, connectivity). Furthermore, by tracking the motion of the individual glass bead, crystallization-induced deformations are quantified.

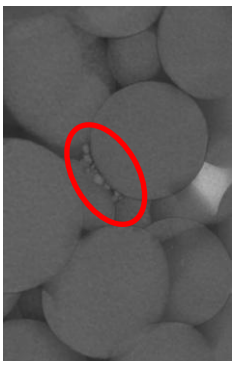

Figure 1: 3D view from CT scan of salt crystals (circled in red) in a glass beads porous medium

Acknowledgement

This research was financially supported by the European Research Council (ERC) under the European Union's Horizon 2020 research and innovation programme (grant agreement No 850853).

References

[1] S. H. Hajiabadi, P. Bedrikovetsky, S. Borazjani, and H. Mahani, " Well Injectivity during CO 2 Geosequestration: A Review of Hydro-Physical, Chemical, and Geomechanical Effects ," *Energy & Fuels*, vol. 35, no. 11, pp. 9240–9267, 2021, doi: 10.1021/acs.energyfuels.1c00931.

[2] T. Klimentos and A. Parker, "The preparation (by an epoxy-resin method) and physical properties of artificial sandstones," *Sediment. Geol.*, vol. 59, no. 3–4, pp. 307–312, 1988, doi: 10.1016/0037-0738(88)90083-8.

[3] R. J. Flatt, F. Caruso, A. M. A. Sanchez, and G. W. Scherer, "Chemo-mechanics of salt damage in stone," *Nat. Commun.*, vol. 5, pp. 1–5, 2014, doi: 10.1038/ncomms5823.

[4] M. Steiger, "Crystal growth in porous materials - I: The crystallization pressure of large crystals," *J. Cryst. Growth*, vol. 282, no. 3–4, pp. 455–469, 2005, doi: 10.1016/j.jcrysgro.2005.05.007.

Une analyse critique des modèles à deux paramètres pour décrire le transport de soluté en milieu poreux : simulations et exemples expérimentaux

N. Benaouag[a], M. Sardin[b], R. Rihani[a]

[a]Laboratoire des Phénomènes de Transfert, Faculté de génie mécanique et de génie des procédés, Université des Sciences et Technologie Houari Boumediene (USTHB), Alger (Algérie).
[b]Laboratoire Réactions et Génie des Procédés (LRGP), École Nationale Supérieure des Industries Chimiques, Université de Lorraine - CNRS, Nancy (France).

Mots clés : Modélisation, courbes de percé, transport, lix fixe,

Résumé

De nombreuses publications sur le transport des polluants en lit fixe en particulier en traitement des eaux utilisent encore des modèles à deux paramètres : un paramètre de capacité, mesurant le retard de la courbe de percée (CP) et un paramètre de cinétique de transfert pour traduire la dispersion observée. Les auteurs négligent totalement le rôle de la dispersion hydrodynamique qui contribue pourtant largement à l'étalement des courbes. A l'aide de trois exemples impliquant des lits fixes de billes adsorbantes homogènes ou de sable, l'un de Xiaoqing Lin et.al (2013) [1] avec des grains de biochar-alginate (diamètre 2.0 mm), le suivant de Jiseon Jang et.al (2018) [2] avec des billes de résine (diamètre 0.8 mm), et nos propres travaux avec un sable de diamètre moyen 0.4 mm Benaouag et al., (2018) [3] nous avons analysé la validité de ces modélisations. Pour cela nous avons utilisé comme support de référence un modèle à 4 paramètres (Mélangeurs en Cascade avec Echanges) tenant compte de la dispersion hydrodynamique et d'une cinétique de transfert de matière du premier ordre.

Dans les deux publications analysées, les auteurs ont modélisé leurs CPs par trois modèles classiques à deux paramètres. Deux d'entre eux donnent d'excellents ajustements sur les CPs des polluants. Nous avons établi la correspondance entre les deux modèles d'un point de vue cinétique, confirmant leur concordance avec le paramètre de transfert du modèle MCE. Pour les deux exemples expérimentaux, nous avons déterminé la dispersion dans les lits de billes à partir des corrélations du génie chimique. Dans le modèle MCE la dispersion est traduite par un nombre de mélangeur J. Trois des paramètres du modèles MCE (J, t_0 et K') ont été déterminés a priori [3]. Le quatrième paramètre qui est le temps de transfert de matière a été ajusté sur les points expérimentaux.

On montre ainsi sur le premier exemple du transport du strontium [2] que la dispersion est principalement contrôlée par la cinétique de transfert justifiant, l'approche proposée par les auteurs de négliger la dispersion et d'utiliser un modèle à deux paramètres. A contrario dans le cas des courbes de percé du butanol sur lit de résine [1] le calcul a priori de la dispersion hydrodynamique montre que toute la dispersion observée sur les courbes de percée est contrôlée par la dispersion hydrodynamique et non par la cinétique de transfert, invalidant ainsi l'interprétation proposée. En conclusion, l'utilisation de modèles à deux paramètres nécessite une analyse critique de la dispersion effective observée. L'utilisation d'un traceur de l'écoulement lors des expériences permet de lever cette hypothèse et de choisir la bonne interprétation.

Références :

[1] Xiaoqing Lin, Renjie Li, Qingshi Wen, Jinglan Wu, Jiansheng Fan, Xiaohong Jin, Wenbin Qian, Dong Liu, Xiaochun Chen, Yong Chen, Jingjing Xie, Jianxin Bai, and Hanjie Ying. **(**2013)**, «Experimental and Modeling Studies on the Sorption Breakthrough Behaviors of Butanol from Aqueous Solution in a Fixed-bed of KA-I Resin.»**. *Biotechnology and Bioprocess Engineering*, 18: 223-233.

[2] Jiseon Jang, Waheed Miran, Sewu D. Divine, Mohsin Nawaz, Asif Shahzad, Seung Han Woo, Dae Sung Lee. (2018)**« Rice straw-based biochar beads for the removal of radioactive strontium from aqueous solution».** Science of the Total Environment 615, 698–707,

[3] Benaouag, N., Sardin, M., Arrar, J., Bentahar, F., (2018). **« Migration of Naphthalene through Low Organic Content Sandy Soil Columns: Comparison of Unsaturated and Saturated Conditions »**. Soil and Sediment Contamination VOL. 27, NO. 5, 408–425.

Coupling between compaction and pressurization during shear waves in drained granular layers: implications for soil liquefaction

S. Ben zeev[a,b], R. Toussaint [b,c], E. Aharonov[a], L. Goren[d], S. Parez[d]

[a] *Institute of Earth Science, Hebrew University of Jerusalem, Israel*
[b] *Institut Terre et Environnement de Strasbourg, UMR7063, CNRS, Univ. Strasbourg & ENGEES, Strasbourg, France*
[c] *SFF PoreLab, The Njord Center, Physics Dept, Univ. Oslo, Norway*
[d] *Geological & Environmental Science, Ben-Gurion University of the Negev, Israel*
[e] *Institute of Chemical Process Fundamentals of the CAS, Prague, Czech Republic*

Keywords: compaction, liquefaction, fluid/granular model, soil mechanics, fluid mechanics

The dynamics of saturated granular layers during shaking is controlled by the coupling between grains and fluid. Understanding such systems is crucial for studies of soil liquefaction, seismically induced landslides and shear along faults. This study focuses on the compaction of a near surface well-drained saturated granular layer during seismic shaking. Compaction is known to promote soil liquefaction, but the exact feedback mechanism between compaction and pressurization remains poorly understood. We use Discrete Element numerical simulations composed of coupled solid grains and fluid phases under cyclic horizontal shear of the bottom undrained boundary and a free, completely drained, top layer. We compare the dynamics under two drainage conditions: First, simulations of "infinite" drainage, where the fluid pressure is maintained hydrostatic during the shaking, similar to the model of Clément et al. (2018) [1]. Second, simulations of "realistic" drainage in a high permeability layer, whereby fluid pressure dynamically deviates from hydrostatic values due to local granular compaction and dilatation, presented in details by Ben Zeev et al. (2020) [2]. Simulation results show two end member behaviours, with a transition controlled by the magnitude of shaking acceleration:

At low acceleration the system behaves rigidly, compaction is negligible and fluid pressure remains constant even during "realistic" drainage simulations, where it is allowed to evolve. At high acceleration, significant compaction occurs in both cases, but the compaction rate is higher in "realistic" drainage simulations.

This rapid compaction trend is temporally correlated to a transient pore pressure increase that reaches lithostatic stress values before it drops back to a lower value. This is an evidence to a feedback mechanism in which compaction causes pressure increase that can persist under drained condition as long as the compaction rate is sufficiently high. On the other hand, this very pressure itself promotes the high compaction rate. (See Fig. 1). From this we conclude that although well-drained soils are considered liquefaction-resistant, dynamic coupling between pore fluid pressure elevation and compaction during seismic shaking provides a previously unrecognized pathway to liquefaction.

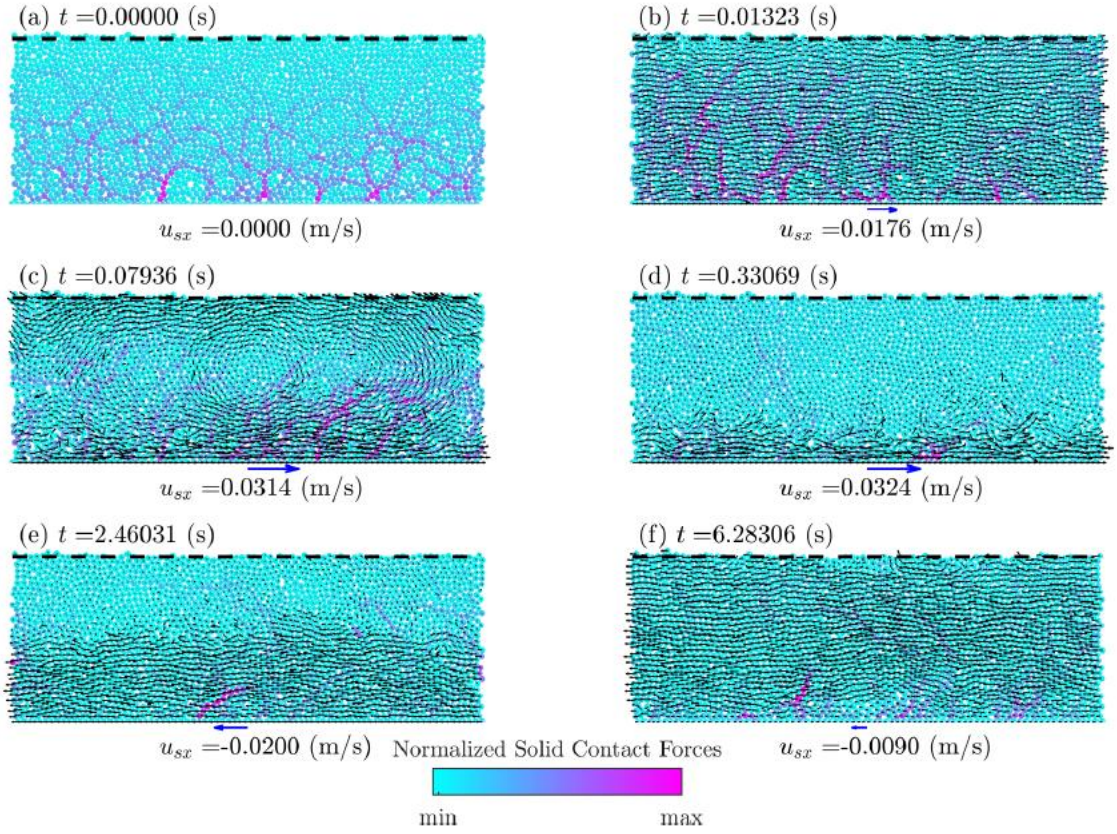

Figure 1: Snapshots of granular dynamics during a high-acceleration simulation (Peak Ground Acceleration = 0.25 g) with dynamic pore pressure. The colors of the grains indicate their relative solid normal contact force, normalized to the maximum normal force in each frame: (a) 3.5 N, (b) 0.7 N, (c) 7.5 N, (d) 1.7 N, (e) 2.6 N, and (f) 1.0 N. Black arrows depict the solid grain velocity. The blue arrow at the base indicates the imposed bottom wall velocity, exaggerated by a factor of 5 with respect to the black arrows. The dashed black line shows the position of the fluid top surface. (a) Before the initiation of shear, the layer is at rest. (b) When the imposed shaking starts, the grain skeleton behaves in a solid manner, with percolating stress chains capable of transmitting the shear waves from the bottom wall. (c) Some of the motion occurs via transient granular vortices. (d) After a few cycles, the stress chains almost vanish and shear is not transmitted through the upper parts of the layer. (e) The thickness of the bottom sheared zone gradually increases. (f) The whole layer is sheared as in the very beginning.

References

[1] Clément, C., Toussaint, R., Stojanova, M., & Aharonov, E. Sinking during earthquakes: Critical acceleration criteria control drained soil liquefaction. *Physical review E*, 97(2), 022905 (2018).
[2] Ben-Zeev, S., Aharonov, E., Toussaint, R., Parez, S., & Goren, L. Compaction front and pore fluid pressurization in horizontally shaken drained granular layers. *Physical Review Fluids*, 5(5), 054301 (2020)

Application of porous media study techniques on natural samples from Western Siberian Lowlands

S. Cazaurang, M. Marcoux[a,b], L. Orgogozo[b], S. Loiko[c,d], A. Lim[c,d], S.Audry[b], L.Shirokova[b,e], O. Pokrovsky[b,c]

[a] Biological Porous Media Lab., Toulouse Institute of Fluid Mechanics (IMFT).National Polytechnical Institute of Toulouse (INPT) - Toulouse, France.
[b] Geoscience Environment Toulouse Lab., Observatoire Midi-Pyrénées. Université Toulouse III - Paul Sabatier - Toulouse, France.
[c] BioGeoClim Laboratory, Tomsk State University - Tomsk, Russian Federation.
[d] Department of Soil Science and Soil Ecology, Tomsk State University - Tomsk, Russian Federation.
[e] N. Laverov Federal Center for Integrated Arctic Research of the Ural Branch of the Russian Academy of Sciences – Russian Federation

Keywords: Representative Elementary Volume, Physical properties, Bryophytes.

1 Introduction

Permafrost can be described as a soil horizon which is perennially frozen during at least two consecutive years. This mainly occurs at high latitudes and more specifically on nearly a quarter of Northern Hemisphere lands [1]. These frozen soils are for the most part of them covered with a complex association of Bryophytes (*i.e.* non-vascular plants), lichens (*i.e.* symbiotic association of *Fungus* and algae) [2] which can be considered as the main interface between the atmosphere and the geosphere. Between 2008 and 2016, global climate change has been strongly correlated to an increase of 0.4 (± 0.2) ° C on mean soil temperature in the Arctic [3]. This lead the IPCC to classify arctic biomes as "highly vulnerable" considering a large scale climate change in the next hundreds of years [4]. Understanding hydrological and thermal dynamics in arctic soils is hence a key to accurately forecast permafrost thaw consequences on natural systems (land erosion) and on human societies (building collapse, greenhouse gas emission). Overlying vegetation cover, which is a strongly multi-scale porous medium, is still poorly characterized in terms of thermal and hydrological properties although its significant role for permafrost's thermo-hydrological dynamics. Therefore, this study aims giving some usage examples of well-established numerical porous media study techniques on X-ray computed tomography samples. A comparative study with previously obtained results available in the literature is also conducted.

2 Sampling and pore-scale imaging

In order to access bryophytic cover's hydrological and thermal properties, 12 samples of *Sphagnum* mosses, lichen and peat were collected in 2018 at the Khanymey Research Station (INTERACT - Tomsk State University) and dried at 40 °C during 48h. Samples were then numerically reconstructed using X-ray computed tomography at a resolution of 94 μm.voxel^{-1}. The obtained numerical reconstruction volumes after pre-processing (cropping and binarization) fluctuate from 783^3 to 995^3 voxels. Examples of some numerical reconstructions are shown in figure 1.

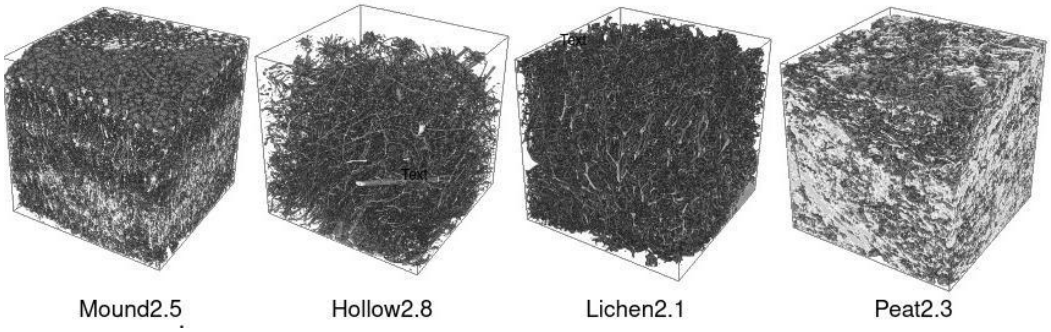

Figure 1: Examples of numerically reconstructed samples for each studied types of samples. *Hollow* stands for samples which were collected in topographical depressions and *Mound* for topographic high points.

3 Numerical assessments of effective properties

The resulting image stacks representing the numerical reconstructions are processed following similar methods traditionally deployed in more conventional porous media (soils [5], sandstones [6] and glass beads [7]). For each of the studied properties (porosity and effective permeability tensor in the first place), a Representative Elementary Volume is accessed using High Performance Computing and dedicated image processing software (IPSDK – Réactiv'IP, France) and Computational Fluid Dynamics open-sourced software (OpenFOAM [8]).

Sample	Global Porosity [%]	Best porosity REV [mm]	Mean porosity of the REV [%]
Hollow1.2	74.43	-	-
Hollow1.4	53.14	13.16	56.565 ± 4.922
Hollow2.7	96.46	2.82	96.143 ± 0.328
Hollow2.8	94.29	7.52	96.266 ± 2.970
Lichen1.3	83.51	1.88	83.422 ± 3.850
Lichen2.1	88.23	14.08	86.675 ± 4.868
Mound1.1	39.13	5.64	38.198 ± 4.905
Mound2.4	57.72	9.40	62.596 ± 2.679
Mound2.5	72.94	11.28	67.872 ± 4.923
Mound2.6	93.29	26.32	93.514 ± 0.999
Peat2.2	49.82	-	-
Peat2.3	55.04	3.76	50.256 ± 2.956

Table 1: Porosity calculation on each sample. REV stands for Representative Elementary Volume.

The obtained results (table 1) show that the air-filled porosity spans from 39 to 96 % of the sample's total volume. Computation converged to Representative Elementary Volumes for 10 of the 12 collected samples with sizes ranging from 1.88 mm to 26.32 mm. Some introductory Direct Numerical Simulations of single-phase flows on arbitrarily chosen sample sub-volumes showed a high values for intrinsic permeability mainly between 10^{-8} and 10^{-19} m² (or 10^{0} to 10^{-2} m.s^{-1} for the saturated aqueous hydraulic conductivity).

The upcoming study of the Representative Elementary Volume on the intrinsic permeability and its careful comparison with experimental results found in the literature. This might open a new sight in the usage of innovative and non-destructive assessments of physical properties applied to new types of samples, and more specifically on natural bryophyte and lichen samples collected in Western Siberia.

References

[1] Brown J., Circum-arctic map of permafrost and ground-ice conditions, *Circum – Pacific Map Series*, 45 (1997).

[2] Soudzilovskaia N., van Bodegom P., Cornelissen J., Schweitzer J., Dominant bryophyte control over high-latitude soil temperature fluctuations predicted by heat transfer traits, field moisture regime and laws of thermal insulation, *Functional Ecology*, 27(6), 1442-1454 (2013)

[3] Biskaborn B., Smith S., Noetzli J, et al. Permafrost is warming at a global scale, *Nature Communications*, 10(1), 264 (2019).

[4] Meredith M., Sommerkorn M., Cassotta S., et al. , IPCC Special Report on the Ocean and Cryosphere in a Changing Climate, *IPCC Special Report on the Ocean and Cryosphere in a Changing Climate* (2020).

[5] Koestel J., Larsbo M., Jarvis, N. , Scale and REV analyses for porosity and pore connectivity measures in undisturbed soil , *Geoderma*, 366, 114-206 (2020).

[6] Guibert R., Nazarova M., Horgue P. et al., Computational Permeability Determination from Pore-Scale Imaging : Sample size, Mesh and Method Sensitivities, *Transport in Porous Media*, 107(3), 641-656 (2015).

[7] Leroy P., Revil A., Kemna A., Cosenza P., Ghorbani A. , Complex conductivity of water-saturated packs of glass beads, *Journal of Colloid and Interface Science*, 323(1), 103-117 (2008).

[8] Weller H., Tabor G., Jasak H., Fureby C., A tensorial approach to computational continuum mechanics using object-oriented techniques, *Computer in physics*, 6(12), 620-631 (1998).

Impact of gravity and inertia in DNAPL spatialization: experimental and numerical studies of stable displacements at laboratory scale

M. Cochennec[a,b], H. Davarzani[a], Y. Davit[b], S. Colombano[a], M. Quintard[b]

[a] *French Geological Survey (BRGM), Orleans, France*
[b] *Insitut de Mécanique des Fluides de Toulouse (IMFT), Université de Toulouse, CNRS, Toulouse, France*

Keywords: two-phase, DNAPL, high permeability, gravity, inertia

The flow of Dense Non-Aqueous Phase Liquid (DNPAL) flow in highly permeable porous media is characterized by a complex interplay between viscous, gravity, and inertial forces. If gravity effects have been discussed in the case of DNAPL flows, and especially in relation with the onset of displacement instability (gravity fingering) [1, 2], little work has been dedicated to studying the impact of inertial effects for stable flows.

We first performed experimental gravity-stabilized DNAPL injections in a 2D tank for different homogeneous and highly permeable porous media. In particular, the permeability, K_0, was changed by using either calibrated 1 mm diameter glass beads (350 darcy) or 2 mm glass beads (4200 darcy). The front displacement was tracked by taking photos (see Fig. 1), continuously recording the volume injected, and by acquiring mean local saturation around an array of Time-Domain Reflectometry (TDR) probes. DNAPL and water have been replaced by canola oil and ethanol, as it is much less hazardous and this fluid couple has similar properties to a coal tar/water couple [3].

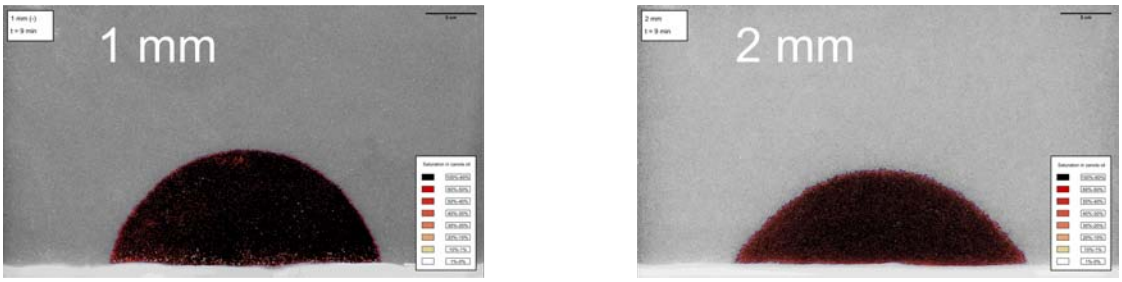

Figure 1: Oil zone after 9 minutes of injection at the bottom of the tank in 1 mm (left) and 2 mm (right) glass beads.

We showed that the experimental injection can be well reproduced with a numerical model that explicitly deals with the fluid front (an Arbitrary Lagrangian-Eulerian method coupled with Darcy-Forchheimer law), and for which less constitutive relations are needed compared to generalized Darcy law. The model was then used to study the impact of gravity and inertial effects on the shape of the DNAPL zone. A parametric study was conducted by varying the dimensionless groups

$$G_r = \frac{\rho_o g K_0}{\mu_o U}, \quad F_o = \frac{\rho_o U K_0}{\mu_o \eta}, \tag{1}$$

namely the gravity and Forchheimer number, respectively, where η is the passability, U is a filtration velocity of reference and μ_o and ρ_o are the dynamic viscosity and density of DNAPL.

We found a strong impact of gravity starting from gravity numbers $G_r \approx 0.2$, which spread the oil laterally. The threshold value for G_r is likely to be reached in contaminant hydrogeology, even with a highly viscous DNAPL such as coal tar. Results depend on the Initial Boundary Value Problem (IBVP) at hand, and inertia impacts the oil zone if the inlet condition is a fixed pressure drop, contrary to a

fixed velocity as for the previous study. Inertial effects tend to decrease the extent of the oil front for Forchheimer numbers $0.25 \lesssim F_o$, as shown in Fig. 2. However, this range of value is hardly obtained in contaminant hydrogeology and might be reached only in particular cases involving active pumping or injection in highly permeable porous media.

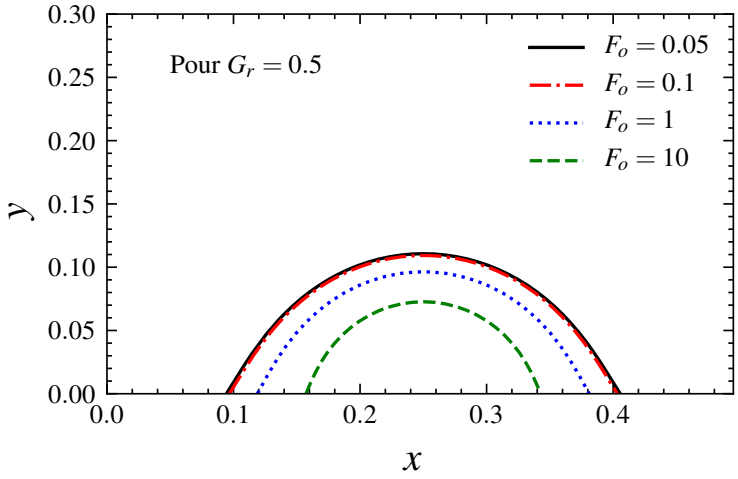

Figure 2: Impact of the Forchheimer number F_o upon the oil front for moderate gravity number.

References

[1] Schwille, Friedrich, and James F. Pankow. "Dense chlorinated solvents in porous and fractured media-model experiments." Lewis Publishers, Chelsea, MI (1988).

[2] Nsir, Khalifa, et al. "Laboratory experiments on DNAPL gravity fingering in water-saturated porous media." International Journal of Multiphase Flow 40 (2012): 83-92.

[3] Philippe, Nicolas, et al. "Experimental study of the temperature effect on two-phase flow properties in highly permeable porous media: Application to the remediation of dense non-aqueous phase liquids (DNAPLs) in polluted soil." Advances in Water Resources 146 (2020): 103783.

Relationship between protection requirements and textile structure and material

O. Douguet[a,b], V. Tschamber[b], K. Gautier[a], G. Leyssens[b], D. Mathieu[a], M.A. Bueno[a], J.F. Brilhac[b], A. Charvet[c], D. Thomas[c], N. Bardin-Monnier[c], M. Pfrimmer[c], C. Vibert-Clement, C. Segovia, L. Jeanmichel

[a] *Université de Haute-Alsace, Laboratoire de Physique et Mécanique Textiles (LPMT UR4365), F-68100 Mulhouse*
[b] *Université de Haute-Alsace, Laboratoire Gestion des Risques et Environnement (LGRE UR 2334), F-68100 Mulhouse*
c Université de Lorraine, CNRS, LRGP, F-54000 Nancy, France
d Centre d'Essais Textile Lorrain (Cetelor), Université de Lorraine, F-88026 Epinal

Keywords Textile fabric, air permeability, filtration efficiency, Face mask

1 Introduction

Face masks for infectious protection are made from nonwoven textile materials and for a single use. The Covid-19 sanitary crisis and the generalisation of the wearing of masks by healthy people, throughout the world, led the textile industry to produce a new type of mask, i.e.the barrier or community face mask, which is reusable. Almost such masks are woven or knitted fabrics, which present an environmental impact lower than nonwovens. Community face mask is a specific and very technical textile product. In France, two specifications have been defined by AFNOR [1]: the air permeability and the particle filtration efficiency (3 μm in diameter). Given the emergency situation, such barrier face masks were produced following an empirical and mimicking approach. No textile rules or theory have been followed. In this study, correlations between air permeability, filtration efficiency and textile structure characteristics were sought in order to provide elements for formalizing their design.

2 Material and Methods

Textile fabrics, made of cotton or a mixture of cotton and linen, with defined and controlled characteristics have been specifically manufactured by a textile company, Emanuel Lang. Two families of textile fabrics were produced, both of them have the same i) weaving pattern, i.e. a plain woven, ii) cotton warp yarns (17 tex, i.e. 17 g/km) and iii) number of warp yarns per centimetre (31 yarns/cm). The two families have been designed to study the influence of two different parameters: i) the number of weft yarns per centimetre and ii) the weft yarn diameter combined with the number of yarns per centimetre. The first family includes two sets of 5 fabrics each made from cotton or flax weft yarns, with from 12 to 18 weft yarns/cm. The second family is composed of 8 cotton fabrics with a constant ratio weft yarn diameter on number of weft yarns/cm, i.e. they are homothetical.

All these samples were observed and some geometrical characteristics are obtained from scanning electron microscopy (SEM) or 3D optical microscopy and the mean yarn diameter and yarn distances are measured. From these parameters, two textile characteristics were calculated named the saturation index defined as the maximum amount of yarn that can be inserted into a given fabric, and the cover factor, characterising the density of threads per unit area. These parameters are linked to the textile porosity.

Air permeability was measured using a AP 36 VVC Air Permeability meter according to the AFNOR specification, as the air flow rate for a given air pressure loss [1].

Particle filtration efficiency measurements were performed using two different protocols. A first protocol, (P1), is based on the injection of a solid aerosol, Holi polydispersed powder, using a RBG Palas generator, then diluted with compressed air in a tunnel. Two similar filter holders (3.5 cm diameter), one empty and the one filled with the mask sample to be tested are placed side by side in the tunnel. An Electrical Low Pressure Impactor (ELPI, Dekati®) is used for continuously measurement of the number concentration of particles. In the second protocol (P2) oil droplets (DEHS) generated by nebulization (AGK 2000, Palas®) were used as aerosol source. An Aerosol Particle Sizer (APS 3321, TSI®) coupled to a dilutor (3302A from TSI®) is connected to two sampling lines located upstream and downstream of the sample, allowing the determination of the concentrations and particle size distributions on either side of tested sample.

3 Results

Fig. 1 presents the correlations of air permeability and filtration efficiency at 3 µm as a function of the number of weft yarns per centimeter of the textile samples. Both air permeability and filtration efficiency are strongly related to yarn density, which appears to be a major parameter for identifying of the most relevant textile for designing an efficient filtering mask. Regardless the composition of the textile fabric, power law correlations are observed, with air permeability increasing and filtration efficiency decreasing with decreasing the density. For a given density, linen fabrics were found to have higher air permeability and lower filtration efficiency than cotton fabrics. Further characterizations revealed that the saturation index and coverage factor are linearly related to both air permeability and filtration efficiency, while fabric superficial hairiness quantity appears to be similar regardless of material composition.

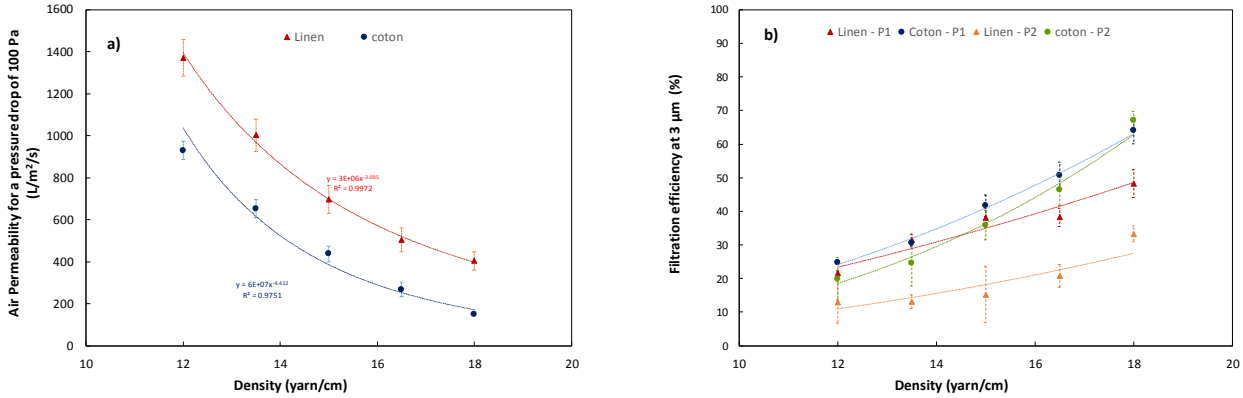

Figure 1: Correlations between weft yarn density of the textile fabrics and air permeability (a) and filtration efficiency (b).

Comparison of filtration efficiency measurements obtained from the two protocols reveals a good agreement for the cotton fabrics, while more discrepancies are observed with linen, or linen samples (Fig. 1b). These ones were attributed to the heterogeneity of such samples (observed by SEM) and to the complex experimental procedures and variability applied of devices used. However, remarkable correlations between air permeability and filtration efficiency are highlighted, considering well-defined textile fabrics, whereas for a wide variety of textiles such relationships are difficult to establish [2] (fig. 2).

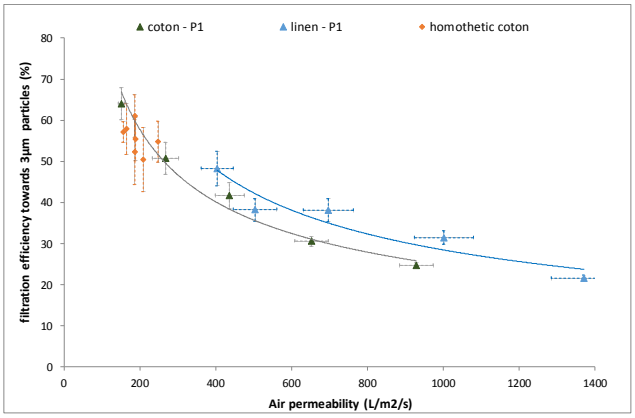

Figure 2: Air permeability versus filtration efficiency to 3 µm according to protocol P1

Finally, it has been shown that homothetic textiles exhibit similar behavior with respect to breathability and filtration which is an important point for the optimization of manufacturing parameters and costs.

References

[1] AFNOR. Masques barrières - Guide d'exigences minimales, de méthodes d'essais, de confection et d'usage. SPEC S76-001. 2020.
[2] S. Bourrous et al., A Performance Evaluation and Inter-laboratory Comparison of Community Face Coverings Media in the Context of COVID-19 Pandemic, *Aerosol and Air Quality Research*, 21, 1-13 (2021).

Identification of the intrinsic optical indexes of fibrous media at high temperature using numerical simulation and infrared spectroscopy

C. Daoût[a,b], O. Rozenbaum[b], D. De Sousa Meneses[b], D. Rochais[a]

[a] *Commissariat à l'Énergie Atomique et aux Énergies Alternatives (CEA), DAM, Le Ripault, F-37260 Monts, France*
[b] *CNRS, Conditions Extrêmes et Matériaux : Haute Température et Irradiation (CEMHTI), UPR 3079, 1D Avenue de la Recherche Scientifique, 45071, Orléans, Cedex 2, France*

Keywords: optical indexes; ray tracing; FTIR spectroscopy; 3D X-ray microtomography; fibrous ceramics

1 Introduction

The French Alternative Energies and Atomic Energy Commission (CEA) is developing a software to forecast the conducto-radiative exchanges within 3D porous and heterogenous media [1]. In order to use this numerical tool on semi-transparent fibrous ceramics, we need to identify the intrinsic optical indexes of each phase of the considered material. However, these spectral quantities are dependent on the chemical composition, the making process and the temperature of the material. The existing experimental devices to measure reflectance, transmittance or direct emittance only allow to retrieve apparent quantities which are calculated according to several physical models. These indexes are strongly linked to the texture of the porous medium and this doesn't fit our requirements. As far as we know, there are currently no experimental method combined with a physical model that permits to quantify the optical indexes of each phase of a material at such small scale and high temperature (about 1000°C). Thus, we propose a new methodology combining measurements and numerical studies to identify these intrinsic optical indexes.

2 Method

A 3D X-ray microtomography investigation was made on a fibrous sample. After extraction of statistical information (fiber dimensions, orientations), we used a code developed by the CEMHTI laboratory to reproduce numerically porous media with simple geometrical objects [2]. In this context, the software has been upgraded to generate cylinders for reproducing the fibers observed by tomography. We carried out normal hemispherical transmittance and reflectance measurements on the fibrous sample with an integrating sphere (both at 300K) and acquired the temperature dependence of its normal spectral emittance by using the emissivity setup of CEMHTI [3]. Then, we have evaluated the same radiative quantities on a numerical sample we generated from the tomography information, by performing Monte Carlo Ray Tracing (MCRT). Since the MCRT code requires the optical indexes as an input, which is the information we are initially looking for, an iterative optimization algorithm is used to retrieve the values from an initial guess. The solution for the material optical indexes is obtained when numerical and experimental values match (see Fig. 1). By repeating the process of optimization on a set of experimental data, we obtained the spectral dependence of the intrinsic optical indexes of the fibers.

We applied this approach to a « template » sample made of silica fibers. As the optical indexes of this material vary greatly in the infrared domain (e. g. opaque or semi-transparent or transparent region) we are able to study the robustness of the numerical procedure and identify its limits, i.e. the validity domain of the geometric optics regime.

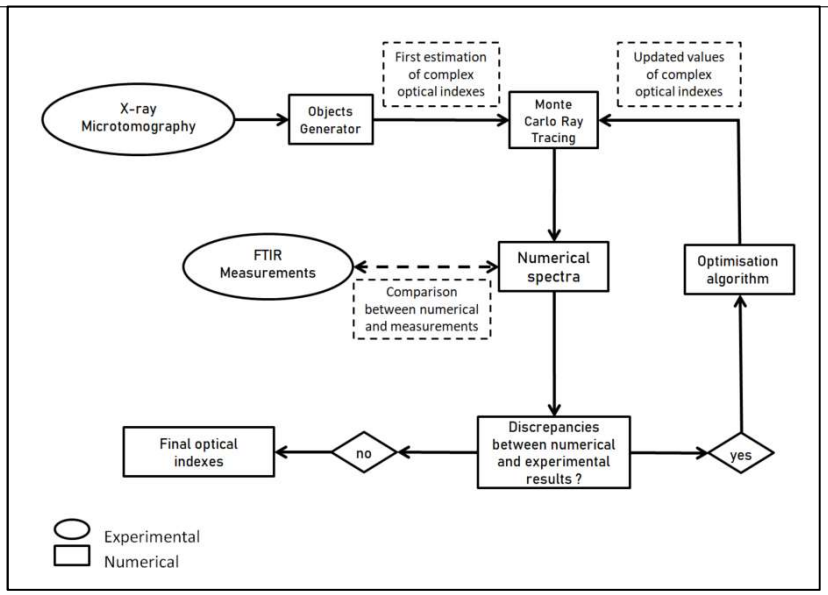

Figure 1: Flow chart of the method

3 Conclusion

The numerical samples generated in this study and their associated optical indexes can be embedded in the CEA numerical tool to compute the conducto-radiative exchanges depending on the frequency of thermal radiation. This heat transfer mode being major at high temperatures, a better forecast of the heat exchanges within the material provides temperature fields that are closer to the observed ones. The approach we present here is advantageous, because it allows to study the sensitivity of several parameters of the material in a very cheap way (whether it is about time, economic or human resources) to design materials that are more relevant to the application for which they are intended.

References

[1] M. Niezgoda and al., Modeling heat transfer within porous multiconstituent materials, *Journal of Physics Conference Series* (Eurotherm Conference 95 - Computational Thermal Radiation in Participating Media), 369, 012001 (2012).
[2] O. Rozenbaum and al., Determination of high-temperature radiative properties of porous silica by combined image analysis, infrared spectroscopy and numerical simulation, *Int. J. Therm. Sci*, 137, 552-559 (2019).
[3] D. De Sousa Meneses and al., Apparatus for measuring the emittance of materials from far infrared to visible wavelengths in extreme conditions of temperature, *Infrared Phys. Technol*, 69, 96-101 (2015)

Treatment of warts with clay

F.Z. Falah[a], M. Bouamrani[a], S. Yousfi[a]

[a]Research Laboratory of Analytical Chemistry and Physical Chemistry of Materials, Sciences Faculty Ben M'sik, University Hassan II - Casablanca, Morocco.

Keywords: Clay, wart, absorption

1 Introduction

Clay plays an important role in several fields of activity; because of its physical-chemical properties and their abundance at their relatively low cost justifying the many uses in the manufacture of drugs, treatment of polluted water as an adsorbent, catalysis, discoloration, drilling fluids...

Clays with a fibrous structure have a high absorbency. Therefore, they have cleansing properties that allow them to absorb impurities or eliminate bad odors. From a therapeutic point of view, it can be used as a gastric bandage, or to absorb various toxins. It is also used to stop internal bleeding in the digestive system, and to correct gastric acidity.

Clays with a layered structure have a high adsorbing power (which in some cases does not exempt them from an effective absorbency). They have an important interest in treating intestinal problems. Through to this absorption ability, they detoxify by capturing viruses, bacteria and other unwanted molecules, while respecting the bacteria necessary for intestinal balance. Their antibacterial ability is coupled with a protective virtue; this is why these clays with adsorbing ability are also used as a gastric bandage against acidity, ulcers and burns. Certain types of clays are used in the dermatological field as healing products. They have also proven their effectiveness in the treatment of warts, which appear on the skin of the human body as small tumors often present in the hand, of the foot and face. These warts often present both a cosmetic problem and a serious health problem.

In Morocco, in the region of Fez, a natural clay has proven its effectiveness in the treatment of vulgar, flat and plantar warts. The study we conducted in this work is part of the characterization and valuation of this clay for the treatment of planar, plantar and common warts.

The first part of our research allowed us to know both the fundamental aspect and the structural aspect of clay materials and generalities about warts.

The second part is devoted to the physical-chemical characterization of our clay samples taken in one of the Moroccan regions, we carried out three analysis techniques (X-ray diffraction, Infrared spectroscopy and X fluorescence), the results show that the three samples are from the same family (Illite, Dolomite, Chlorite) and we then verified the effectiveness of A1 (clay1) for the removal of planar, plantar and vulgar warts compared to other samples this effectiveness may be due either to the presence of the elements (like: SiO2 and AlOH) shown by IR or by the importance of the difference in the contents of some compounds already shown by X fluorescence. However, we cannot confirm the presence of the specific compounds or elements involved in the efficacy of A1.

The rheological study is a study that consists of characterizing the specific criteria of a sample and informs us of its kinetic character. For this reason, we carried out different tests, mainly oriented around the knowledge of the different characteristics of clays, the results obtained enhancing the sample A1 compared

to the other samples, (A2, A3) are characterized by a low percentage of plasticity water; higher linear shrinkage on drying; higher fire retardation; a lower water absorption percentage.

The last part includes the drying study on several shapes of which the cylindrical shape S3 is the ideal packaging shape, which minimizes the transfer of water by the drying process and allows the preservation of our product A1 in the long term.

2 Section

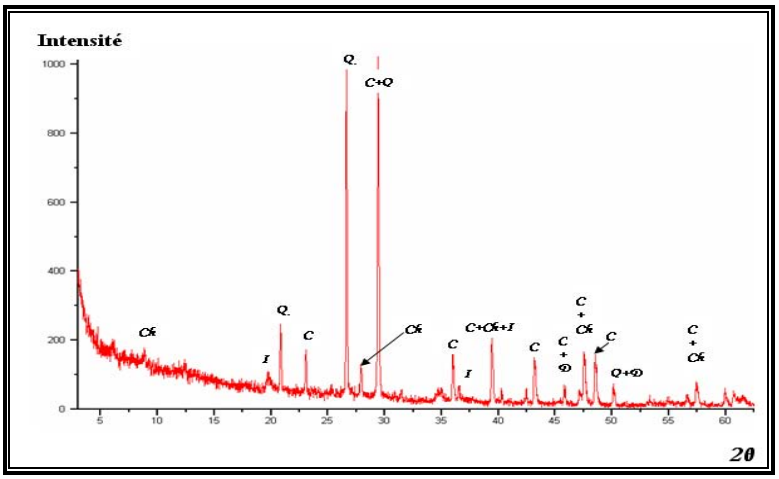

Figure 1: Diffraction diffraction diagram of sample A1
Q : quartz ; D : Dolomite ; C : Calcite ; I : Illite ; Ch : Chlorite

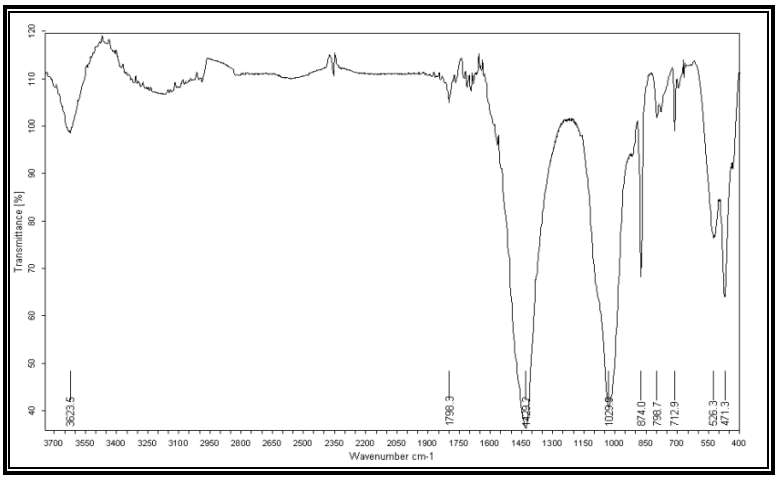

Figure 2: IRTF spectrum of sample A1

Influence of the water table oscillation on the mechanical and petrophysical properties of chalk

Davide Geremia[a], Christian David[a], Temenuga Georgieva[b], Fanny Descamps[b], Sara Vandycke[b], Beatriz Menéndez[a], Christophe Barnes[a]

[a]CY Cergy Paris Université, Département géosciences et environnement, Neuville-sur-Oise, France
[b]Université de Mons, Mining Engineering unit, Mons, Belgium

Keywords: water-weakening, mechanical tests, chalk

It is well known that pore fluids can affect rock physical properties, like Young's modulus, mechanical strength and elastic wave propagation, especially in environments where gas and water coexist in the pores and a cyclic saturation/desaturation produces mechanical weakening.

We performed a series of mechanical tests on the Ciply chalk, a phosphatic rock from the Mons basin (Belgium), collected from "La Malogne" underground quarry in which the rock strata cyclically imbibe due to the oscillation of the water table.

We designed different experiments at different pressure conditions to highlight how the cyclic capillary imbibition or the injection of water influence the static and dynamic Young's modulus and the peak failure through uniaxial and triaxial tests. Furthermore, piezoelectric sensors are installed onto the sample's surface for P-wave ultrasonic surveys.

It is likely an interplay between the strengthening due to the closure of the initial crack content and a weakening triggered by the water that influence the mechanical properties of this chalk. Indeed, in 1 cycle of loading/unloading in unconfined uniaxial stress conditions and up to 55% of the peak strength (i.e. in the elastic domain), this chalk can accumulate 0.16% of irreversible plastic deformation (compared to 0.52% of axial strain at failure), which results in a strengthening of the Young's modulus observed in the sequent cycles, in a similar manner as the Kaiser effect for acoustic emissions. On the other hand, a water-induced strain rate acceleration caused by a reduction in strength is observed when water is injected in constantly axially loaded samples.

Results from the active seismic monitoring showed that the P-wave velocity is affected by the water saturation, providing useful information about the distribution of the air-water mixture while imbibition/injection is taking place.

We conclude that the outcomes of these experiments can provide interesting information on water-induced variations on the fatigue behaviour of chalk, which is recognised to control the stability of underground quarries.

Gas flows in microporous media

M. V. Johansson[a,b], P. Perrier[a], I. Graur[a]

[a] *Aix-Marseille University, CNRS, IUSTI UMR 7343, 5 rue E. Fermi, 13453, Marseille, France*
[b] *SINTEF Energy Research, P.O. Box 4761 Torgarden, NO-7465 Trondheim, Norway*

Keywords: microporous media, permeability, conductance, Knudsen number, thermal transpiration

The transient method of the mass flow rate and permeability measurements through microporous media, developed previously [1], [2], is used to extract different characteristics of these media. By implementing the model of a porous medium as a bundle of capillaries, the effective pore dimension is extracted from the measurements, and its physical interpretation is given. This methodology shows promising results to be used as a non-destructive method of micro-and- nanoporous media analysis. The permeability is also extracted directly from the measurements of the pressure variation in time. By using additional information about the sample porosity, the number of capillaries, the tortuosity, and the internal surface of the sample are calculated. The extracted values are very close to that obtained by the mercury porosimetry and by microtomography.

When a microporous media is subject to a temperature gradient, the thermal transpiration effect [3], [4] causes gas flows from the cold side toward the hot end. Both the transient and stationary properties of the thermal transpiration in microporous media are analyzed. One of the thermal transpiration phenomena applications could be the development of the motionless Knudsen compressor/pump (a pump with no moving parts). Since the motion is brought about only by a temperature difference, this device has attracted attention as a possible candidate to generate a stable fluid flow in micro-electro-mechanical systems (MEMS) [5].

References

[1] W. F. Brace, J. B. Walsh, W. T. Frangos, Permeability of granite under high pressure, Journal of Geophysical Research 73 (6) (1968) 2225–2236.
[2] M. V. Johansson, F. Testa, I. Zaier, P. Perrier, J. P. Bonnet, P. Moulin, I. Graur, Mass flow rate and permeability measurements in microporous media, Vacuum 158 (2018) 75–85.
[3] O. Reynolds, On certain dimensional properties of matter in the gaseous state, Philos. Trans. R. Soc. London 170 (1879) 727–845.
[4] M. Rojas Cardenas, I. Graur, P. Perrier, J. G. Méolans, Thermal transpiration flow: a circular cross-section microtube submitted to a temperature gradient, Phys. Fluids 23 (2011) 031702.
[5] S. An, N. K. Gupta, Y. B. Gianchandani, A si-micromachined 162-stage two-part a si-micromachined 162-stage two-part knudsen pump for on-chip vacuum, Journal of Microelectromechanical Systems 23 (2) (2014) 406–416.

Rheological modelling of the flowability of aerated fine powders

O. Hadjam[a], K. Allia[a]

[a] *Lab of Science in Industrial Process Engineering (LSGPI)– University of Science and Technology -USTHB. Algiers – Algeria*

Keywords: Aerated powders, flowability, Rheology, Failure properties

1 Introduction

Powders and bulk solids are widely used in a variety of industries such as materials production, food processing, pharmaceutical development and the processes used in manufacturing cycle are multiple and can be very different in nature. As a product, powders are diverse in nature and may be in the form of a bulk powder in a bag, as a toner in a laser printer or as a compacted powder in tablet form [1]. Whether the focus is on the formulation of a particular product, scale-up, process development, technology transfer or quality assurance, the flow properties of powders are essential in many aspects as they have properties which, if properly understood, can be used to develop useful and specific products. Also, quantifying powder flow and link the measured values to the powder behavior during a given process is not an easy task, indeed, the flowability [2] is affected by powder physical characteristics (e.g., the particle size distribution, the morphology, the presence of satellite particles, the density and the surface interaction) as well as the environmental and surface conditions. Handling conditions (e.g., humidity, temperature, atmosphere pressure and measurement methods). In addition, depending on the process, the powders are exposed to different flow conditions, including plastic, inertial, fluidized, and entrained flow [2].Despite their importance in the industrial world, current knowledge associated with powders is limited due to their behavior as a function of the imposed conditions; the powder can be considered as a solid, as a liquid, or as a gas, their behavior therefore remains complicated and very difficult to apprehend [3]. The object of this study is based on this issue and with different technical measures that could help to understand the behavior of a fine powder, in particular its flowability (case of marble powder 51.45µm), we have examined the physical properties (dp, ρ ,..), Flow properties (Carr index, Hausner index), and mechanical properties (Cohesion, Cohesion of the wall, static angle of internal friction) then using a fluidization column equipped with a stirrer, we studied classical fluidization, and the effect of agitation on fluidization under aerated conditions and below the fluidization threshold, then we developed a rheological model to estimate the stresses at the fixed bed level and predict the value of the stress of the wall shear τw, as well as the torque T, and finally, a study on the effect of aeration on the rheology of the powder

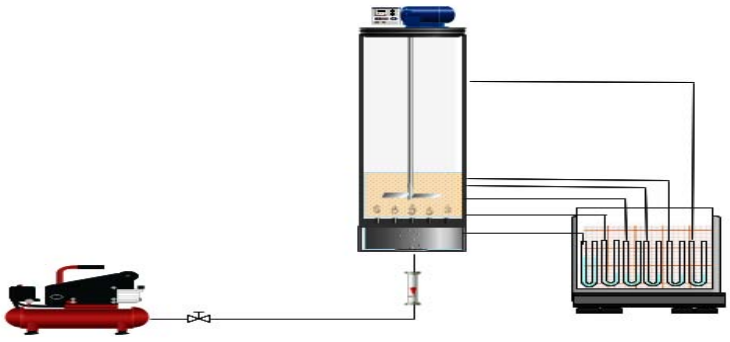

Figure 2: Experimental setup.

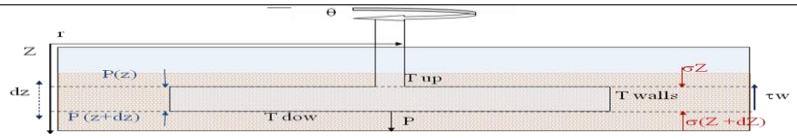

Figure 2: Representation of the balance of forces exerted on the layer at depth z.

Poudre	dp(µm)	ε_{mf}	ρ_p(g/cm^3)	ρ_b(g/cm^3)	ρ_T(g/cm^3)	ρ_a(g/cm^3)	I_c	H_R	θ(°)
Marbre	51.	0,53	27,63	1,28	1,4	1,08	22,8	1,29	41,2

Table 1: The physical properties and Flow properties of the marble powder.

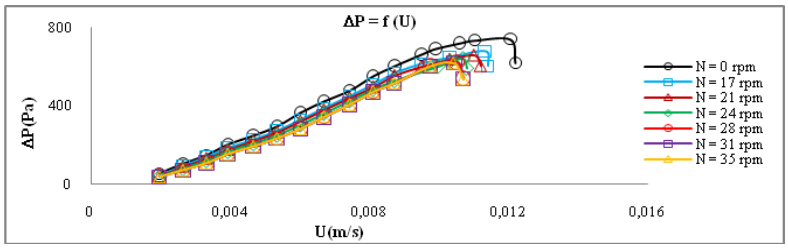

Figure 3: Effect of agitation on fluidization.

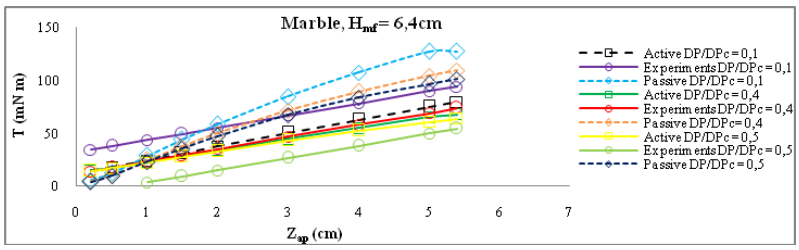

Figure 4: Z_{ap} and aeration effect on torque.

References

[1] Duran, J. Sables, Poudres et Grains. Eyrolles Sciences. 1997

[2] A. Castellanos, J.M. Valverde, A.T. Pérez, A. Ramos, P.K. Watson, Flow regimes in fine cohesive powders, Phys. Rev. Lett. 82 (6) (1999) 1156 – 1159, https://doi.org/ 10.1103/PhysRevLett.82.1156.

[3] Jaeger, H.M., Nagel, S.R. et Behringer, R.P. (1996) Granular solids, liquids, and gases. Reviews of Modem Physics, 68 , p. 1259. 1273

Coupling Navier-stokes, Brinkman and Darcy equations for modelling pollutant transfer at the sediment-water interface in rivers

Perla Gulbeyaz Ibrahim[1,2], Marwan Fahs[2], Gwenaël Imfeld[2], Sylvain Payraudeau[2]
[1]*Lebanese university, Faculty of Engendering, Beirut, Lebanon*
[2]*ITES , University of Strasbourg, CNRS, ENGEES, 67000, Strasbourg, France.*

Keywords: sediment-water interface, coupled flow and transport, modelling, Darcy, Brinkman

Most pollutant transformations such as sorption, chemical reactions, biological transformations and, ion exchange in rivers mainly occur at the sediment water interface (SWI). Modeling pollutant transfer at SWI requires accurate evaluation of the velocity field as this latter control mass transfer processes by advection and hydrodynamic dispersion. However, in such a configuration, accurate simulation of the velocity field is a challenging task as it involves surface flow in the upper water layer, high flow velocity in the high permeable intermediate layer of sediment and low velocity in the bottom layer of sediment (see figure 1).

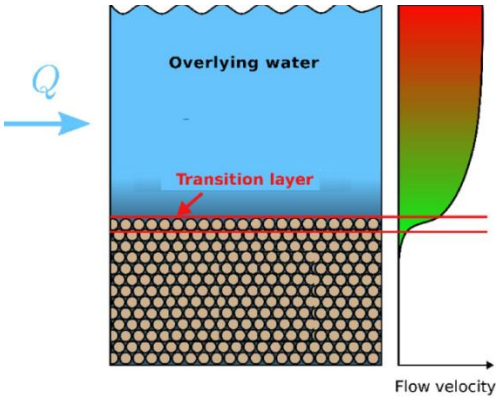

Figure 1. Different flow regimes at the SWI

In several existing models, Darcy's law is used for both fluid and porous regions. The flow in the overlaying water and transition layers is approximated with the Darcy's law by assuming a high permeability. However, this approximation is not accurate as it neglects viscosity and convection effects. In this work, we presented a new model by coupling, Navier-stokes equation for the overlying water layer, Brinkman's model for the transition layer and Darcy's law for the sediment layer. The model is developed in the finite element framework of COMSOL. Specific boundary conditions have been implemented in COMSOL to handle the exchange between different layers. The developed model is used to simulate an experimental benchmark developed in Drouin et al. 2021. The new model, based on coupled Navier Stokes, Brinkman and Darcy equations, provides better agreement with observations than a standard model based on Darcy equations.

References

Drouin, G., Fahs, M., Droz, B., Younes, A., Imfeld, G., & Payraudeau, S. (2021). Pollutant dissipation at the sediment-water-interface: A robust discrete continuum numerical model and recirculating laboratory experiments. Water Resources Research, 57, e2020WR028932. https://doi.org/10.1029/2020WR028932

Multiple-porosity model based on density functional theory and poromechanics

Y. Khaldouni[a], L. Perrier[a], T. Bernet[b], C. Miqueu[a], D. Grégoire[a,c]
[a] *Universite de Pau et de Pays de l'Adour, E2S UPPA, CNRS, LFCR, Anglet, France*
[b]*Department of Chemical Engineering, Imperial College London, UK*
[c]*Institut Universitaire de France, Paris, France*

Keywords: microporous media, adsorption, deformation

Abstract:

At nanoscale, fluid adsorption occurs in the vicinity of solid surfaces because of a strong attractive solid-fluid interaction, which takes effect up to few nanometers away from the solid wall. This interaction makes the adsorbed fluid in an inhomogeneous condensed phase. In the case of micropores, the solid surface encloses and confines the fluid within a space of dimension less than 2 nanometers. For that reason, micropores adsorb more fluid, which in turn induces a simultaneous mechanical reaction on the pore walls at the nanoscale. Consequently, at the macroscale, microporous media swell due to fluid adsorption while classical poromechanics predicts shrinkage.

Our objective is to study microporous material deformation induced by fluid adsorption. Recently, we proposed a poromechanical framework [1] able to predict adsorption-induced swelling in double porosity media where the fluid confinement is deduced from the experimental measurement of an excess adsorption isotherm. In order to avoid this experimental measurement and develop a pure modeling approach, we propose here to couple the latter enhanced poromechanics framework with a classical Density Functional Theory (cDFT) [2], which allows to predict the adsorbed fluid quantity directly in each pore. That means that the adsorbed fluid quantity in each pore size of the material Pore Size Distribution is estimated by cDFT and each corresponding pore volume is then considered independently. The double-porosity poromechanical framework is consequently extended to a *n*-porosity framework in order to estimate the global deformation induced by the fluid confinement in each evolving pore volume.

This coupled cDFT/poromechanics approach is validated by experimental comparison with simultaneous measurement of CH_4 and CO_2 adsorption quantities and volumetric swelling deformation in activated carbon [3].

Acknowledgements: This work is partially financed by the *Institut Carnot ISIFOR* and the *Investissement d'Avenir* French programme (ANR-16-IDEX-0002) under the framework of the E2S UPPA hub Newpores.

References:

[1] Perrier, L.; Pijaudier-Carbot, G.; Grégoire, D., "Extended poromechanics for adsorption-induced swelling prediction in double porosity media: modeling and experimental validation on activated carbon," *Int. J. Solids Struct.,* vol. 146, pp. 192-202, 2018.

[2] Bernet, T.; Müller, A. E.; Jackson, G. "A tensorial fundamental measure density functional theory for the description of adsorption in substrates of arbitrary threedimensional geometry," *J. Chem. Phys.,* Vols. 152 (22), 224701, 2020.

[3] Perrier, L.; Plantier, F.; Grégoire, D.; "A novel experimental setup for simultaneous adsorption and induced deformation measurements in microporous materials," *Rev. Sci. Instrum,* Vols. 88 (3), 035104, 2017.

Capillary imbibition in particle-bed 3D printing

E. Keita, W. Zuo, P. Belin, N. Roussel

Laboratoire Navier; Université Gustave Eiffel, ENPC, CNRS, Marne-la-Vallée, France

Keywords: Imbibition; 3D printing; Cement; Thickener

1 Introduction

This paper deals with controlling the net geometry of a printed object in the case of powder-bed or particle bed binding technologies. In the specific case of these printing technologies, this concern finds its origin in the ability of the liquid injected into the bed to move under the effect of capillary forces freely. This paper first compares water penetration as a function of time in a cement powder-bed, a plaster powder-bed, and a commercial plaster powder-bed specifically designed for powder-bed printing. Our results show that water penetration goes through various penetration regimes and is fully uncontrolled in standard powders. We then measure water penetration in a cement powder-bed containing various amounts of dispersed organic water thickeners. Our results suggest that the use of water thickeners at an optimal dosage for a given powder-bed and a given water droplet leads to the formation of a non-Newtonian fluid between the grains. The formation of this non-Newtonian fluid allows, in turn, for the control of the naturally uncontrolled capillary-driven liquid penetration in the powder-bed [1–3].

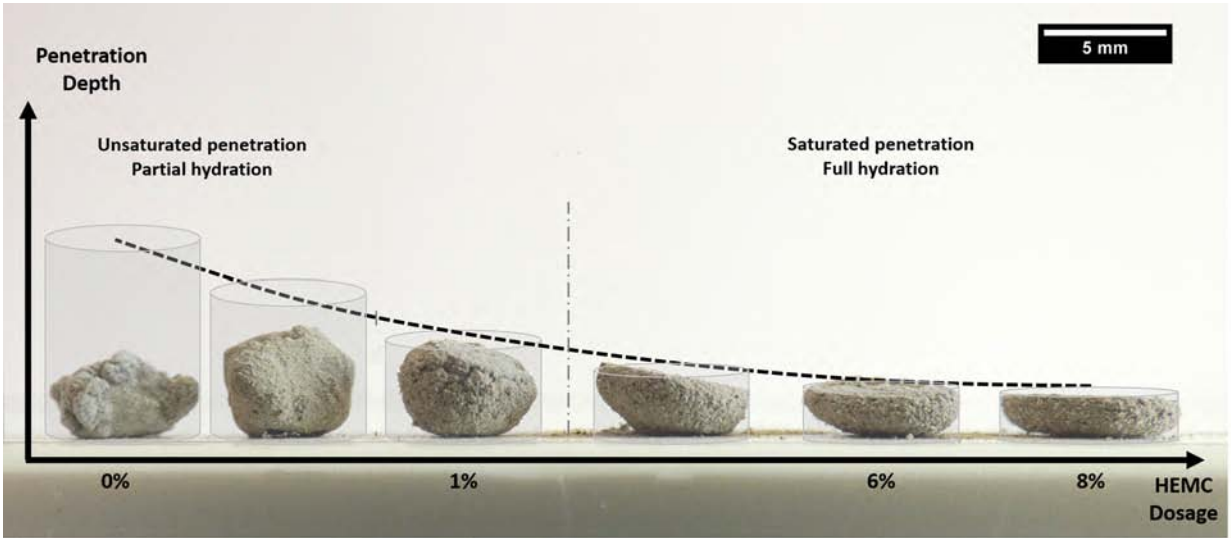

Figure 1:Morphology of the liquid penetrated area after hardening. The dash line is the excepted imbibition depth.

References

[1] A. Pierre, D. Weger, A. Perrot, D. Lowke, Penetration of cement pastes into sand packings during 3D printing: analytical and experimental study, Mater. Struct. Constr. 51 (2018) 22. doi:10.1617/s11527-018-1148-5.

[2] W. Zuo, C. Dong, E. Keita, N. Roussel, Penetration Study of Liquid in Powder Bed for 3D Powder-Bed Printing, in: Second RILEM Int. Conf. Concr. Digit. Fabr., 2020: pp. 379–386. doi:10.1007/978-3-030-49916-7_39.

[3] W. Zuo, C. Dong, P. Belin, N. Roussel, E. Keita, Control of capillary imbibition by thickeners in particle-bed 3D printing, Submitted. (2021).

3D finite volume simulation of flow and passive transport within a real watershed

G. Latour[a], P. Horgue[a], F. Renard[b], R. Guibert[a], G. Debenest[a]

[a] *Institut de Mécanique des Fluides de Toulouse (IMFT) - Université de Toulouse, CNRS-INPT-UPS, Toulouse FRANCE*
[b] *CEA, DAM, DIF, F-91297 Arpajon*

Keywords: porous media, finite volumes, transport, OpenFOAM

Numerical simulation of flow in porous media is a key feature in many fields ranging from oil extraction to environmental risk assessment. In particular, predicting the fate of pollutants in real heterogeneous geological environments involves the implementation of three-dimensional simulations which require huge numerical resources. In this context, the finite volume OpenFOAM environment address such concerns as it is modular and massively parallel.

An OpenFOAM toolbox for multiphase flow in porous media has already been created [1] and is still under development. The hydrological solver deals both with the generalized Darcy's equations [1] or the mixed form of Richard's equation for groundwater flow applications [2]. For unsaturated flows solved by the Richard's equations, the non-linearity can be treated either with Picard's or Newton's algorithm for transient problems. The transport solver uses the classical advection-dispersion equation in porous media. For our analysis, three main cases are set up using a real domain and many more using a modular theoretical domain.

The theoretical domain represented on figure 1 is a simple cubic domain regularly meshed with hexahedral cells, under a constant infiltration chronicle from the upper face. It may contain most of the features of a real one : (i) a slope can be added on the bottom face, as well as (ii) heterogeneous permeability and (iii) seepage on the top face. The different degrees of complexity constitute a test case for numerical methods and a bridge towards real applications. Satisfying comparisons between 2D and 3D water tables are obtained. The effects of different numerical parameters such as discretization, tolerance and numerical methods are explored.

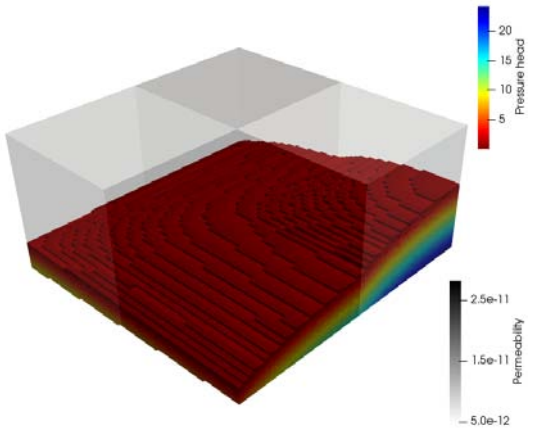

Figure 1: Quarter of the theoretical domain

The real domain, illustrated on figure 2, is then created from a set of geological data (figure 2a), for which the infiltration chronicles are known. It spans over about 5 km in both horizontal directions, and 125 m vertically. There, the stationary and transient solvers are both first run with an average constant infiltration (figure 2b) and the transient solver is then used with a time-variable infiltration. Finally, the

transport solver is employed for a passive tracer (figure 2c). Results are then confronted to the 2D cases and disparities are compared and analyzed. As the unsaturated phase and the water fluxes are taken into account with three-dimensional simulations, the general water table height is slightly changed. The mesh refinement is also studied and in particular its visible effects on the concentration dispersion.

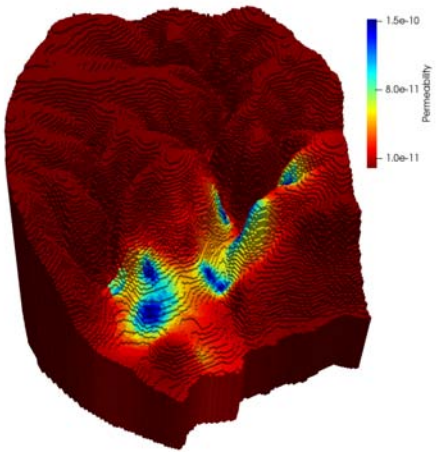

(a) Mesh and permeability

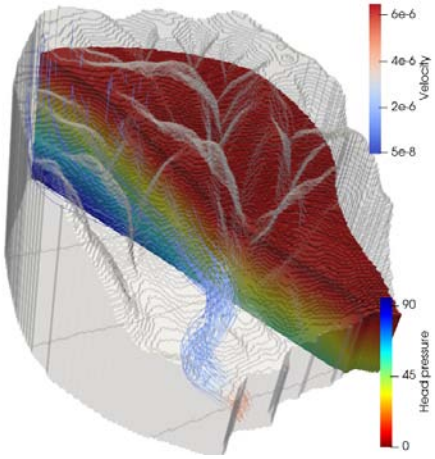

(b) Flow under a constant infiltration

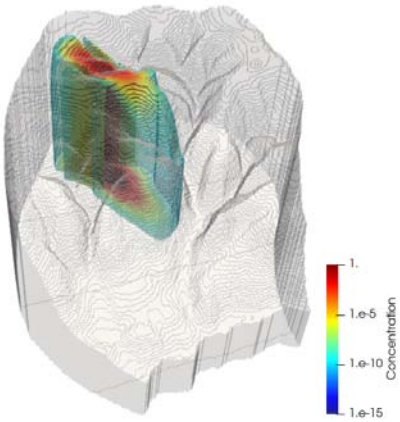

(c) Passive transport

Figure 2: Real domain, vertically extended for clarity

With regard to our current results, we conclude that mesh refinement is mandatory to correctly track localized fronts of concentration with through a realistic, therefore highly heterogeneous domain. Because of the high computational costs that would be induced by these refined meshes, the next step of the work will be to adapt OpenFOAM's Adaptive Mesh Refinement (AMR) module to dynamically refine according to the flow and/or transport properties.

References

[1] Horgue, Soulaine, Franc, Guibert, Debenest, An open-source toolbox for multiphase flow in porous media, *Computer Physics Communications*, 187, 217–226 (2015)

[2] Horgue, Franc, Guibert, Debenest, An extension of the open-source porousMultiphaseFoam toolbox dedicated to groundwater flows solving the Richards' equation, arXiv:1510.01364, (2015)

Faulting in volcaniclastic rocks: architecture, deformation mechanisms, structural diagenesis and petrological properties

E. Leroy[a], T. Cavailhes[a], Y. Anguy[b], C. Gaborieau[b]

[a]*UMR EPOC, Université de Bordeaux, Bâtiment B18N, 33400 Talence, France*
[b] *I2M, UMR CNRS 5295, 33405 Talence, France*

Keywords: Deformation bands, volcaniclastic rocks, porous rocks, fluid/rock interaction.

1 Introduction

Volcaniclastic rocks are composed of consolidated volcaniclastic and pyroclastic materials mainly made of volcanic glass, ashes and/or phenocrysts; such rocks are ubiquitous in geothermal areas, may be highly porous (up to 38%), and thus may have excellent potential for fluid storage and/or flow.
Deformation affecting porous volcaniclastic rocks ($\phi > 15\%$) in the 0.5 -3 km depth interval is expressed by the presence of catasclastic deformation bands (CDB) in which a reduction in grain size is caused by (i)grain rotation, (ii)intragranular and (iii) transgranular fracturing. These deformation mechanisms result in a drastic reduction of porosity (and permeability). Yet, little attention has been paid to CBD affecting volcanoclastites, despite the growing interest of the scientific community in volcanosedimentary reservoirs where volcanic glasses and cleavage minerals make these porous and granular media mechanically heterogeneous and complex to understand.
Thus, this work focuses on (i) fault development in volcaniclastic rocks and (ii) the implications of faults and fault-related structures on subsurface fluid-flow and petrophysical properties.

2 Geological context

The studied area is located in the Milos Volcanic Island, which forms part of the Southern Aegean Volcanic Arc. The Calc-alkaline Pliocene to present-day volcanic edifices are the surface expression of the northward subduction of the African plate beneath the Aegean microplate. The complex subduction-related tectonics has caused poly-phasal and multi-directional extensional tectonism affecting the Aegean microplate, during which multiple types of structural heterogeneities have formed. The studied normal faults of Milos cut Pliocene subhorizontal strata of white and porous felsic pumice tuffs at the Saranikiniko beach.

The regional fracture network consists of four sets of structural heterogeneities oriented N70, N15, N135 and N90 and all dipping ~ 75-90°. The relationship and timing between the different sets are consistent with regional dynamics and post-Pliocene peri-volcanic deformation.

3 Structural and petrological analysis

At the outcrop scale, we show (i) cm-wide *clusters* and (ii) mm-wide isolated anastomosed *deformation bands* exhibiting strong positive reliefs due to their higher resistance to erosion compared to the surrounding host rock.

At the sample scale (Cf. Fig. 1), the strain is accommodated by the formation of deformation bands which are characterized by (i) a rearrangement of volcanic glass particles (ii), pore collapse, and (iii) grain fracturing (Cf. Fig. 1.C), which tends to be localized to narrow zones within each deformation band. The core zone is ~ 4.6 mm wide while the damage zone is ~ 1mm wide (Cf. Fig. 1.A). The bands present an anastomosed morphology where *cataclasite* and *protocatalasite* coexists (Cf. Fig. 1.A), depending on the intensity of the deformation. Thus, the *cataclasis* affecting the glasses appears to be the main deformation mechanism, inducing a reduction in grain size (from 42 μm to 23 μm) and therefore in porosity (from 28% to 4%) (Cf. Fig. 1.F) in the band compared to the host rock.

Micrometric clay filaments (illite) are observed (Cf. Fig. 1.E) and represent the main evidence of the volcanic glass alteration in interaction with water(s). These filaments are preferentially located in the CBD where they reflect a high degree of alteration favored by the fresh reaction surfaces created by the cataclastic processes. Halite mineralization along the edge of the CBD (Cf. Fig. 1.D) may support a past circulation of seawater in the vadose zone, locally stopped by the CDB.

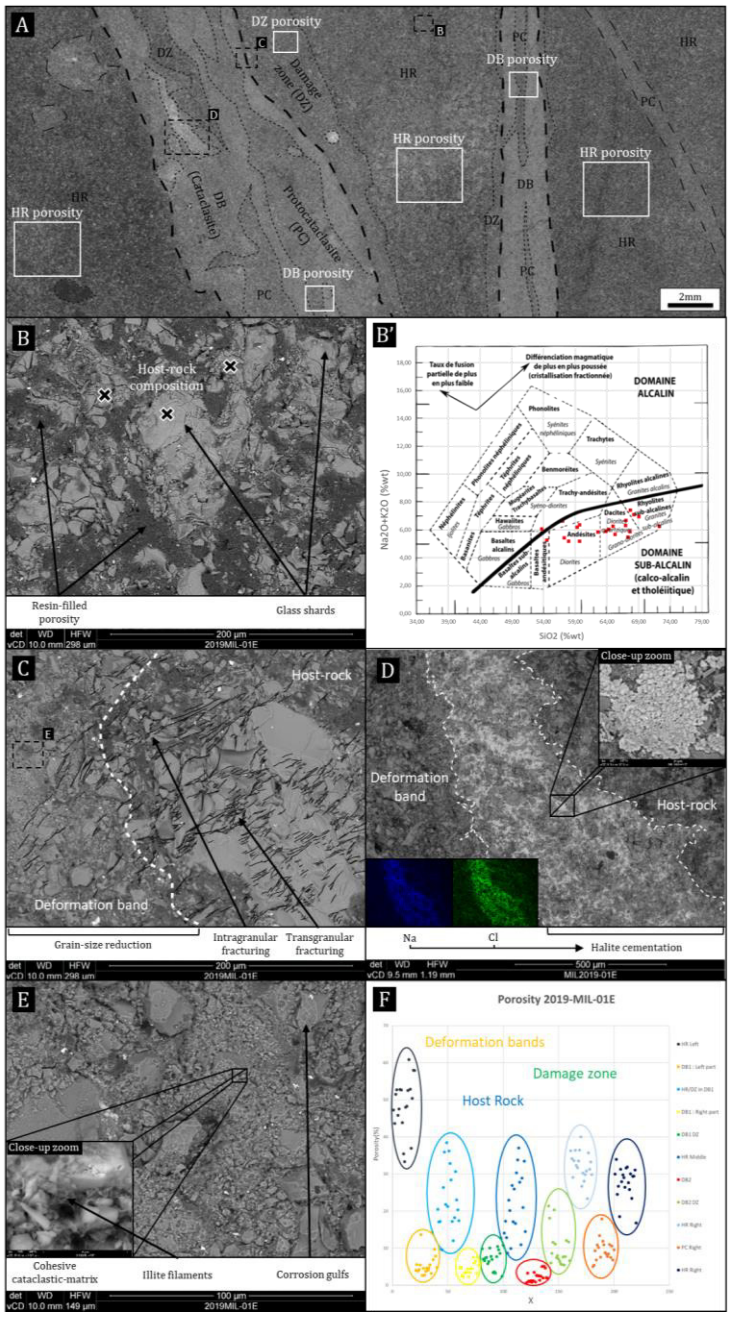

Figure 1: SEM imagery of deformation bands in volcaniclastic bands. (A: general view of the bands; B: Host-Rock; B': Host-rock nature; C: CDB/Host rock transition; D: Halite cementation; E: In-band cementation; F: Petrological properties)

4 Conclusion

These observations highlight the immediate impact of deformation on the petrological characteristics of the volcaniclastic rock, inducing a decrease in grain size, porosity and a concentration of alteration and mineralization processes on the edges of the deformation bands.

Homogénéisation séquentielle par méthode “grid-block” de milieux poreux hétérogènes: application à l’ostéosarcome

Moreno Adel[a], Quintard Michel[a], Mancini Anthony[a], Gomez-Brouchet Anne[b], Swider Pascal[a], Assemat Pauline[a]

[a] *IMFT (Institut de Méecanique des Fluides de Toulouse), Universitée de Toulouse, Allèe Camille Soula, 31400 Toulouse, France.*
[b] *CHU de Toulouse-IUCT Oncopole, Toulouse, France.*

Mots-clés : Homogénéisation, Séquentielle, Milieux poreux hétérogènes

1. Introduction

L’ostéosarcome est une tumeur osseuse primitive, caractérisée par la production anarchique de tissu osseux, et qui survient principalement chez les adolescents et les jeunes adultes. Le taux de survie à 5 ans est de 70% et chute à 25% pour les patients présentant des métastases ou répondant mal aux traitements [1]. Les stratégies thérapeutiques n’ont pas évolué depuis plus de trois décennies et de nouveaux développements sont nécessaires pour améliorer la prise en charge spécifique des patients. Comme la majorité des sarcomes à génomique complexe, ce type de tumeurs présente de fortes hétérogénéités spatiales.
Dans le cas de l’ostéosarcome, il existe des hétérogénéités dans la micro-architecture osseuse, la densité cellulaire mais aussi dans la réponse au traitement en raison de l’effet potentiellement localisé de la chimiothérapie. Compte tenu des populations cellulaires impliquées dans l’évolution des ostéosarcomes, telles que les ostéoblastes, les ostéoclastes ou les ostéocytes [2], il est supposé que l’ostéosarcome est très sensible aux effets mécaniques se produisant à différentes échelles spatiales [3]. Il est en particulier admis que les mécanismes de transport et les déformations structurelles jouent un rôle fondamental dans l’évolution de la maladie mais aussi sur l’efficacité du traitement.
L’objectif de ce travail est d’étudier les différents mécanismes de transport (flux interstitiel, diffusion), la mécanique structurelle (élasticité linéaire) et la poromécanique de la tumeur poreuse à l’échelle du tissu par une approche basée sur des méthodes de changement d’échelle.

2. Méthode et résultats

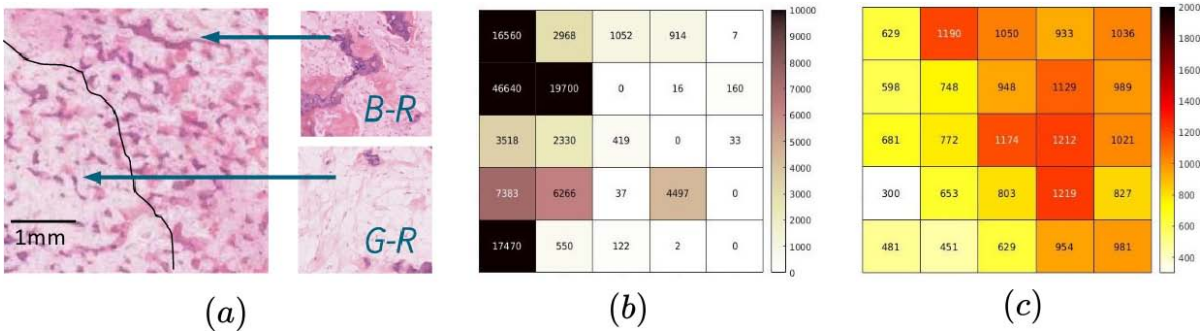

Figure 1: a) Coupe histologique présentant une réponse mixte au traitement (BR= Bad Response, nombreuses cellules présentes dans le tissu après traitement par chimiothérapie, GR= Good Response, peu de cellules résiduelles), résolution $466nm$. b) Carte de la magnitude adimensionnée κ des perméabilités. c) Carte de la densité surfacique cellulaire C.

Cette méthodologie s'appuie sur des coupes histologiques de pièces chirurgicales issues d'une cohorte de patients toulousains (CRB Cancer Toulouse). Les lames sont scannées (figure 1a) et l'image est segmentée puis binarisée (thèse Anthony Mancini). L'étude statistique de la micro-architecture des ostéosarcomes montre que l'identification des longueurs caractéristiques est complexe et qu'une séparation des échelles spatiales n'est pas nécessairement observée.

Dans cette étude, l'approche choisie pour caractériser le transport et les déformations de ce milieu poreux biologique est une méthode séquentielle du type "grid-block" [4, 5] en deux étapes. Afin de réduire l'influence des conditions aux limites sur le processus séquentiel, une méthode "extend-local" a été développée pour le premier changement d'échelle. Ces méthodes ont été mises en oeuvre avec la toolbox d'éléments finis FEniCS [6]. Cette approche permet en particulier d'obtenir une cartographie des propriétés équivalentes de l'objet d'étude. La dépendance des tenseurs équivalents aux différents paramètres (conditions aux limites, taille de la grille, etc.) a été explorée. Grâce à cette approche, les propriétés mécaniques et les paramètres biologiques (par exemple, la densité de la population cellulaire) peuvent être mis en relation (figure 1b-c). Dans l'exemple illustré ici, une corrélation négative est trouvée entre la densité cellulaire et la perméabilité du milieu.
De manière plus générale, les développements numériques mis en oeuvre dans ces travaux permettent d'obtenir de nouvelles informations quantitatives mécano-biologiques sur les tumeurs osseuses à partir d'images issues du suivi des patients et potentiellement d'obtenir des marqueurs utiles pour une prise en charge thérapeutique personnalisée des malades.

References

[1] P Casali, N Abecassis, Sebastian Bauer, R Biagini, S Bielack, Sylvie Bonvalot, Ioannis Boukovinas, Judith Bovee, T Brodowicz, Javier Martin-Broto, Angela Buonadonna, E Ãlava, Angelo Tos, X Muro, Palma Dileo, Mikael Eriksson, A Fedenko, V Ferraresi, A Ferrari, and Jean-Yves Blay. Soft tissue and visceral sarcomas: Esmo-euracan clinical practice guidelines for diagnosis, treatment and follow-up. *Annals of oncology : official journal of the European Society for Medical Oncology*, 29, 05 2018.

[2] Anne Gomez-Brouchet, Julia Gilhodes, Nathalie Van Acker, Regis Brion, Corinne Bouvier, Pauline Assemat, Nathalie Gaspar, Sebastien Aubert, Jean-Marc Guinebretiere, Beatrice Marie, Frederique Larousserie, Natacha Entz-Werlé, Gonzague De Pinieux, Eric Mascard, Francois Gouin, Pierre Brousset, Marie-Dominique Tabone, Marta Jimenez, Marie-Cecile Le Deley, Jean-Yves Blay, Laurence Brugieres, Sophie Piperno-Neumann, and Francoise Rédini. Characterization of macrophages and osteoclasts in the osteosarcoma tumor microenvironment at diagnosis: New perspective for osteosarcoma treatment? *Cancers*, 13(3), 2021.

[3] Stephen Cowin. Mechanosensation and fluid transport in living bone. *Journal of musculoskeletal & neuronal interactions*, 2:256–60, 04 2002.

[4] Moussa Kfoury, Benoit Noetinger, Michel Quintard, and Rachid Ababou. Upscaling fractured heterogeneous media: Permeability and mass exchange coefficient. *Journal of Applied Mechanics*, 73, 01 2006.

[5] Louis Durlofsky. Numerical calculation of equivalent gridblock permeability tensors for heterogeneous porous media. *Water Resources Research*, 27:699–708, 05 1991.

[6] Martin S. Alnæs, Jan Blechta, Johan Hake, August Johansson, Benjamin Kehlet, Anders Logg, Chris Richardson, Johannes Ring, Marie E. Rognes, and Garth N. Wells. The fenics project version 1.5. *Archive of Numerical Software*, 3(100), 2015.

Deplacements diphasiques de liquides organiques en milieux poreux - suivi et analyse par micromodeles

E. M. Niang[a], M. Marcoux[a]

[a] *Institut de Mecanique des Fluides de Toulouse.*

Keywords: Chemin percolant, Mouillabilite, Drainage, Imbibition, Saturation residuelle

1. Introduction

L'etude des deplacements de fluides non miscibles dans les milieux poreux modeles a un interet croissant. En effet, l'etude de l'hydrologie des milieux peu permeables, susceptibles de confiner des dechets industriels ou nucleaires, et actuellement en pleine expansion. L'amelioration des ressources en eaux souterraines en particulier et un objectif d'autant plus important que les risques de pollutions des eaux de surface augmentent. La recuperation des produits petroliers du sous-sol, la migration primaire d'hydrocarbure, les fuites de gaz ou de liquide par percage capillaire de roches couverture et l'amelioration des ressources geothermiques sont egalement des enjeux ecologiques et economiques importants qui doivent faire appel a des approches microfluidique.

2. Objectif

Dans le cas present, nous nous interessons aux ecoulements isothermes se produisant dans des milieux poreux modeles de mouillabilites homogene a l'eau ou a l'huile.

L'objectif est de visualiser a l'aide d'un micromodele (voir figure : 1) le comportement d'un polluant organique a pouvoir d'etalement positif ou negatif dans les differentes zones du sous-sol (zones saturees et non saturees) ainsi que lors de la fluctuation saisonniere de la nappe phreatique, et d'en deduire les mecanismes de mouvement qui regissent son deplacement et afin d'optimiser les predictions de contamination des sols et d'ameliorer la depollution.

3. Resultats

Figure 1: Drainage par de l'eau (en jaune) d'un milieu initalement sature par de l'huile (en rouge)

Le principal verrou qui a ete leve dans cette etude est la realisation de micromodeles en resine avec une resolution micrometrique pouvant supporter l'utilisation de fluides organiques, generalement problematiques pour ce type de milieux modeles.

Des comportements tres differents ont ete observes suivant les couples de fluides utilises et la geometrie du milieu poreux.

Ces observations et analyses seront confrontees aux modeles theoriques pour une validation ou amelioration de ces derniers.

Applying high performance computing techniques to the simulation of heat and water transfers within permafrost

L. Orgogozo[a], C. Grenier[b], M. Marcoux[c], O. Pokrovsky[a,d] E. Mouche[b], M. Quintard[c,e]

a GET (Geosciences Environment Toulouse), Toulouse, France
b LSCE (Laboratory of the Sciences of Climate and Environment), Gif-sur-Yvette, France
c IMFT (Toulouse Institute of Fluid Mechanics), Toulouse, France
d BIO-GEO-CLIM laboratory, Tomsk, Russian Federation
e CNRS, IMFT, Toulouse, France

Keywords: heat transfer, freeze/thaw, variable saturation, permafrost, numerical simulation, high performance computing, OpenFOAM

1 Introduction

Permafrost covers a quarter of the land of the northern hemisphere. Due to the intimate coupling that it provokes between water and heat fluxes, the presence of permafrost has strong impacts on biogeochemical fluxes and geomechanical processes[1]. The global warming induced permafrost thaw has thus important consequences both at local scale (e.g. : hydrogeology, terrain stability) and at global scale (e.g. : hydro-biogeochemical cycles, including C-cycle). Water and heat fluxes in such environments correspond to highly coupled and non-linear transport phenomena. Thus, mechanistic modeling approaches are key tools for studying quantitatively the thermo-hydrological dynamics of permafrost, and for predicting their responses to climate change. However, the huge computational power that these approaches require is an obstacle toward their application. In this work, we discuss the potential application of the High-Performance Computing (HPC) tool for permafrost modeling permaFoam[2] in the framework of the HiPerBorea project (hiperborea.omp.eu).

2 The permaFoam solver for permafrost modelling

Permafoam is a cryohydrogeological simulator that allows to model the coupled heat and water fluxes in variably saturated soils with freeze/thaw of the pore water by solving a set of governing partial differential equations that describes the involved physics. The validation of permaFoam has been done in the framework of the Interfrost international benchmark[3]. In order to benefit from good High-Performance Computing capabilities[4], it has been developed in the framework of the open source Computational Fluid Dynamics modeling tool box OpenFOAM® (openfoam.com / openfoam.org). The first application of the permaFoam solver has been devoted to the study of the evapotranspiration fluxes in a taiga covered watershed of Central Siberia, in the continuous permafrost area, the Kulingdakan watershed[2]. This previous study has been performed with a simplified 2D representation of the slopes of the considered catchment, and now 3D computations of the permafrost dynamics are on-going[5].

3 Parallel performances

Dealing with complete 3D modeling of thermo-hydrological fluxes in this 40 km² watershed for multi-annual simulations leads to important computational loads, and thus we use national level supercomputers for performing these simulations. Obtained using more than 1.3 millions of CPU hours on Occigen (CINES, ~80 000 cores) and IRENE-ROME (TGCC, ~300 000 cores) since 2019, our results are in good agreement with the available observations in term of maximum active (i.e. seasonally thawed) layer thicknesses. To illustrate the High-Performance Computing capabilities of permaFoam, Figure 1 presents the elapsed time ("real world" time) needed for the simulation of the month of January under current climate, as well as the CPU time (elapsed time multiplied by the number of used cores) as a function of the number of cores used in parallel, from 1 024 to 16 382 cores. Such a strong scaling curve allow to assess the parallel performances of the used numerical tool.

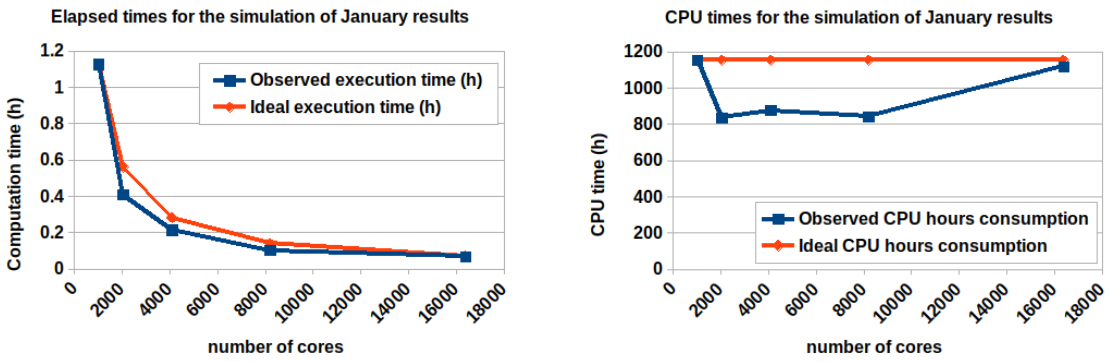

Figure 1: Elapsed times (i.e. : real worl times) and CPU times (i.e.: computing hours consumption) observed for the presented 3D simulation for January, using 2x64 AMD Rome@2.6Ghz (AVX2) processors (TGCC IRENE-ROME).

The ideal elapsed times and CPU times are obtained by assuming a linear speed up for the computations while increasing the used number of cores (references values at 1024 cores). Thus in these ideal conditions, no effects such as data transfer related effects or differential loading effects damage the efficiency of the parallel speed up. It means that, in ideal conditions, by using n time more cores a n-fold decrease of elapsed time is obtained while the CPU times stays strictly constant. The superlinear behaviours observed here are classical when applying OpenFOAM® to modeling in geosciences[6].

References

[1] McKenzie J.M. et al. Invited perspective: What lies beneath a changing Arctic? The Cryosphere, 15, 479–484 (2021).
[2] Orgogozo L. et al. Water and energy transfer modelling in a permafrost-dominated, forested catchment of Central Siberia: the key role of rooting depth. Permafrost and Periglacial Processes 30:75–89 (2019).
[3] Grenier C. et al. Groundwater flow and heat transport for systems undergoing freeze-thaw: Intercomparison of numerical simulators for 2D test cases. Advances in Water Resources. 2018;114:196-218 (2018).
[4] Orgogozo L. et al. Application of OpenFOAM® to permafrost modeling – the permaFoam solver. 7th ESI OpenFOAM Conference, Berlin (2019).
[5] Orgogozo L. et al. 2020. Numerical modeling of coupled heat and water transport for the study of permafrost dynamics: High Performance Computing simulations for watershed scale analysis. 12th INTERPORE Conference, Tsingtao (online conference), https://hal.archives-ouvertes.fr/hal-02931744 (2020).
[6] Orgogozo L. et al. An open source massively parallel solver for Richards equation: Mechanistic modelling of water fluxes at the watershed scale. Computer Physics Communications 185 : 3358-3371 (2014).

High performance numerical simulation of Thermo-Hydro-Chemical processes in porous media.

N. Pillardou[a,1], E. Ahusborde[a], F. Croccolo[b]

[a] *Universite de Pau et des Pays de l'Adour, E2S UPPA, CNRS, LMAP, Pau, France*
[b] *Universite de Pau et des Pays de l'Adour, E2S UPPA, CNRS, Total, LFCR, Anglet, France*

Keywords: Finite volume, HPC, THC, Numerical simulation, Multiphase flows in porous media, Reactive transport, Nonisothermal, CO_2 geological storage.

1. Introduction

Reactive multiphase flows in porous media appear in diverse energetic and environmental problematics. Without being exhaustive, one can mention geological gas storage (CO_2, natural gas and H_2), nuclear waste management, petroleum engineering or geothermal energy production. In this talk, we will mainly focus on the application of CO_2 storage.

Nowadays, the effects of global warming start to be clearly visible all around the world. The evidence reported by many scientists increased the pressure exerted by the scientific community to the general public and politicians in order to take actions against further dramatic climate changes. Therefore, some projects have been studied in order to reduce greenhouse gas emissions. CO_2 storage in geological reservoirs represents a good alternative to cut off these emissions by injecting the CO_2 underground and keep it trapped due to different trapping mechanisms. Saline aquifers reservoirs seems to be one of the most promising storage type to store CO_2 thanks to huge available volumes and to a diversity widespread worldwide. Numerical simulations are widely used in geological reservoir modeling due to their flexibility to treat wide range of sizes of reservoirs and span a wide range of time scales for investigating the behaviour of the injected fluid.

Despite the large effort of the scientific community, simulations of Thermo-Hydro-Chemical (THC) processes in complexes porous media remains a challenge. In this talk, we consider a parallel fully coupled fully implicit finite volume scheme for modeling nonisothermal multiphase flow and geochemical interactions by implementation in the DuMu^X platform [1].

2. Mathematical model for reactive multiphase flows

Reactive multiphase flows are modeled by mass conservation laws written for each chemical component in each phase (liquid or gaseous). These equations are coupled with the Darcy law to characterize the flow velocity of each phase. The energy balance equation is added in order to take into account temperature effects in nonisothermal simulations.

Chemical reactions are described thanks to reaction rates that are either function of concentration in case of kinetic reactions or unknown for equilibrium reactions. Reactions rates at equilibrium can be eliminated by means of linear transformation by using Morel's formalism. The chemical system is then closed with the help of mass action laws which are algebraic equations linking activities (or molar fractions) of the different species.

Finally, the system is closed by capillary pressure laws, equations of state and solubility laws characterizing each phase equilibrium. Thus, the unknowns of the system are pressures, saturations, molar fractions and the temperature. These flows are governed by a non-linear system of degenerated partial differential equations (modeling the flow), coupled with algebraic or ordinary differential equations (provided by chemical reactions).

3. Numerical simulations

In order to solve the system, a fully coupled fully implicit finite volume method has been developed and implemented within the DuMu^{X}platform [1]. The temporal discretization is done by using a Backward Differentiation Formula 2 (BDF2) scheme while the spatial discretization is based on a "cell-centered" method. Hence, the global resolution of the problem is written as a non-linear system that is solved using a Newton method with an adaptive time step. Linear systems are solved with the help of solvers provided by the DUNE library [3] (solver Bi-Conjugate Gradient Stabilized (BiCG-STAB) coupled with an AMG preconditionner). Parallelization is carried out taking advantage again of the DUNE library package based on MPI, providing high parallel efficiency and allowing simulations with several millions of degrees of freedom, ideal for large-scale field applications involving multicomponent chemistry.

To validate our methodology, we have adapted a 3D CO_2 injection test case proposed in [2] that aims at modeling mineral trapping which is the safest sequestration phenomenon. This test case considers five equilibrium reactions between three minerals (Calcite, MinA, MinB) and seven aqueous reacting species. Since this test considers an isothermal configuration, the complexity of the model is increased in order to take into account temperature effects due to nonisothermal CO_2 injection. Results in Figure 1 show briefly that the reservoir is cooled near the well due to injection. Moreover, after the injection, the gaseous CO_2 rises to the top of the domain and accumulates. It is dissolved in the aqueous phase and the $CO_{2(aq)}$ reacts with water to release H^+. Due to the decrease of pH, Calcite and MinA are dissolved by the front of low pH water stream. Finally, the dissolution of MinA provides free ions Me^{3+}, inducing the precipitation of MinB. One comparison with an isothermal simulation [4] will be presented in order to highlight the influence of the temperature as well as parallel computations.

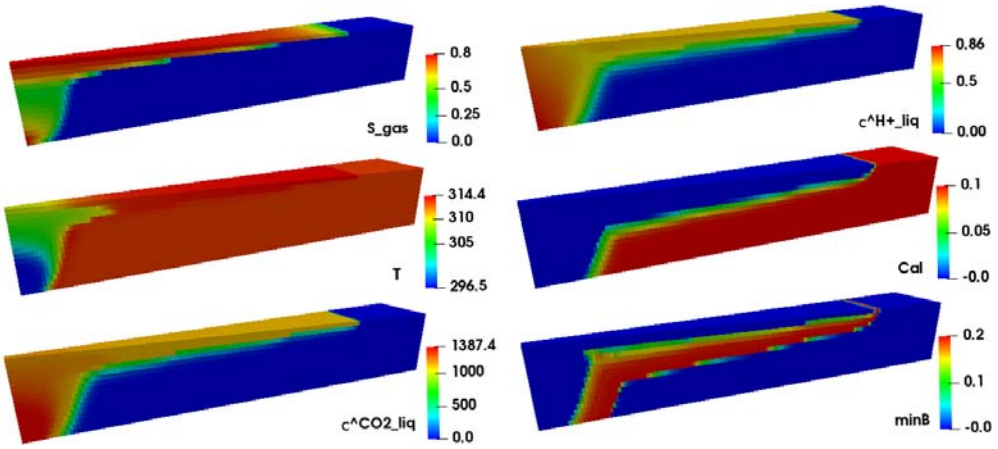

Figure 1: Profile of several quantities after 85 years of injection.

Acknowledgements - This research was carried out under the framework of the E2S-UPPA, Hub Newpores and Industrial Chair CO_2ES supported by the Investissements d'Avenir French programme managed by ANR (ANR16IDEX0002). We acknowledge financial support from E2S-UPPA, TOTAL Energies, BRGM and CNES. Computer time for this study was provided by CINES (allocation A0100610019 made by GENCI) and the computing facilities MCIA of the Université de Bordeaux and of the Université de Pau et des Pays de l'Adour.

References

[1] Koch, T., Gläser, D., Weishaupt, K. et al., DuMu^{X}3 - an open-source simulator for solving flow and transport problems in porous media with a focus on model coupling, *Computers & Mathematics with Applications*, 81, 423-443 (2021).

[2] Brunner, F., Knabner, P., A global implicit solver for miscible reactive multiphase multicomponent flow in porous media, *Computational Geosciences*, 23, 127-148 (2019).

[3] Bastian, P., Blatt, M., Dedner, A. et al., The DUNE framework: Basic concepts and recent developments, *Computers & Mathematics with Applications*, 81, 75-112 (2021).

[4] Ahusborde, E., Amaziane, B., Id Moulay, M., High Performance Computing of 3D reactive multiphase flow in porous media: application to geological storage of CO_2, *Submitted to Computational Geosciences* (2020).

Computation of macroscopic properties for 3D real bio-sourced morphologies

El-Houssaine Quenjel[a], Patrick Perré[a]

[a] *Chair of Biotechnology, LGPM, CentraleSupélec, Centre Européen de Biotechnologie et de Bioéconomie (CEBB), 3 rue des Rouges Terres, 51110 Pomacle, France.*

Keywords: Porosity, 3D real morphology, thermal and mass conductivities.

In this work, we are interested in the numerical computation of macroscopic properties of bio-based materials following their orthotropic directions. We focus on typical wood species such as : spruce, poplar and balsa. Porosity, thermal conductivity and mass diffusivity were investigated. At first, each sample is scanned at a resolution of the order of the micrometer thanks to a lab X-ray nanotomograph (UltraTom by RX-solutions). Then, a suitable set of 3D image processing operations, coded as a Python script in ImageJ, allows a digital representation of 3D morphology to be obtained.

This representation is used as input mesh of a in-house software, based on the finite volume method. By achieving the permanent regime, we deduce the macroscopic properties consisting of directional thermal conductivities and mass diffusivities. Several numerical experiments are carried out to validate the prediction approach. The focus will be on the effect of the REV (Representative Elementary Volume) on the macroscopic property, which depends on the property itself (porosity, thermal conductivity and mass diffusivity), the species, and the material direction.

Acknowledgment
The authors would like to thank SaTT Paris-Saclay for their support under the contract of the project Predict Bio-Mat. They also acknowledge Grand Reims, the Marne department and the Grand Est region for their funds.

References

[1] Louërat, M and Ayouz, M and Perré, P, Heat and moisture diffusion in spruce and wood panels computed from 3-D morphologies using the Lattice Boltzmann method, *International Journal of Thermal Sciences*, 130, 471–483 (2018).
[2] Schindelin, J, et al. Fiji: an open-source platform for biological-image analysis, *Nature methods* 9, 676-682, (2012).
[3] Perré, P, A review of modern computational and experimental tools relevant to the field of drying, *Drying technology*, 29(13), 1529-1541 (2011).
[4] Eymard, R., Gallouët, T., and Herbin, R. Finite volume methods. Handbook of numerical analysis, 7, 713-1018. *Finite volume methods, Handbook of numerical analysis*, Vol. VII, 713-1020, North-Holland, Amsterdam, (2000).

The class of weighted interior penalty discontinuous Galerkin methods for groundwater flow models

V. Fontaine[a], N. Rajaonison[a,c], P. Ackerer[b], H.T. Rakotondramiarana[c]

[a] *Department of Building and Environmental Sciences, University of La Réunion - South Campus, France.*
[b] *Université de Strasbourg, CNRS, ENGEES, LHYGES UMR 7517, F-67000 Strasbourg, France.*
[c] *Institute for the Management of Energy (IME), University of Antananarivo. P.O. Box 566 - Antananarivo 101, Madagascar.*

Keywords: Primal discontinuous Galerkin, weighted interior penalty, Péclet-dependent weights, advection or diffusion-dominated regime, numerical experiments

Abstract

Advection-diffusion-reaction equations are easily encountered in groundwater flow models, which is the principal motivation for the present work. We focus on mass or energy transport processes characterized by a significant variation of (local) Péclet numbers. It is well-known that the presence of a high Péclet number can trigger internal layers that are delicate to be well-captured by discretization methods [1]. This detrimental situation is generally characterized by a small diffusivity or a large velocity field at the element level. The analysis of Discontinuous Galerkin (DG) methods to address this kind of issue has been extensively covered in the literature (see, e.g., [3] and references therein). The success story of DG methods is because they combine advantages of finite volume and finite element methods, and they are well-suited to capture large gradients or discontinuities of exact solutions. However, despite all of these advantages, DG methods are generally more expensive than most other numerical methods due to their high number of coupled degrees of freedom (DOFs) and large stencils. To overcome these weaknesses, we focus here on families of Interior Penalty (IP) methods since they have the advantage of being one of the most compact DG schemes [4], i.e., only DOFs belonging to the direct neighboring elements are connected in the discretization. Thus, we propose a novel class of Weighted Interior Penalty (WIP) methods to approximate in a DG sense ADR equations. Several authors have preferred utilizing weighted trace operators in the IPDG formalism instead of arithmetic averages during the last decades. Specifically, Ern et al. selected the weights appropriately based on (normal) diffusivities on both sides of an interface [3]. Here, the originality of the proposed WIP method relies on the use of Péclet-dependent weights and penalty parameters to capture internal layers better. Furthermore, these quantities are selected accordingly to the nature of the local cellwise problem characterized by an advection- or diffusion-dominated regime. Thus, the stated DG-WIP formalism can automatically treat ADR processes for a wide range of Péclet numbers. Our penalty strategy is inspired by the recent work of Etangsale et al. [2] using a Scharfetter-Gummel technique to improve the stability of the HDG scheme. Numerical experiments are then presented to illustrate the performance and robustness of the proposed DG-WIP method.

References

[1] Di Pietro, D.A. and Ern, A., *Mathematical aspects of discontinuous Galerkin methods*, Springer Science & Business Media, (2011).
[2] Etangsale G., Fahs M., Fontaine V. and Isa-Abadi A.R., Families of hybridizable interior penalty discontinuous Galerkin methods for degenerate advection-diffusion-reaction problems, *arXiv:2106.00226* [math.NA], June 2021.
[3] Ern, A. and Stephansen, A.F. and Zunino, P., A discontinuous Galerkin method with weighted averages for advection–diffusion equations with locally small and anisotropic diffusivity, *IMA Journal of Numerical Analysis*, 29, 235–256 (2009).
[4] Rivière, B., *Discontinuous Galerkin methods for solving elliptic and parabolic equations: theory and implementation*, SIAM(2008).

Identification and understanding of colloidal destabilization mechanisms in geothermal processes

I. Raies[a,b], B. Ledésert[b], E. Kohler[a], M. Fleury[a]

[a] *IFP Energies nouvelles, 1 et 4 avenue de Bois-Préau, 92852 Rueil-Malmaison, France.*
[b] *Laboratoire Geosciences et Environnement Cergy, 1 rue Descartes, 95000 Neuville-sur-Oise, France.*

Keywords: Geothermal energy, reinjection, clays, colloids, retention, porosity, permeability decline, clogging, characterization, XRD, SEM-EDS, STEM, DLS, coreflooding experiments.

Abstract

In this work, the impact of clay minerals on formation damage of sandstone reservoirs is studied in order to provide a better understanding to the problem of deep geothermal reservoirs clogging due to fine particle dispersion and migration.

Our study is carried out on cores from a Triassic reservoir in the Paris Basin (Feigneux, 60 km NorthEast of Paris). Our goal being to first identify the clays responsible for clogging, a mineralogical characterization of these natural samples was carried out by coupling X-Ray Diffraction (XRD), Scanning Electron Microscopy (SEM) and Energy Dispersive X-ray Spectroscopy (EDS). The obtained results show that the stratigraphic interval studied contains mostly illites and chlorites [Figure 1 (a)]. Nevertheless, several parameters, notably the spatial arrangement of the clays in the rocks as well as the morphology and size of the particles, suggest that the illites are more easily mobilized by the flow of the pore fluid than chlorites.

Thus, based on these results, illite particles are next used to carry out laboratory experiments in order to better understand the factors leading to the aggregation and deposition of this type of clay particles in geothermal reservoirs under variant physicochemical and hydrodynamic conditions. To do so, the stability of illite suspensions under geothermal conditions will be investigated using different characterization techniques including Dynamic Light Scattering (DLS) and Scanning Transmission Electron Microscopy (STEM). Various parameters such as the hydrodynamic radius, the morphology and surface area of aggregates are measured.

Then, core-flooding experiments [Figure 1 (b)] are carried out using sand columns in order to highlight the permeability decline due to the injection of illite-containing fluids in sandstone reservoirs. In particular, the effects of the salinity, temperature, particle concentration and flowrate of the injected fluid are investigated. In order to localize the particles retained in the columns, Nuclear Magnetic Resonance (NMR) and X-ray Tomography are used to obtain porosity profiles before and after the injection.

The correlation of the results obtained in static and dynamic conditions allows thus a better understanding of the clogging problem encountered in the Triassic reservoirs of the Paris basin.

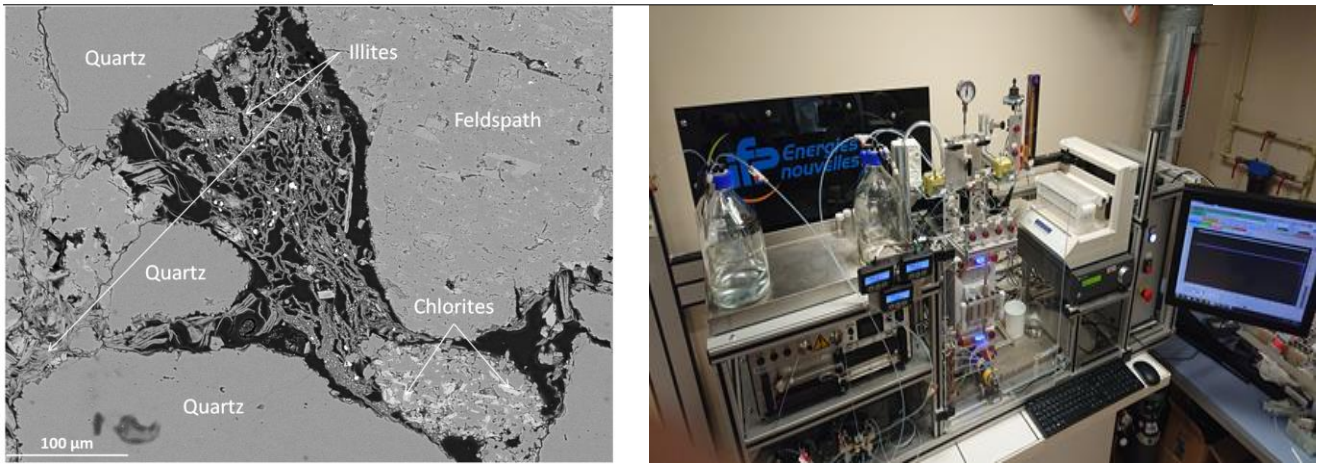

a b

Figure 1 : (a) SEM image showing pore-filling illites - Sample from the triassic FEX-1 series at Feigneux ; (b) Injection device used to carry out the core-flooding experiments in the framework of the present thesis (IFP Energies Nouvelles)

Microporous insulation behaviour under pressure

G. André, S. Chupin, D. Rochais

CEA, DAM, LE RIPAULT, F-37260 Monts, France

Keywords: insulation, pressure, microporous, thermal conductivity

1 Introduction

Thermal batteries are single-use power generators. Their safety and reliability make them an ideal source of auxiliary or backup energy. After being primed by a pyrotechnic device, the electrolyte contained in the battery liquefies and becomes a conductor. As long as the electrolyte remains liquid, the battery can supply current. The duration of the electric discharge operation depends on the ability to keep the heat at its core. For this purpose, super-insulators are used around the electrochemical heart of these batteries. These materials are made from silica nanoparticle compaction and have 90% porosity [1]. The nanoparticle matrix creates a pore network whose characteristic dimension is smaller than the average free range of air molecules. This structure means that the material has the particularity of having a lower thermal conductivity than the uncontained still gas. Heat transfer is carried out by conduction and radiation. To limit the latter, opacifying microparticles are present in a proportion of about 1% by volume. However, this superinsulation behaviour is only true when the material is in normal temperature and pressure (or vacuum) conditions. During battery priming, combustion gases are generated from pyrotechnic materials and degrade the insulation performance.

The objective of our study is to be able to characterize the behaviour of a super-insulator when it is in an operating environment degraded from its nominal use. Its behaviour will depend on the operating temperature level, the pressure, the type of gas in the battery. To achieve this, a numerical material approach is developed to determine the effective properties of a representative elementary volume. Complementary to this numerical approach, a flash method characterization bench has been adapted to perform thermal diffusivity measurements in temperature and under pressure of gases of different nature (up to 5 bar).

At the 15th JEMP 2021, the first estimations in the apparent conductivity of the material as a function of temperature and pressure, obtained from digital experiments of guarded hot plate carried out on a structure representative of the nanostructure of the insulation, will be presented.

2 Theoretical approach to determine the apparent conductivity of the WDS

In super-insulators, heat transfer is carried out by conduction and radiation. The latter becomes the dominant transfer mode in the WDS for high temperature applications. To understand its thermal behaviour, the approach chosen consists of 2 steps:

- homogenization of the conductive transfer in the medium, based on a description of the material at the scale of its smallest constituents, *id-est* nanoparticles (scale ~10 nm) and knowledge of the conductivity of the constituents from [2] for silica and [3] for gases in the contained state as a function of temperature and pressure.

- the determination of a radiative thermal conductivity derived from Rosseland's so-called diffusion approximation, which allows, on the basis of laws of optical and radiative homogenization, on the one hand to integrate the contributions of the various solid constituents to the overall infrared opacity of the microporous medium, and on the other hand to understand the different phenomena of radiation-matter interaction occurring within the material [4].

This means that we assume that it is possible to define an apparent thermal conductivity, $\boldsymbol{k^{app}}$ such as the sum of the effective conductivity $\boldsymbol{k_C}$ (calculated by a digital hot plate) and a radiative conductivity k_R of the

Rosseland type defined by $\boldsymbol{k_R(T) = \frac{16\sigma T^3}{3}\langle\frac{n^2}{\beta}\rangle}$, where n, optical medium index and β, medium absorption coefficient, depend on the wavelength.

3 Estimated apparent conductivity of WDS with temperature and pressure

Figure 1a is a 3D reconstruction of the insulation structure and Figure 1b is an example of a temperature field obtained when simulating a guarded hot plate to estimate the effective conductivity $\boldsymbol{k_c}$ for a given temperature and pressure condition.

(a) (b)

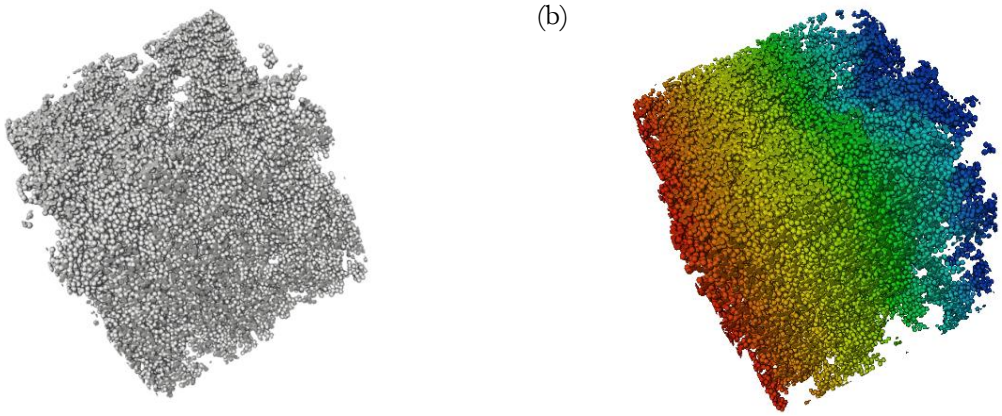

Figure 1: (a) a fractal structure representing a agglomeration of silica nanoparticles (size = 1x1x1 µm ; silica volumetric fraction = 10 %) and (b) the temperature field obtained when simulating a guarded hot plate to estimate the effective conductivity k_C for T = 400°C and P = 5 bar.

An estimate of $\boldsymbol{k_c}$ is obtained on the basis of these simulations to which the contribution of k_R is added to obtain the apparent thermal conductivity k^{app} of the insulation as a function of temperature and pressure as shown in Figure 2.

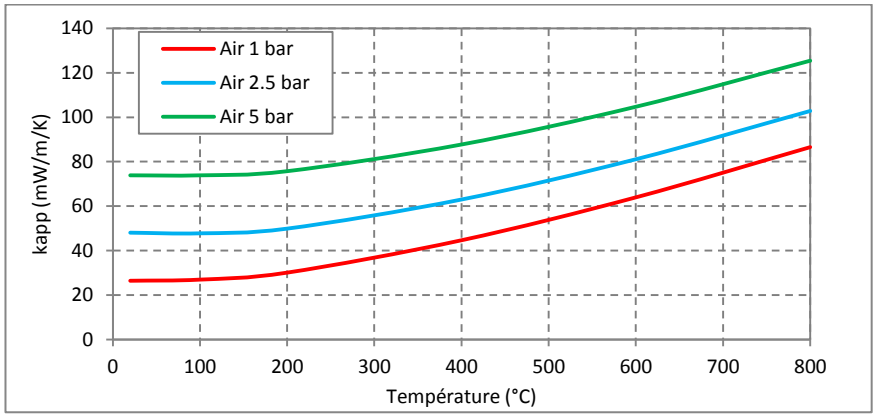

Figure 2: evolution of the apparent thermal conductivity, as a function of the temperature and pressure of the WDS by considering the air contained in 150 nm pores.

References

[1] Société PROMAT, « High temperature microporous insulation », technical documentation.
[2] Y. S. Touloukian, *Thermophysical properties of matter*. IFI/PLENUM New York-Washington, 1970.
[3] F. Bourret, « Mesure de la diffusivité thermique de mousse de carbone par la méthode flash et modélisation de la conductivité thermique radiative », Thèse de Doctorat de l'Université de Bourgogne, (1995)..
[4] F. Enguehard, « Multi-scale modeling of radiation heat transfer through nanoporous superinsulating materials », *International Journal of Thermophysics*, 28 (5), 1693 (2007).

Author Index

JEMP 2021

Biennial French InterPore Conference

Understanding porous media complexity